

1999

# A Fibre Optical Strain Sensor

Allsop, Thomas David Paul

<http://hdl.handle.net/10026.1/2779>

---

<http://dx.doi.org/10.24382/4018>

University of Plymouth

---

*All content in PEARL is protected by copyright law. Author manuscripts are made available in accordance with publisher policies. Please cite only the published version using the details provided on the item record or document. In the absence of an open licence (e.g. Creative Commons), permissions for further reuse of content should be sought from the publisher or author.*

# **A Fibre Optical Strain Sensor**

by

**Thomas David Paul Allsop**

BSc(Hons) , MSc

collaborators

( British Aerospace System and Equipment , BASE )

( Department of Electronic Engineering and Applied Physics, Aston University )



A Thesis submitted to the University of Plymouth  
in partial fulfilment for the degree of

**Doctor of Philosophy**

99

School of Electronic Communications and Electrical Engineering  
Faculty of Technology

## LIBRARY STORE

90 0392047 1



UNIVERSITY OF PLYMOUTH	
Item No.	<del>9003920471</del>
Date	- 8 JUL 1999 T
Class No.	T 681.25 ALL
Contl. No.	X 703901558
LIBRARY SERVICES	

REFERENCE ONLY

## **Abstract :**

Strain-sensing elements, fabricated in standard communications-grade single mode optical fibre, are increasingly being considered for application in structural health monitoring. The reason for this is the numerous advantages demonstrated by these devices compared with traditional indicators. This thesis describes work carried out on optical sensors at the University of Plymouth. The aim of this work was to achieve an optical fibre strain sensing system capable of measuring absolute strain with good resolution and having wide dynamic range, without bulky optical equipment and not susceptible to misalignment due to handling.

Earlier work was devoted to study on an intrinsic Fabry-Perot interferometric sensor and an optical phase-shift detection technique. The sensing element investigated relied on the end face of an optical fibre as one mirror and the second mirror being a layer of Titanium Dioxide ( $\text{TiO}_2$ ). Although some results are included, it was soon realised that this sensor had a number of problems, particularly with fabrication. As no simple solution presented itself, consideration was given to a sensor that made use of the change in reflectance of an intra-core fibre Bragg grating when the grating was subjected to strain. The bulk of work described in this thesis is concerned with this type of sensing element. The grating structure is inherently flexible and a number of structural formats were studied and investigated. The first and simplest grating considered was two linearly chirped Bragg gratings used in a Fabry-Perot configuration (a grating resonator). The sensor was tested using the sensing detection system and although the fabrication problems were overcome absolute strain measurement was unattainable.

To achieve this end, a theoretical study of a number of grating structures was carried out using the T-matrix Formalism. Confidence in using this approach was gained by comparing the spectral behaviour of a proposed grating with results, which were given by another theoretical model for the same proposed grating. The outcome of this study was that two structures in particular showed promise with regard to absolutism (the measure of true strain) and linearity. Discussions held with the department of Applied Physics at Aston University about fabrication resulted in one of the proposed designs being abandoned due to difficulties of fabrication.

The second structure showed more promise and fabrication attempts were put in hand. This grating is linearly-chirped with a Top-hat function and a sinusoidal perturbation as a taper function of the refractive index modulation. Experiments were performed, data were acquired and system performance for this sensor is presented. The thesis concludes that using such a fibre Bragg grating as the sensing element of a strain sensing system enables it to measure absolute strain without using bulky optical equipment. At present, the resolution of strain is limited by the quality of the grating being fabricated (anomalies on profile), this should improve once the fabrication technique is refined.



*This copy of the thesis has been supplied on condition that that anyone who consults it is understood to recognise that its copyright rests with its author and that no quotations from the thesis and no information derived from it may be published without the author's prior consent.*

## ***Acknowledgements :***

I would like to thank Ron Neal who as been my Director of Studies for making it possible for me to do and complete this project at University of Plymouth . Dr Alan Malvern my supervisor from British Aerospace (BASE) for his thought provoking discussions and guidance . To the fabricators of the fibre Bragg gratings the Department of Applied Physics and Electronic Engineering at Aston University particularly Dr Kate Sugden and Karen Chisholm for their helpful advice and Karen's tenacity in producing the final sensing element . To Dr Mansel Davies and Peter Van-Eetvelt for the help and laughs with some of the mathematics dealing with Bragg gratings . Also to Dave Jones and Bill Mckee for their help and company in the Lab and the office , which made it a lot more bearable .

Last to mention but first too mind , my parents , The-Old-Dear and Pop's , for their support and love over the years and who always kept faith with me .

## **(1) The Fibre Optical Sensor .**

1.1	The fibre optical sensor .	1
1.1.2	Smart Structures .	2
1.1.3	The physical attributes of a fibre optical sensors.	3
1.2	Classification of fibre optical sensor .	5
1.2.1	The intensimetric sensor .	5
1.2.2	The interferometric sensor .	5
1.2.3	The modalmetric sensor .	6
1.2.4	The polarimetric sensor .	6
1.2.5	The Fabry Perot sensor .	7
1.2.6	The fibre Bragg grating sensor .	8
1.2.7	The general parameters of the fibre strain sensors .	9
1.3	Multiplexing Techniques .	10
1.3.1	Frequency division multiplexing .	11
1.3.2	Time division multiplexing .	12
1.3.3	Intensity ; quasi-distributed sensors .	13
1.3.4	Coherence multiplexing .	14
1.3.5	Low coherence multiplexing .	14
1.3.6	Wavelength division multiplexing .	15
1.3.7	Demodulation techniques for multiplexed sensors .	16
1.3.7.1	Demodulation techniques suitable for multiplexed interferometric sensors .	16
1.3.7.2	Demodulation techniques suitable for multiplexed Bragg grating based sensors .	18
1.3.7.3	Broadband and edge filters .	19
1.3.7.4	The interferometric detection technique .	20
1.3.7.5	Detection techniques using tuneable narrowband filter .	21
1.4	Basic principles of a fibre optical strain sensor .	23
1.4.1	The strain optics effect , $\Delta n$ .	24

## **(2) The Fabry Perot sensor ( F.F.P. sensor ) .**

2.1	The Fabry Perot sensor .	27
2.2	Fabrication of the fibre fabry Perot sensor (FFPS) .	28
2.3	Fibre Fabry Perot optical strain sensor .	31
2.3.1	The relationship between optical phase change of a F.F.P. sensor and longitudinal strain .	33
2.4	Signal processing for the fibre Fabry Perot sensors .	36
2.5	Experimental test rig .	39
2.6	Experimental results for the fibre Fabry Perot sensor .	40
2.6.1	Processed information from the F.F.P. sensor .	43
2.7	Observations and results of the F.F.P. sensor .	45

## **(3) The intra-core fibre Bragg grating sensor .**

3.1	The fibre Bragg grating sensor .	49
3.2	Properties of a uniform fibre Bragg grating .	50
3.3	Nonuniform fibre Bragg grating .	52
3.3.1	Aperiodic or chirped fibre Bragg grating .	52
3.3.2	Apodising of a uniform or chirped fibre Bragg grating .	53
3.4	Principle of operation of a Bragg grating strain sensor .	54
3.5	Fabrication techniques .	55
3.6	Theoretical representation of the fibre Bragg gratings .	58
3.6.1	Methods used to obtain an analytical expressions for Bragg gratings .	58
3.6.2	The Perturbation approach to modelling a grating .	59
3.6.3	Rouard's Method .	59
3.6.4	Alternative methods to model Bragg gratings .	61
3.6.5	T-matrix formalism of fibre Bragg gratings .	61
3.7	Development of a theoretical model of the fibre Bragg grating ( a spectral reflection response with no longitudinal strain )	62
3.7.1	The chirp factor for a linearly chirped Bragg grating .	64

3.7.2	Spectral Reflective response of a fibre Bragg grating under longitudinal strain .	65
3.8	Simulations of fibre Bragg grating .	67
3.8.1	Flexibility of C program for the T-matrix formalism .	67
3.8.2	Implementation of the C program for the T-matrix formalism .	68
3.8.3	Technique to predict how a Bragg grating under longitudinal strain behaves using the prescribed signal process method .	73

#### **(4) The fibre Bragg grating resonator .**

4.1	The fibre Bragg grating resonator .	74
4.2	A Bragg grating resonator with a 27nm bandwidth and gratings having identical reflectivities of five percent ( Spectral response ) .	74
4.3	A Bragg grating resonator with a 27nm bandwidth and gratings having identical reflectivities of ten percent ( Spectral response ) .	76
4.4	Theoretical reflectivity response with longitudinal strain .	78
4.5	Experimental and theoretical results of the fibre Bragg grating resonators .	80
4.5.1	Theoretical results of a fibre Bragg grating resonators .	82
4.5.2	Experimental results of the fibre Bragg grating resonators .	84
4.6	Modified fibre Bragg grating resonator .	89
4.6.1	The static response of the resonator to longitudinal strain .	90
4.6.2	Experimental results of the modified resonator .	92
4.7	Observations and results of the fibre Bragg grating resonator sensor .	94

#### **(5) The fibre Bragg grating strain sensor .**

5.1	Description of the grating to be investigated and theoretical spectral responses .	98
5.2	The theoretical response of the proposed gratings subjected to longitudinal strain .	101

5.3	Physical interpretation of the fibre Bragg gratings .	104
5.4	The fibre Bragg grating strain sensor ( the spectral response) .	106
5.5	Experimental results from the fibre Bragg grating sensor subjected to longitudinal strain .	110
5.5.1	The static reflectivity response of the Bragg grating sensors to longitudinal strain .	111
5.5.2	Experimental results of the sensing system using the fibre Bragg grating sensors .	113
5.6	Observations and results of the sensing system using sensor Bragg grating that is linearly chirped and has a Top-Hat taper function with a sinusoidal variation in the refractive index modulation .	118

## **(6) Conclusion .**

6.1	General discussion .	122
6.2	General discussion of the performance of the new sensing elements .	124
6.3	General comparison of the three sensing elements .	125
6.4	Suggestion for multiplexing .	128
6.5	Robustness of the system .	129
6.6	A comparison of specification to existing systems .	130
6.7	Concluding remarks	131

## **(7) References .**

## **Appendices .**

<b>I</b>	<b>Mode Coupling Theory .</b>	<b>140</b>
Ia	Coupled equations of Motion .	140
Ib	Backward Coupling : The Grating reflector .	144
Ic	Solution to the mode Coupled Equations ( Uniform Grating ) .	148
Id	Approach for Nonuniform gratings .	154

<b>II</b>	<b>The Runge-Kutta method for solving the coupled equations .</b>	<b>155</b>
IIa	Derivation of the equations used in the Runge-Kutta method .	155
IIb	Implementation of the FORTRAN90 program of the R-K method .	157
IIc	Listing of the FORTRAN90 program for Runge-Kutta method .	158
<b>III</b>	<b>The Analytical solution to a linearly chirped fibre Bragg grating .</b>	<b>160</b>
IIIa	Derivation of the two independent second order ordinary differential equations .	160
IIIb	Parabolic Cylinder function and its relationship to confluent hypergeometric functions .	165
IIIc	Using the boundary conditions ; $a(0) = 1$ , $b(L) = 0$ and the derivatives at the those points to obtain the constants of integration .	168
IIId	Implementation of the MATHEMATICA program .	170
IIIe	Listing of the MATHEMATICA program .	171
<b>IV</b>	<b>Theoretical prediction of the spectral response and of longitudinal strain ( Mathcad +6 Programs ) .</b>	
IVa	Results ( spectral response ) for a uniform Bragg grating using Rouard's method , T-matrix formalism and the Derived analytical expression .	173
IVb	Results ( spectral response ) uniform and nonuniform grating ( linearly chirped period ) with constant $\Delta n$ using <u>Rouard's method</u> .	178
IVc	Results ( spectral response ) for a uniform and nonuniform grating ( linearly chirped period ) with constant $\Delta n$ using <u>T-Matrix formalism</u> .	180
IVd	Results ( spectral response ) for a combination of nonuniform gratings ( linearly chirped period , three gratings ) with constant $\Delta n$ using <u>Rouard's method</u> .	182
IVe	Results ( spectral response ) for a combination of nonuniform gratings ( linearly chirped period , three gratings ) with constant $\Delta n$ using <u>T-Matrix formalism</u> .	185

IVf	Resultant response ( single wavelength ) for a uniform and nonuniform grating ( linearly chirped period ) with constant $\Delta n$ subjected to longitudinal strain using <u>Rouard's method</u> .	188
IVg	Spectral response using the T-matrix Formalism technique a single uniform grating and single nonuniform grating ( linearly chirped ) with envelope function for $\Delta n$ ( a sinusoidal variation with a Top-Hat function ) .	190
IVh	Resultant response ( single wavelength ) for either a single or combination of uniform or nonuniform ( linearly chirped ) with a constant $\Delta n$ or a taper function for $\Delta n$ subjected to longitudinal strain using <u>T-Matrix formalism</u> .	193
<b>V</b>	<b>The Modelling of the signal processing technique employed by this scheme ( Mathcad +6 programs ) .</b>	
Va	The General Implementation and modelling of the strain sensing system for a Fabry-Perot configured sensor .	200
Vb	The General Implementation and modelling of the strain sensing system for a individual fibre Bragg grating sensor .	203
Vc	Schematic of the system .	205
Vd	A derivation of the magnitudes of the first and second harmonics from the system using a Fabry-Perot type sensor .	208
Ve	Theoretical prediction of the response of the system using a Grating resonator consisting of two approximately 27nm bandwidth and approximately five percent ( sensor 24-7-1 ) reflectivity , ( a Mathcad +6 program ) .	213
Vf	Theoretical prediction of the response of the system using a Grating resonator consisting of two approximately 27nm bandwidth and approximately ten percent ( sensor 24-7-2 ) reflectivity ( a Mathcad +6 program ) .	221



Vg	A theoretical prediction of the system using wavelength modulation in conjunction with a fibre Bragg grating which as a sinusoidal behaviour in it's spectral response and is subjected to longitudinal strain .	229
Vh	Theoretical prediction of the system using single nonuniform Bragg grating ( linearly chirped with a Taper function : envelope function for $\Delta n$ ; a sinusoidal variation with a Top-Hat function ( a Mathcad +6 program ) .	235
Vj	Theoretical prediction of the system using single nonuniform Bragg grating ( linearly chirped with a Taper function : envelope function for $\Delta n$ ; a sinusoidal variation with a Top-Hat function ( a Mathcad +6 program ) .	241
Vk	A theoretical prediction of the system using the experimental static reflection response data of the fabricated single nonuniform Bragg grating ( linearly chirped with a Taper function : envelope function for $\Delta n$ ; a sinusoidal variation with a Top-Hat function ( a Mathcad +6 program ) .	247
VI	The C program for the linearising of the data obtained from the demodulation technique for extraction of strain information .	253
<b>VI A</b>	<b>code listing of the C program for the T-Matrix formalism .</b>	<b>258</b>

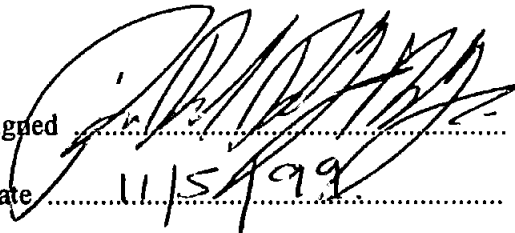
### **AUTHOR'S DECLARATION**

At no time during the registration for the degree of Doctor of Philosophy has the author been registered for any other University award.

This study was financed with the aid of a studentship from the University of Plymouth and carried out in collaboration with British Aerospace (BASE), Plymouth.

A conference was attended and work was presented. External institutions were visited for consultation purposes and several papers are being prepared for publication.

Conference attended: Bio-Sensors, 1996, Vienna, Austria

Signed  .....

Date 11/5/99 .....

# **1      The fibre optical sensor.**

## **1.1 The fibre optical sensor.**

Fibre optics first gained prominence in the field of telecommunications. This was dictated almost entirely by economics, changing from wires and coaxial cables to optical fibres. The increasing cost and demand for high-data-rate or large-bandwidth-per-transmission channels and the lack of available space in already congested conduits in metropolitan areas are the reasons for the increase in the popularity of fibre optics. Furthermore, fibre optical devices interface well with digital data-processing equipment, and their technology is compatible with modern microelectronic technology.

This success is also due to low-loss fibres and to the ability to drastically reduce group-velocity dispersion in such fibre so that extremely short optical pulses (  $\sim 5 \times 10^{-12}$  s ) undergo minimal spreading in propagation. Also the availability of laser sources as emission devices for fibre optical lines. These fibre optical lines are based upon electric fields that are confined and lossless by the process of total internal reflection from the dielectric interface between the core and the cladding of the fibre optic. This requires that the index of refraction of the core be greater than the cladding.

In the 1970's several researchers [1,2,50,51] showed the potential of fibre optics in the field of instrumentation, as sensors to monitor environmental changes. Interest in optical fibre sensors began in earnest in the late 1970's with the development of fibre optic hydrophones by J.A.Bucaro et al [1] and J.H. Cole et al [2]. The main motivation for researchers in maturing fibre optical sensor technology is the number of advantages they have over conventional sensors / indicators. One of the main advantages is that they do not generate electrical interference and therefore require no electrical isolation. These sensors can be embedded into or becomes part of a structure, are inert and corrosion resistant. These physical properties have led to a large number of applications in the structural health of materials monitoring of the structure when exposed to various environments. The physical make-up of an optical fibre sensor allows the sensor to be embedded into a material, for example a composite material. The sensor now becomes an integral part of the material. This technique allows real-time monitoring of fatigue in an aeroplane superstructure [3] see Figure 1.

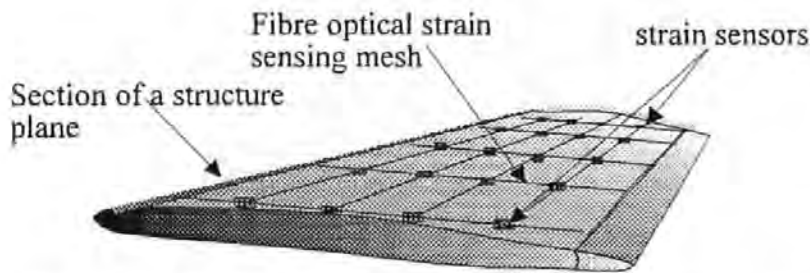


Figure (1). A section of a wing from an aeroplane with a fibre optical network sensing array.

The reliability and non-electrical nature of these sensors will have a great impact in the petro-chemical industry, in that they can be classified as being “intrinsically safe” instrumentation i.e. “non-electrical spark”. Their application will yield a reduction in costs that stems from the reduction in plant downtime. Ease of sterilisation, chemical inertness and their non-electrical nature has resulted in a number of medical applications [4,5]. An added bonus in this area of application is the geometric versatility permitting configuration into any arbitrary shape.

#### 1.1.2 Smart structures.

Optical fibre sensors are playing an increasing role in an emerging area of technology termed “Smart Materials and Structures”, sometimes called “Active Materials and Adaptive Structures”. There are two distinctive types of smart structures. Type I the “Passive smart structures” which possess a structurally integrated microsensor system for determining the state of the structure and also in certain instances determining the environment in which the system is operating. Type II the “Reactive smart structures” which can be said to possess a nervous system, a sensor array and an actuator control loop to effect a change in some aspect such as stiffness, shape, position, orientation or velocity of the structure to counteract environmental effects on the structure.

The development of a structurally integrated optical fibre sensing system represents a necessary first step in the evolution of this field of smart materials which will lead to advances in process control of material fabrication and to improvements in safety / economics of many diverse industrial products. Although there are a number of sensor systems that could be used for smart-material sensing networks, optical fibre sensors are being rapidly recognised as a sensing system capable of fulfilling this roll [6-9].

### 1.1.3 The physical attributes of fibre optical sensors.

The main advantages of an optical fibre sensor are as follows:

- 1 ) Light in weight.
- 2 ) Very small.
- 3 ) Immune to electromagnetic interference.
- 4 ) Inert and corrosion resistant ( Silica doped material ).
- 5 ) Safe and cannot initiate fires.
- 6 ) Very sensitive ( temperature, strain , pressure ,etc. ) .
- 7 ) Non - perturbing of structural properties.
- 8 ) Multifunctional capability.
- 9 ) Optical bus or network compatible.
- 10 ) Amenable to multiplexing and signal processing with integrated optics.
- 11 ) Provide high spatial resolution.
- 12 ) Can make integrated ( strain ) measurements over large distances.

Progress in demonstrating these advantages has been substantial in the past few years with a large number of different sensor types being developed. This large number of individual devices is usually categorised into amplitude or phase ( interferometric ) sensor or can be categorised into four basic types ( see section 1.2 ). In amplitude sensor the physical perturbation interacts with the fibre or some device attached to the fibre to directly modulate the intensity of the light in the fibre. The general advantages of intensity sensors, are the simplicity of construction and the compatibility with multimode fibre technology.

The phase ( interferometric ) sensor offers greater sensitivity than the intensity sensor and generally employs some kind of Mach-Zehnder arrangement, which uses phase change induced in the radiation field as it propagates along the fibre optical sensor. A suitable demodulator is employed to detect the original phase change of the sensor. Various demodulation techniques can be utilised including frequency modulation discrimination, stabilised homodyne, synthetic heterodyne, as well as several others ( see section 1.3 ).

Two fibre optic sensors showing most promise are based upon the intracore fibre Bragg grating and the intrinsic fibre Fabry Perot. There are still a number of problems to be overcome with these sensors before full commercialisation is possible. Further discussions of these topics occur later in this thesis.

For the application of fibre optical sensors to measure strain of some structure, more than one sensor is usually required. So one sensor becomes an array of sensors. This produces its own problem, how to address individual sensor within the array of sensors? Signals from individual sensors need to be separated and monitored without interference from other sensors. This requires assigning each sensor a distinct address that can be used to identify signals from individual sensors at the detector location; multiplexing.

The question of which multiplexing techniques are adopted can be dependent upon the particular application of the sensing system and the environment in which it is functioning. Also, other factors have to be considered such as cost, durability, size and required system specification (strain resolution, range of measurements and dynamic range) and is dependent upon the type of sensor being used in the array. This could be time division multiplexing (T.D.M.), frequency division multiplexing (F.D.M.), coherence multiplexing, and wavelength division multiplexing (W.D.M.) or it could be a combination. Various multiplexing and encoding procedures are highlighted in section 1.3 which have been adopted by various researchers.

The rest of this chapter discusses the various kinds of sensors and schemes that have been developed as a sensing system / array at the present time and also the working principles of the sensing element itself. The interferometric dielectric Fabry Perot strain sensor and the proposed sensing scheme are explained more fully and experimental results are shown in chapter 2. The subject of fibre Bragg grating (F.B.G.) is expanded in chapter 3, from the various kinds of gratings available to how they can be fabricated and their physical interpretation. Following on chapter 4 discusses the change from using a interferometric dielectric Fabry Perot strain sensing element to a fibre Bragg grating resonator as a strain sensing element. Experimental results of the sensing system using a fibre Bragg grating resonator as a sensing element is given. Chapter 5 deals with the final sensing element, the fibre Bragg grating strain sensor from a theoretical point of view and also gives experimental verification of its behaviour. In chapter 6 a general discussion of the work in the thesis is given with a conclusion. Also aspects of the sensing system are addressed, such as comparisons to existing systems and robustness.

## **1.2 Classification of optical fibre sensors.**

Fibre optic sensors can be classified into four main basic categories. These are intensimetric, interferometric, polarimetric and modalmetric sensors. The two fibre sensors with the most promise at this time are based upon the intracore Bragg grating and the intrinsic Fabry- Perot and most research is being conducted with these types of sensors.

### **1.2.1 The intensimetric sensor.**

The intensimetric sensor depends upon a variations of the radiant power transmitted through the fibre; i.e. the presence or absence of light. The absence of light would show a fracture has occurred.

### **1.2.2 The interferometric sensor.**

This type of sensor relies on the detection of a phase change induced in the radiation field as it propagates along the fibre optical sensor. The Michelson, Fabry - Perot and the Bragg grating are examples of this type of sensor. The Bragg grating has shown the greatest potential and has therefore been the subject of intense research and continues to be so. The working principles of the intrinsic Fabry - Perot sensor and the intracore fibre Bragg grating sensor are discussed in later sections of the report.

The differential Michelson (Figure 2 ) uses two closely spaced single mode optical fibres, in which one optical fibre serves as a reference to the other fibre . The actual sensing region is localised between the mirrored ends of the two optical fibres. As changes in the relative length of the two arms occurs due to strain / compression or temperature, an interference pattern is produced. Sinusoidal modulation of the light intensity occurs and is incident upon the detector. In order to extract the intensity variation, the two sensing arms need to be linked, this is achieved by means of a coupler.

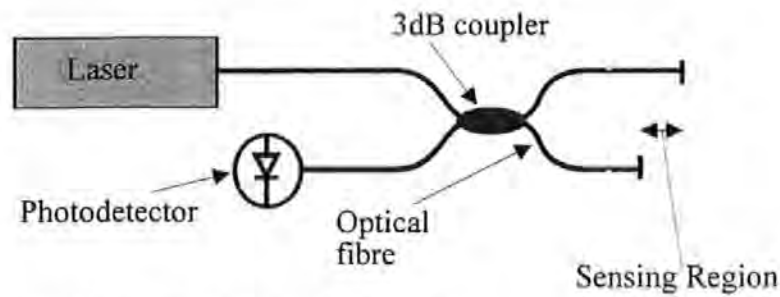


Figure (2) . Michelson fibre optical sensor.

An example of such a system is described and demonstrated by T. Berkoff et al [10] using an unbalanced fibre Mach-Zehnder interferometer based on source coherence synthesis.

The coupler used must preserve the phase relationship between the two sensing fibres. Any transient phase variation that is introduced by coupling will degrade the performance. The main difficulty is to produce a connector that can provide phase preservation between the two optical fibres at all times. That is to say, no transient variation in the phase difference between the pair of the optical fibres can be introduced by the connector during a practical operation.

### 1.2.3 The Modalmetric sensor.

Modalmetric sensors involve changes in the distribution of the modal energy, an example of which is the twin core fibre. The evanescent field in the cladding can be used to make possible the transfer of optical energy from one core to the other under the action of strain or temperature [11].

### 1.2.4 The Polarimetric sensor.

Phase differences can be induced in the orthogonal polarisation eigenmodes of a single mode optical fibre. The state of the polarisation reflects the strain or temperature change to which the optical fibre is subjected. A measurement of the change in the state of polarisation of the radiation emanating from the optical fibre can be employed to determine changes in the two physical effects [12,13].



### 1.2.5 The Fabry-Perot sensor.

A number of fibre-sensors have been investigated that make use of the change in the resonant frequency of a Fabry-Perot optical cavity. The cavity is formed by two reflective surfaces that are parallel to each other and both are orthogonal to the axis of the fibre core. A change in the optical path length between the mirrors leads to a shift in the frequencies of the cavity modes. In some ways the Fabry-Perot fibre cavity represents the simplest interferometric sensor. The response function for a low finesse fibre Fabry-Perot sensor with respect to longitudinal strain is practically identical to that of the Michelson sensor and is therefore sinusoidal in nature. Consequently any signal recovery technique should address the five problems associated with this type of response function with strain, these being signal fading, interrupt immunity, sign ambiguity, nonlinearity and multi-valued response.

These sensors can be sub - divided into the intrinsic Fabry-Perot [14] and the extrinsic Fabry-Perot [15,16]. The extrinsic sensor differs from the intrinsic counterpart in that the cavity is formed in air instead of a glass waveguide. Extrinsic sensors are based upon a mechanical [15], fusion or a combination fabrication process to produce the Fabry-Perot cavity. These have been developed with varying degrees of success [ 15-24 ].

A Wang et al [21] used the extrinsic fibre Fabry-Perot sensor ( EFFPS ) in conjunction with micro - lens to improve fringe contrast ( fringe counting ). These sensors are used with a variety of multiplexing and modulation / demodulation schemes; Ph Nellen et al [24] devised a system with the intrinsic fibre Fabry - Perot sensor ( IFFPS ) obtaining measurements of static longitudinal strain with a resolution of a few micro - strain (  $16.9 \pm 0.7$  )  $\text{rad}(\mu\epsilon)^{-1}$  using a low coherence demodulation technique. Another example of an approach was demonstrated by K.A. Murphy et al [17] using EFFPS and a quadrature phase shift, quoting a strain sensitivity of (  $9.67$  )  $\text{rad}(\mu\epsilon)^{-1}$  which is a similar strain sensitivity stated by C.E. Lee et al [18]; (  $9.1$  )  $\text{rad}(\mu\epsilon)^{-1}$  using an IFFPS .

A particular problem with these sensors is the high sensitivity to temperature, pressure and acoustic waves. The problem arises when only one measurand is needed; which parameter is causing the change in the measurand? These sensors are also sensitive to shear strain because of the length of the sensor for reasonable strain resolution. The effect of shear as been studied by researchers such as Sirkis et al [25-27] and K.Kim et al [28].

There are more obvious possible problem that need to be addressed such as the question of mirror degradation with time and also fabrication difficulties ( discussed in chapter 2 ).

#### 1.2.6 The fibre Bragg grating ( F.B.G. ) sensor.

A major portion of the effort in this research programme has been devoted to this sensor. For this reason, discussion of the device at this stage is limited to a few general background comments. The Bragg-grating is an optical element developed for the telecommunications industry and is having a very significant impact on the evolution of these systems.

Inducing a periodic variation of the refractive index in the core of the step-index, single mode optical fibre, forms Bragg-gratings. The grating behaves as a wavelength sensitive reflector, the spectral bandwidth of which is in the form of a narrow spike, with a centre wavelength that depends linearly on the product of the mean core refractive index and the period of the variation of the refractive index.

The general characteristics of these sensors are discussed in a later section in the report. This type of sensor has generated a great deal of interest over the past few years. There are two distinctive advantages. Firstly, automation of fabrication and secondly, the detected signal is absolute, that is to say that the wavelength shift is directly proportional to strain if temperature affects are calibrated out. F.B.G. are also sensitive to changes in temperature ( thermal expansion and contraction ).

A variety of schemes have been proposed and demonstrated over several years. These include numerous multiplexing schemes [6,27] and various demodulation techniques [ 30-33] to achieve an effective sensor array. These include the edge - filter demodulation method where a sharp edge of a filter is used to convert wavelength changes to amplitude variations [34], interferometric based approaches [35,36], the use of frequency locked grating pairs [37] and the laser sensor concept where the grating sensor determines the lasing frequency [38].

A.B. Ribeiro et al [42] used time and spatial multiplexing techniques for F.B.G. sensors and an interferometric-wavelength shift detection method giving a reported static strain resolution of  $( 0.0041 ) \text{ rad}(\mu\epsilon)^{-1}$ . This requires a reference F.B.G. sensor and sensing F.B.G. sensor that is subjected to the measurand of interest. This sensing system suggests a

problem with robustness and general costs. A similar detection technique was reported by Y.J. Rao et al [39] obtaining a phase to strain response of  $(0.168) \text{ rad}(\mu\epsilon)^{-1}$ . The robustness of the scheme would be questionable away from the laboratory environment due to the use of two scanning Michelson interferometers. T. Coroy et al [34] used an optical spectrum analyser and filter detection system based upon a quantum well electroabsorption filter with a resultant static strain resolution of  $(\pm 8.04) \mu\epsilon$ . Other filter schemes have been developed for example A.D. Kersey et al [40]  $(\pm 3) \mu\epsilon$ . Other techniques that have been investigated are the sensor - receiving grating pair. In this arrangement, the receiving sensor tracks the sensor using a piezotranslator (P.Z.T.) to induce a mirror strain in the receiving grating. The multiplexing system employed is time division multiplexing (T.D.M.), obtaining a static resolution of  $(4.12) \mu\epsilon$  [41]. These are only a few of a large number of papers published using fibre Bragg gratings as strain sensors. Of these systems reviewed a majority of them require bulky optical equipment for signal recovery. Robustness and cost must be questioned away from the laboratory.

#### 1.2.7 The general parameters of fibre strain sensors.

The fibre optical sensors which seem to be showing the most promise at this moment in time would seem to be the extrinsic and intrinsic fibre Fabry-Perot sensor (IFFPS and EFFPS) and the fibre Bragg grating sensor (F.B.G.). Both of these sensors have a number of distinct advantages. Many of the schemes reviewed using the IFFPS and EFFPS measure only apparent strain; do not measure absolute strain, but relative strain. To obtain absolute strain measurement, coherent multiplexing has to be employed [24] but this decreases the response time of the system. A F.B.G. sensor wavelength shift gives a direct measurement of absolute strain but problems arise when trying to recover that information. The use of an optical spectrum analyser is required which is bulky and costly.

In general the resolution of the IFFPS and EFFPS is better than the F.B.G. sensors but again both these sensors are sensitive to temperature variations. The effects of temperature can be calibrated out by using a control sensor.

### **1.3 Multiplexing Techniques.**

The technique of multiplexing sensors is an important issue in many of the proposed application areas for fibre optic sensors. For example industrial process control, structural sensing and medical sensing ( prosthetics ), the use of multiplexing techniques can be beneficial in regard of the number of system aspects including reduced component costs, lower fibre count in telemetry cables , ease of the electrical / optical interface and overall system immunity to electromagnetic interference. The development of efficient multiplexing techniques can thus be expected to lead to general improvements in the competitiveness of the fibre sensors compared with conventional technologies in a broad range of applications. A large number of factors determine the suitability of a sensor-networking scheme for a particular application. These include the format of the data or information (i.e. analog or digital), the optical parameter onto which the sensor information is encoded, for example intensity, phase, wavelength and modulation ( subcarrier ) frequency and the application requirements for electrical passivity of the sensors and telemetry for reasons of safety.

There have been several multiplexing techniques ( networking scheme ) that have been applied to this problem. These multiplexing techniques include;

Frequency - Division Multiplexing.

Time - Division Multiplexing.

Coherence Multiplexing.

Low Coherence Multiplexing.

Wavelength - Division Multiplexing.

The multiplexing technique used for a given sensor is usually dependent upon the nature of the sensor itself. Some sensors have an intensity variation, which is a function of change of phase with regard to some reference signal due to some external parameter. Another example is variation in the wavelength of the signal; resulting from some external parameter changing. The number of sensors which can be multiplexed using a specific multiplexing technique is dependent on several factors and a given architecture array. These factors include power budget considerations, sampling criteria, bandwidth requirements and crosstalk [7].

### 1.3.1 Frequency - Division Multiplexing.

Frequency - division multiplexing can be achieved by frequency modulating the light source which illuminates the sensor. Ramping or sinusoidal perturbation of the injection current to the laser diode will bring this about. The change of injection current causes a frequency shift of the laser at the modulation frequency, which can be used to read effective changes in an interferometer. There is a simultaneous intensity modulation, which needs to be removed. Consider the case of a monomode fibre optic interferometer as a sensor, a path length imbalance in an interferometer will then produce an amplitude modulation of the photodetector output. The optical path imbalance and the frequency determine the phase of the signal, by the product of the swept number of fringes and the frequency of the sinusoidal perturbation of the injection current to the laser diode. By arranging each sensor to be at different multiples of the minimum path - length imbalance swept over  $2\pi$  radians by the frequency - modulation source, the detector output consists of distinct frequencies corresponding to each sensor. This output is then demultiplexed by bandpass filtering and phase detection, leading to the path imbalance of each sensor. Generally speaking this technique is used in conjunction with interferometric sensors. An example is shown in Figure 3.

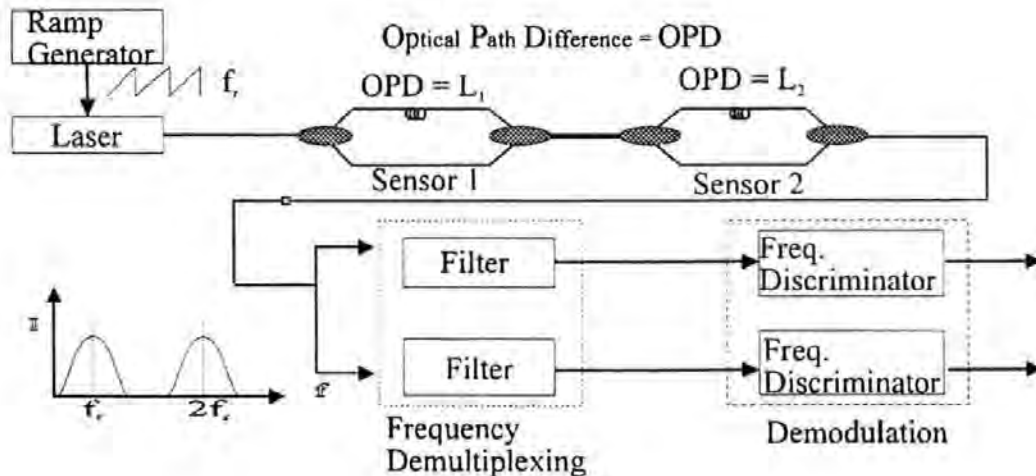


Figure (3). A frequency - division multiplexing concept ( pseudo heterodyne technique ).

The laser is modulated using a current ramp waveform of frequency  $f_r$ , which in turn produces an optical frequency deviation. This technique can be used to track the phase of the beat signals. This method can also be used in conjunction with a pseudo - or synthetic - heterodyne technique to monitor the phase of the beat signal. This technique is also used in the case of a Bragg grating sensor with other in - line optical elements as well as interferometric sensors [43].

### 1.3.2 Time - Division Multiplexing.

The basic principle of Time - Division Multiplexing ( T.D.M. ) involves a series of sensors in an optical line, which are illuminated by a pulsed optical source. Grating pulses are produced with time delays from the different sensors such that the pulses returned from each sensor do not overlap in time at the detector. The output signals corresponding to a specific sensor can be recovered by appropriately gating the detector signal; so matching in time the arrival of a signal from a given sensor. Different fibre optic topologies have been proposed [30,44] and demonstrated using the T.D.M. One of the main drawbacks is the relative complexity of the fibre optical networks in field applications. There is also question marks about the robustness of a system using time - division multiplexing. Figure 4 shows an example of time - division multiplexing, this method has been applied to interferometric, intensity and Bragg grating sensors.

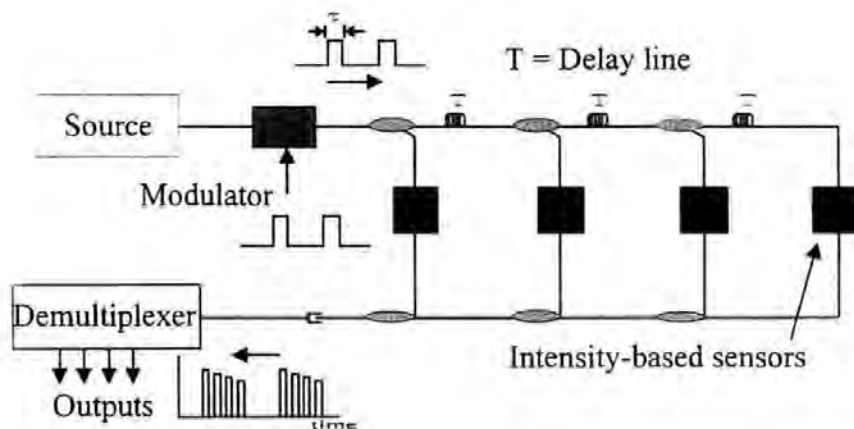


Figure (4) . Basic time - division multiplexing technique for intensity - based optical fibre sensor.

Here the sensors are spaced at different distances from the source and detector such that a single pulse of appropriate duration input to the network produces in the output a series of distinct pulses. These pulses represent time samples of the sensors outputs interleaved in time sequence, as shown. The required duration of the input pulse  $t$  is determined by the effective optical delay of the fibre connecting the sensor elements and repetitive pulsing of the system allows each sensor to be addressed by a simple time selective gating of the detector output. In this case the intensity of the returned signal forms a measure of the measurand.

### 1.3.3. An intensity quasi-distributed Sensor.

In the simplest quasi - distributed sensor concept, modified fibre sections are spliced into a long fibre at certain intervals to provide localised variations in the loss, backscattering intensity, polarisation, fluorescence etc. An example of this is the discrete extrinsic - type nonfibre sensor element in which transmittance or reflectance varies ( see Figure 5 ). An example is Ruby glass elements in which the attenuation increases with temperature for light of wavelength  $\sim 600\text{nm}$  to  $620\text{nm}$  ( absorption edge shift  $\sim 0.12\text{nm} / ^\circ\text{C}$  ).

The major limitation of this type of loss - dependent backscatter - based system is that the attenuation is accumulative. The light level at the most distant sensor thus depends on the measurand at each sensor along the fibre. This places demanding requirements on the dynamic range of the optical time domain reflectometer ( OTDR ) detection system and limits the number of sensors that can be used in a practical system.

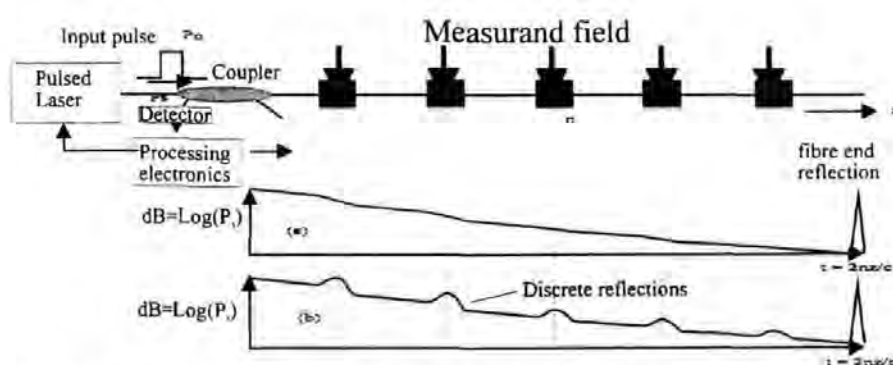


Figure (5) . Principles of quasi - distributed sensing based on (a) absorption and (b) reflective element

#### 1.3.4. Coherence Multiplexing.

A schematic diagram of a coherent-multiplexing sensor scheme is shown in Figure 6. Although there was initially significant interest in coherence multiplexing [45], problems associated with crosstalk, excess phase noise and poor power budget have limited the practical use of this approach especially with interferometric sensors. This multiplexing technique has also been demonstrated with polarimetric sensor [46].

One arrangement is to use two bulk optical “ sensor ” interferometers of optical path difference ( O.P.D. ) that is much larger than that of the coherence length of the source. A single receiver interferometer at the output could be used to selectively reconstruct the interference associated with the sensors by tuning its optical path difference to match that of each sensor. This is achieved by the use of a PZT to change the OPD of the receiver interferometer to match that OPD of the sensor to obtain the interference pattern. This can be used to track a sensor’s OPD, thus monitoring the measurand via the tracking of the receiver OPD by the applied voltage to the PZT.

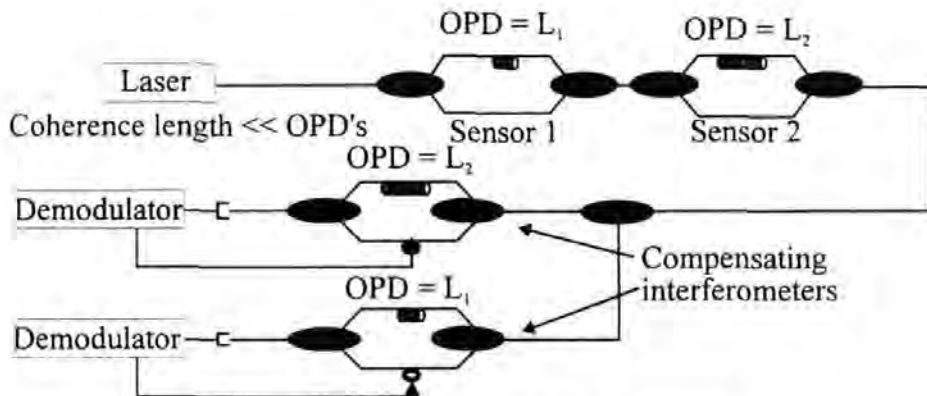


Figure (6) . Coherence multiplexed interferometric array.

#### 1.3.5 Low Coherence multiplexing.

This technique is used for the measurement of absolute path difference. In a typical fibre optic sensing system, two interferometers operate in tandem, where one is the remote sensor and the second interferometer is the receiving sensor, which is isolated from the environment.



The system is illuminated with light from a source with a very short coherence length; hence no optical interference will be seen at the sensor. This optical signal is injected into the receiving ( reference ) interferometer sensor, optical interference is only observed when the difference in the optical path difference of sensor and reference sensor is less than the coherence length of the illuminating source .

For a typical low coherence source the intensity / amplitude profile gives an auto-correlation function with a Gaussian or Lorentzian profile. This in turn gives an envelope function for the visibility of interference signal, which decreases very rapidly. The rapid reduction in fringe visibility is used to locate a reference point / feature for the two interferometers working together. This is used to determine the optical path difference of the sensor by scanning the optical path difference of reference interferometer to obtain the reference point / feature [24].

#### 1.3.6. Wavelength - Division multiplexing.

Sensor information is allocated to a particular optical wavelength. This multiplexing technique is applicable to intensity, interferometric and in particular Bragg grating sensors [47]. Theoretically this is the most efficient technique possible, as all the light from a source could in principle be directed to a particular sensor element and then onto a corresponding photodetector with minimal excess loss. The reason for the lack of practical demonstrations to date of this technique is due to the limited availability of wavelength-selective couplers ( splitters and recombiners ) which are required to implement this technique, plus the availability of sources. The source has to have a bandwidth of the order of approximately 100nm. This limits the number of sensors in the array because each sensor needs a finite bandwidth to operate. At this moment in time there is extensive interest in this multiplexing technique because of the intrinsic wavelength encoding of Bragg grating sensors or a hybrid system using another multiplexing technique in conjunction with wavelength - division technique [44] see Figure 7 .

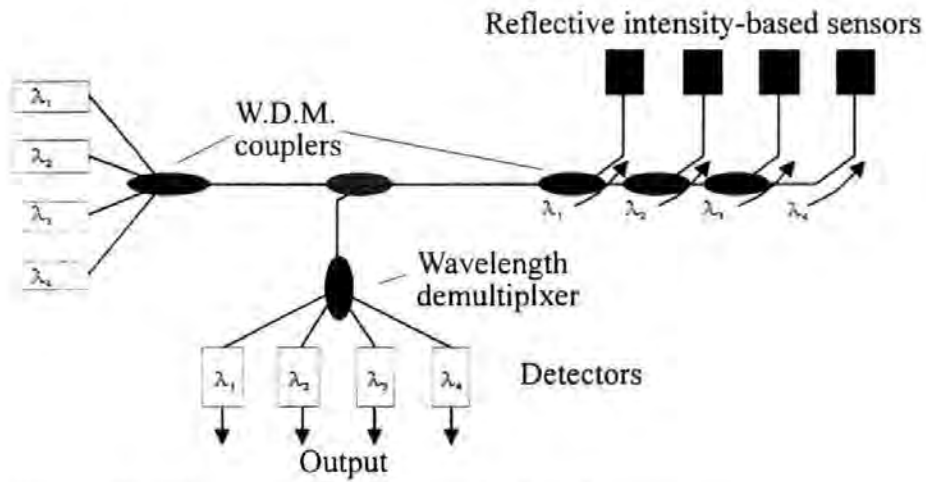


Figure (7) . Wavelength division multiplexed sensor array.

### 1.3.7. Demodulation Techniques for Multiplexed Sensors.

The method of remote demodulation of multiplexed sensors is dependent on the type of sensor that is being multiplexed. The two types of sensor that are receiving most attention are interferometric and Bragg grating based sensors.

#### 1.3.7.1 Demodulation techniques suitable for multiplexed interferometric sensors.

##### 1.3.7.1a Phase-generated carriers ( PGC ).

Phase-generated carriers ( PGC ) use homodyne or synthetic heterodyne techniques that rely on frequency modulation of the laser and a slightly unbalanced in the sensing interferometer. The phase difference between the optical fields is derived from the signal and the reference arms of the interferometer. This is a function of the input optical frequency. The laser frequency modulation is converted to phase modulation by the interferometer. The output signal from the interferometer is detected with a photo-detector and is used to synchronously detect the amplitudes of the components at the fundamental laser modulation frequency and the second harmonic of the frequency. These two outputs represent the in - phase and quadrature components of the interferometer phase shift [48 , 111 ].

#### 1.3.7.1b Path matched differential interferometry ( PMDI ).

This method uses matched unbalanced sensor and compensator ( receiver ) interferometers. This approach is not a demodulation technique as such, but it facilitates demodulation by splitting the interferometer into two sections. One is referred to as the sensor interferometer and the other a compensating interferometer. Demodulation of the compensating interferometer output can be accomplished using several techniques. When PMDI is used in a single sensor application, demodulation by active phase-tracking homodyne detection is possible by feedback to a phase shifter in one of the compensator arms. Generally, in a multiplexed system based on PMDI, active phase tracking may not be feasible due to the diversity of phase signals detected. Other approaches are adopted such as PGC to provide the in - phase and quadrature components of the interferometric signals [48 , 111 ].

#### 1.3.7.1c Differential delay heterodyning.

This approach uses an unbalanced sensor interferometer and a pulsed frequency modulated laser source. Differential delay heterodyning is a phase-shift detection technique for use with interferometric sensors which produce a phase modulated heterodyne carrier output without recourse to the use of a frequency - shifting element in either arm of the interferometer. Two pulses are sequentially fed into the interferometer. The temporal separation of these pulses is equal to the differential delay between the fibre arms of the interferometer. The components of the first optical pulse, which passes through the long arm of the interferometer will be coincident at the detector with the arrival of the component of the second pulse, which passes through the short arm .If the optical frequencies of the two pulses are offset, mixing between the two coincident pulses produces a burst of heterodyne beat signals at the detector. Repetitive pulsing of the system and time selective gating of the detector output produces a gated carrier and a continuous wave carrier can be generated by filtering. This signal can then be fed to a FM discriminator or phase-locked loop and integrated for phase demodulation [ 111 ].

### 1.3.7.2 Demodulation techniques suitable for multiplexed Bragg grating based sensors.

Intra - core fibre Bragg grating sensors have attracted considerable interest over the past few years because of their intrinsic nature and wavelength - encoded operation. Generally fibre Bragg grating sensors are illuminated by a broadband light source, such as an edge emitting LED, superluminescent diode or superfluorescent fibre source ( a section of Erbium doped fibre, which is optical, pumped by a laser ). In the application of monitoring longitudinal strain or / and temperature there is a shift in the wavelength which is reflected by the Bragg grating sensor. This wavelength shift is proportional to the strain / temperature change induced in the sensor. The gratings are assigned a wavelength range for operation, which do not overlap. The Bragg wavelengths of the individual gratings can thus be determined by illuminating the system with a broadband source and using an optical spectrum analyser to analyse the returning signal. There are two problems with this scheme. There is a practical limit to the number of sensors for a given broadband source, and the conventional optical spectrum analyser is a costly piece of equipment. This reduces the cost effectiveness of this scheme and there are questions over the robustness of systems ( breakage during handling of the sensing array ).

Several options for measuring the wavelength of the optical signal reflected from the Bragg grating sensor exist. These include the use of a simple miniaturised spectrometer, passive optical filtering, tracking using tuneable filter and interferometric detection, where the fractional power transmitted are linear functions of the wavelength over the wavelength range of interest. Other techniques are matched receiving - sensing grating pairs, where the receiving grating tracks the Bragg wavelength shift of the sensing grating. A similar scheme uses a Mach - Zehnder interferometer and an isolated reference grating. Another option is a fibre laser cavity the lasing wavelength of which depends on the Bragg gratings.

The optical characteristics of these filtering options are shown in Figure 8.

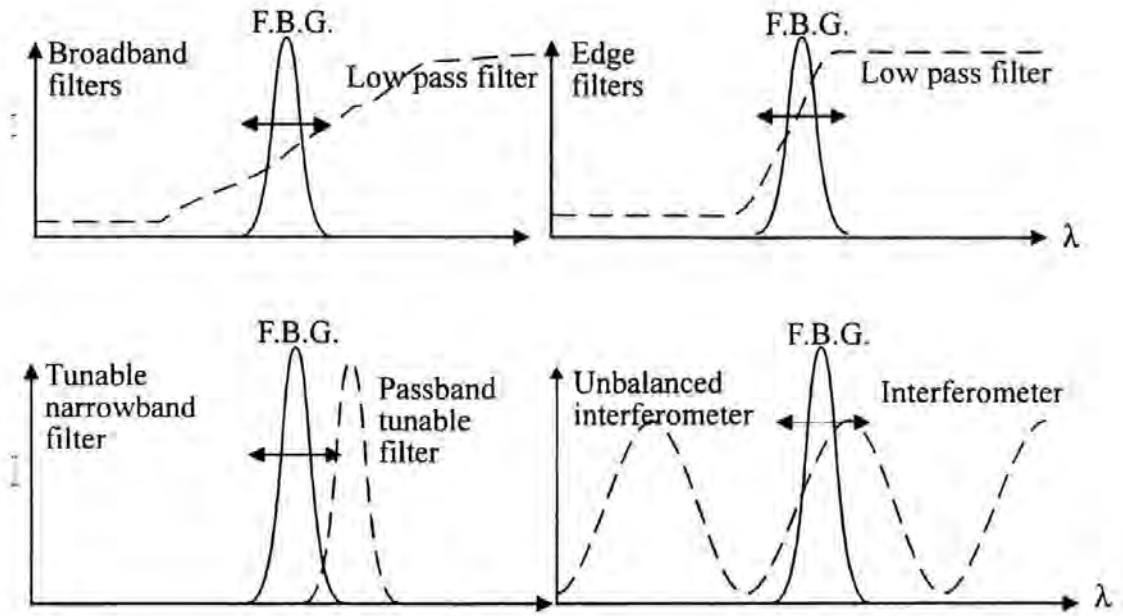


Figure (8) . Showing various filters that can be used in conjunction with a fibre Bragg grating to obtain information about strain.

#### 1.3.7.3 Broadband and edge filters.

Wavelength shift is assessed by comparing the transmittance through the filter to a direct reference path. The sensitivity is limited with this approach due to problems of using bulk - optical components and their inherent alignment stability. The sensitivity can be improved by using a wavelength demultiplexing ( W.D.M. ) coupler, a fibre device that has a wavelength-dependent transfer function. This provides a monotonic change in the coupling ratio between two output fibres for an input optical signal over the entire optical spectrum of the broadband source. A suitable transfer function for the wavelength discrimination over this bandwidth is required ( i.e. linear variation of intensity with variation of wavelength).

A resolution of  $\pm 5\mu\epsilon$  has been demonstrated using this technique [34] (an edge filter can however, limit the dynamic range of the system ).

#### 1.3.7.4 The interferometric detection technique.

The interferometric detection technique is a filtering method with a transfer function of the form  $\{1 + \cos[\Psi(\lambda) + \phi(t)]\}$ . The phase term is dependent upon the input wavelength. In this case the interferometer output can be modulated via control of the imbalance between the interferometer arms to allow the phase reading technique to be implemented to determine the fibre Bragg grating wavelength.

Light from a broadband source is coupled by means of a feeder fibre to the F.B.G. sensor. The wavelength component reflected back along the fibre towards the source is tapped off and fed to an unbalanced Mach-Zehnder interferometer. The reflected light becomes the source light into the interferometer and wavelength shifts induced in the F.B.G. sensor resemble a wavelength ( optical frequency ) modulated source. The unbalanced interferometer behaves as a spectral filter with a raised cosine transfer function. The wavelength dependence on the interferometer output can be expressed as:

$$I(\lambda) = A\{1 + K\cos[\Psi(\lambda) + \phi(t)]\}$$

where  $\Psi(\lambda) = \psi(\lambda) + \Delta\psi(\lambda)$

$$\psi(\lambda) = (2\pi nd) / \lambda$$

and  $\Delta\psi(\lambda) = [(2\pi nd) / \lambda^2] \cdot \Delta\lambda = [(2\pi nd) / \lambda] \cdot \zeta \cdot \Delta\lambda$

where  $\zeta = [1 / \lambda] \cdot [\delta\lambda / \delta\epsilon]$

$A$  is proportional to the input intensity and system losses.

$K$  is the interference visibility.

$d$  is the length imbalance between fibre arms.

$n$  is the effective refractive index fibre core.

$\lambda$  is the wavelength of the returned light from the sensor.

$\zeta$  is the normalised strain-to-wavelength shift responsivity.

$\phi(t)$  represents an environmentally induced variation in  $d$  and  $n$ . This is usually a thermally induced phase drift. For a well shielded fibre interferometer  $\phi(t)$  is a slowly varying random parameter.

The unbalanced interferometer acts as a discriminator to detect the wavelength shifts in the effective source which is being generated by the strained sensor. A.D. Kersey

et al used this technique and proposed a using time-division multiplexing technique for an array of sensors [36].

#### 1.3.7.5 Detection techniques using a tuneable narrowband filter.

This technique can be used with any tuneable narrowband filter.

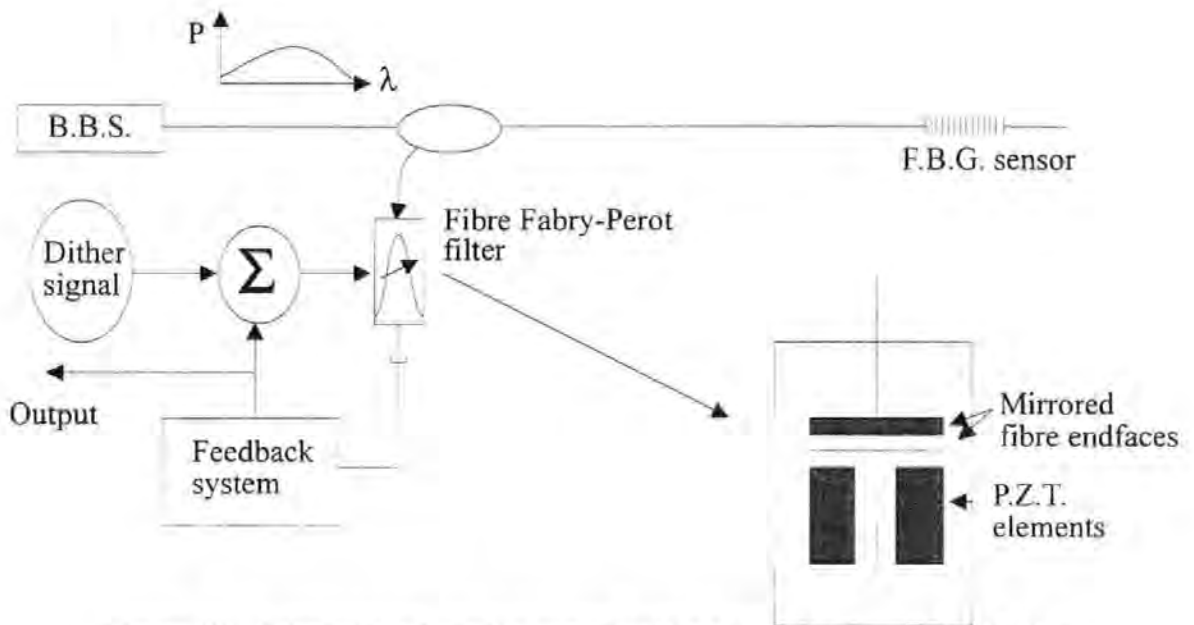


Figure (9) . Schematic of sensing system using a tuneable narrowband filter.

Figure 9 shows a system for single sensor operation. The F.F.P. filter passband is locked to the F.B.G. sensor return signal, using a simple feedback loop arrangement. This is accomplished by dithering the F.F.P. resonance wavelength by a small amount (  $\sim 0.01\text{nm}$  ) and using a loop to lock on to the Bragg wavelength of the sensor-returned signal. This system can also be used in a F.F.P. scanning mode for a series of sensors. This gives a limited resolution capability in terms of the minimum resolvable Bragg wavelength shifts which can be detected as the observed peaks are line - broadened by the convolution of the F.F.P. passband and the F.B.G. signals [49].

If the F.F.P. dither signal is maintained and the detector output is passed into an electrical mixer and low-pass filter the output component signal at the dither frequency can be detected.

A derivative response to the spectral components can be obtained using the described arrangement. This produces a zero crossing at each of the F.B.G. centre wavelengths and allows improved resolution in determining the Bragg wavelength shift, see Figure 10.

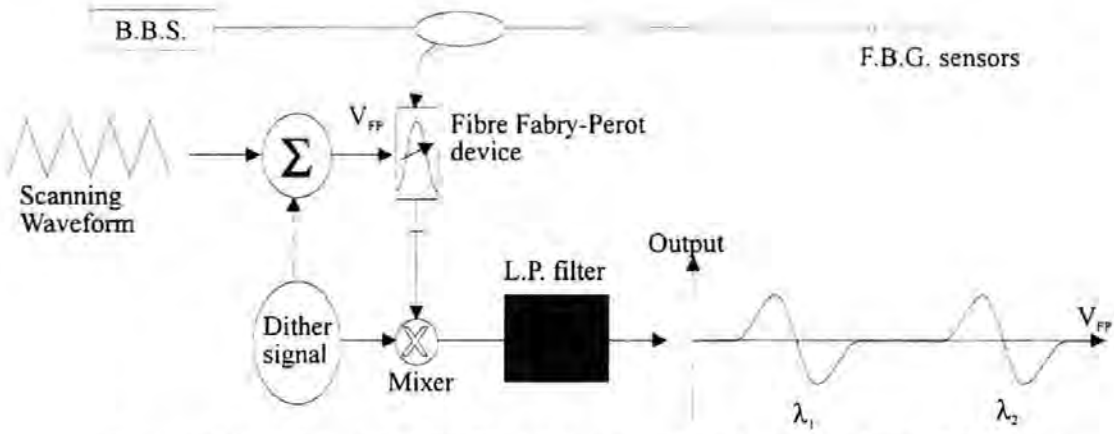


Figure (10) . Schematic of a fibre Bragg sensing element using a F.F.P. as a filter to extract strain information.

The above descriptions of the demodulation techniques are basic concepts used in conjunction with Fibre Bragg Gratings. These techniques, or variations of them, have been reported in the literature, see A.D. Kersey et al [36]. A sensing and reference F.B.G. sensor are placed in the output arms of an unbalanced fibre Mach - Zehnder interferometer using light from a broadband source. Each sensor reflects a narrow - band portion of the interferometer output signal which is monitored by tap - off couplers. The reference sensor then is used to eliminate temperature variations experienced by both sensors. A resolution of  $\sim 6 \times 10^{-3} \mu\epsilon/\text{Hz}$  at 1Hz was obtained by A.D. Kersey et al [36].



## 1.4 Basic principles of a fibre optical strain sensor.

The fibre optical strain sensor was first proposed and demonstrated by Butter and Hocker [50,51].

When light from a laser, having sufficient coherence length, is launched into two single-mode fibres of approximately the same length, the light coming from the other two ends can be made to interfere and produce a fringe pattern, when the optical path length of one fibre is changed with respect to the optical path length of the other fibre, the fringes will shift. The amount of fringe shift is proportional to the relative change in the optical path length. By observing the motion of the fringes, the changes in the optical path length can be determined. Introducing different strains in the two fibres causes a difference in the optical path lengths of the fibres and the motion of the fringes. This effect is utilised to produce a sensitive fibre optic strain sensor.

Calculation of the fringe shift due to longitudinal strain of a single fibre of length  $L$  can be obtained as follows. Assuming

$\beta$  is the propagation constant of the fibre.

$\kappa_0$  is the free space propagation constant.

$n$  is the fibre's core refractive index.

$D$  is the core diameter of the fibre.

$\mu$  is Poisson's ratio.

The phase of the light through the fibre is;

$$\delta = \beta L$$

If the fibre is strained by  $\epsilon$ , then the change in the phase is given by;

$$\Delta\delta = \beta \cdot \Delta L + \Delta\beta \cdot L$$

Considering the first term in the above expression represents the physical change of the length of the fibre produced by the longitudinal strain  $\epsilon$ .

so

$$\beta \Delta L = \beta \epsilon L$$

Considering the second term, where the changes in the phase is due to  $\Delta\beta$ , can come about by two effects. These mechanisms are the strain - optic effect whereby the strain changes the refractive index of the fibre and the other is waveguide mode dispersion, an effect due to changes in the fibre diameter  $\Delta D$  ( $\Delta D = \mu \epsilon D$ ), produced by the longitudinal strain .

So the change in the propagation constant  $\Delta\beta$ , which contributes to the change in optical phase is dependent upon changes to the refractive index which is related to strain this being the strain-optic effect; photoelastic effect and is symbolised by  $\Delta n$ . Also the change in the diameter of the optical fibre affects the normalised propagation constant which is a function of the diameter of the fibre, the diameter of the optical fibre is also a function strain. This is given by the expression below:

$$L\Delta\beta = L \frac{d\beta}{dn} \Delta n + L \frac{d\beta}{dD} \Delta D$$

Consider the parts of the above equation;  $\frac{d\beta}{dn}$  and  $\frac{d\beta}{dD} \cdot \Delta D$ .

The propagation constant  $\beta = n_{\text{eff}}\kappa_0$  where  $n_{\text{eff}}$  is the effective index of refraction and lies between the core and the cladding values. This difference is of the order of a few percent so the propagation constant can be approximated to  $\beta \approx n\kappa_0$

Thus 
$$\frac{d\beta}{dn} = \kappa_0 = \frac{\beta}{n}$$

It as been shown by Sirkis, Butter and Hocker [25,50] that

$$\frac{d\beta}{dD} = \frac{V^3}{2\beta D^3} \cdot \frac{db}{dV}$$

Where  $V$  and  $b$  are normalised parameters of the fibre and  $\frac{db}{dV}$  is the slope of the  $b$ - $V$  dispersion curve at the point which describes the waveguide mode.

#### 1.4.1 The strain - optic effect; $\Delta n$ .

The strain - optic effect / photoelastic effect is an well-understood effect in which a material couples mechanical strain to the optical index of refraction. This is described by a change in the optical impermeability tensor, which is a function of the strain-optic tensor and the strain tensor of the material. The original indices of the optical impermeability tensor may be simplified by considering the symmetries of the tensor, which becomes a change in the optical indicatrix [103]:

$$\Delta \left[ \frac{1}{n^2} \right]_i = \sum_{j=1}^6 P_{i,j} s_j$$

Where  $s_j$  is the strain vector and  $p_{i,j}$  is the strain - optic tensor.

It has been shown by Sirkis et al [25] and Kim et al [28] that for longitudinal strain in the  $x$  direction, that as no shear strain (  $s_4, s_5, s_6 = 0$  ) along the fibre axis for a homogeneous isotropic medium  $p_{i,j}$  has only two numerical values, which represents the strain in the material designated by  $p_{11}$  and  $p_{12}$  . The change in optical indicatrix in the  $y$  and  $z$  direction (  $i = 2, 3$  ) elements is just

$$\Delta \left[ \frac{1}{n^2} \right]_{2,3} = \varepsilon(1 - \mu)P_{12} - \mu\varepsilon P_{11}$$

So the change in the refractive index in the  $x$  direction due to longitudinal strain is

$$\Delta n = \frac{-1}{2} n^3 \Delta \left[ \frac{1}{n^2} \right]_{2,3} = \frac{-1}{2} n^3 \left[ \varepsilon(1 - \mu)P_{12} - \mu\varepsilon P_{11} \right]$$

So the phase change per unit strain unit fibre length is:

$$\frac{\Delta \delta}{\varepsilon L} = \beta - \beta n^2 \left[ (1 - \mu)P_{12} - \mu P_{11} \right] + \frac{V^3}{2\beta D^2} \cdot \frac{db}{dV}$$

This expression can be simplified because the waveguide dispersion is negligible compared to the first term in the above expression, which becomes

$$\frac{\Delta \delta}{\varepsilon L} = \beta - \beta n^2 \left[ (1 - \mu)p_{12} - \mu p_{11} \right]$$

Butter and Hocker confirmed this expression and verified it against experimental results.

This work had been continued by Sirkis, Haslash and Kim [25-28,52] establishing a fundamental strain-phase relationship. They showed that the axial component of the strain in a surface-mounted optical fibre significantly affects the refractive index. They also derived the same expression between phase and strain in a fibre as did Butter and Hocker but including a birefringence effect; this expression being

$$\delta = \beta_0 \int_0^L (1 - c \varepsilon_n) (1 - \varepsilon_n) ds$$

This becomes

$$\delta = \beta_0 L + \beta_0 (1 - c) \int_0^L \varepsilon_n ds$$

where  $\varepsilon_n$  is the axial strain.

$c$  is a constant that depends upon the Pockels coefficients;  $P_{ij}$  and on the fibre Poisson ratio.

$$c = \frac{n_0^2}{2} \left[ P_{12} - \mu (P_{11} + P_{22}) \right]$$

In this expression there are two factors contributing to the phase change. Difference in length of the fibre and change in the optical path length,  $\beta_0 (L + \partial)$  where  $\partial$  is the net elongation of the strained fibre and a birefringence effect  $\beta_0 c \int_0^L \varepsilon_n ds$ .

The original Butter and Hocker relationship can be extracted from the above integral giving

$$\Delta \delta = \beta_0 (1 - c) \hat{\varepsilon}_n$$

where  $\hat{\varepsilon}_n$  is the average strain in the fibre.

Optical fibre sensors are sensitive to temperature variations. Hocker [51] showed that a change in temperature  $\Delta T$  of the fibre changes the optical phase  $\Delta \delta$  of the light going through it. The change in  $\delta$  results from two effects. These are changes in the physical dimensions of the fibre due to thermal expansion or contraction and the temperature - induced change in the index of refraction.

As 
$$\delta = \frac{2\pi n L}{\lambda}$$

then 
$$\frac{\Delta \delta}{L \Delta T} = \frac{2\pi}{\lambda} \left( \frac{n}{L} \frac{dL}{dT} + \frac{dn}{dT} \right)$$

## **2      The Fibre Fabry Perot sensor ( F.F.P. sensor ).**

### **2.1 The fibre Fabry-Perot sensor.**

A Fabry - Perot optic sensor involves a single monomode optical fibre with a sensing region defined by a cavity comprising two mirrored surfaces. These mirrors are parallel to each other and perpendicular to the axis of the optical fibre. A change in the optical path length between the two mirrors leads to a shift in the frequencies of the cavity modes. This shift in the cavity modes introduces a phase change in the light emitted from the cavity, thus an interference pattern ( fringes ) is generated from the change in the optical path length. In some ways the Fabry - Perot cavity represents the simplest interferometric sensor. The cavity can be formed by using mechanical splices [15] or by fusion spliced ( first mirror ) and a cleaved endface as the second mirror ( Fresnel reflection ) [14]. The F.F.P. sensor can be sub - divided into two categories; intrinsic F.F.P. sensor and extrinsic F.F.P. sensor [14-16]. The intrinsic Fabry - Perot sensor creates an all - fibre cavity where interference occurs. The extrinsic F.F.P. sensor differs from its counterpart in that the cavity is formed in air instead of a glass waveguide, see Figures 11 and 12.

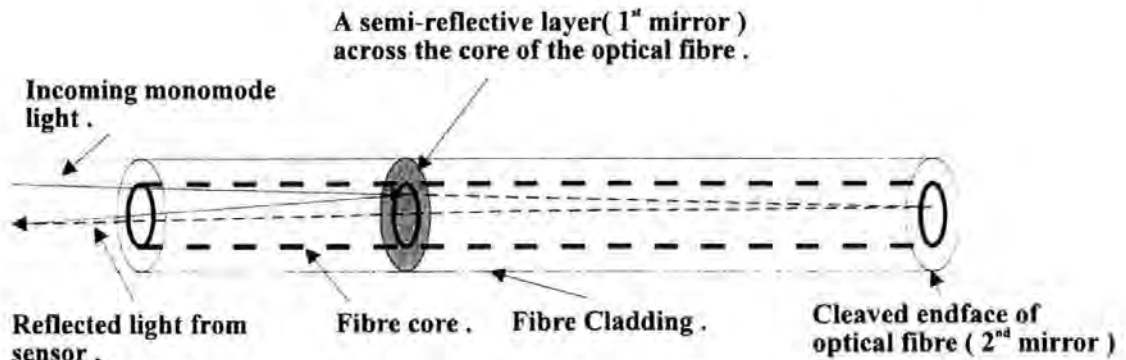


Figure (11). A schematic of an intrinsic F.F.P. sensor.

The semi - reflective layer across the optical fibre can be a thin metal layer or dielectric material such as Titanium dioxide (  $\text{TiO}_2$  ); Titanium dioxide was used in the fabrication of the Fibre Fabry Perot sensors .

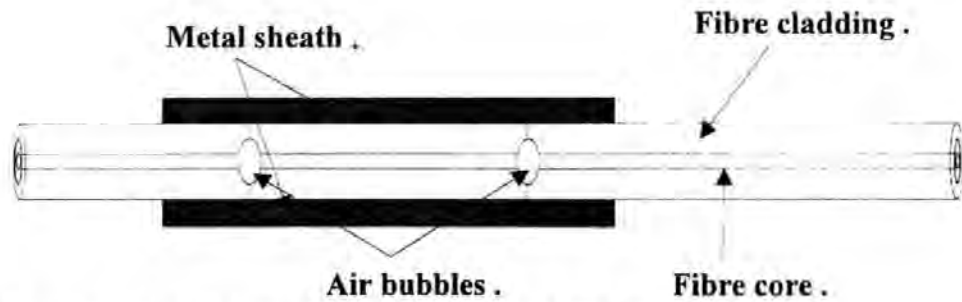


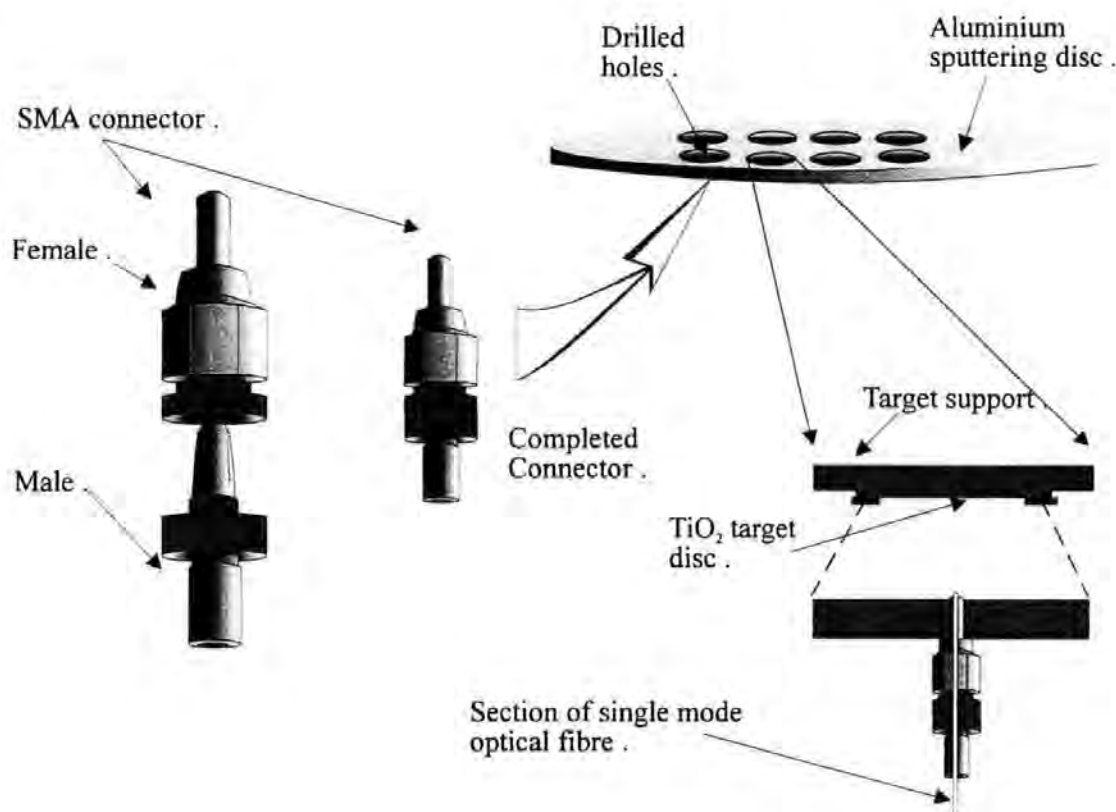
Figure (12) . A schematic of an extrinsic F.F.P. sensor.

An example of an extrinsic F.F.P. sensor is shown in Figure 12. As the extrinsic F.F.P. was not investigated the term intrinsic is dropped from use.

## 2.2 Fabrication of the Fibre Fabry Perot sensor ( FFPS ).

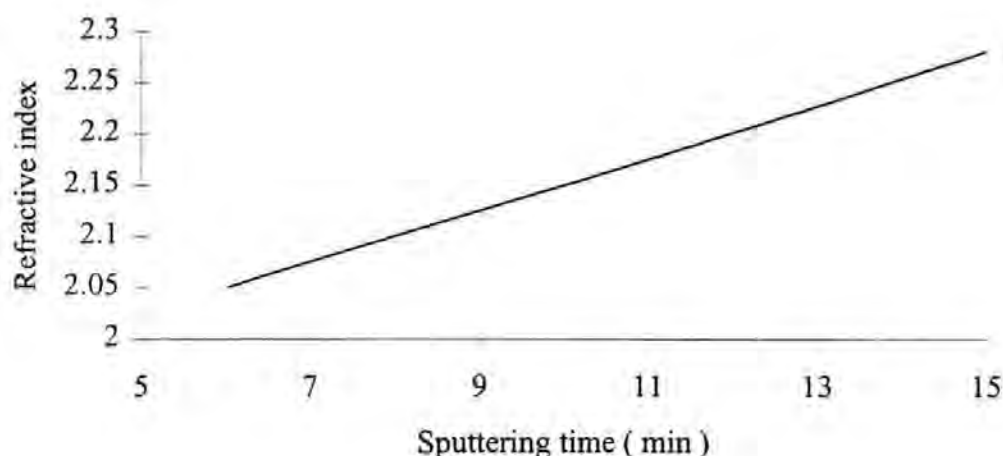
The partially reflecting layer of Titanium Dioxide ( mirror ) was formed by depositing the  $\text{TiO}_2$  on a cleaned and cleaved endface of a section of single mode fibre . The depositing of the  $\text{TiO}_2$  is achieved by using a standard sputtering machine, where the target is  $\text{TiO}_2$  .The sputtering machine used was a Material Research Corporation machine maximum power 1200 Watts, typical vacuum pressure of  $2 \times 10^{-6}$  Torr, base pressure and process gas used is Argon, in this application. Titanium Dioxide has similar physical properties to those of glass used in fibre optical cable and has a melting point of  $1640^\circ\text{C}$ . A series of experiments were conducted to see if a vacuum coater could be used to deposit the  $\text{TiO}_2$  layer. This technique was not successful in producing a layer of  $\text{TiO}_2$  on test slides, probably due to the crucibles used to vaporise the  $\text{TiO}_2$  material.

To facilitate the coating of the fibre endfaces, the fibres were held by means of sub-miniature assembly ( SMA ) connectors. The SMA connectors were fitted into holes drilled in an Aluminium disc with a length of the fibre protruding out of the connector end. Prior to mounting the fibre, the buffer coating removal and cleaning were carried out before cleaving. This was accomplished using a Fujikura CT-07 high precision fibre-cleaving tool.

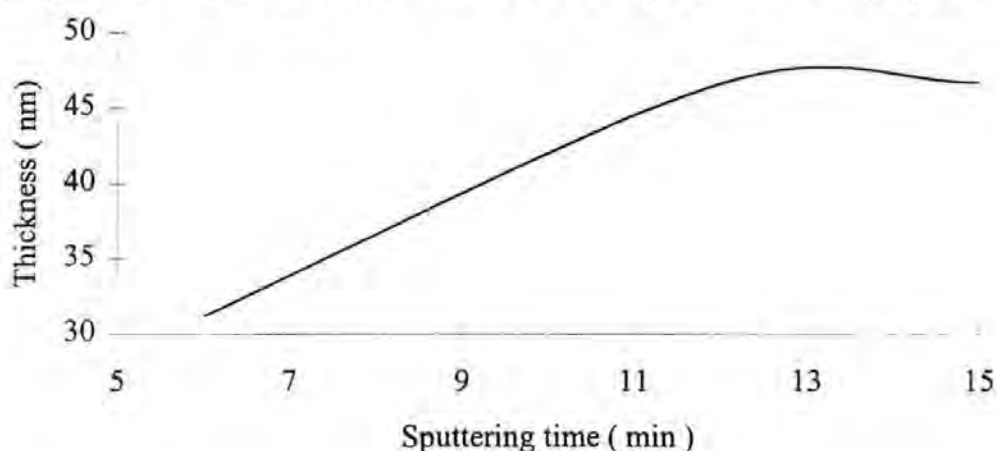


Figure(13) . Apparatus used in the sputtering machine.

At an early stage of the research it became apparent that a major difficulty existed when incorporating the sensor into an optical fibre. This difficulty arose from the process of fusion splicing. Although the sensor performed satisfactorily when mechanically spliced or butt coupled, a large number of the sensors failed after fusion - splicing. The cause of the failure of the sensors was identified as being the loss of the  $\text{TiO}_2$  layer ( mirror ). To address this problem a number of samples were prepared; each having a different thickness of the  $\text{TiO}_2$  layer achieved by varying the duration of sputtering. All the conditions for sputtering were exactly the same, base pressure  $2 \times 10^{-6}$  Torr, power 400Watts and the process gas pressure  $4 \mu\text{m}$  of Argon but for time duration which varied from 3 minutes to 27 minutes. The deposition rate for the Titanium Dioxide is 5 nm per minute. Calibration of the coating process was achieved by using a glass slide mounted on the Aluminium disc and using an ellipsometer to measure the thickness and the index of refraction of the Titanium Dioxide layer ( see graphs 1 and 2 ).



**Graph 1 .** Refractive index of Titanium Dioxide layer as a function of sputtering time.



**Graph 2 .** Thickness of Titanium Dioxide layer as a function of sputtering time.

The refractive index ( effective index ) increases with thickness of the layer, this is due to the so-called “ Island effect ”. At the beginning of the deposition of the thin layer, it does not build up a homogeneous layer but lumpy; islands of material (  $\text{TiO}_2$  ). So this gives an effective refractive index.

Fusion splicing the sensor onto the feed fibre was carried out using a Fujikura Arc Fusion splicer, type FSM - 200. Two parameters were varied on the control panel of the splicer, these being i) power of the fusion arc ii) the duration of the arc. Over the range permissible by the splicer for the parameters, no noticeable improvement was observed; the fusion arc still vaporised the  $\text{TiO}_2$  layer, thus destroying the layer so the spliced joint is not semi - reflective. The success rate with the available equipment is low. Two methods were used to detect whether the coating was successful in producing a semi - reflective splice. One using the optical arrangement shown in Figure 14, the other is using the test rig for strain and the associated electronics to detect the generation of a cardoid (see section (2.5)).



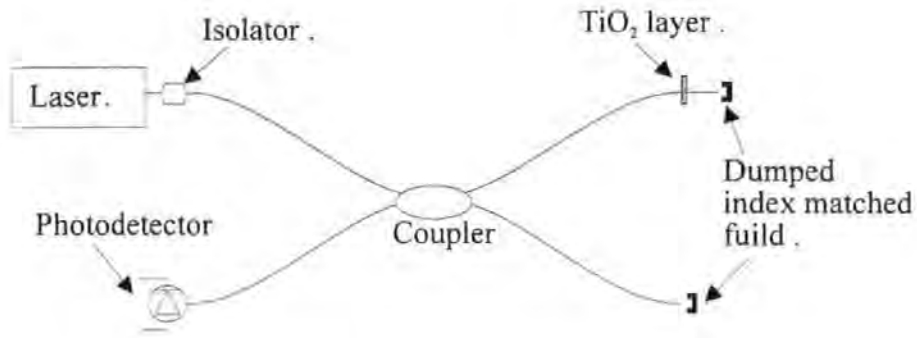


Figure (14) . Detection of the semi-reflective Titanium Dioxide layer / fusion splice.

### 2.3 Fibre Fabry Perot Optical Strain Sensor.

The intrinsic Fabry - Perot sensor creates an all - fibre cavity where multiple reflection interference occurs. The intensity function of a Fabry Perot sensor is an Airy formula [53]. However Fabry - Perot cavity can be considered Fizeau in form if the reflectivities of the cavity forming surfaces are less than approximately 5%. In this case the intensity function is identical to that of a Michelson interferometer if a negative sign, resulting from the  $\pi$  phase shift induced by Frensel reflection precedes the cosine, see Figure 15.

The reflected intensity is given by:

$$I_{Re} = I_O \left( 1 - \frac{c}{1 + F \sin^2 \frac{\delta}{2}} \right)$$

Where  $I_o$  is irradiance being subjected to the Fabry-Perot cavity,  $\frac{1}{1 + F \sin^2 \frac{\delta}{2}}$  is an Airy

function.  $F$  depends on the reflectivity of the mirrors; this being the semi - reflective fusion splice of approximately  $\sim 4\%$  reflectivity and second mirror being the endface of the optical fibre again  $\sim 4\%$ .  $F$  is commonly known as the coefficient of finesse, which is approximately 1 for these types of sensors with a low reflectivity.

$$F \text{ is defined as } F = \frac{\sqrt{R_1 R_2}}{1 - \sqrt{R_1 R_2}} .$$

$R_1, R_2$  are the reflectivities of two mirrors.

$c$  depends on the loss of the mirrors and equates to 1 for lossless reflectors.

$\delta$  is the optical phase which is given by

$$\delta = \frac{2\pi nL}{\lambda}$$

where  $L$  is the length of the sensor.

$n$  is the index of refraction of the fibre.

$\lambda$  is the wavelength of the laser.

A longitudinal strain causes the length  $L$  to change. This in turn causes the optical path length of the sensor to change. So when the sensor is subjected to a longitudinal strain the optical phase changes, the resultant reflected irradiance changes according to the above equation. This results in an intensity profile with respect to a change in the optical phase of the sensor, see Figure 15.

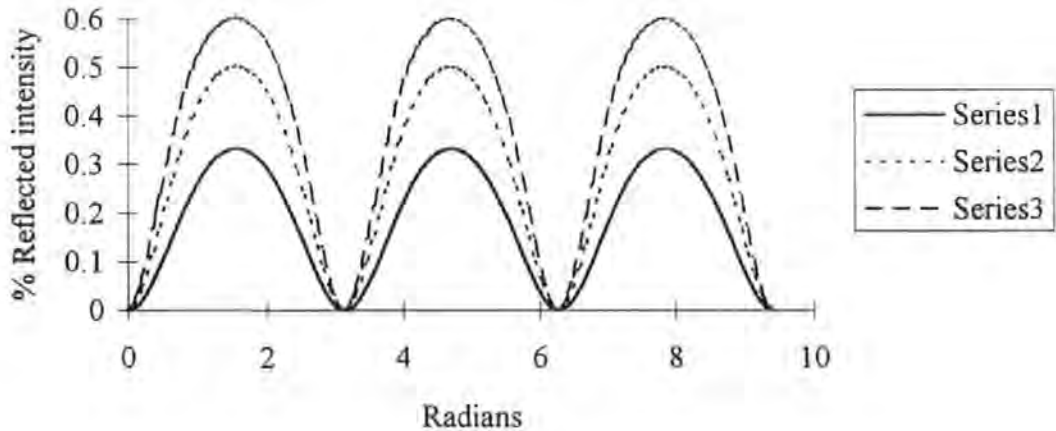


Figure (15) . Irradiance as a function of the change in optical phase.

In Figure 15, series 1 has a finesse value of 0.5, series 2 a finesse value of 1.0 and series 3 a finesse value of 1.5. Notice that as the finesse increases, the sinusoidal waveform of the reflected intensity becomes more distorted and takes on a rectified sine function.

### 2.3.1 The relationship between optical phase change of a F.F.P. sensor and the longitudinal strain.

If a function is defined as  $F(x) = \frac{1}{1+x}$  the function can be approximated by a series as long as  $|x| \leq 1$ . The Airy function is such a function when the coefficient of finesse is less than one.

So  $\frac{1}{1+x} \approx 1 - x + x^2 - \dots + (-1)^n x^n$  is the approximation, so the Airy function can therefore be written as.

$$\frac{1}{1 + F \sin^2\left(\frac{\delta}{2}\right)} = 1 - F \sin^2\left(\frac{\delta}{2}\right) + F^2 \sin^4\left(\frac{\delta}{2}\right) - \dots$$

as long as  $F \leq 1$

then 
$$F \sin^2\left(\frac{\delta}{2}\right) \gg F^2 \sin^4\left(\frac{\delta}{2}\right)$$

The reflected intensity from the F.F.P. sensor becomes

$$1 - \frac{c}{1 + F \sin^2\left(\frac{\delta}{2}\right)} \approx 1 - c \left[ 1 - F \sin^2\left(\frac{\delta}{2}\right) \right]$$

with first derivative

$$\frac{\partial I_{Re}}{\partial \delta} \approx cF \cos\left(\frac{\delta}{2}\right) \sin\left(\frac{\delta}{2}\right) \approx \frac{cF}{2} \sin(\delta)$$

and second derivative

$$\frac{\partial^2 I_{Re}}{\partial \delta^2} \approx \frac{cF}{2} \cos(\delta)$$

The ratio  $\frac{\frac{\partial A_{Re}}{\partial \delta}}{\frac{\partial^2 I_{Re}}{\partial \delta^2}}$  of the two derivatives gives a  $\tan(\delta)$  function from which the

optical phase change  $\delta$  can be recovered, i.e.

$$\delta \approx \arctan \left[ \frac{\frac{\partial A_{Re}}{\partial \delta}}{\frac{\partial^2 I_{Re}}{\partial \delta^2}} \right]$$

where  $\delta = \frac{2\pi nL}{\lambda}$ .

The extraction of the first and second derivative is obtained by a signal processing demodulation technique ( see appendix V and section 2.4 ), which involves the extraction of the first and second harmonics at a given modulation frequency of the irradiance.

By definition, strain = ( change in linear length ) / ( original linear length ) =  $\varepsilon = \frac{\Delta L}{L}$

$L$  is the original linear length.

Thus the total optical phase is

$$\delta = \frac{2\pi n}{\lambda} [L + \Delta L]$$

$\delta = \delta_s + \delta_\varepsilon$ , where  $\delta_\varepsilon$  is the change in optical phase due to strain and  $\delta_s$  is the phase change due to temperature. Thus the relationship between longitudinal strain and the change in optical phase is:

$$\varepsilon = \frac{\lambda}{2\pi nL} \arctan \left[ \frac{\frac{\partial A_{Re}}{\partial \delta}}{\frac{\partial^2 I_{Re}}{\partial \delta^2}} \right]$$

Researchers Butter, Hocker and Sirkis [25-28] has shown that the optical phase change is due to longitudinal strain, photoelastic effect and a change in the diameter of the fibre ( see section 1.4 ) is given by:

$$\varepsilon = \frac{\lambda}{2\pi n \left[ 1 - \frac{n}{2}(1-\mu)P_{12} - \mu P_{11} \right] L} \arctan \left[ \frac{\frac{\partial I_{Re}}{\partial \delta}}{\frac{\partial^2 I_{Re}}{\partial \delta^2}} \right]$$

which can be written as

$$\varepsilon = const * \arctan \left[ \frac{\frac{\partial I_{Re}}{\partial \delta}}{\frac{\partial^2 I_{Re}}{\partial \delta^2}} \right]$$

This expression states clearly that for a F.F.P. sensor, there exists a quasi - linear relationship between the longitudinal strain applied to the sensor and the resulting optical phase change of the light from the sensor. The reason why a quasi - linear relationship is due to the value of finesse  $F$  of the Fabry-Perot cavity. The expression is not exact because of the temperature effect ( see Butter and Hocker [50,51] ); and because the expression ignores thermal expansion and contraction of the glass sensor itself see Figure 16 .

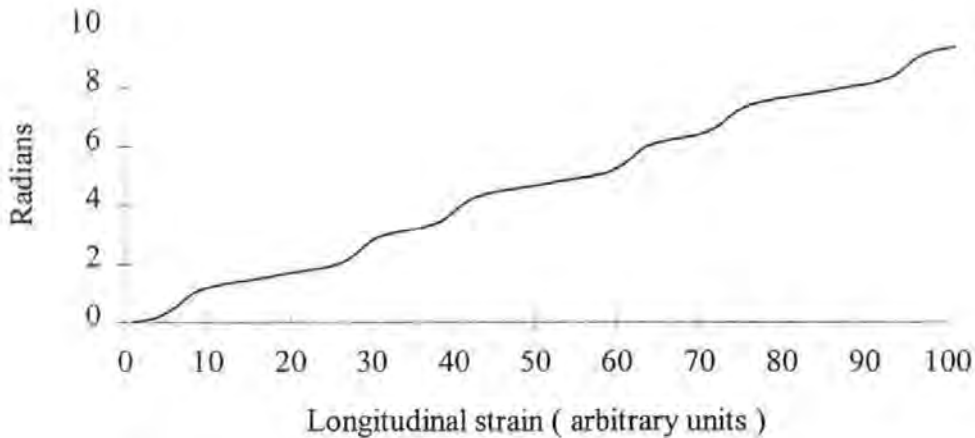


Figure (16) . Quasi-linear relationship between longitudinal strain and optical phase change, a theoretical plot with a finesse of 0.5 for constant temperature.

## **2.4 Signal processing for the Fibre Fabry Perot sensors.**

The tracking of the first and second derivatives of the reflected intensity profile is possible by using a phase generated carrier technique ( see section 1.3.7.1 ). This is achieved by modulating the frequency of a distributed feedback ( D.F.B. ) laser that is used as the optical source. This is achieved by modulating the injection current to the laser. In a conventional Fabry Perot cavity diode laser there are two effects which brings this modulation about. First, changes in the current result in small changes in the cavity temperature, which leads to a modulation in the effective cavity length via temperature-dependent refractive index and thermal expansion. Secondly, the carrier concentration in the laser region increases with increased current, causing a modification in the refractive index, thus giving rise to a current-frequency conversion factor for diode lasers. In this work a modulation frequency of approximately 5KHz is used and a current-frequency factor of approximately 3GHz/mA which is given by the manufactures ( Nortel ) for the D.F.B. laser LC111 - 18 series.

A D.F.B. ( Distributed Feedback ) laser diode generates optical power into one longitudinal mode. The laser-drive unit provides the necessary functions for optical power and temperature stability. This ensures that there is no drift in the wavelength generated by the laser.

The effect of this modulation is to convert the frequency modulation of the light to an intensity modulation dependent upon the length of the sensor. Thus when the sensor length increases by a half wavelength of the light used to illuminate the sensor. The sensor passes through one complete cycle i.e. shifts through one fringe and one complete cardioid is produced.

The signal generated from the F.F.P. sensor is recovered by a Germanium photo-diode. A signal at the modulation frequency of the laser is extracted from the photo-detector ( the first harmonic ); this signal is proportional to the first derivative of the intensity profile of the sensor. A second signal at twice the modulation frequency is also extracted, this being the second harmonic which is proportional to the second derivative of the intensity profile of the sensor. This is used to track positions across each fringe and thus determines the change in optical phase from which the longitudinal strain subjected to the F.F.P. sensor can be calculated.

The analysis in appendix V derives the expressions for the harmonics these being:

$$1^{\text{st}} \text{ Harmonic : } \left[ \left( 2F - \frac{3}{2}F^2 \right) \sin(\delta) - F^2 J_2(\Delta\delta) \sin(2\delta) \right] \cdot J_1(\Delta\delta) \sin(\omega_c t)$$

and

$$2^{\text{nd}} \text{ Harmonic : } \left( \frac{3}{2}F^2 - 2F \right) \cdot J_2(\Delta\delta) \cos(\delta) \cos(2\omega_c t)$$

for a value of  $F < 1$ , then the  $F^2$  terms become less significant compared to the  $F$  terms and thus becomes:

$$1^{\text{st}} \text{ Harmonic : } (2F) \sin(\delta) \cdot J_1(\Delta\delta) \sin(\omega_c t)$$

and

$$2^{\text{nd}} \text{ Harmonic : } (-2F) \cos(\delta) \cdot J_2(\Delta\delta) \cos(2\omega_c t)$$

Where  $\omega_c$  is the modulation frequency,  $\delta$  is the optical phase change

$\Delta\delta$  is a phase shift, which is a quantity dependent upon current - frequency factor of the D.F.B. laser and the change of length of the Fabry Perot sensor due to longitudinal strain.

$$\Delta\delta = \frac{2\pi n \Delta L}{c} \cdot \Delta i \frac{\delta\nu}{\delta i}$$

where  $\frac{\delta\nu}{\delta i}$  is the current - frequency factor and  $\Delta i$  is the induced change in the drive current to the D.F.B. laser. The functions  $J_1(\Delta\delta)$  and  $J_2(\Delta\delta)$  are Bessel functions of the First kind of order 1 and 2.

Thus under this condition of  $F < 1$  the ratio of the two harmonics is a  $\tan(\delta)$  function of the optical phase change.

The signal extraction is performed by a lock-in-amplifier (L.I.A.), Jupiter Microsystems LA1130 with synchronous phase detection. Synchronisation of the L.I.A.'s with the modulation frequency is achieved by means of a square wave signal generator (Farnell sine square oscillator LF1) which is synchronous with the modulation of the D.F.B. laser.

Phase control and optimisation of the signals to maximise the signal to noise ratio is provide by the L.I.A.'s. Using an analogue to digital converter facilitates direct coupling to a desk - top personal computer. The computer controls the L.I.A.s via a general-purpose output / input board ( programs for controlling the L.I.A.s and data acquisition ).

The data obtained from the L.I.A.s at the first harmonic and second harmonic can be used to generate a quadrature diagram; a cardioid figure, see Figure 17. This shows that at every position on the cardioid the two “ harmonics ” have a unique value, so it is possible to interpolate between fringes. Using these data and the relationship on page 34 in section (2.3.1) it is possible to extract the longitudinal strain subject to the sensor and this is demonstrated in the next section.

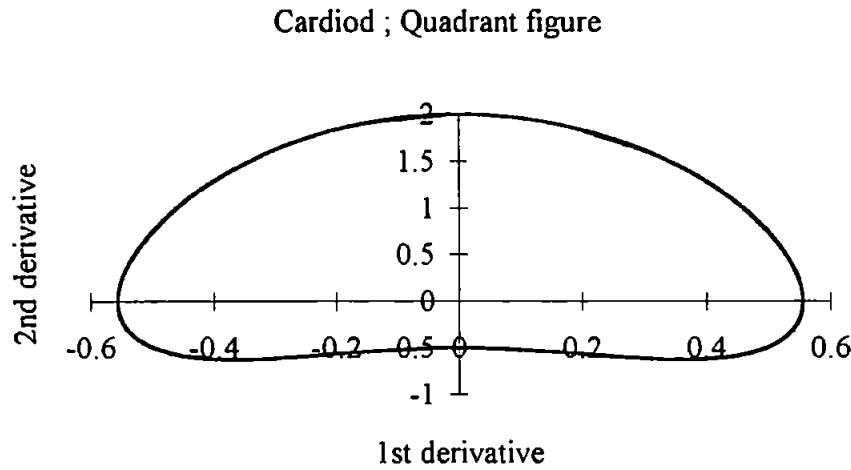


Figure (17) ; A Theoretical plot of a cardioid generated from the first and second derivatives of the reflected intensity profile of the F.F.P. sensor with a finesse of 1.0.



## 2.5 Experimental Test Rig.

An F.F.P. sensor is adhered to the surface of an Aluminium cantilever beam by using an optical epoxy EpoTek 301 Interonics. The dimensions of the cantilever beam are 171mm in length, 59mm in width and 1mm thick. Attached also to the Al cantilever beam are two electrical strain gauges which are used for calibration purposes, Micro - Measurement a division of Measurements Group inc, gauge type EA-13-240LZ-120 which are self - temperature compensated. The two electrical gauges are positioned on either side of the F.F.P. sensor and parallel to the F.F.P. sensor. Both gauges are connected to a switch and balance unit Vishay Instruments model SB-1 and in turn this unit is connected to a strain indicator Measurements Group Inc, model P-3500.

One end of the cantilever is connected to a rigid support. The opposite end is attached to a linear micro - position tracker that is used to exert a force on the beam. This force manifests itself as a longitudinal strain in the beam and therefore on the sensor. This is accomplished by using the vernier. The vernier is attached to the tracker, the vernier pushes against an end support and moves the tracker, see Figure 18. The vernier is turned, the strain is observed by the electrical strain gauges and noted. The change in the optical phase is generated in the reflected light from the sensor and is detected by the rest of the apparatus of the test rig, see Figure 19.

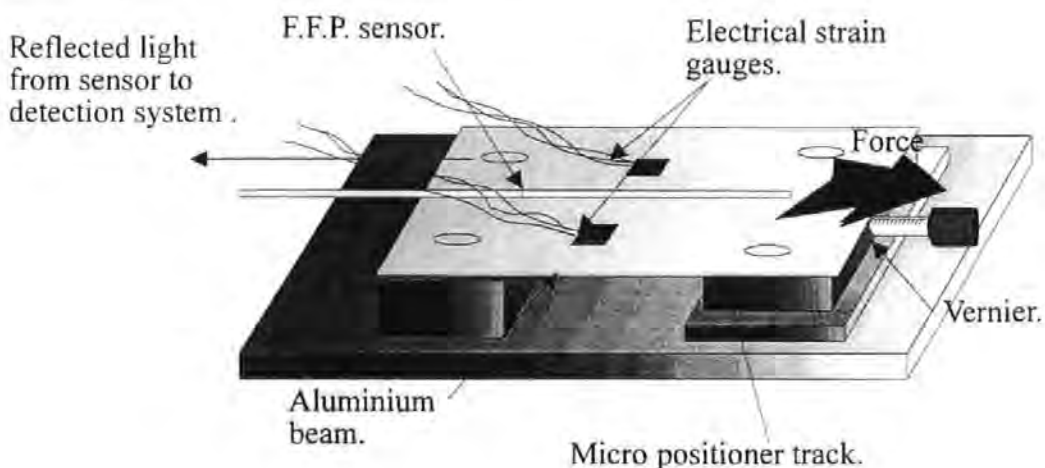


Figure (18) . The mechanical test rig for testing the F.F.P. sensors.

The experimental arrangement of the rest of the apparatus is shown in Figure 19. The apparatus is used to generate / detect the first and second harmonics from the F.F.P. sensor, thus a cardioid can be generated. Finally the information on the longitudinal strain subjected to the F.F.P. sensor can be calculated from the first and second harmonics.

The F.F.P. sensor is not temperature compensated at this stage, so strain effects resulting from thermal changes ( thermal expansion and contraction ) will cause error signals to be generated. These effects are not considered at this stage.

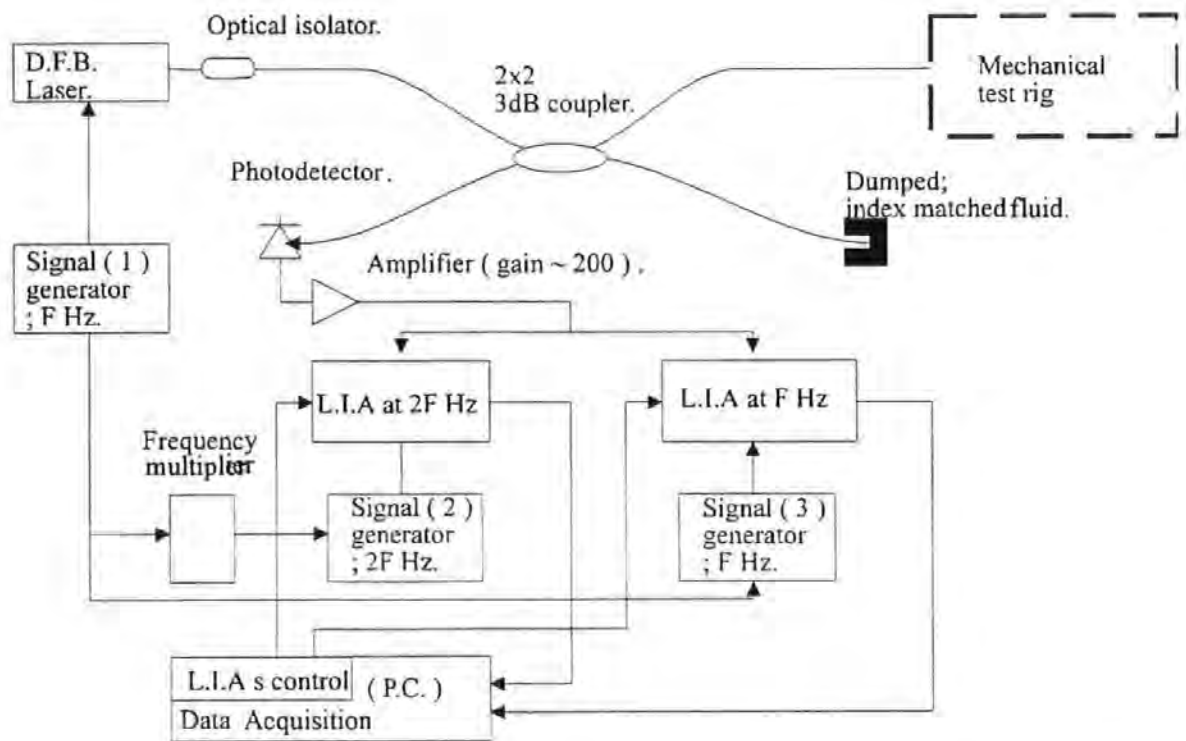


Figure (19) . Shows the experimental arrangement used to investigate and assess The performance of the sensor, system and signal processing.

## 2.6 Experimental results for the Fibre Fabry-Perot sensor.

A number of experiments were carried out on the sensor under the procedure described in the above section 2.5 and section 2.3. Applying longitudinal strains to the F.F.P. sensor generated a number of cardioids; these are shown in Figures 20 to 24.

The differing shapes of the cardioids are due to a number of reasons, such as varying the gain of the amplifier and changes to the phase of the electronic signals. Figures 20, 21 show the amplification factor for each of the two harmonics by the lock-in-amplifiers.

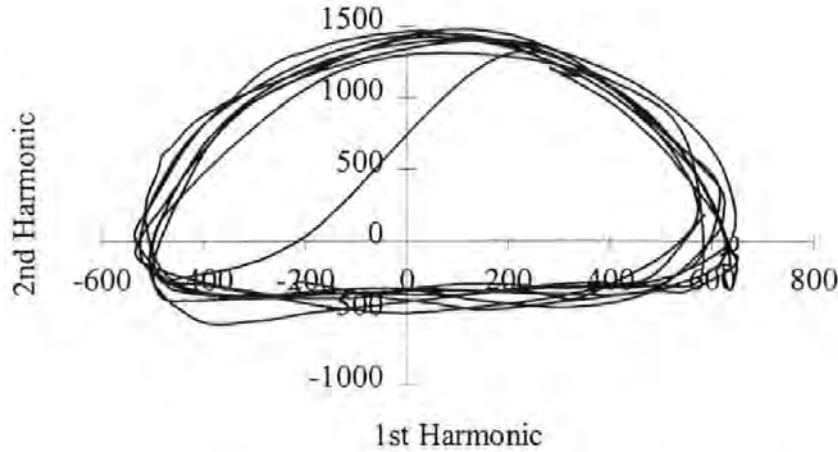


Figure (20) . Example one, cardioid results from the F.F.P. sensor adhered to the Aluminium beam.

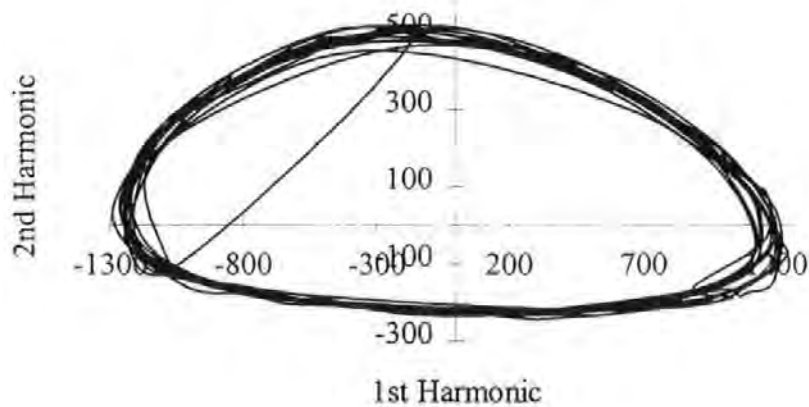


Figure (21) . Example two, cardioid results from the F.F.P. sensor adhered to the Aluminium beam.

Figures 22,23 show the variation of the cardioid shape due to the phase relationship between the various parts of the electronic equipment and the lock in-amplifiers. Thus the

shape of the cardioid can be optimised by a change in the L.I.A.'s phase relationship to the rest of the equipment. Secondly optimisation can be achieved by changing the phase difference between the signal generators; signal generator (1) and signal generator (2).

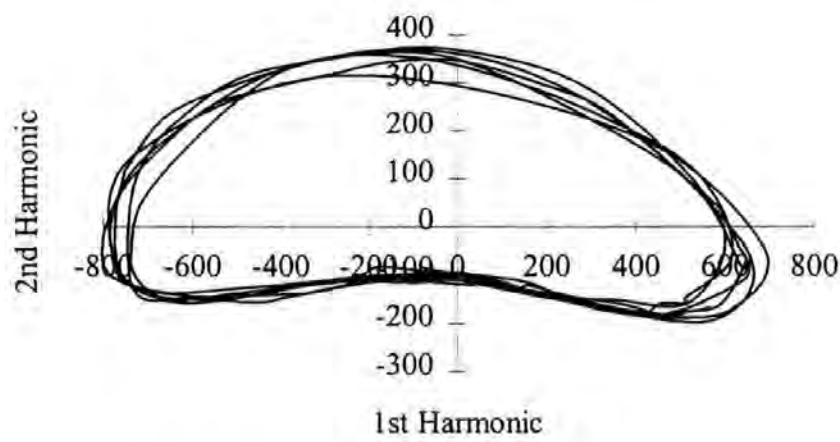


Figure (22) . Example three, a cardioid from the same test-rig and F.F.P. sensor but the phase relationship changed.

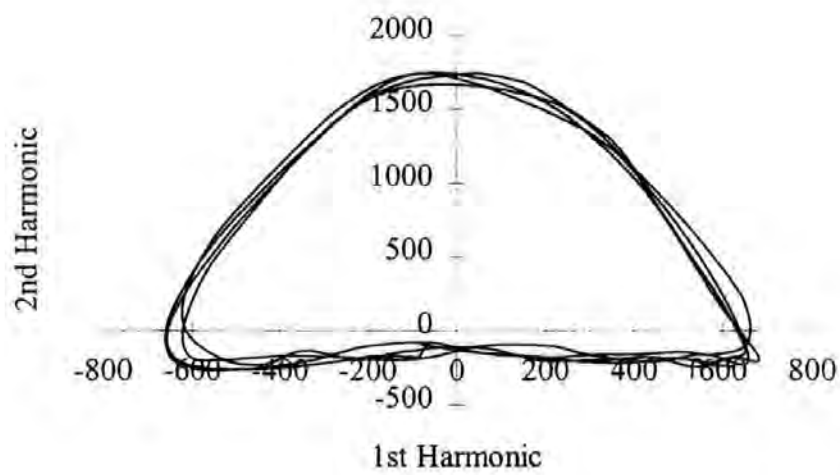


Figure (23) . Example four, a cardioid from the same test-rig and F.F.P. sensor but again changing the phase relationship.

Signal fading is observed when the longitudinal strain is continued, see Figure 24. This is expected because of the signal processing technique used ( see appendix V ).

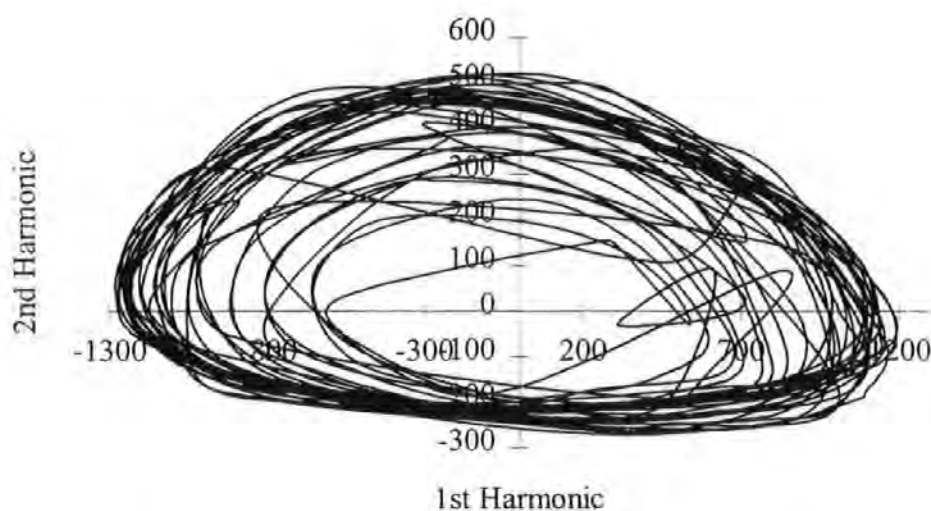


Figure (24) . An example of signal fading, using the described processing technique.

#### 2.6.1 Processed information from the F.F.P. sensor.

After or during the acquisition of the data, the inverse tangent is taken of the ratio of the first to second harmonic. This gives interpolation between fringes but it is essential that the number of fringes, which are covered or gone through, be detected and this fact be used for the overall change in optical phase. This is achieved by a short C++ program that looks for the value of  $\pm\pi/2$  from the inverse tangent operation. At these points  $\pm\pi/2$  the tangent function is discontinuous, so the addition of  $\pi$  ( for phase progression ) or the subtraction of  $\pi$  ( for phase retardation ) is needed to achieve a continuous function. This is because the inverse tangent function is periodic and discontinuous. A code listing of the program is given appendix V.

An increase or retardation in phase of the signal can occur depending whether anti-clockwise or clockwise generation of the cardioids is used. The reason for the two ways of generation of a cardioid is due to the electronic equipment's ( signal generators ) phase relationships to the local-in-amplifiers can be changed by the various methods which have already been discussed in section 2.6. Figures 25, 26 shows what happens if the phase relationship changes between sensor and electronics, i.e. increasing phase and phase retardation. Also Figure 26 shows what happens if temperature is not calibrated for.

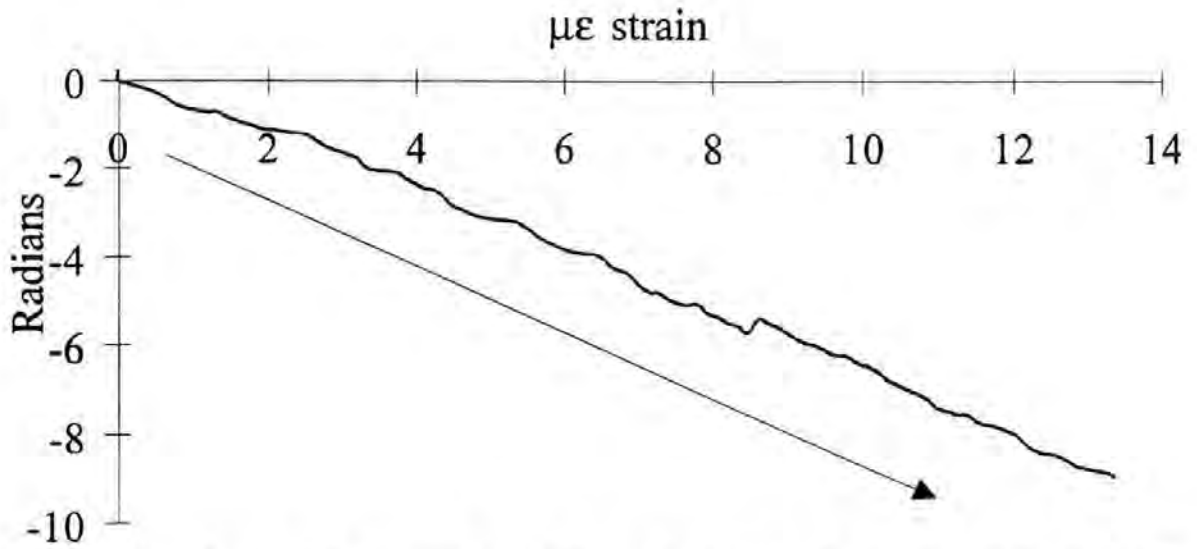


Figure (25) . Optical phase change as a function of longitudinal strain, exhibiting phase retardation.

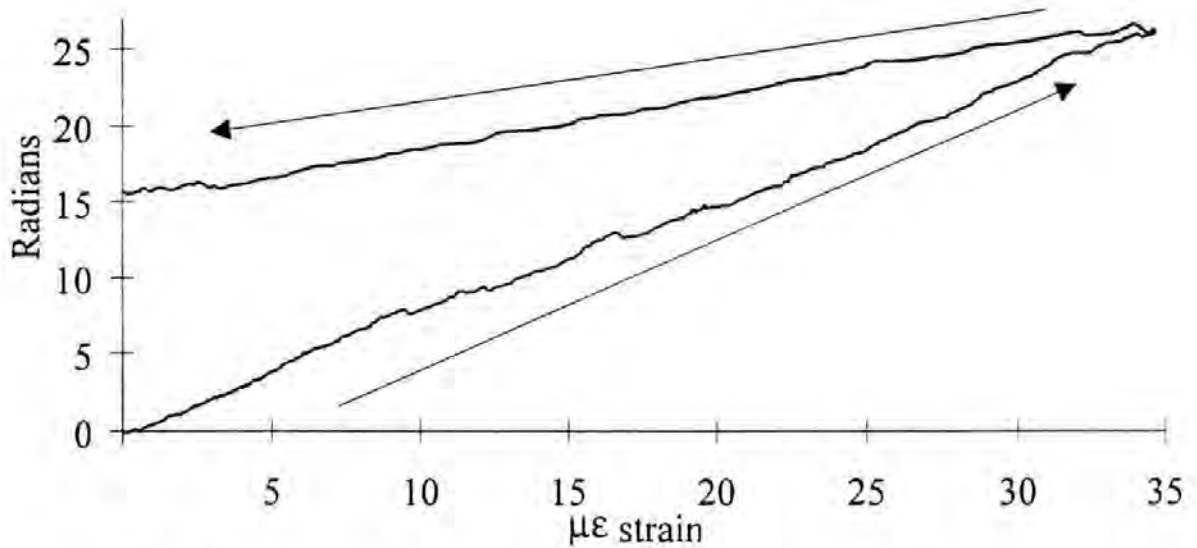


Figure (26) . Optical phase change as a function of longitudinal strain.

In Figure (26) there is an increase in optical phase with an increase in longitudinal strain and decrease in optical phase with a decrease in longitudinal strain. This graph also demonstrates the effect of temperature on the sensor when it has not been compensated for. This results in a hysteresis effect.

## 2.6 Observations and Results of the F.F.P. sensor.

Figures 25 and 26 shows the quasi-linear relationship between longitudinal strain applied to a F.F.P. sensor and the change in the optical phase generated by the F.F.P. sensor with regard to the synchronous detection system ( the lock in amplifiers ).

The reason for the quasi-linear relationship is because the signal generated by the F.F.P. sensor does not respond sinusoidally to changes in longitudinal strain i.e. it is not a true Fizeau response. This is due to the approximation used in the inverse tangent function to obtain the phase information ( see section 2.3 ) and it is this that causes the ripple in the graph.

Assuming a linear relationship between the phase generated and the longitudinal strain, the error derivation due to the approximation for a given response; Figure 26 is  $\pm 0.5 \mu\epsilon$ . This is a typical value of deviation away from linearity for the length of the F.F.P. sensor used. These error numbers are calculated from the residuals of the linear regression of the processed data and taken as the root mean squares of the residuals, i.e.

$$Error = \frac{\sum_{i=1}^n \sqrt{[\mu\epsilon(\delta)_i - \{con \cdot \delta_i\}]^2}}{n}$$

where

$\mu\epsilon(\delta)_i$  is the experimental data for a given phase change for a given longitudinal strain.

$con \cdot \delta_i$  is the longitudinal strain where  $con$  is the constant of proportionality and  $\delta_i$  is the experimental phase.

A comparison is also made against the Butter and Hocker model for longitudinal strain in optical fibre and associated optical phase change [50]. According to Butter and Hocker, neglecting minor terms ( section 1.4 ) the constant of proportionality for the change in optical phase;  $\delta$  to longitudinal strain;  $\mu\epsilon$  is given by;

$$\mu\epsilon = \frac{\lambda}{4\pi n \left[ 1 - \frac{n^2}{2}(1 - \mu)P_{12} - \mu P_{11} \right] L} \delta$$

A small note concerning the Butter and Hocker original equation. These equations assume that the optical path length through the sensor is  $2\pi nL$ , the transmission change in the optical path length. In this application the detection system looks at the reflected light coming from the sensor, thus the optical path length is doubled hence  $4\pi nL$ ; a round trip of the F.F.P sensor.

Using the following values for the Pockel's coefficient for fused silica  $P_{11} = 0.121$  and  $P_{12} = 0.270$  and a Poisson's ratio of 0.17. Assuming a core refractive index  $n = 1.456$  and the length of the F.F.P. sensor as 8.4 cm. A theoretical constant of proportionality was calculated for a F.F.P. sensor with the stated specification, this being  $0.733 \text{ rad}(\mu\epsilon)^{-1}$ . Conducting a series of 28 individual experiments with a specific F.F.P. sensor with a approximate length of 8.4 cm, an average constant of proportionality was found to be  $0.728 \text{ rad}(\mu\epsilon)^{-1}$  with an error of  $\pm 0.289 \text{ rad}(\mu\epsilon)^{-1}$ . The large variation in this constant can be probably due to experimental error ( measurements ), fluctuations in the equipment used and the effects of temperature variation ; the crudeness of the experiment [51].

The process was repeated and an average value obtained was 0.613 with an error of  $\pm 0.066 \text{ rad}(\mu\epsilon)^{-1}$ , in case one 1% error between the theoretical and the experimental test rig but with a large variation and in case two the error was 16%. The results seem to have reasonable agreement with the theoretical results, the deviation between results maybe due to the crudeness of the experimental test rig.

A number of problems were evident with the F.F.P. sensor. These are:

- ( I ) Fabrication.
- ( II ) Multiplexing.
- ( III ) Measures apparent strain, i.e. changes in strain.
- ( IV ) The length of the sensor.

( I ) The problem with the fabrication of the F.F.P. sensor is the fusion splicing of the  $\text{TiO}_2$  semi-reflective layer onto the feeder fibre. This usually results in the destruction of the  $\text{TiO}_2$  layer or a low rate of successful splicing; thus no sensor. The reflectivity of the  $\text{TiO}_2$  layer can vary due to splicing; depending how much of the  $\text{TiO}_2$  layer evaporates in joining the sensor to an optical line. This would change the cardiod's shape ( the response



of the sensor ), so optimising the system for each individual F.F.P. sensor would have to take place. These problems above would cause major difficulties for automation production.

( II ) The problem with multiplexing is that there is no simple satisfactory solution, which has been devised yet for this type of sensor. The  $\text{TiO}_2$  layer is an ideal mirror; reflecting at all wavelengths, so time division multiplexing is the only feasible technique at the present time which causes additional problems with sensor network architecture.

( III ) The F.F.P. sensor measures only apparent strain not absolute strain, that is to say it measures changes in strain and does not know the original strain / the intrinsic strain of the structure when sensor was incorporated.

( IV ) Another problem is the length of the F.F.P. sensor. In general all the sensors investigated had lengths ranging from 6.5 cm to 9.6 cm. A problem with having relatively long sensors is that there may be possibility of a shear strain subjected to the sensor and thus rendering the sensor useless [25-29]. Decreasing the length of the sensor decreases the strain resolution of the sensor and causes additional problems in fabrication.

Temperature sensitivity has been observed during experiments. This problem can be overcome by using two identical F.F.P. sensors; both having the same environmental conditions but only one sensor subjected to the strain. Thus using a signal from the nonstrained sensor as a reference signal ( phase variations due to changes in temperature ) for the strained sensor any resultant signal from this system would be due to changes in longitudinal strain. This scheme was not pursued because of the above difficulties.

The F.F.P. sensor has good strain resolution compared to other systems that have been investigated by various researchers [14-24] but taking the above problems into account the F.F.P. sensor ( with a  $\text{TiO}_2$  layer ) would not be a practical solution for a strain sensing array network.

To overcome the fabrication problems it was decided to move away from using  $\text{TiO}_2$  layer as a semi - reflective layer and use fibre Bragg gratings as a semi - reflective layer substituting for the  $\text{TiO}_2$  layer and the endface. Fibre grating are " written " into the fibre core using a U.V. side writing technique [54]. This process is a much more controllable and repeatable for producing semi - reflective layer.

Sensors fabricated this way have been investigated both theoretically and experimentally. The results are considered in sections 3 and 4 using the prescribed signal-processing scheme.

With this type of sensor it may be possible to measure absolute phase changes. This is investigated in section 5. Also the problem of multiplexing may be addressed; Fibre Bragg gratings have wavelength-dependent reflectivity profiles; a finite bandwidth of major reflectivity.

### 3      The intra-core fibre Bragg Grating Sensor.

#### 3.1 The fibre Bragg grating sensor.

A number of optical elements and devices have recently come into general use in the telecommunication industry. These components have a number of interesting properties. They are robust, have low insertion loss, can be easily integrated into optical fibre systems and in some cases have the potential for automated fabrication. The intra-core fibre Bragg grating is one of these elements. The Bragg grating consists of a short length ( 1 to 10 mm ) of standard telecommunications grade single-mode step index optical fibre, which has a periodic perturbation of the core refractive index  $n$ . This is brought about by means of exposure to an interference pattern of ultra-violet radiation in the range of 240 - 250 nm. This was first achieved by Hill [58] in 1978 and is known as uniform gratings, the spatial variation ( period ) of the refractive index is constant. The grating is used as a wavelength selective reflector, rejection filter, wavelength-tuning device and as a sensing device. Figure 27 shows a schematic diagram of a uniform grating and Figure 28 shows the spectral reflective response of such a fibre Bragg grating.

The wavelength of peak reflectance is known as the Bragg wavelength  $\lambda_B$  and is a function of the spatial period of the perturbation of the core refractive index;  $\Lambda$ . This is also known as Bragg resonance. The spectral bandwidth of the reflection response depends on the grating profile. This may be narrow for a uniform grating or in the case of nonuniform gratings maybe much wider.

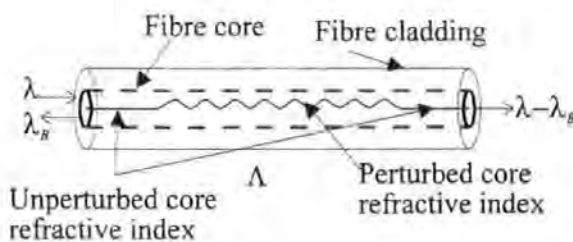


Figure (27) . A simple uniform Bragg grating.

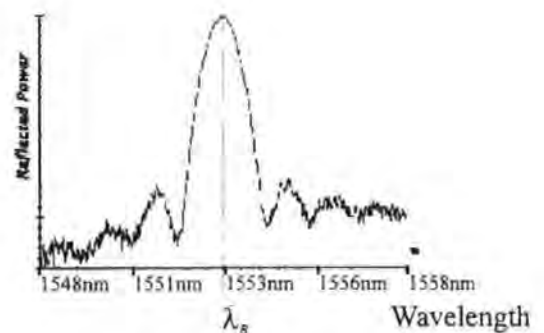


Figure (28) . Spectral Response of a fibre uniform fibre Bragg grating.

Mechanically-induced change in the spacing  $\Lambda$  of the core refractive index perturbation gives rise to a proportional change in the Bragg wavelength  $\lambda_B$  of the reflected power. It is this simple linear relationship that triggered a widespread interest in using these optical elements to measure strain.

### 3.2 Properties of a uniform fibre Bragg grating.

A grating that has a non-varying spatial period  $\Lambda$  and a constant value of the effective refractive index is known as a uniform grating. When the optical radiation incident on the grating has a wavelength at or close to the Bragg wavelength  $\lambda_B$ , it suffers a strong reflection. The mechanism of this reflection can be described as follows. Each individual corrugational change in the index causes an infinitesimal amount of Fresnel reflection. A large number of such corrugations correctly spaced will have a cumulative effect and will cause the reflection to approach 100% at the Bragg wavelength. The Bragg wavelength is determined by the average / effective refractive index of the core  $n_{eff}$  and the grating period  $\Lambda$ , the periodic spacing of the core refractive index perturbations:

$$\lambda_B = 2n_{eff} \Lambda$$

Reflection of the incident optical power at a specific wavelength is caused by the forward propagating modes coupling energy into the backward propagating modes, caused by the grating's structure. A schematic diagram of a simple one-dimensional Bragg grating showing the overall physical interaction is shown in Figure 29.

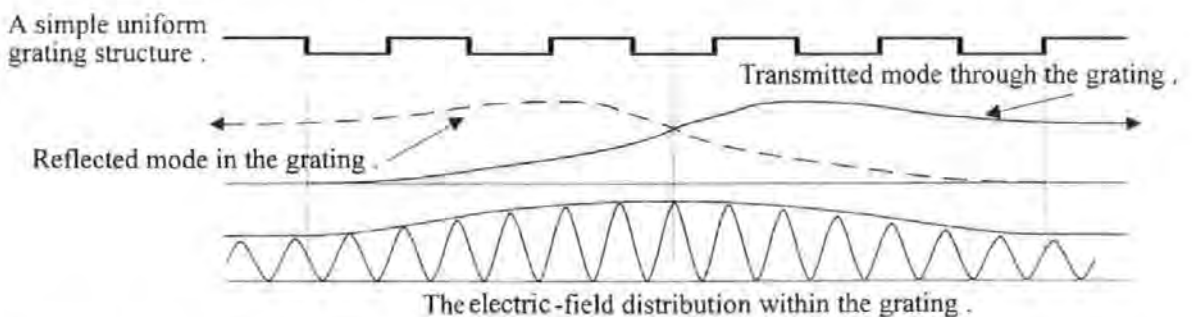


Figure (29) . The general build up of the reflected waves from a simple uniform Bragg grating.

A more realistic model of a uniform Bragg grating for simple analytical purposes is one in which the perturbation of the core's refractive index is sinusoidal. Where strong

reflection occurs over a spectral bandwidth  $\Delta\lambda_B$ , inside this region is the so called photonic band gap where the waves are evanescent, which is smaller than  $\Delta\lambda_B$  it as be shown by researchers [81,104-110] that;

$$\Delta\lambda_B = \frac{\lambda_B^2}{\pi m_{eff} L} \sqrt{\pi^2 + \left( \frac{\pi \Delta n L}{\lambda_B} \right)^2}$$

where  $L$  is the grating length and  $\Delta n$  is the amplitude of the refractive index perturbation.

In the case of the sinusoidal uniform Bragg grating, the coupling strength between the forward and backward modes can be described by a coupling coefficient:

$$\kappa = \frac{\pi \delta n}{\lambda_B} \eta$$

and the maximum grating reflectivity is

$$R_{Max} = \tanh^2(\kappa L)$$

The variable  $\eta$  represents the fraction of fibre mode power contained by the fibre's core and can be estimated using the normalised parameter  $V$ . On the basis that the grating is uniform then  $\eta$  can be approximated by:

$$\eta \approx 1 - V^{-2}$$

and using

$$V = \frac{2\pi a}{\lambda_0} \sqrt{n_1^2 - n_2^2}$$

$a$  is the core radius.  $n_1$  is the core refractive index.  $n_2$  is the cladding refractive index.

$\lambda_0$  is the wavelength of the light in free space.

A more complete analysis of a Bragg grating shows that wave propagation behaviour is quite different outside and inside the band-gap  $\Delta\lambda_B$ . The range of wavelengths just outside the band-gap experience reflection as a consequence of an interaction between the standing wave and the propagation of interference wave-packets within the periodic structure. The result is a natural resonance that is a function of the total length of the grating [55]. Within the band-gap the reflectance is at a maximum and the waves are evanescent (exponential functions) and most of the light is reflected. A very small amount of light is transmitted through the evanescent region. This is analogous to strong reflection in barrier tunnelling problems in quantum mechanics. In addition to the strong reflections at the band edges, there are weak reflections at the front and back ends of the grating; this

can be viewed essentially as an impedance mismatch effect. The above parameters are derived from waveguide mode-coupling theory applied to gratings as reflectors [56,57]; contradirectional coupling ( see appendix I on analysis of grating using mode coupling theory and the T - matrix formalism ).

### 3.3 Nonuniform fibre Bragg gratings.

The demand by the telecommunications industry for gratings to carry out various functions has led to a number of nonuniform gratings. To produce a nonuniform grating a number of changes to the refractive index variations can be introduced during or after fabrication, these are chirping ( linear, quadratic, cubic) [59-61], tapering [62], apodisation [63,64].

#### 3.3.1 Aperiodic or chirped fibre Bragg gratings.

The reflection bandwidth of a uniform - period grating is narrow. Varying the Bragg condition continuously along the grating's length can increase the reflection bandwidth. When light at a given wavelength travels through the grating it will encounter two types of region. If Irradiance wavelength lies outside the local reflection band gap, this condition is where the optical field interacts weakly with the grating and the light propagates through the grating without coupling to the reflected mode. If the Irradiance wavelength lies within the local reflection band gap coupling occurs between this light and the reflected mode. The Bragg condition is given by  $\lambda_B = 2n_{eff}\Lambda$  by making the value of the gratings period or effective refractive index a function of the length of the grating;  $\Lambda(z)$  and  $n_{eff}(z)$  or both, it becomes possible for a range of wavelengths to satisfy the Bragg condition at given points within the grating length .

$$\lambda_B(z) = n_{eff}(z)\Lambda(z)$$

Doing this widens the maximum peak of the Bragg grating reflection profile and also decreases the maximum value of reflectivity if the grating length is constant. The variation in the grating period or chirp can be for example, linear, quadratic or cubic. The fabrication techniques of producing a chirped grating are discussed in section 3.4.

Chirped gratings can be divided into two categories, wavelength or frequency. A chirped grating is created by varying the grating periodicity, noting that frequency chirping to first order can be approximated by wavelength chirping. When the refractive index is varied as a function of the length of the grating ( Taper function ), this is called amplitude chirping occurs providing the grating periodicity is held constant. Figure 30 shows how the reflectance varies for both of these conditions also [65].

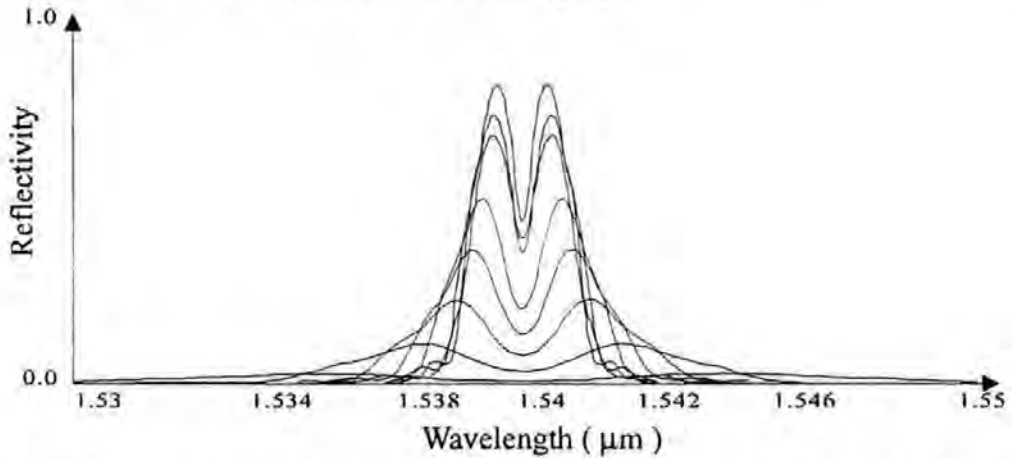


Figure (30) . Some spectral reflectivity responses calculated using the T-matrix formalism.

The above spectral responses are for gratings that consist of a combination of three chirps, which have a continuous phase relationship between each section along the grating length, that is to say, no discontinuities. Also there is a taper function ( Gaussian ) for the modulation of the refractive index. These effects are discussed in section 3.5. Each curve in Figure 30 represents a grating with a constant chirp for a given length.

### 3.3.2 Apodisation of a uniform or chirped fibre Bragg grating.

Apodisation is the gradual change in the refractive index modulation. In the case of a chirped grating this is necessary when the coherence length of a signal determined by the bandwidth of the chirp is a few per - cent of the length of the chirped grating. This can effect the reflectivity response of grating because of dispersion occurring in different parts of the grating. An example of this technique is the perfect cosine apodisation of fibre grating by repetitive symmetric longitudinal stretching of the fibre around the centre of the grating while the grating is being written .The effect of stretching by exactly half the period at the ends of the grating results in the interference pattern at the ends of the grating being completely smeared out (see section 3.5 fabrication techniques). The composite interference



pattern follows a linear mark - space ratio if the stretch is a triangle ramp function ( see Figure 31 ), [63,64].

change in O.P.D ( Optical Path Difference ) by  $\Delta n$

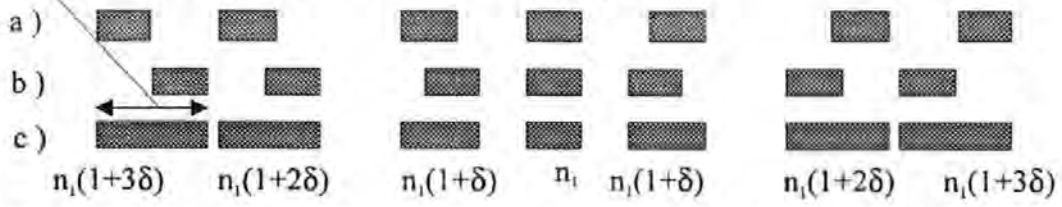


Figure (31) . Apodisation by stretching a grating. Figures 31a and 31b shows the maximum positions of stretch of the grating and Figure 31c shows the resultant grating refractive index variation.

### 3.4 Principle of operation of a Bragg grating strain sensor.

The fibre Bragg grating sensor is illuminated using a broadband source, such as an edge-emitting LED or a superluminescent diode. The narrow wavelength component reflected by the sensor is determined by the Bragg wavelength  $\lambda_B$  where  $\lambda_B$  is equal to  $\lambda_B = 2n_{eff} \Lambda$ . When the fibre is strained the Bragg wavelength varies due to the change in the grating spatial period  $\Lambda$  and the photoelastic-induced change in the refractive index. The fractional change in the Bragg wavelength with a longitudinal strain  $\epsilon$  is given by:

$$\frac{\Delta \lambda_B}{\lambda_B} = (1 - p_e) \epsilon$$

where  $p_e$  is the effective photoelastic constant given by:

$$p_e = \left( \frac{n^2}{2} \right) [P_{12} - \mu(P_{11} + P_{12})]$$

$P_{12}$  and  $P_{11}$  are components of the strain optic tensor,  $n$  is the index of the core and  $\mu$  is Poisson's ratio ( see section 1.4 ). Shifts in the Bragg Wavelength can occur and are most likely due to fluctuations in temperature, causing changes in the period  $\Lambda$  due to thermal expansion or contraction [65]. The fractional change in the Bragg wavelength due to temperature variations is given by:  $\frac{\Delta \lambda_B}{\lambda_B} = (a + \xi) \cdot \Delta T$ . Where  $a$  is the thermal expansion coefficient of the fibre and  $\xi$  is the thermo-optic coefficient [44].



The most important advantage of a sensor based on gratings over other sensing schemes is the self - referencing nature of the output. The shift in the wavelength of the grating is an absolute parameter and doesn't depend upon the total light level. This is reason for the considerable amount of research on multiplexing schemes based upon wavelength division addressing [29-41]. Researchers in the pursuit of sensing system based upon the wavelength shift to determine strain or temperature variations have obtained and quoted responses of wavelength shift to strain / temperature given below [35, 44, 49, 65].

$$\varepsilon = \left( \frac{1}{\lambda_B} \right) \frac{d\lambda_B}{d\varepsilon} \approx 0.74 \times 10^{-6} \mu\varepsilon^{-1} \text{ which relates to } 1.15 \times 10^{-3} \text{ nm}\mu\varepsilon^{-1}.$$

$$T = \left( \frac{1}{\lambda_B} \right) \frac{d\lambda_B}{dT} \approx 8.9 \times 10^{-6} \text{ C}^{-1} \text{ which relates to } 1.3 \times 10^{-2} \text{ nmC}^{-1}.$$

### 3.5 Fabrication Techniques.

The fibre Bragg grating is formed in the core of the fibre using a U.V. - induced refractive index change. If a Germanium doped fibre is exposed to U.V. light then photobleaching occurs at the oxygen deficient Ge-Si bonds and there is a change in the refractive index at the position of the photobleaching. The sensitivity of the doped fibre can be increased by pressure soaking the fibre in Hydrogen or using Boron and Germanium codoped fibre [66].

The corrugation of the index in the core is produced by the variation of intensity of the U.V. light from the interference pattern. The fabrication technique employs a Michelson interferometer arrangement but there are alignment problems using this approach.

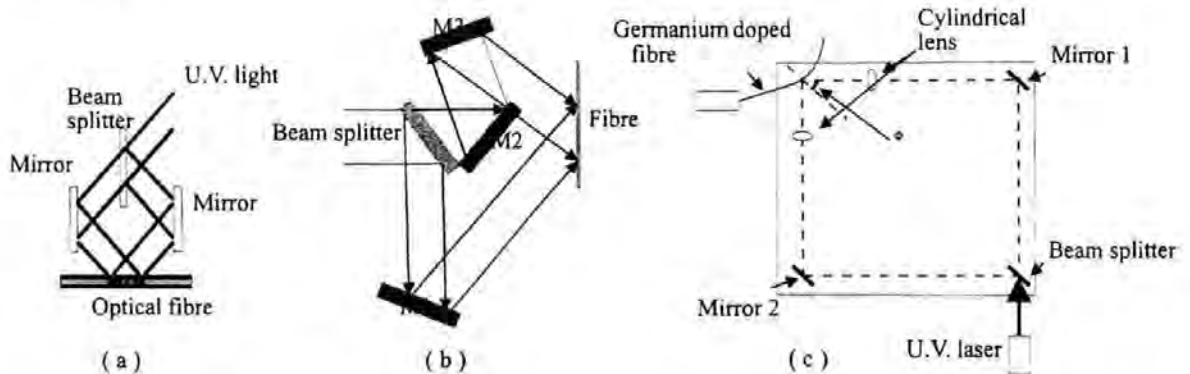


Figure (32) . Interferometric optical arrangements to fabricate gratings.

In Figure 32 all three diagrams shows various optical arrangements for the holographic side writing technique for producing fibre Bragg gratings. Figure 32c was the arrangement employed by G. Meltz et al [54].

Another technique uses a phase mask. Using a single pulse from a U.V. source such as an excimer laser in conjunction with a phase mask, a near - field intersection of two diffracted orders from a surface relief phase grating generates the field pattern. This requires only a concentrating lens plus the phase mask. This technique simplifies optical alignment, allows the use of short coherence - length lasers [67-70] and reduces the chance of mechanical misalignment due to vibration, see Figure 33.

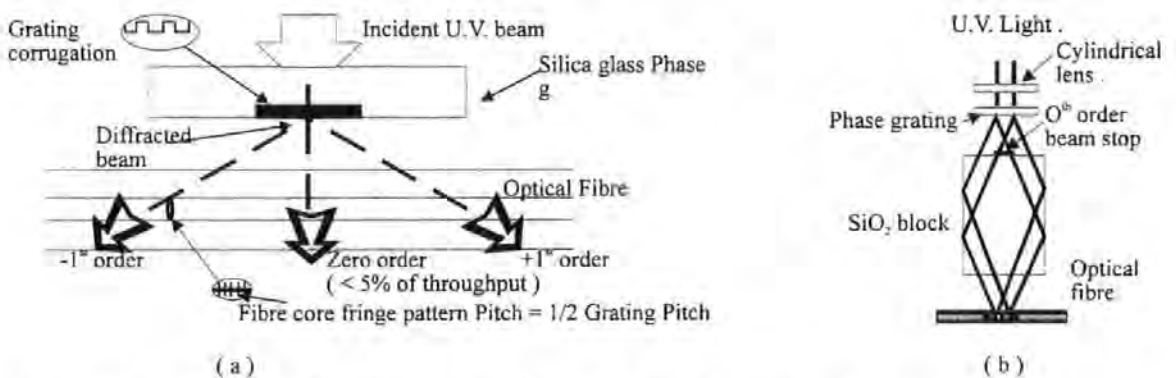


Figure (33) . The use of phase masks to fabricate fibre Bragg gratings.

A third technique is the prism interferometer method, which is a variation on the holographic method see Figure (34), [71].

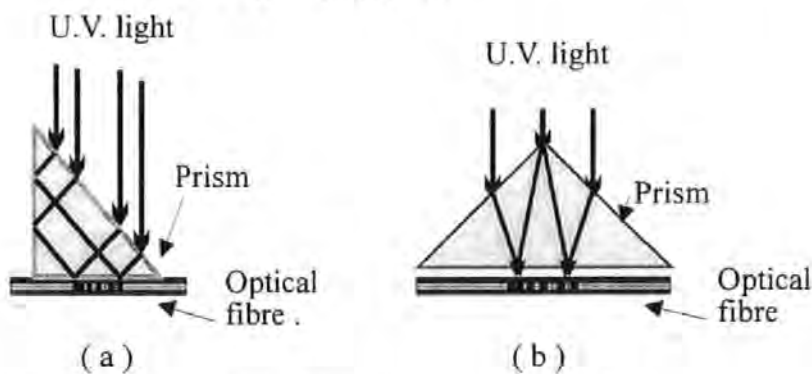


Figure (34) . The prism interferometric method.

The true mechanism of photobleaching is still not fully understood. Various explanations have been offered such as the Kramers - Kronig model, Dipole model and Compaction model [72-76]. It would seem that the Bragg grating formation in part is due to germanium oxygen deficiency centres. The germanium oxygen deficiency centres are photobleached by UV laser illumination and that this sensitivity to UV can be increased by

hydrogen loading of the optical fibre [66]. The dissolved  $H_2$  reacts at the Ge defect sites,  $GeO_2$  doped glass react with  $H_2$  molecule at a normal Si-O-Ge site resulting in the formation of a Si-OH bond and oxygen deficient Ge defects which both contribute to the refractive index change.

It is also believed [66] that an additional contribution to the refractive index change is densification of the glass structure initiated by the annihilation of the defects. The addition of Boron to the core of the fibre enhances the densification contribution to the induced change in the refractive index.

The fabrication techniques vary depending on the type of grating that is required. The fabrication techniques shown in Figure 34 are for uniform gratings. The fabrication of nonuniform gratings have the same basic optical arrangement but some additional apparatus is required to produce the tapering function for the refractive index or the chirp for the period of the perturbation, see Figure 35. The chirping of the effective grating period is accomplished by tapering the fibre diameter, by bending the exposed fibre, or the constant period interference pattern derived from two plane wavefronts of dissimilar curvatures [61].

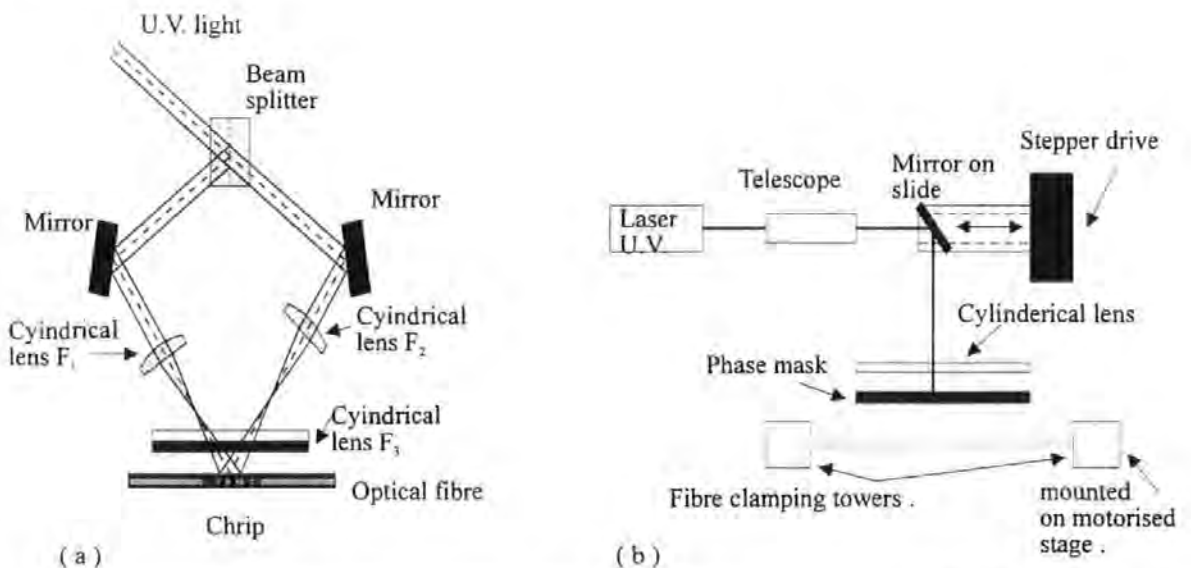


Figure (35) Some typical modification of the basic arrangement of the holographic technique to produce chirped fibre Bragg gratings.

### 3.6 Theoretical representation of fibre Bragg gratings.

#### 3.6.1 Methods used to obtain an analytical expressions for Bragg gratings.

The analysis of gratings was first developed as a means to understand the characteristics of the Distributed Feedback ( D.F.B. ) laser and the Distributed Bragg reflection ( D.B.R. ) laser. The analysis was then used to optimise the parameters that govern the behaviour of the D.F.B./D.B.R. lasers [77-79]. There have been several techniques used to predict the behaviour of a given kind / type of grating.

The general starting point for these methods is the mode coupled equations ( see appendix I ) .The mode coupled equations can be solved in some cases; these being a grating with a uniform period and a given tapering ( envelope ) function for the change in the perturbed refractive index ( see appendix III , II ) [56,57]. Problems arise when a chirp is introduced, a variation in period along the grating length.

Over the past several years there has been several techniques developed to solve the coupled mode equations with a nonuniform period along the grating length (chirp) . One approach to this problem is the development of a Riccati differential equation from the coupled - wave theory ( see appendix II ), then using a fourth order Runge - Kutta method to numerically evaluate the differential equation. H. Kogelnik [80,81] first used these techniques.

In some cases researchers have obtained closed form expressions for the spectral reflection profile of a chirped grating. An example of this is by J.B. Shellan et al [82]. Shellan's method is based upon a direct integration of the coupled mode equations using the method of stationary phase. In this technique the coupling coefficient  $\kappa(z)$  is evaluated at a point  $\kappa(z_B)$  and expanding the attenuation term;  $e^{-\alpha z}$  about  $z = z_B$  . Since the phase is a rapidly varying quantity except near  $z = z_B$  . The point  $z_B$  being the position where the Bragg condition is satisfied and mathematically is the point of stationary phase. The phase term is expanded around the stationary phase point. For the lossless case, the coupling coefficient is then expanded about the stationary phase point and integrated term by term. A similar method had been adopted by C.S. Hong et al [83]. In Hong's approach he combined the coupled mode equations to obtain second order differential equations and

solved these equations. The solutions of these equations were parabolic cylinder functions and using the asymptotic expansions of these functions found expression for reflectivity of a given chirped grating. It was found that the expressions derived by Hong et al were in good agreement with experimental data in the case where the Bragg condition applies but not close to Bragg condition edges. Other examples of this technique can be found in the literature; M. Matsuhara et al [84,85], T. Fukuzawa et al [86] B.Kim et al [87].

### 3.6.2 The perturbation approach to modelling a grating.

The perturbation technique is known also as the W.K.B. technique or phase - integral approximation. In a nonuniform grating there are regions where the field will have a strong interaction or a weak interaction. So the field in each propagating or evanescent region is written as the product of the local oscillatory or exponentially varying field and a slowly varying amplitude. The W.K.B. method is essentially a standard slowly varying amplitude analysis supplemented by a procedure to match the fields across the turning points between propagating and evanescent regions. This technique is used by L. Poladian [88] considering three separate effects; barrier tunnelling through evanescent regions, simple propagation ( weak interaction ) and end reflections from the grating itself. Again this method was adopted by J.E. Sipe [89]. This technique is good for selective structures and provides an accurate analytical approximation for the spectral reflective profile of a given grating. Otherwise more approximations of the phase integral are required.

### 3.6.3 Rouard's Method.

Another approach to solve this problem is using Rouard's method [90,91]. Rouard's method is a recursive technique that is widely used in the thin-film design to extend the derivation of the reflection coefficients for a single layer to the case of multilayer films. The fundamental step in this technique is the replacement of a thin-film layer characterised by an effective complex reflectivity by a single interface having the same properties. In this approach the amplitude reflectivity of each period of the grating are found; instead of solving coupled mode differential equations for the entire grating including any period variation. There is only a need to solve the equations once to obtain

the reflectivity of a single grating period using the general expression for amplitude reflectivity derived from the coupled mode theory.

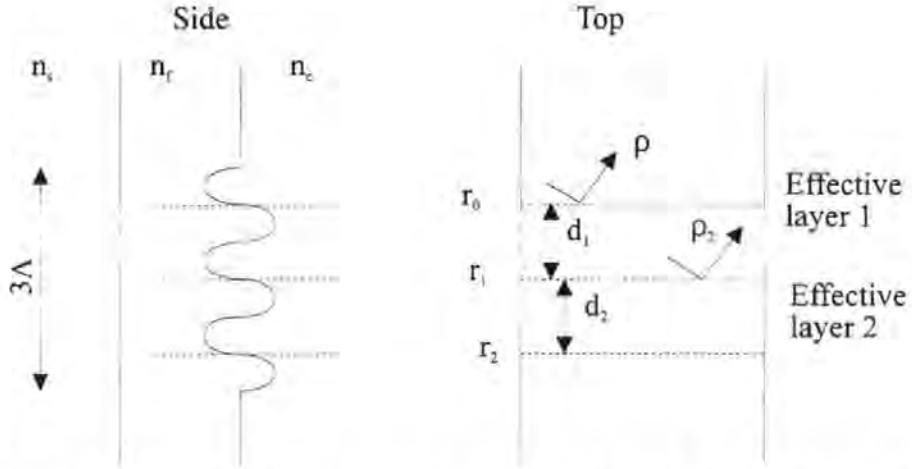


Figure (36) . Schematic drawing showing side and top views of a small grating using Rouard's method.

Figure 36 shows a three-period periodic waveguide grating of length  $3\Lambda$ , illustrating the application of Rouard's method. The reflectivities of the effective interfaces are given by  $r_0$ ,  $r_1$  and  $r_2$ . The complex reflectivity layer is defined by  $\rho_2$ ; that of the entire grating is given by  $\rho$ . Using the grating described in Figure 36 starting with the second effective layer gives an effective Airy equation which is applied to determine the effective complex reflectivity of the layer.

$$\rho_2 = \frac{r_1 + r_2 e^{-2i\Delta_2}}{1 + r_1 r_2 e^{-2i\Delta_2}}$$

The recursive nature of this technique implies that the Airy equation is used once again by Rouard's method to find the complex reflectivity of the entire grating;

$$\rho = \frac{r_0 + \rho_2 e^{-2i\Delta_1}}{1 + r_0 \rho_2 e^{-2i\Delta_1}}$$

where  $\Delta_k$  is the phase shift occurring on traversal of the  $k^{\text{th}}$  layer. This method was first used by L.A. Weller-Brophy et al [90] and it was found that the predictions made were in good agreement with the results obtained from coupled-mode theory using Kogelnik's approach [80]. A comparison between the two techniques is given by L.A. Weller-Brophy and D.G. Hall [91].

#### 3.6.4 Alternative methods to model Bragg gratings.

There are a number of methods available for finding solutions to the coupled mode equations. A brief mention will be made of the other methods. G.H. Song et al [92,93] for example, uses an inverse-scattering method known as Gel'fand - Levitan - Marchenko inverse-scattering method. Using scattering data the shape and / or the characteristics of a scatterer can be obtained. This method is similar to electronic filter design using s-parameters. Yet another approach is the resonance mode expansions. This method is basically derived from how waveguide modes in waveguide-mode theory behave. The general solution for wave propagation down a linear waveguide can be expressed as a superposition of its waveguide modes. So a nonuniform grating is considered as a resonator, which resonates at several of these modes as opposed to a single mode for a uniform grating, and the response is considered as a superposition of those resonant modes. The quantity analogous to the propagation constant of a waveguide mode is the characteristic or resonant frequency of the grating resonance mode. These resonant frequencies relate to reflection and transmission bands of a grating, this method was developed by L. Poladian [94].

#### 3.6.5 T-Matrix Formalism of fibre Bragg gratings.

T - matrix formalism is a method derived from the work of D. Kermisch [95,96] on the analysis of hologram gratings and was proposed by M. Yamada and K. Sakuda [97,98] for detailed studies of D.F.B. lasers and then later used by S. Huang et al [99] for fibre Bragg gratings. This technique has become a useful tool for characterising a given profile of a nonuniform grating. In this approach the fibre grating is divided into short segments which are assumed to be periodic. In each segment of the grating the coupling coefficient, grating phase and deviation from the Bragg condition are constant and independent of the position along that section of the grating length. These sections of the grating are then characterised by a scattering matrix. The multiplying of each scattering matrix in succession with the proper grating phase conditions at the interface between the successive matrices obtains the complete grating response.

The scattering matrices are derived later in this report and this T - matrix formalism approach is used to predict response of particular kinds of gratings.

### 3.7 Development of a theoretical model of a Fibre Bragg grating ( a spectral reflection response with no longitudinal strain ).

The first step in the development of the theoretical model was to consider a uniform Bragg grating. For a uniform Bragg grating a closed analytical expression can be derived from the coupled-mode equations ( see appendix I ), [56,57] .This expression being

$$R = \frac{\kappa^2 \sinh^2(Ls)}{s^2 \cosh^2(Ls) + \left(\frac{\Delta k}{2}\right)^2 \sinh^2(sL)}$$

Where

$R$  is the reflectivity of the grating.

$k$  is the coupling coefficient  $\kappa = \frac{\Delta n \pi}{\lambda}$

$\Delta k$  is the detuning parameter from the Bragg condition  $\Delta k = 2k_0 - \delta$

with  $k_0 = \frac{2n_{eff}\pi}{\lambda}$  and  $\delta = \frac{2\pi}{\Lambda}$ .

$s$  is a parameter of convenience  $s = \sqrt{|k|^2 - \left(\frac{\Delta k}{2}\right)^2}$  and  $L$  is the length of the grating.

Using a Mathcad +6 environment a procedure for the T - matrix formalism and the other techniques was produced. A theoretical comparison between the numerical procedures and the known solution of a uniform Bragg grating were made Figure 37.

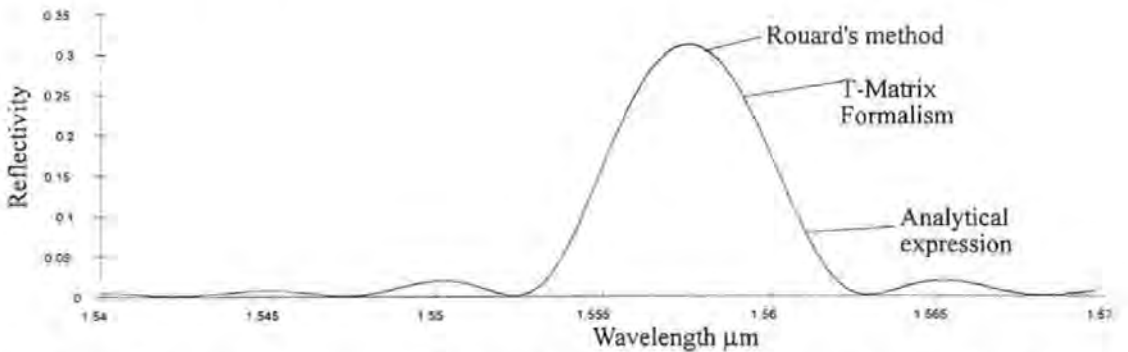


Figure (37) . Spectral response of a given Bragg grating structure obtained from three methods.



Figure 37 shows the results from three of the techniques. The structure chosen in this case has no chirp with an initial / constant spatial period of  $\Lambda = 520$  nm and a total length of  $1.56 \times 10^{-4}$  metres and index of modulation of 0.001. These results were also checked with the formula in section 3.1 for the grating peak reflection and its total bandwidth.

Introducing a linear chirp into the period of the Bragg grating complicates the situation to obtain a true closed analytical expression which still requires introducing approximations ( see section 3.5 and refs [72-76] ). Using the Mathematica 2.2 environment it was possible to produce a solution to the coupled mode equations with a linear chirp in the period of the grating ( see appendix III ). Again this is used to confirm the T-matrix formalism and the other techniques being used. A comparison was performed between the various methods and good agreement was observed. Figure 38 shows a reflectivity plot using the four techniques being used with good agreement.

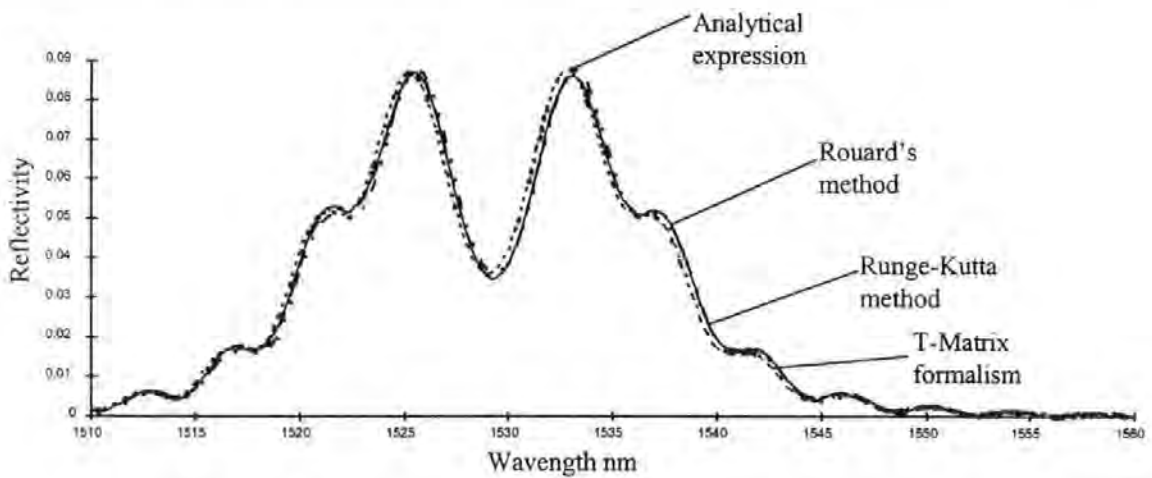


Figure (38) . The spectral reflection responses of a linearly chirped Bragg grating with a uniform  $\Delta n$ , obtained from four methods.

The parameters for the grating that gives the spectral reflection response shown in Figure 38 is as follows, the initial spatial period of the grating is  $\Lambda(z=0) = 492$  nm, a total grating length of  $1.989 \times 10^{-4}$  metres approximately, index of modulation of  $\Delta n = 0.003$  and a chirp factor of  $F = 0.02$  nm change per period of the grating .

### 3.7.1 The chirp factor for a linearly chirped Bragg grating.

The chirp factor for the analytical expression and the Runge-Kutta technique has a different definition to that of the T-matrix formalism and Rouard's method. All the techniques start with the coupled mode equations but for the analytical approach and the Runge-Kutta method. The spatial variation of the period along the grating length for a linear chirp is defined as

$$\frac{2\pi}{\Lambda(z)} = \frac{2\pi}{\Lambda(0)} - 2\gamma z$$

where  $z$  is the distance along the grating not to be confused with length  $L$ .

The coupled mode equations become;

$$\frac{dA}{dz} - i\delta A = -i\kappa B \exp(i\gamma z^2)$$

and

$$\frac{dB}{dz} + i\delta B = i\kappa A \exp(-i\gamma z^2)$$

with  $A$  and  $B$  being the complex amplitudes and  $\delta = \pi/\Lambda(0) - \beta$ ; the phase mismatch factor, see refs. [56,57] and appendices I, II.

In the T-matrix formalism the chirp factor is defined as the rate of change of the period per period of the fibre Bragg grating;

$$\Lambda(z) = \Lambda(0) + \frac{F}{\Lambda(0)} \cdot z$$

So conversion between the two chirp factors is as follows.

$$\frac{2\pi}{\Lambda(z)} = \frac{2\pi}{\Lambda(0)} - 2\gamma z$$

which maybe written as

$$\frac{\Lambda(z)}{2\pi} = \frac{\Lambda(0)}{2\pi - 2\gamma z \Lambda(0)}$$

therefore

$$\Lambda(z) = \Lambda(0) \left[ 1 - \frac{\gamma \Lambda(0)}{\pi} \cdot z \right]^{-1}$$

If the changes in  $\Lambda(z)$  are small then

$$\Lambda(z) \sim \Lambda(0) \left[ 1 - \frac{\gamma \Lambda(0)}{\pi} \cdot z \right] = \Lambda(0) - \frac{F}{\Lambda(0)} \cdot z$$

thus

$$\gamma = \frac{\pi}{\Lambda(0)^3} \cdot F$$

The theoretical models used [80,85,90,99] have produced good agreement with each other and has given confidence in the spectral reflection profiles predicted by the various techniques. A number of types of Bragg grating structures have been used with the various approaches to obtain the spectral responses, these include uniform period with a uniform perturbation in refractive index, a linear chirped period and uniform perturbation of  $\Delta n$  and uniform period with a taper function for the perturbation of  $\Delta n$ . Also chirped period and uniform  $\Delta n$  gratings in a Fabry - Perot configuration. This has been confirmed using some experimental gratings.

### 3.7.2 Spectral Reflective response of a fibre Bragg grating under longitudinal strain.

This is achieved by incremented increases of the grating period and calculating the reflection response of the grating at a specific wavelength. This is repeated for a range of increased values of the grating period. The incrementation of the period is of a few micro-strains, so for a constant period  $\Lambda_0$  becomes

$$\Lambda_0 \rightarrow \Lambda_0 (1 + inc \cdot 10^{-6})$$

For a chirped grating this would become

$$\Lambda(z) \rightarrow \left( \Lambda_0 + \frac{F}{\Lambda_0} \cdot z \right) (1 + inc \cdot 10^{-6})$$

The resultant behaviour of the gratings to this simulated longitudinal strain is to shift the spectral reflection response to longer wavelengths. This is to be expected because of the behaviour of a uniform grating [37,65]. An example of this is shown in Figure 39.

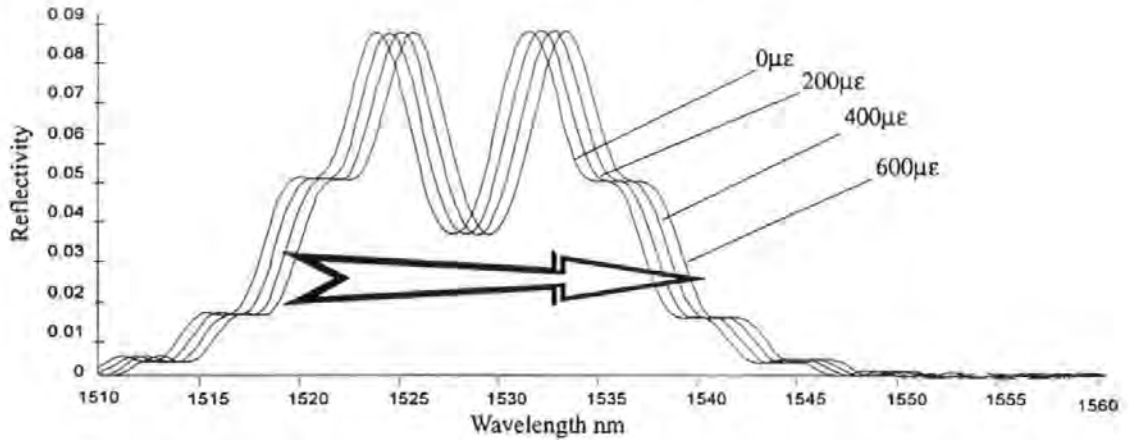


Figure (39) . The predicted effects of longitudinal strain on a linearly chirped Bragg grating.

The parameters used to produced these graphs are the same has in Figure 38. The method used to produce the predictions is the T- Matrix formalism. Further studies of various types and designs of fibre Bragg grating were carried out using the T-matrix formalism to investigate the spectral reflection response with and without longitudinal strain. There are several reasons for pursuing the investigation with the T matrix formalism, one of these being there are fewer approximations made than the Runge - Kutta method. Secondly, a more physical understanding of the structures under inspection is obtainable than using the solutions obtained for the coupled-mode equations with a linear chirp. So considering a combination of gratings with chirps, the solution becomes even more complex and there is a general loss of physical understanding of how the light is acting with the grating. The choice between the T- matrix formalism and Rouard's method is one of personal preference. Rouard's method is not too dissimilar to the matrix procedure. The matrix procedure is more intuitive when taking into account a tapering function for the refractive index perturbation and the effects of the longitudinal strain upon the refractive index of the fibre Bragg grating [65]. This being the strain optics effect [25,28,103];

$$n(z) = n - \frac{1}{2}n^3 \left[ P_{12} - \nu(P_{11} + P_{12}) \right] \varepsilon_z(z)$$

The definitions can be found in section (1.4) .

### **3.8 Simulations of Fibre Bragg grating.**

The various techniques employed to solve these coupled-mode equations had been constructed in software environments to try and improve accuracy and computational run-time. These being Mathcad +6 for Rouard's method, the T- matrix formalism for the uniform Bragg grating ( Appendix IV ) and used Mathematica 2.2 to obtain the solution for a linearly chirped Bragg grating. The Runge - Kutta method was in FORTRAN 90 code, using this method no or little physical interpretation could be made. Also the Runge - Kutta method was the worst-case approximation method to be used, in computer run-time compared to the other techniques, this because of the number of iterations required to obtain a result comparable to the other methods used. Several Mathcad files were generated for the above techniques ( see appendices IV ). It was found that using a Mathcad environment was a serious drain on the computer resources and limited cases were used due to the lengthy time taken to run the simulation. This was true for both models used in the Mathcad +6 environment and the other package used, the reason for this was the limited computational computer power available. Adapting the Mathcad +6 programs increased the scope of the investigation but was restrictive, as the run-time required was of the order of a few hours.

To decrease the running time and free the computer resources for the calculations, a C program was developed using the T-matrix formalism ( see appendix VI for program listing ). This allowed more complicated structures to be studied. For example, chirped, tapered or apodisation gratings or a combinations of these features in one grating. In addition the behaviour of different gratings in series can be addressed.

#### **3.8.1 Flexibility of C program for the T-Matrix formalism.**

The model developed can take into account the various types of gratings that experimentalists can fabricate. For example a chirped period, tapering function of the refractive index perturbation in a single grating. A resonator can be formed by two identical gratings in series along a fibre length separated by some distance of normal fibre. Other alternative arrangements of gratings can, and have been, considered. For example, a series of gratings with a continuous or noncontinuous phase relation between each grating (

see Figure 40 below as an example ). The spectral reflectivity response is obtained in an output file and if required an output file, which contains the DC intensity variation at a specific wavelength ( $\lambda$ ) with a variation in the longitudinal strain, subjected to a grating type and / or structure. This file is used has an indicator that this response of a grating arrangement can use the prescribed signal-processing technique ( see appendix V ) where the response of the signal processing technique is calculated in a Mathcad program using the parameters of the system. Also a more complicated grating structure, a sinusoidal time variation, perturbation centred at  $\lambda$  is introduced into the model to see if the harmonics generated from the structure can be used and allow the extraction of some useful information by the prescribed signal processing technique.

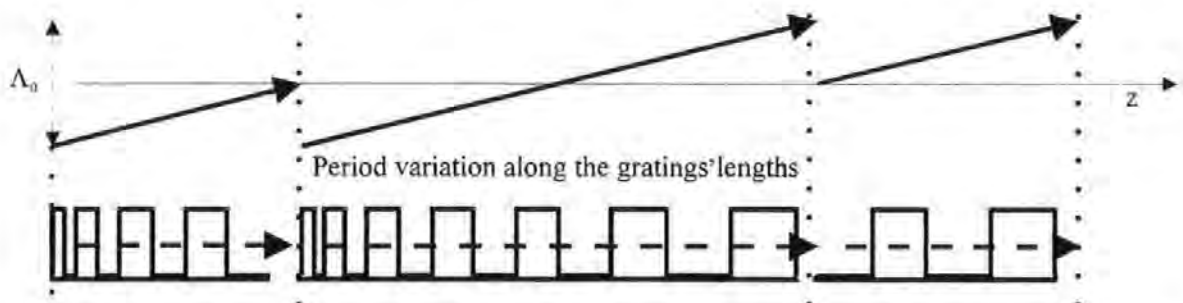


Figure (40) . The period change along the length of three gratings that have a continuous phase relationship between each grating, ( with uniform  $\Delta n$ ).

### 3.8.2 Implementation of the C program for T-Matrix formalism.

There are several parameters that need to be fed into the simulation.

These are:

**n0** : The original core refractive index of the optical fibre.

**n11** : The perturbed core refractive index of the optical fibre.

**F** : Chirp factor ( nano metres ), the rate of change of the period per period. This is an option, with or without chirp.

**Para** : This is a tapering function for the grating perturbed core refractive index, which can also be uniform . The choices in this category are, for example, a Gaussian envelope function or a top hat function ( using tanh functions) see Figures 41 and 42 below.

**lam0** and **laminc** : These are the values that govern the range and the incremental change in the wavelength ( for spectral response ).

**Lambda** : This being the initial spatial period of the grating in the case of a chirp being used or is the spatial period of the grating for a uniform structure.

**Wave\_str** : This gives a choice of simulation to produce a spectral response or the grating response to longitudinal stain.

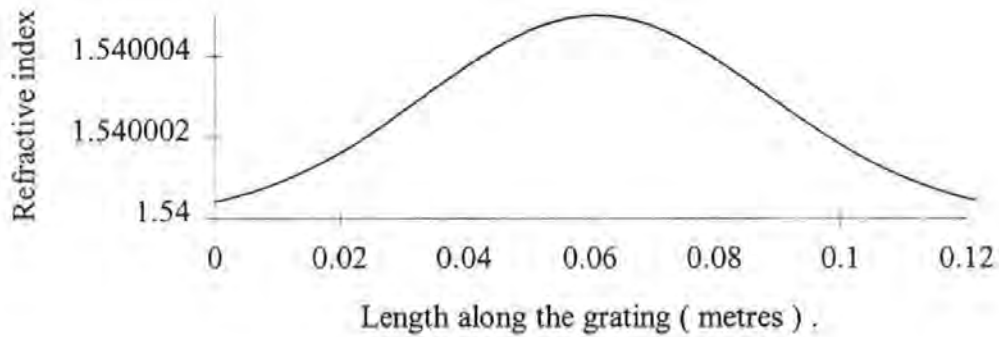


Figure (41) . Gaussian index variation along a Bragg grating length; a taper function for the refractive index, thus  $\Delta n$ . The width of the Gaussian is arbitrary and depends upon the intensity profile of the U.V. laser source.

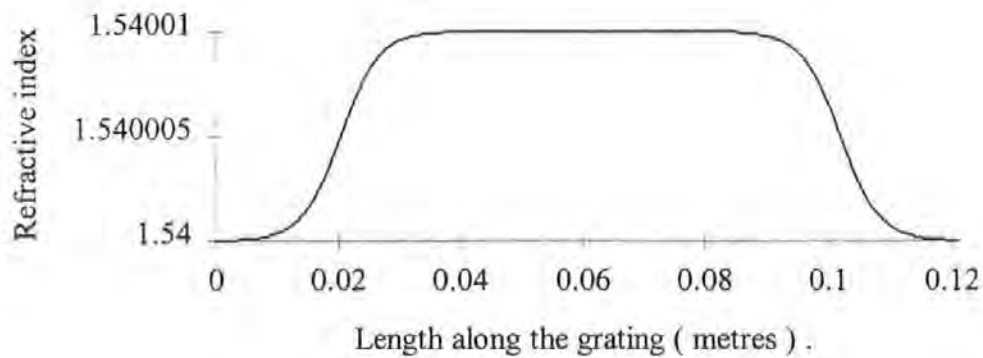


Figure (42) . A TopHat taper function ( this is generated using tanh functions ) for the refractive index, thus  $\Delta n$  variations along the grating length .

Figure 43 below shows a general application of the program with options on the  $\Delta n$  variation per grating or all gratings i)  $\Delta n$  uniform ii) Gaussian  $\Delta n$  per grating iii) single Gaussian  $\Delta n$  for the structure.

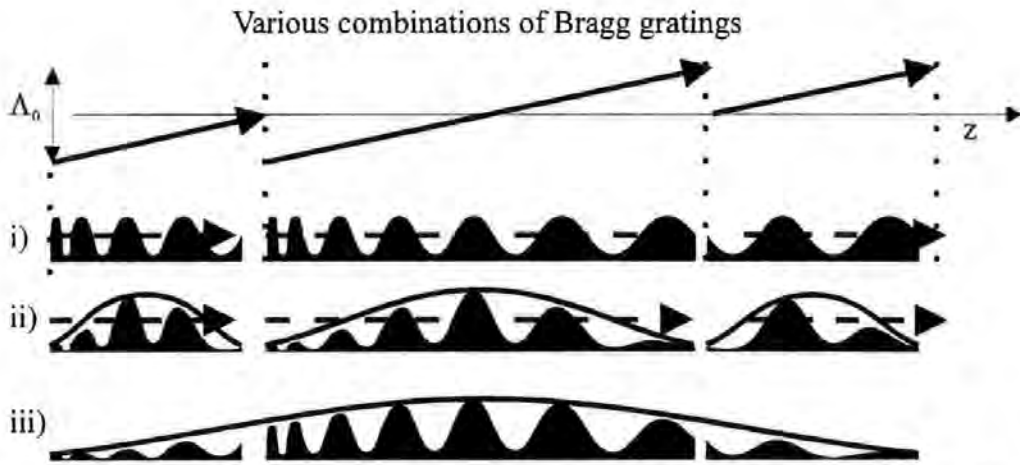


Figure (43) . Some of the various taper functions for refractive index modulation;  $\Delta n$ , with a linear chirp. i) uniform  $\Delta n$ , ii) single Gaussian  $\Delta n$ , iii) combination of three Gaussian  $\Delta n$ 's.

The length of the grating is obtained by inputting the total number of periods in the grating;  $z$ . Following this there is an option on how many calculations are required per period. Sub-dividing each period of the grating into smaller sections to increase the accuracy of the calculations; **SubM**, see Figure 44.

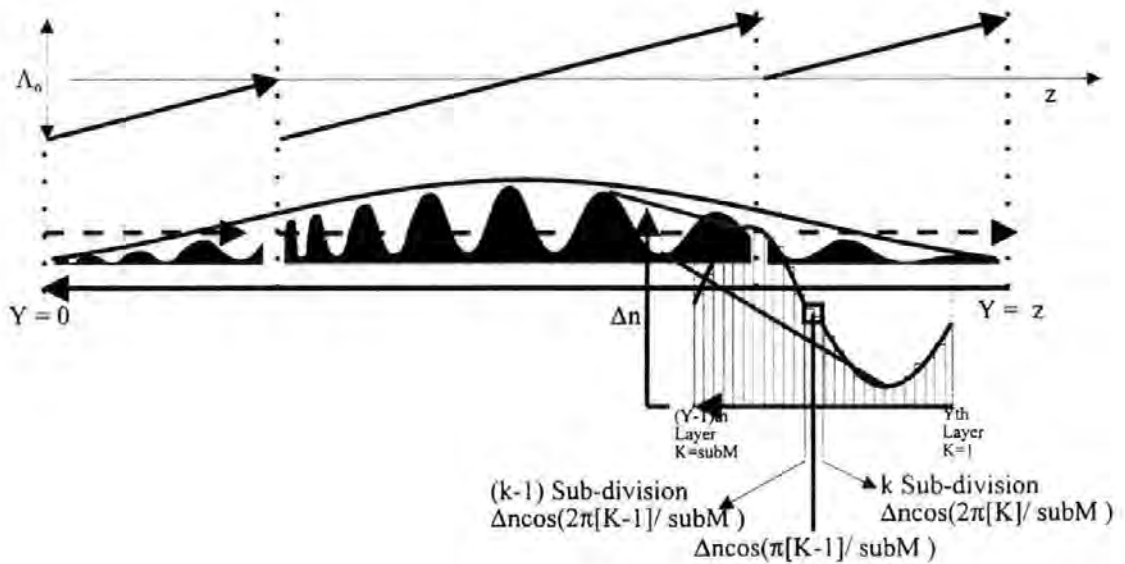


Figure (44) . The procedure for sub-dividing a period of the grating.

The above parameters define the grating or gratings. The pattern and type of chirp of the grating must be changed at the code level ( see appendix VI for listing of program ). There have been various types of patterns of linear chirps and quadratic chirps; see for examples in Figure 45.



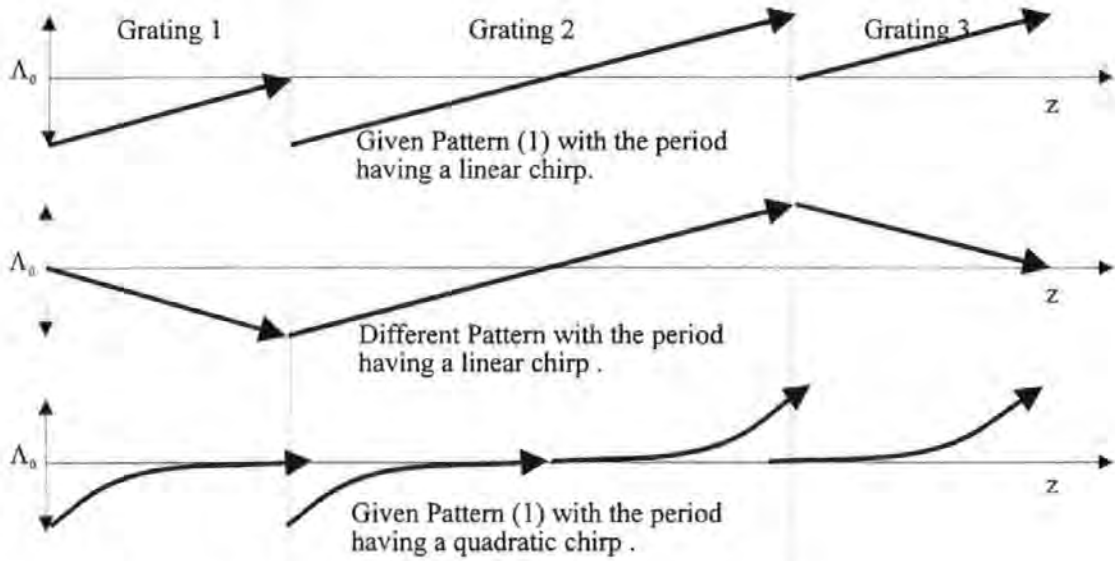


Figure (45) . The variation in chirp obtainable with the C program.

The implementation of the Bragg condition has to be separated into three regimes because of functions that govern the behaviour of the grating. These being hyperbolic and the argument of the hyperbolic functions involve square roots which can be complex, real or zero, depending upon the  $s$ -parameter or the phase mismatch between the Bragg resonance of the grating and the illuminating light on the grating. From appendix I on the T-Matrix formalism the functions that represent the scattering matrix for each segment are:

$$\begin{bmatrix} a(0) \\ b(0) \end{bmatrix} = \begin{bmatrix} T_{11} & T_{12} \\ T_{21} & T_{22} \end{bmatrix} \begin{bmatrix} a(l) \\ b(l) \end{bmatrix}$$

where

$$T_{11} = T_{22}^* = \frac{\Delta\beta \sinh(sl) + is \cosh(sl)}{is} \exp(-i\beta_0 l) ,$$

and

$$T_{12} = T_{21}^* = \frac{\kappa \sinh(sl)}{is} \exp(i\beta_0 l) .$$

and  $s$  is defined as  $s = \sqrt{|\kappa|^2 - \Delta\beta^2}$

where  $\kappa$  and  $\Delta\beta$  have the usual definition ( appendix I )

These functions above determine the spectral response of the grating and the response of the grating due to longitudinal strain.

Three conditions are defined in the C program has follows:

( Condition one )  $|\kappa|^2 > \Delta\beta^2$

$$T_{11} = \left[ -i \frac{\Delta\beta}{s} \sinh(sl) + \cosh(sl) \right] \cdot \left( \cos(\beta_0 l) + i \sin(\beta_0 l) \right)$$

and

$$T_{12} = -i \frac{\kappa}{s} \sinh(sl) \left( \cos(\beta_0 l) + i \sin(\beta_0 l) \right)$$

( Condition two )  $|\kappa|^2 < \Delta\beta^2$

Changing the variable from  $s = \sqrt{|\kappa|^2 - \Delta\beta^2}$  to  $s' = \sqrt{\Delta\beta^2 - |\kappa|^2}$

so  $s = is'$

thus  $T_{11}$  becomes

$$T_{11} = \left[ -i \frac{\Delta\beta}{is'} \sinh(is'l) + \cosh(is'l) \right] \cdot \left( \cos(\beta_0 l) - i \sin(\beta_0 l) \right)$$

but  $\sin(ix) = -i \sinh(ix)$  and  $\cos(x) = \cosh(ix)$  so  $T_{11}$  and  $T_{12}$  becomes:

$$T_{11} = \left[ \frac{-i\Delta\beta}{s'} \cdot \sin(s'l) + \cos(s'l) \right] \cdot \left( \cos(\beta_0 l) - i \sin(\beta_0 l) \right)$$

and

$$T_{12} = \left[ \frac{-i\kappa}{s'} \cdot \sin(s'l) \right] \cdot \left( \cos(\beta_0 l) + i \sin(\beta_0 l) \right)$$

( Condition three )  $|\kappa|^2 = \Delta\beta^2$

Using the series expansion for sinh and cosh;

$$\sinh(x) = x + \frac{x^3}{3!} + \frac{x^5}{5!} + \dots, \text{ and } \cosh(x) = 1 + \frac{x^2}{2!} + \frac{x^4}{4!} + \dots$$

$T_{11}$  and  $T_{12}$  become:

$$T_{11} = [-i\Delta\beta l + 1] \cdot \left( \cos(\beta_0 l) - i \sin(\beta_0 l) \right)$$

and

$$T_{12} = [-i\kappa l] \left( \cos(\beta_0 l) + i \sin(\beta_0 l) \right)$$

For more details of the C program see appendix VI for code listing.

### 3.8.3 Technique to predict how a Bragg grating under longitudinal strain behaves using the signal processing technique.

The C program produces several output files. One is the response of the grating at a single wavelength  $\lambda$  to varying amounts of longitudinal strain. In the strain-monitoring system, the D.F.B. laser is modulated at a frequency  $\omega_0$  centred at  $\lambda$ . So instead of irradiance at  $\lambda$  it becomes:

$$\lambda(t) = \lambda + \Delta\lambda(i(\text{Drive}, \text{Modulation}))\sin(\omega_0 t)$$

Where  $\Delta\lambda$  is dependent upon the parameters of the drive circuit for the D.F.B. laser and the magnitude of the input modulation signal to the drive circuit. Several approaches were adopted depending upon the proposed structure under investigation. These methods are outlined here but more detail of the approaches is given in appendix V.

The time variation is taken into account in the C program for the more complicated structures under consideration by replacing  $\lambda$  by  $\lambda(t)$  and generating an output file which contains the response of a grating under longitudinal strain being irradiated by  $\lambda(t)$ . The values of the irradiance in the output file are taken at given time intervals, determined by the operator of the program ( Note :- changing the sampling rate is done at the code level ). This file is used by a Mathcad +6 program ( see appendix V ) to obtain the magnitude of the first, second and third harmonics of  $\omega_0$  present in the response of the grating. This was found to be a drain on the computer resources and the run-time was very long for the simulation. An alternative approach was adopted, using just the  $\lambda$  and a Mathcad +6 program to obtain data when a sinusoidal perturbation of wavelength dependent upon time is put upon the DC response of the grating. Finally extracting the magnitudes of the harmonics from these data points is performed within this program ( see appendix V ).

For Bragg gratings in a Fabry - Perot configuration ( Bragg grating resonator ) yet another approach was used. The C program is run with a single wavelength  $\lambda$ . The output file contains the DC levels of the irradiance from the Bragg grating resonator. The Bragg grating resonator response is modelled exactly like the fibre Fabry Perot response. Another Mathcad +6 program is used to obtain the response of the system using the prescribed signal process method, to see if the sensor and signal processing can produce meaningful results ( see appendix V ).

## 4 The fibre Bragg grating resonator.

### **4.1 The fibre Bragg grating resonator.**

An alternative method to using thin - film dielectric coatings to form Fabry - Perot resonator mirrors is the use of two identical fibre Bragg gratings. Figure 46 shows a schematic diagram of the arrangement. A theoretical study [101] and methods of fabrication, using the side-writing technique [100,102] of a resonator has been done.

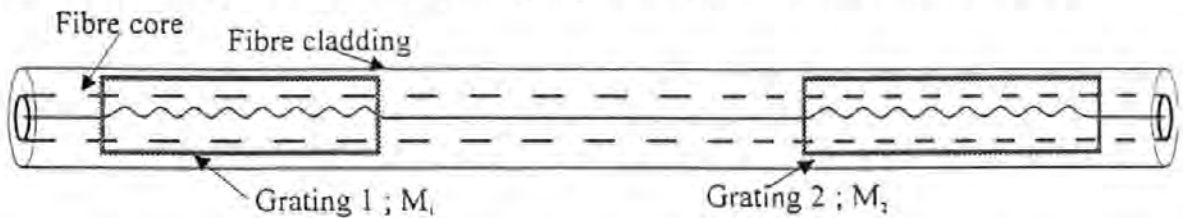


Figure (46) . A Fabry Perot resonator, using two identical gratings as the effective mirrors.

The resonator can be narrow or broadband depending on the grating structure but to act as a resonator, the wavelength of the irradiance illuminating the structure must fall within the spectral bandwidth of the gratings, which are acting as mirrors. The signal generated by the device subjected to strain is then of the same form as that of the previous sensor, which had reflective mirrors allowing the same signal processing to be used.

### **4.2 A Bragg grating resonator with a 27nm bandwidth and gratings having identical reflectivities of five percent ( spectral response ).**

A Bragg grating Fabry Perot resonator or just Bragg grating resonator was fabricated using the following design specification.

A bandwidth ~ 30 nm.

Mirror ( grating ) reflectance 5%.

Nominal central wavelength 1550 nm.

Grating separation 6 cm.

Spectral reflectance measurements were provided by the fabricators, Figure 47. Using their data, additional information was generated, using the C program of the T-matrix formalism, in the form of a spectral response curve, Figure 48.

$\Delta n = 0.002$ , Chirp factor = 0.013 nm change per period.

An initial spatial period of refractive index perturbation  $\Lambda(0) = 510 \text{ nm}$ .

Grating length =  $5.04 \times 10^{-4} \text{ m}$ .

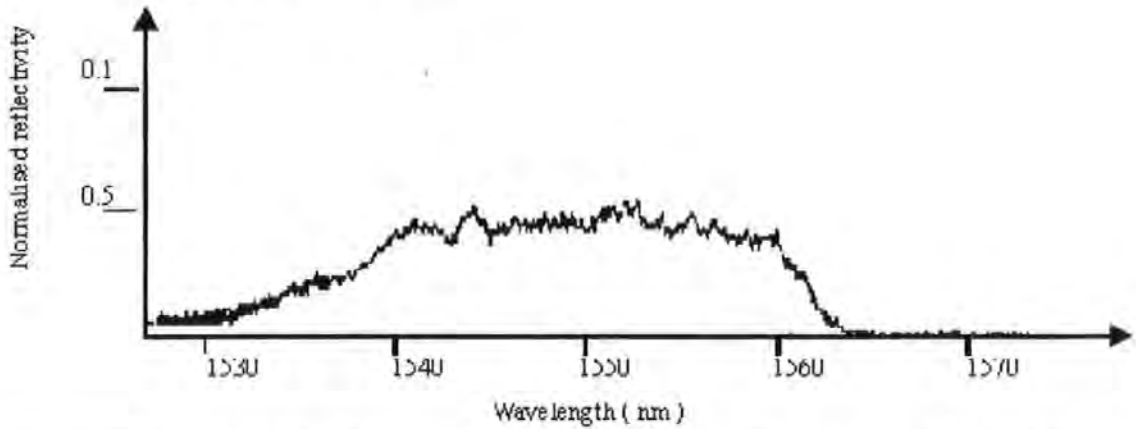


Figure (47) . Measured reflectance of one 5% grating used in resonator ( 24-4-71 ) using an optical spectrum analyser Hewlett Packard 7004A O.S.A.

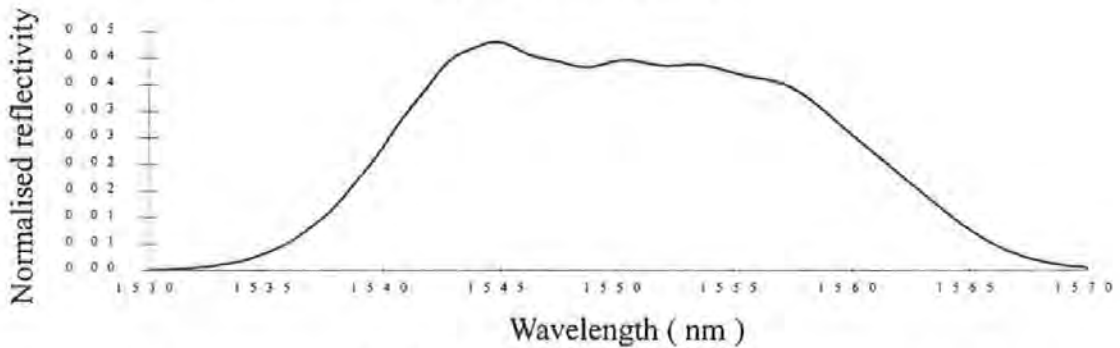


Figure (48) . The theoretical reflectance of the 5% grating shown in Figure 47.

It was not possible to measure, using the optical spectrum analyser, the fine detail of the spectral response of this 5% grating resonator (a separation of 6cm between the gratings ). This was due to a lack of resolution of the instrument.

A theoretical prediction of this fine detail is shown on Figures 49a and 49b. This was obtained by using the C program for the T-matrix formalism.

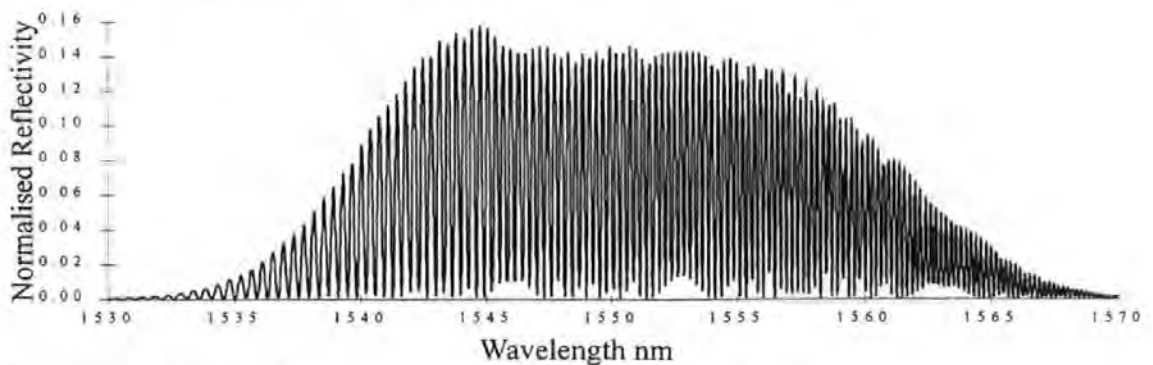


Figure ( 49a ) . The theoretical spectral response of a grating resonator, using two identical single gratings with  $R \sim 5\%$  and 27 nm bandwidth.

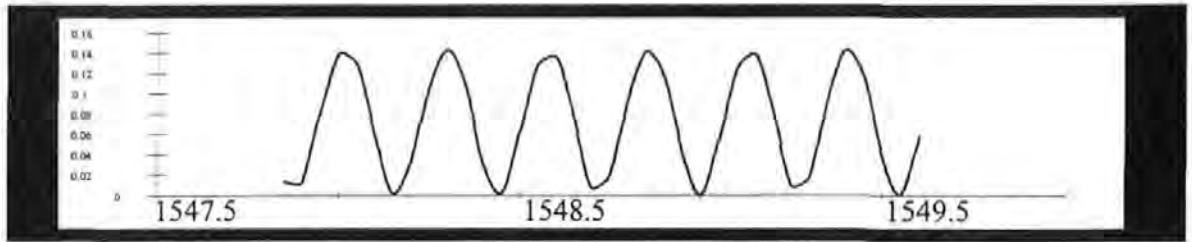


Figure (49b) . An expanded version of Figure 49a, showing the sinusoidal behaviour of the resonator to a variation in wavelength.

### 4.3 A Bragg grating resonator with a 27nm bandwidth and gratings of identical reflectivities, ten percent ( spectral response ).

A second resonator was fabricated with the same specification but with the gratings reflectance increased to 10 %.

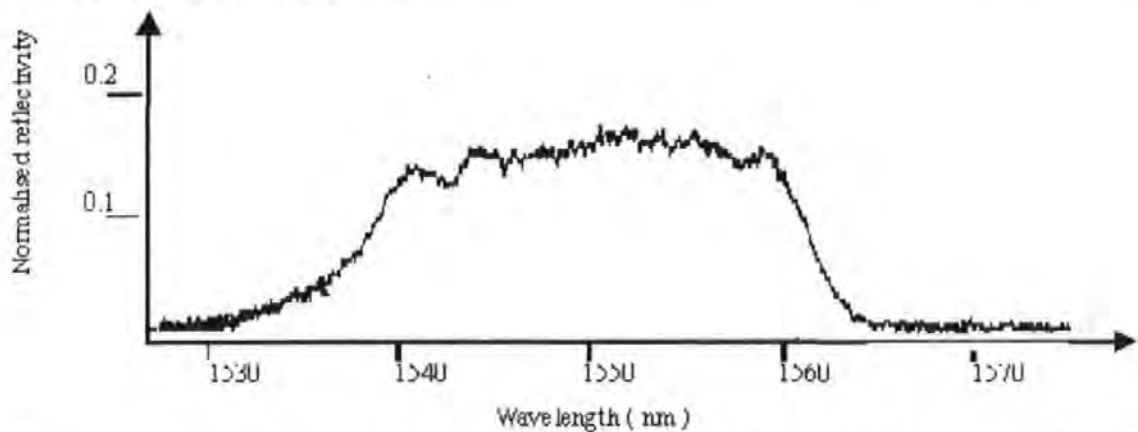


Figure ( 50 ) . The measured reflectance of one 10% grating used in resonator( 24-4-71 ). This was obtained from an optical spectrum analyser (Hewlett Packard 7004A O.S.A.).

The same procedure was adopted for this resonator as for the previous one. A reasonable match was again found between the experimental data Figure 50, and the theoretical response Figure 51. In this case a value of  $\Delta n \sim 0.003$  is used in the C program for the T matrix formalism.

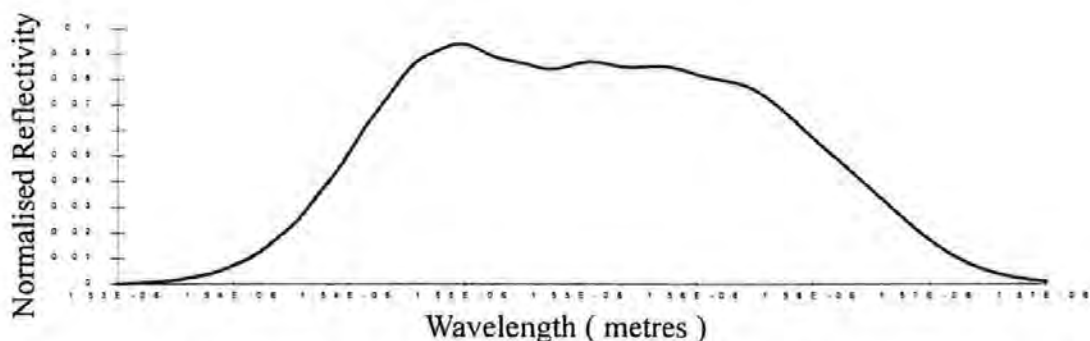


Figure (51) .The theoretical spectral response of the grating of Figure 50 using the T matrix formalism C program.

Again it was not possible to display the fine detail for this 10% gratings in a Fabry-Perot configuration with a separation of 6cm between the gratings. Figures 52a and 52b show the theoretical response of a Fabry-Perot resonator formed from two identical 10% reflectance Bragg gratings with a 6cm separation.

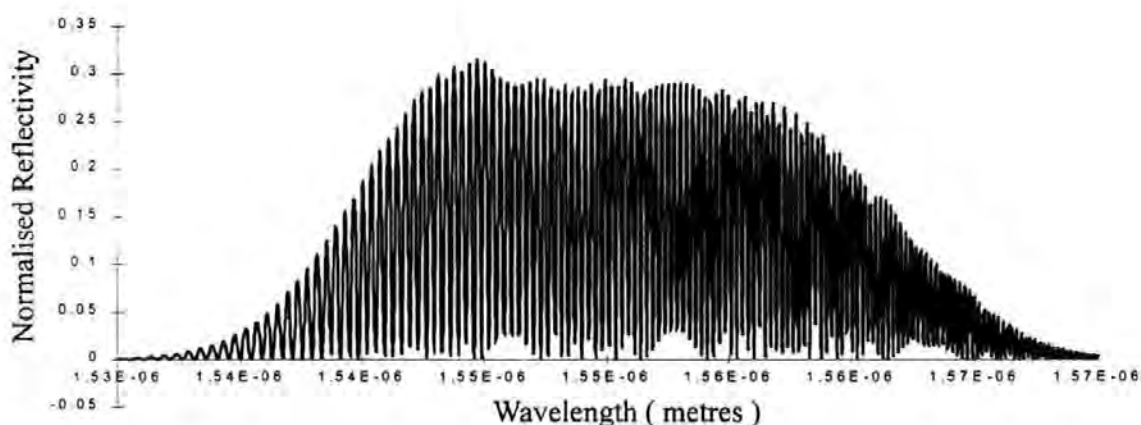


Figure (52a) . The theoretical spectral response of a grating resonator, using two identical single gratings with  $R \sim 10\%$  and 27nm bandwidth.

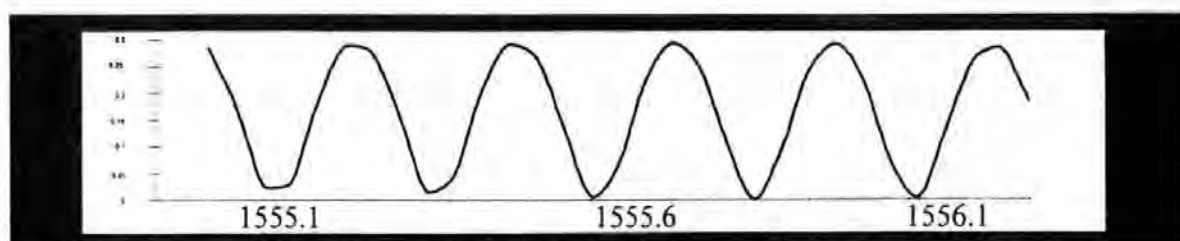


Figure (52b) . An expanded version of Figure 52a. Note the deviation away from sinusoid as a function of wavelength. This demonstrates a normal behaviour of a F.F.P. sensor as the mirror reflectance increases.

#### 4.4 Theoretical reflectivity response with longitudinal strain.

A theoretical response of the reflectance as a function of longitudinal strain of the described resonator using the parameters for the 5% reflectance Bragg grating are given below in Figures 53a and 53b. The optical radiation source used in the calculation is assumed to be monochromatic in wavelength. The procedure to obtain these results is shown in appendix V.

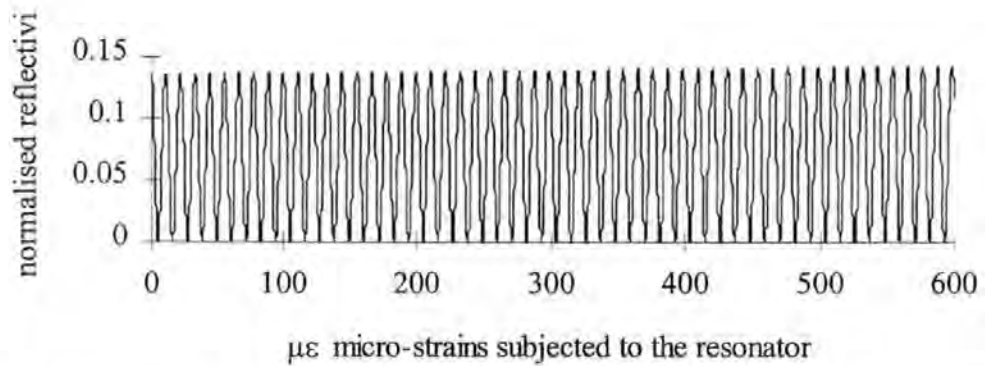


Figure ( 53a ) . The behaviour of the grating when subjected to longitudinal strain over a range of  $0\mu\epsilon$  to  $600\mu\epsilon$ . There is no radical change in the peak reflectivity of the resonator.

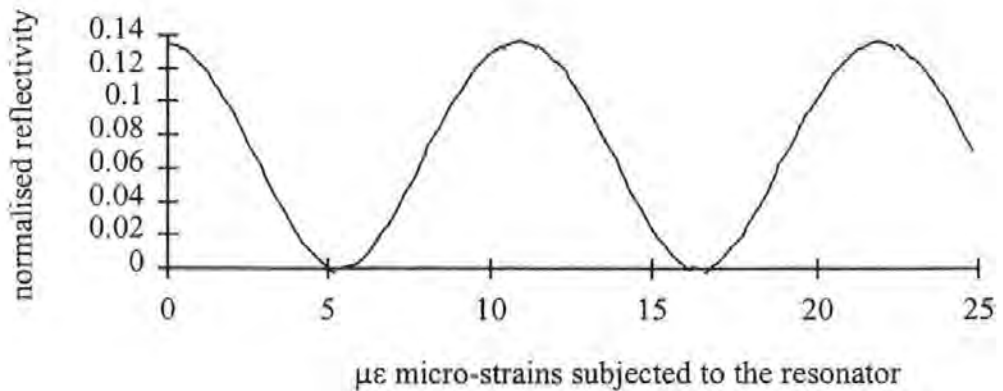


Figure (53b) . This is an expanded version of Figure 53a. Note that the resonators reflectance is a sinusoid function as longitudinal strain increases.



Figures 54a and 54b show the predicted theoretical reflectance response as a function of longitudinal strain of a resonator using the parameters for the 10% reflectance Bragg grating. Again the resonator is assumed to be illuminated by monochromatic radiation. Using the T matrix formalism produces these figures.

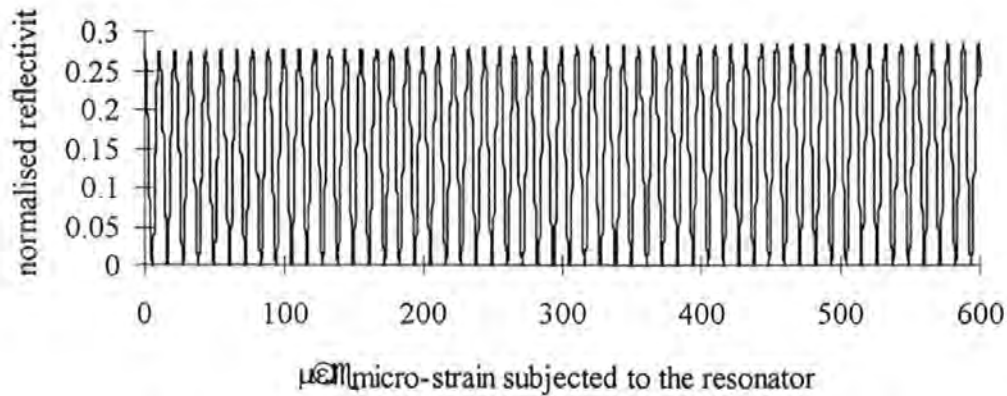
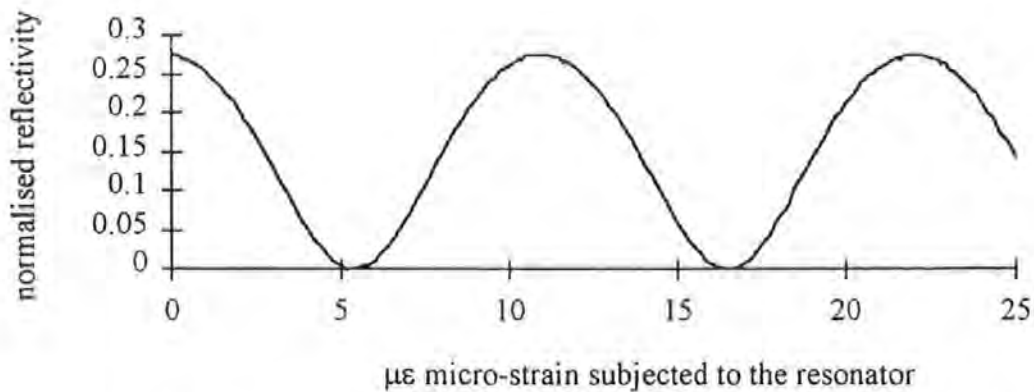


Figure (54a) . The reflectance of the resonator using gratings with 10% reflectance as a function of longitudinal strain.



Figure(54b) . This is an expanded version of Figure 54a. It can be seen by making a direct comparison between the two resonators ( Resonator with F.BG.s at  $R \sim 10\%$  to Resonator with F.BG.s at  $R \sim 5\%$  ) that the sinusoidal behaviour is beginning to distort. This distortion is a direct result of Airy functional behaviour as the coefficient of finesse is increased, Figure 55 shows a direct comparison between the two resonators.

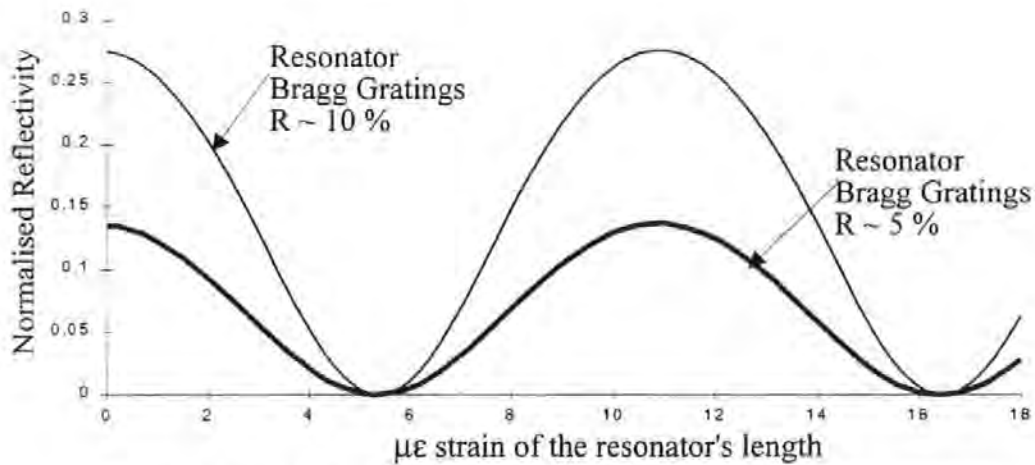


Figure (55) . The increase in the reflectance of the “mirrors”; gratings.

At relatively low reflectance of the Bragg gratings used as mirrors a sinusoidal response is produced. Increasing the reflectance of the Bragg gratings produces a deviation away from a sinusoidal response to a distorted sinusoid.

#### 4.5 Experimental and Theoretical results of the Fibre Bragg grating resonators.

A number of design changes were incorporated into the experimental mechanical test-rig in order to improve the precision and resolution of the applied strain. The original test-rig had difficulties in producing small incremental changes in strain. There were two main modifications, these being:

(I) The incorporation of a piezotranslator (PZT) Physik Instrumente P-841.xx LVPZ translator. A force of up to 2000 Newtons could be applied to induce the strain in the Aluminium beam. Very small changes in strain were possible by changing the voltage to the PZT from the controller ThorLAB inc. 3axis piezo controller model MDT690, using this would hopefully improve repeatability and accuracy. In early experiments the modified mechanical test-rig improved the fineness of strain increase to the Aluminium beam.

(II) The inclusion of a worm and wheel reduction box HPC Drives, worm/wheel reduction box; P60 with a ratio of 60:1 with an output torque of approximately  $\sim 120$  Nm was incorporated so that small increases in strain were obtainable with the 60:1 ratio.

Also a greater force could be applied to the Aluminium beam, see Figure 56a and 56b below. The tests conducted on the mechanical test-rig are exactly the same as for the investigation into the behaviour F.F.P. (  $\text{TiO}_2$  ) sensing element.

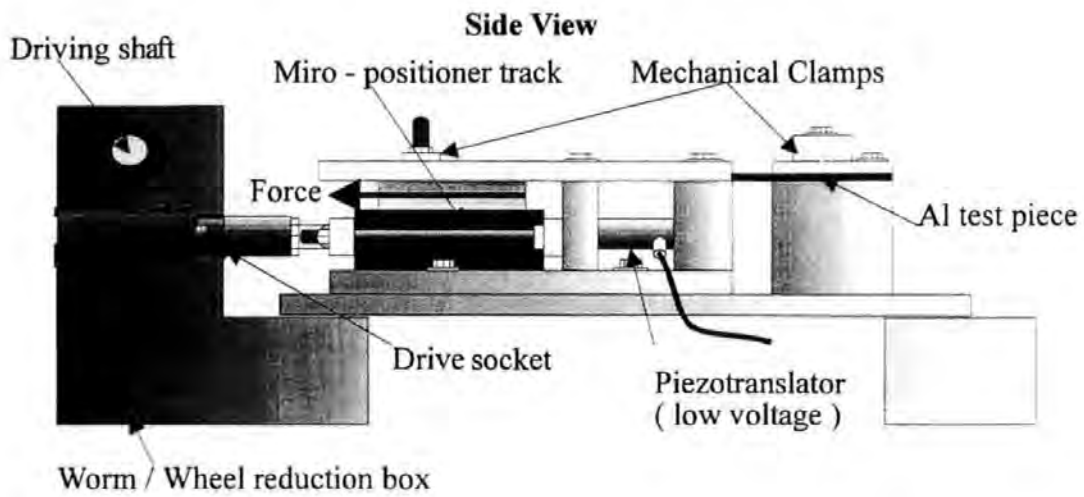


Figure (56a) . The side view of the mechanical test-rig.

The mechanical test-rig is shown in Figure 56a. As the worm/wheel reduction gearbox drive shaft is turned, a fine-threaded bolt, which is connected to the micro-positioner track, pulls on the Aluminium beam to which the sensor is adhered. The Aluminium is clamped to the micro-positioner track and to a block support. As the beam is stretched, strain is induced in the beam. The mechanical clamps are serrated to improve grip.

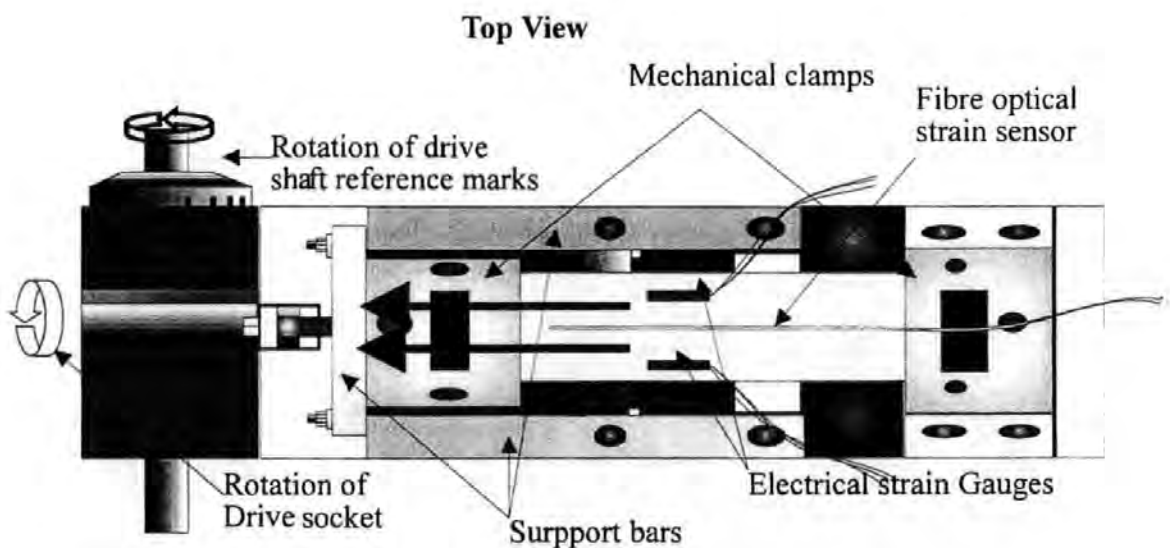


Figure (56b) . Top view of the mechanical test rig.

Figure 56b shows the positioning of the conventional electrical strain gauges to the fibre optical sensing element. The fibre optical sensing element was positioned well away from the edges of the Aluminium beam to ensure that only longitudinal strain is experienced.

#### 4.5.1 Theoretical results of a Fibre Bragg grating resonator.

Plotting values of the second harmonic against those of the first harmonic as a function of longitudinal strain results in a lissajou figure often called a cardioid. Figure 57a and 57b shows cardioids for the 5% and 10% grating reflectances.

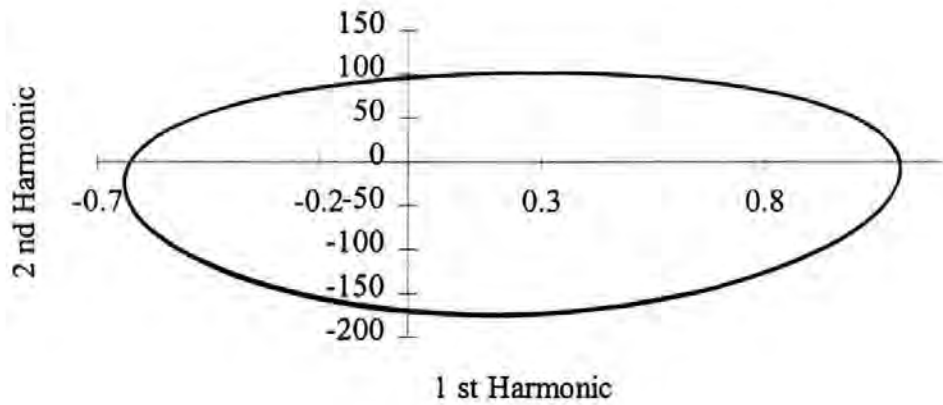


Figure (57a) . The theoretical prediction of a fibre Bragg resonator with the 5% grating mirrors under the influence of strain. A model of the signal processing technique (see appendix V) is generating the cardioid.

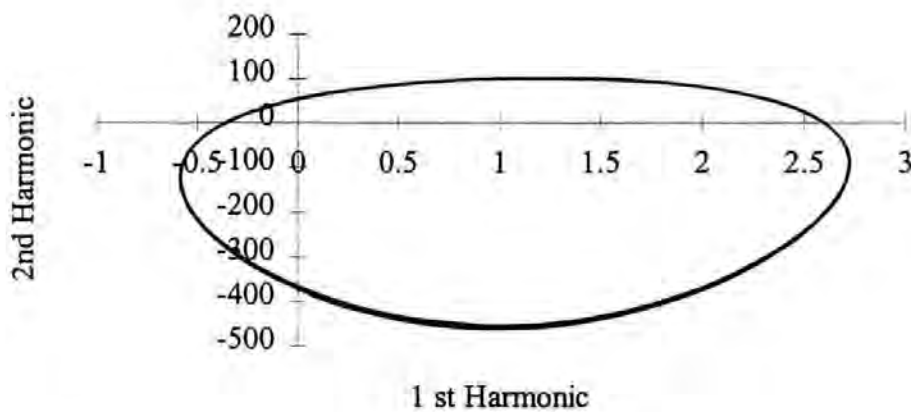


Figure (57b) . The theoretical prediction of a fibre Bragg grating resonator with the 10% grating mirrors under the influence of strain. A model of the signal processing technique (see appendix V) is generating the cardioid.

The two cardioids shapes are slightly different. This is expected because of the increase in finesse as the Airy function becomes more pronounced. It was observed that the predicted voltage from the photodetector to the Lock- in-Amplifiers would not require a pre-amplifier. Using theoretical data from a fibre Bragg grating resonator sensing element subjected to longitudinal strain ( Figures 57a and 57b ) would produce a quasi-linear relationship, similar to the  $\text{TiO}_2$  F.F.P. sensor. The approximation of the inverse tangent function of optical phase change to longitudinal strain begins to deviate as the reflectance increases as Figures 58, 59 show.

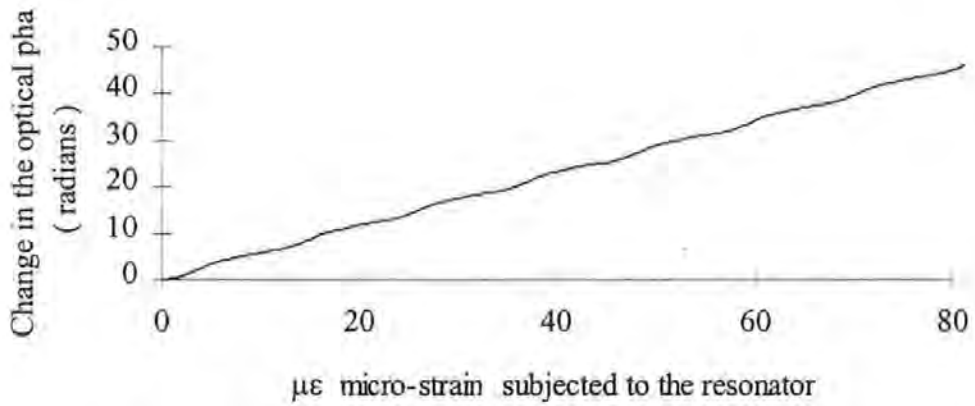


Figure (58) . The further processed data from the lock-in-amplifiers, using F.B.G. resonator with the 5% reflectance grating mirrors.

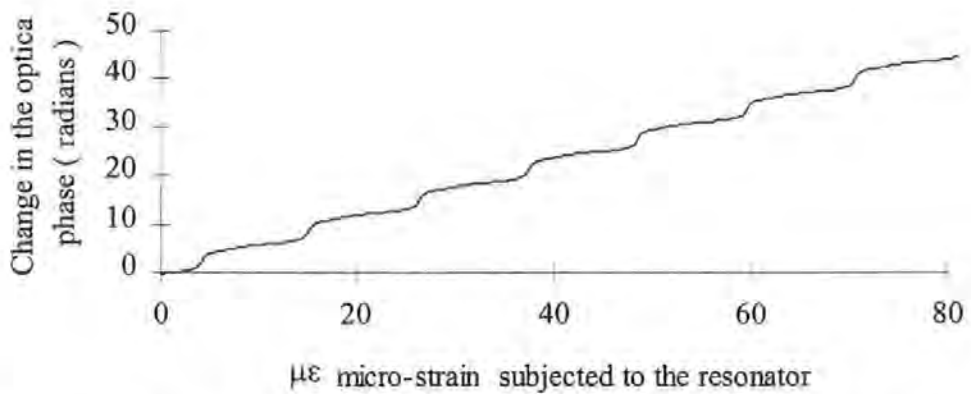


Figure (59) . The further processed data from the lock-in-amplifiers, using F.B.G. resonator with the 10% reflectance grating mirrors.

#### 4.5.2 Experimental results of the Fibre Bragg grating resonators.

The two grating resonators of 5% and 10% reflectances were attached to the test-rig and strained. The results are plotted as cardioids, which are generated by the detection system and a P.C. The difference in the shape of the cardioids is due to changes in reflectance. The undulation on Figure 61 is due to temperature fluctuations / effects caused by additional changes in the optical path length. The temperature is affecting both F.B.G. resonators; the reason for the greater fluctuations with resonator 24-4-71 is due to the more rapid variation of the derivatives for a given change in the optical path length ( temperature and strain ) with this resonator.

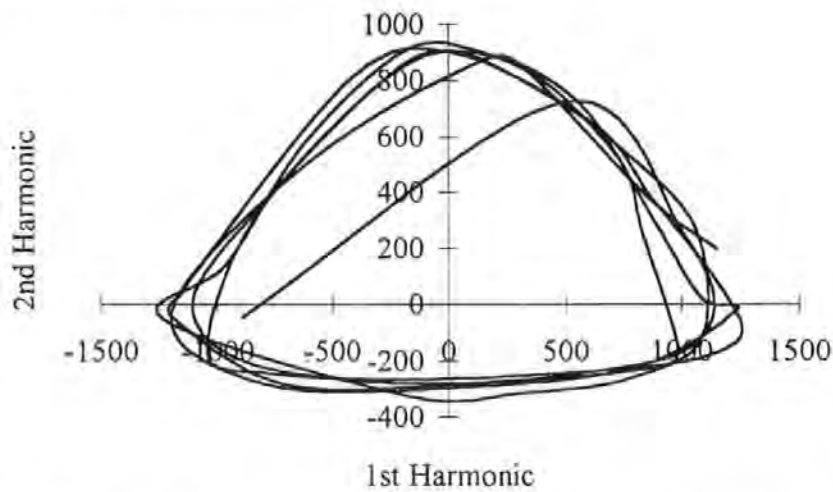


Figure (60) .The experimental data, the strain sensing system using resonator 24-4-72, which has mirror gratings at  $\sim 5\%$  reflectance.

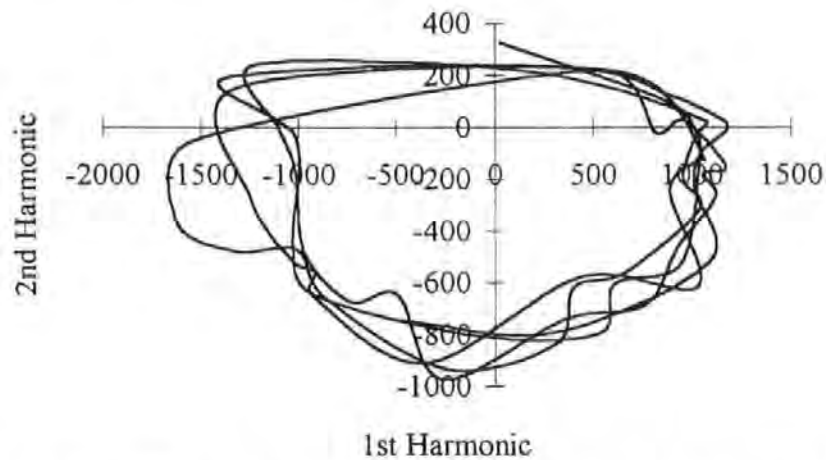


Figure (61) . The experimental data, the strain sensing system using resonator 24-4-71, which has mirror gratings at  $\sim 10\%$  reflectance .

The two cardioids shown in Figures 62 and 63 are one complete cycle, which corresponds to approximately 11 - 12  $\mu\epsilon$ . The readings are taken at increments of one micro-strain. It was observed that the points around the cardioid generated from resonator (  $R_{\text{single}} \sim 10\%$  ) are not a uniform spread. This was expected due to the distortion of the sinusoidal reflectance response to strain. The points are more uniform for the resonator (  $R_{\text{single}} \sim 5\%$  ); this is expected because the reflectance response to strain is nearly sinusoidal.

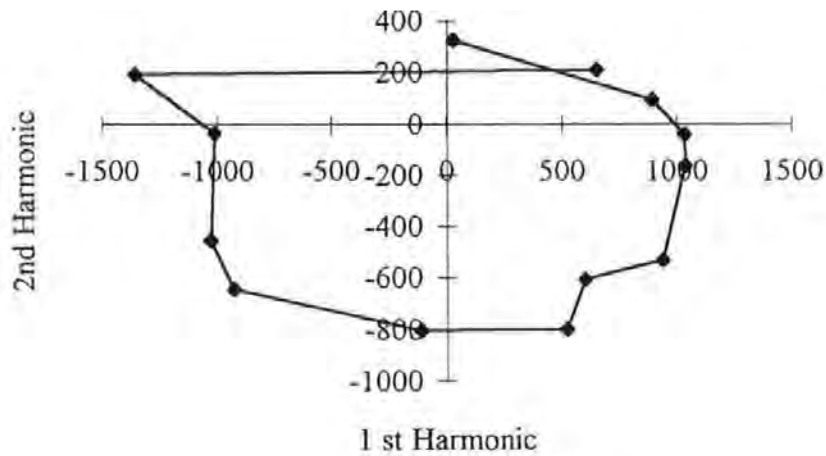


Figure (62) . Experimental data of a single cardioid, generated using sensing element fibre Bragg grating resonator 24-4-71, with a single mirror reflectance of 10 %.

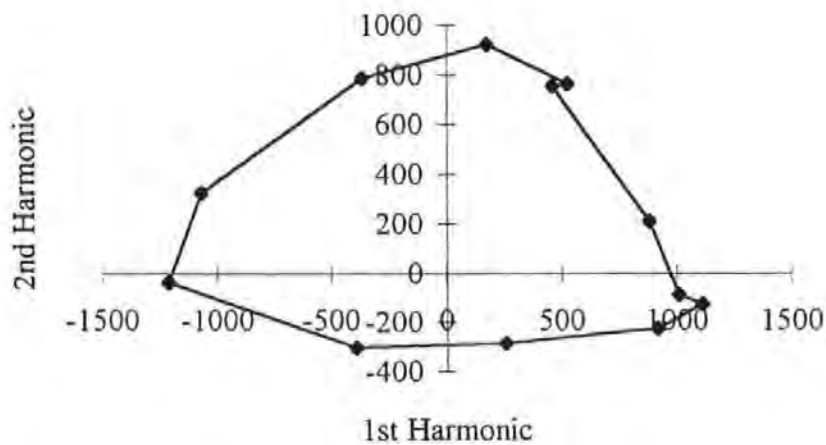


Figure (63) . Experimental data of a single cardioid, generated using sensing element fibre Bragg grating resonator 24-4-72, with a single mirror reflectance of 5 %.



The experimental data from the Lock-in-amplifiers are shown in Figure 64 and the final processed data from the Lock-in-amplifiers and the P.C. are also shown, Figure 65. The Figure 65 shows the experimental data having a quasi-linearly relationship between longitudinal strain and optical phase change which was predicted theoretically. In Figure 64, the cardioid of the 10% mirrors resonator shows a deviation or an error at any point on that quadrature diagram which was "thought" to be due to temperature variations during the experiment which have already been observed in previous experiments, Figure 61.

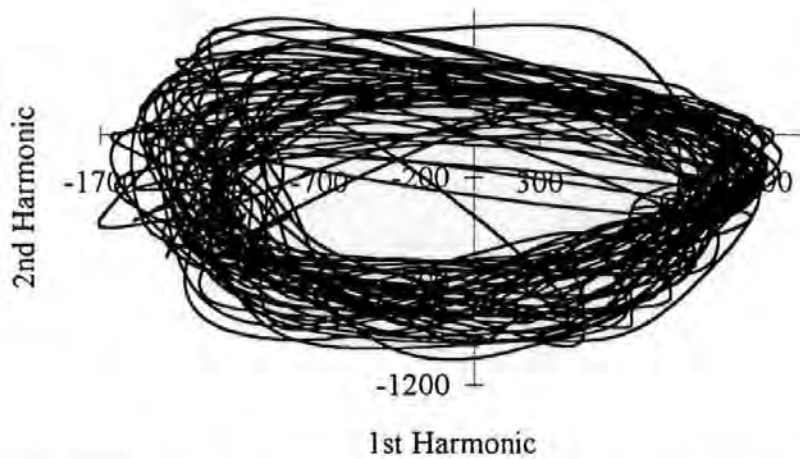


Figure (64) . The generation of cardioids from the Lock-in-Amplifiers due to longitudinal strain subjected to the sensing element, resonator 24-4-71 with F.B.G.s at  $R \sim 10\%$ .

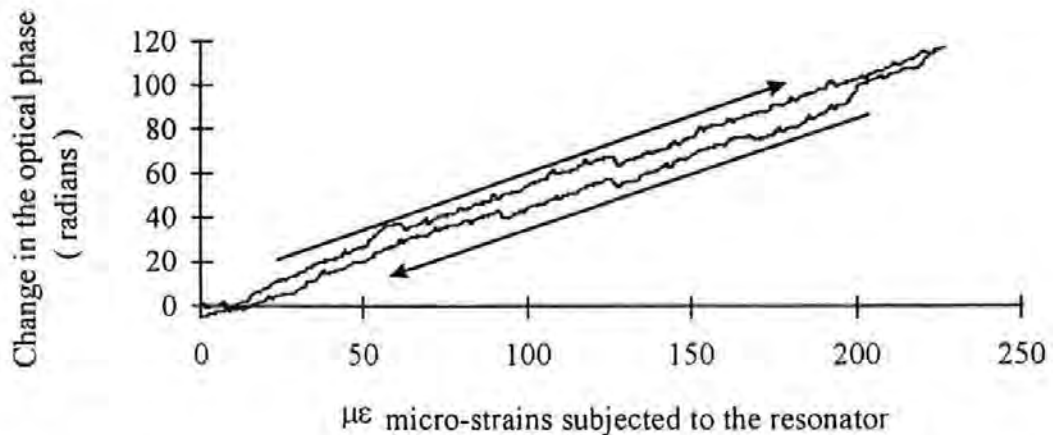


Figure (65) . The processed experimental data from resonator 24-7-1 ( Fibre Bragg grating resonator with single mirror reflectance of  $\sim 10\%$  ). This Figure also shows the effect of temperature on the sensor giving an hysteresis effect.



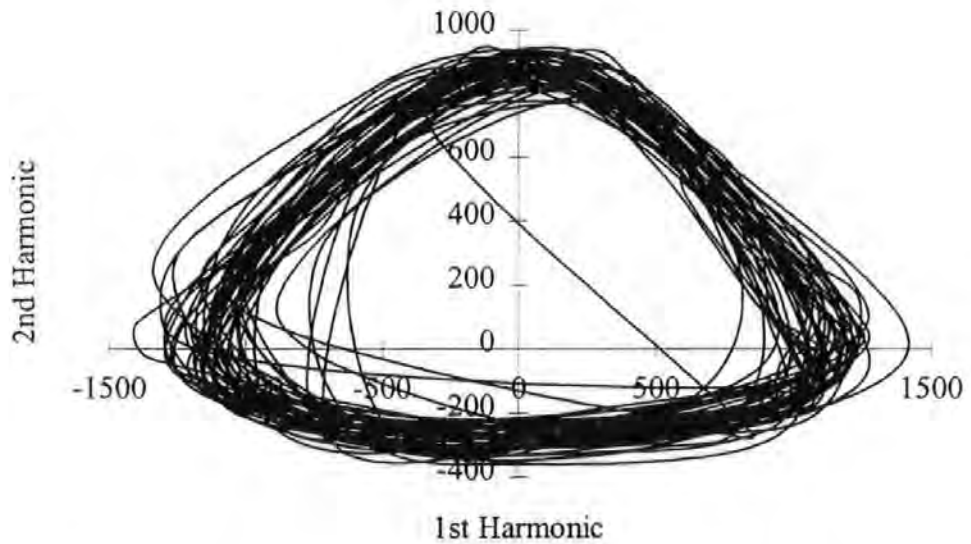
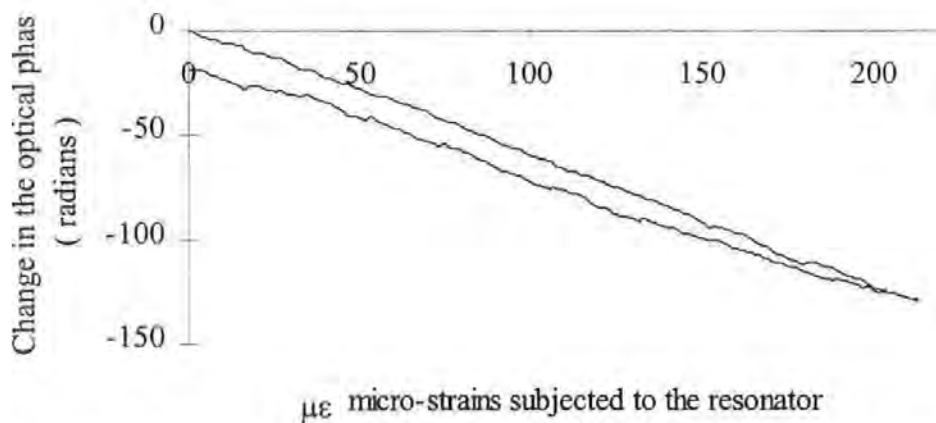


Figure (66) . Experimental data from the Lock-in-Amplifiers. The generation of the cardioids due to longitudinal strain being subjected to a sensing element ( 5% F.B.G. resonator 24-7-2 ) on the mechanical test rig.



Figure(67) . The processed experimental data from resonator 24-7-2 ( Fibre Bragg grating resonator with single mirror reflectance of  $\sim 5\%$  ).

Both Figures 65 and 67 shows how temperature variations can affect the data. This effect can be calibrated out by using a reference element that is only subjected to the environmental temperature variations of the sensing element. A simple electronic subtraction of the two signals generated by the reference and the sensing element.

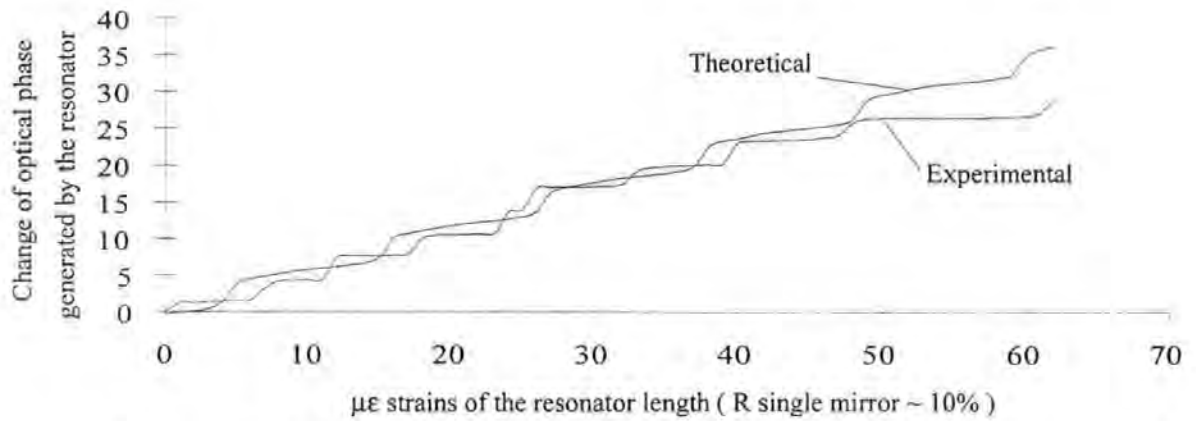


Figure (68). A comparison between experimental data and theoretical results. In Figure 68 the experimental processed data is from the lock-in-amplifiers with the sensing element F.B.G. resonator ( 24-4-71 ); mirrors with  $R \sim 10\%$ . The theoretical results were obtained from the C program for the T-Matrix formalism.

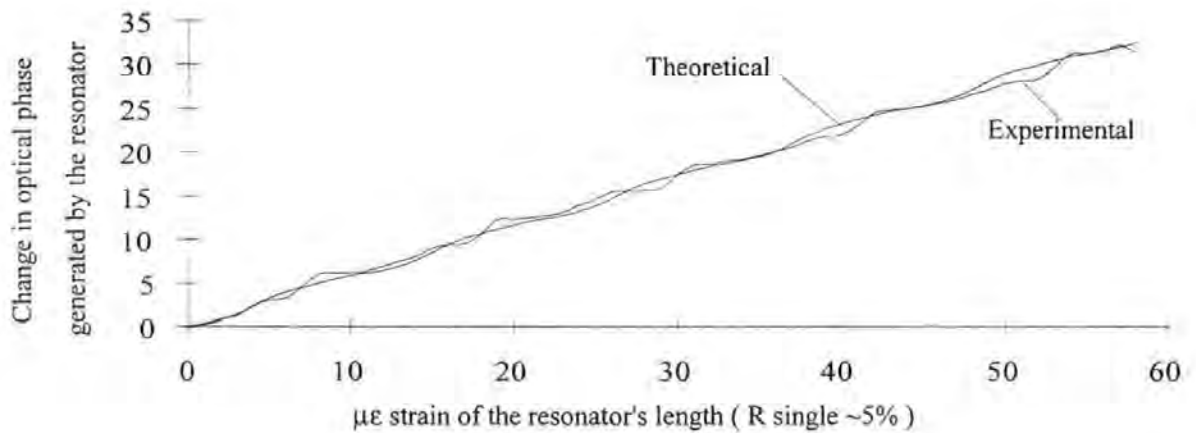


Figure (69) . A comparison between experimental data and theoretical results. In Figure 69 the experimental processed data is from the lock-in-amplifiers with the sensing element F.B.G. resonator ( 24-4-72 ) mirrors with  $R \sim 5\%$ . Again theoretical results come from the T-Matrix formalism. For above Figures 68 to 69 the strain was measured by the electrical strain gauges type EA-13-240LZ-120 from Measurements Group inc., which are self-temperature, compensated, which were attached to the Aluminium beam to which the fibre sensor had been adhered.

#### 4.6 Modified fibre Bragg grating resonator.

The spectral response of a resonator is also a function of gratings ( mirrors ). This is achieved by varying the separation between the gratings. Two resonators of different spacing were supplied, the spectral response of which were obtained using equipment at Nortel Optoelectronic Division at Paignton ( see section 5.4 ) Figures 70 and 71 below.

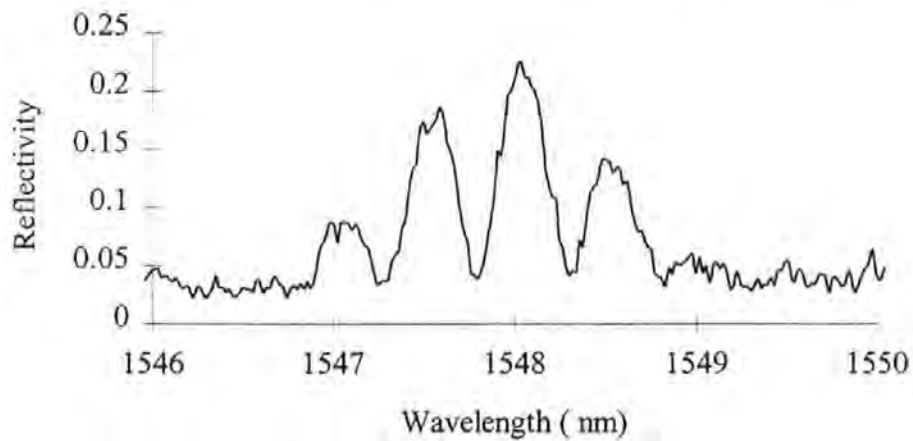


Figure (70) . The observed spectral response of resonator 14-3-4.

The 14-3-4 resonator has an approximate cavity length of less than 1mm, a total separation of 1.5 mm and a free spectral range  $\sim 0.46\text{nm}$  with a bandwidth of approximately 1.7 nm.

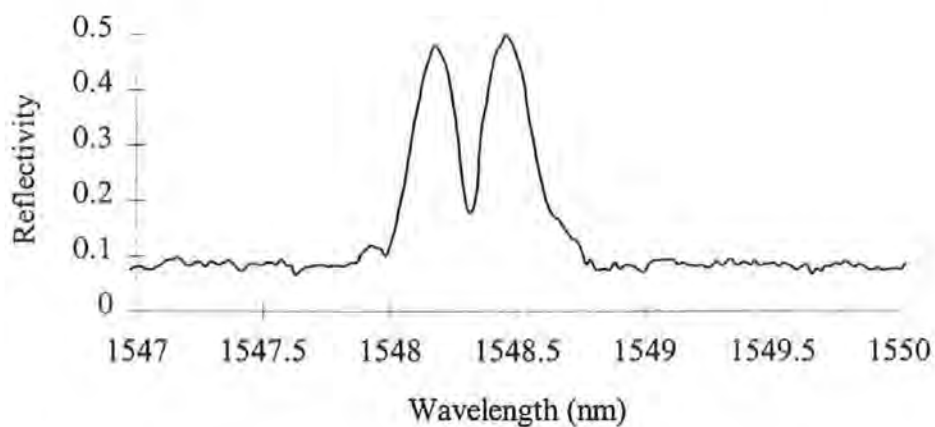


Figure (71) . The observed spectral response of resonator 14-3-3.

The 14-3-3 resonator has an approximate cavity length of  $\sim 2\text{mm}$ , a total separation of 2.5 mm and a bandwidth of approximately 0.46 nm.

The D.F.B. laser wavelength was set to be just outside the profile of the resonators. This is achieved by adjusting the temperature control of the drive unit of the D.F.B. laser ( type LDC100 ). The figure below shows the wavelength variation obtainable via the control voltage for the temperature setting.

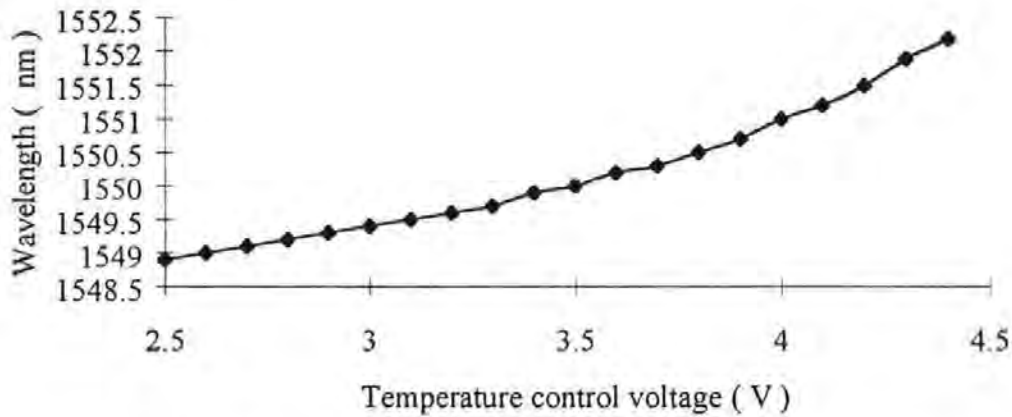


Figure (72) . The variation of wavelength from the D.F.B. laser using the temperature control of the drive unit.

The wavelength is obtained by feeding the output of the pigtailed D.F.B. laser into a wavemeter type Burleigh WA-25000 with an accuracy of 0.1nm.

#### 4.6.1 The static response of the resonator to longitudinal strain.

The constant levels of reflected irradiance from the resonators is obtained by using the strain system without modulating the D.F.B. laser light source and subjecting the resonator to longitudinal strain on the test-rig. The Ge photodetector output voltage is then fed to an oscilloscope and the voltage observed. This operation was carried out on both resonators (14-3-3 and 14-3-4). The operational wavelength of the D.F.B. laser was chosen to obtain the resonator's full response with respect to strain. The wavelength of the D.F.B. laser in the spectral domain was such that, as the longitudinal strain experienced by the resonator increases the resonator's complete profile would sweep through the D.F.B. laser wavelength; see Figures 73 and 74 below.

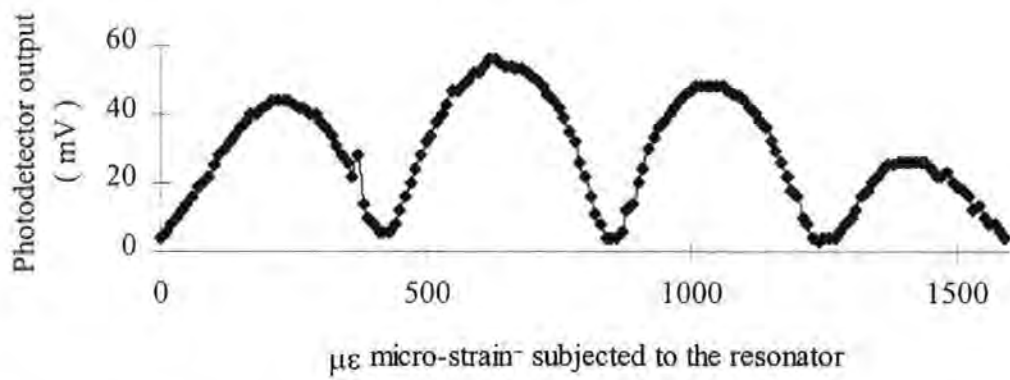


Figure (73) . The reflective power profile with respect to longitudinal strain for resonator ( 14-3-4 ).

The static reflective intensity response of the resonator (14-3-4) when subjected to strain. The voltage measurement is directly from the photodetector, thus a measure of the reflected light intensity from resonator. The voltage was observed on an oscilloscope.

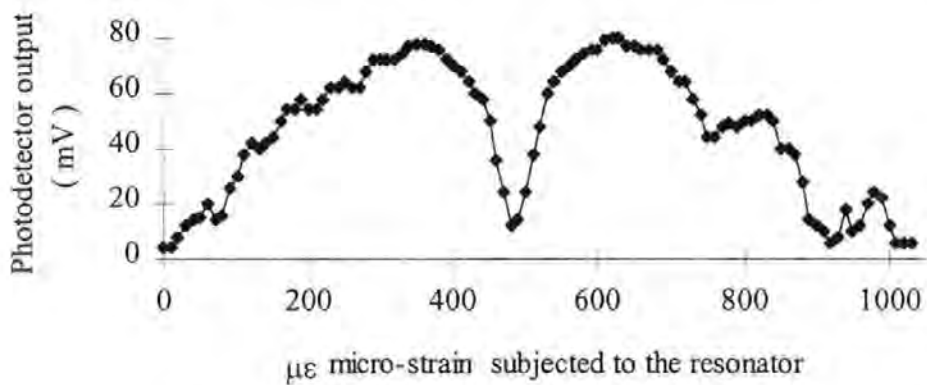


Figure 74 . The reflective power profile with respect to longitudinal strain for resonator ( 14-3-3 ).

The static reflective intensity response of the resonator 14-3-3 when subjected to strain. The voltage was measured using the same technique as for resonator 14-3-4.

The results shown in Figures 73 and 74 were obtained by increasing the longitudinal strain in steps of 10 micro strains and the output voltage of the photodetector was noted and the strain increased again. The step increases in strain are marked on the two graphs.

The general shape of resonator 14-3-3 suggests that the adopted signal-processing scheme may not work because of the deviations from a sinusoidal profile and the anomalies on the profile itself.

#### 4.6.2 Experimental results of the modified resonators.

Some typical cardioids generated from the system using both sensing elements, resonator 14-3-4 and resonator 14-3-3 are shown in Figures 75 and 76 respectively where each mark is an increase of ten micro-strain being subjected to the sensing element. Modulation of the D.F.B. laser was chosen to maximise the second harmonic to generate a more linear relationship between longitudinal strain and change in optical phase shift. Also, the anomalies on the profiles had to be considered because this would cause deviations or add noise to the magnitudes of the harmonics ( the harmonics are a measure of the 1<sup>st</sup> and 2<sup>nd</sup> derivatives ), these deviations would also appear in the final processed data .

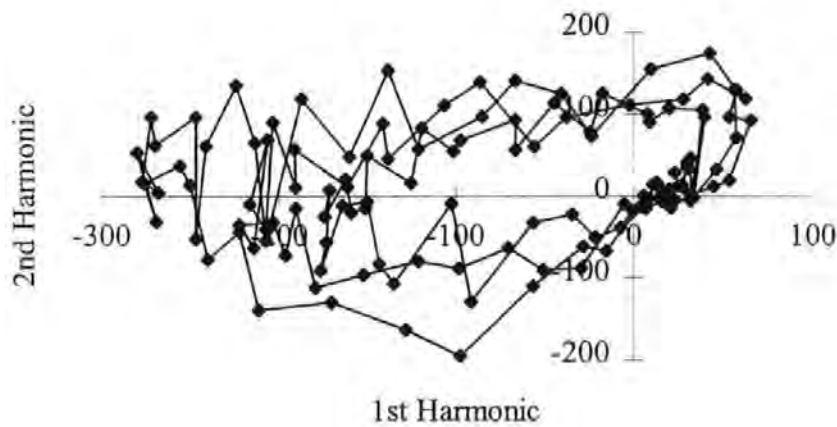


Figure (75) . Cardioids generated using sensing element F.B.G. resonator 14-3-4.

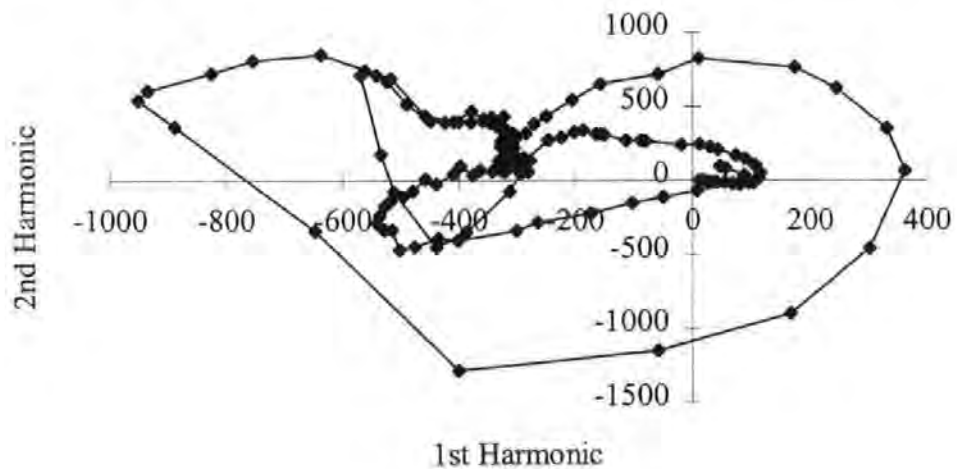


Figure (76) . Cardioids generated using sensing element F.B.G. resonator 14-3-3.

Figures 77 and 78 show typical processed data from the sensing system. Figure 77 shows results using 14-3-4 resonator and which demonstrates the quasi - linear relationship between change in optical phase and longitudinal strain. The dynamic range can be seen to be 0 to 1200  $\mu\epsilon$ . This is due to the nature of the fibre Bragg grating that is to say that the reflected bandwidth profile of the grating is dependent upon the period of the perturbation of the refractive index, which changes the spectral period response of the grating. This also effects the grating response to strain. It can also be seen that over the linear range there exists some noise that is most likely due to temperature variations in addition to causing the hysteresis effect. The anomalies on the profile response of the grating itself would add to the noise effect.

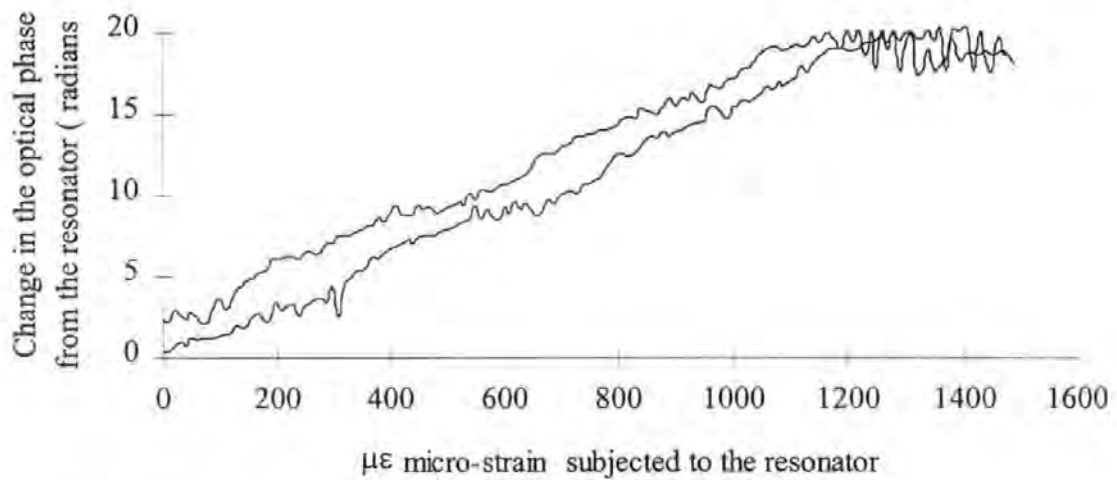


Figure (77) . Processed experimental data from sensing element F.B.G. resonator 14-3-4.

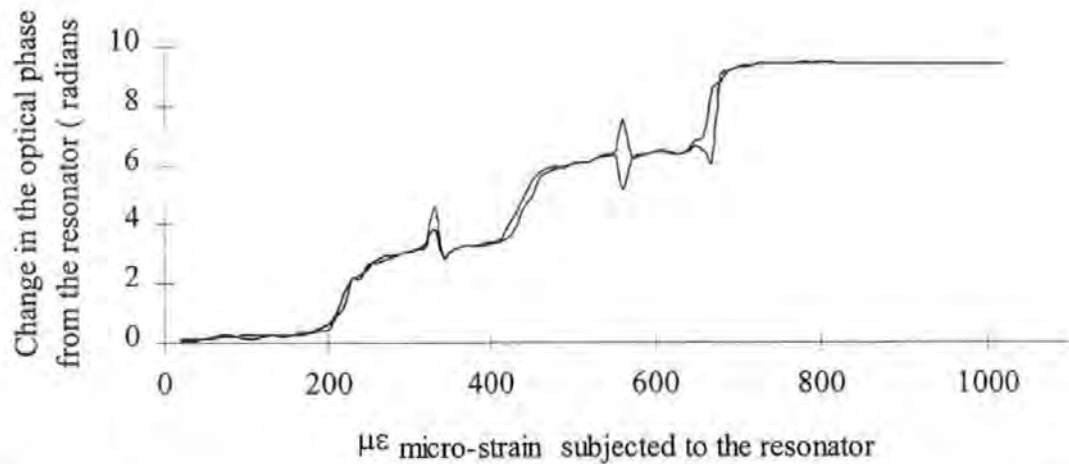


Figure (78) . Processed experimental data from sensing element F.B.G. resonator 14-3-3.



Figure 78 also shows reduced linearity, which is to be expected because of the reflectivity response profile according to longitudinal strain, which is more like a rectified sinewave. This profile gives a “stepped” response after the data are processed ( see section 2.3 ).

#### 4.7 Observations and results of the fibre Bragg grating resonator.

The results given in section 4.2 show that a relatively broadband fibre Bragg grating can be used instead of a  $\text{TiO}_2$  layer as a semi-reflective layer. The same problems exist with the grating mirrors increasing the reflectivity of the mirrors distorts the sinusoidal behaviour of the optical phase change of the sensor, thus producing a quasi-linear relationship. There is the problem of also measuring only apparent phase change.

The major advantage of the fibre Bragg grating over the  $\text{TiO}_2$  layer is in fabrication and repeatability. This was the major problem with the  $\text{TiO}_2$  layer. The wavelength selectivity of the fibre Bragg grating is a very useful property when considering multiplexing. The additional pre-amplifier used between the Ga photodetector and the lock-in-amplifiers (L.I.A.s) was removed when investigating the 10% reflectivity mirrors.

Following the same procedure as in section 2 but instead of using the Butter and Hocker model the T-matrix formalism was used to derive the constant of proportionality between change in optical phase and longitudinal strain. The photoelastic effect was also taken into account in a similar way to Butter and Hocker. The T-matrix formalism was used because of the grating sensitivity to longitudinal strain:

A theoretical value of  $0.567 \text{ rad } (\mu\epsilon)^{-1}$  was obtained for a grating resonator defined by the following parameters that gives mirrors with 5% reflectance;  $\Delta n \sim 0.002$ ,  $n_{\text{core}} = 1.45$ , a uniform  $\Delta n$ , chirp factor of  $F = 0.013 \text{ nm per change per period}$ . A starting / initial spatial period of  $\Lambda(0) = 510 \text{ nm}$  and the number of periods in the grating equal to 1000. A separation of 6 cm between the two identical gratings of 5% reflectance.

Assuming linearity between change in optical phase and longitudinal strain the deviation away from linearity is  $\pm 0.3 \mu\epsilon$  per radian.

A theoretical value of  $0.568 \text{ rad } (\mu\epsilon)^{-1}$  was obtained for a grating resonator defined by the following parameters that gives mirrors with 10% reflectance;  $\Delta n \sim 0.003$ ,  $n_{\text{core}} = 1.45$ , a uniform  $\Delta n$ , chirp factor of  $F = 0.013 \text{ nm per change per period}$ .



A starting period of  $\Lambda(0) = 510$  nm and the number of periods in the grating equal to 1000. A separation of 6 cm between the two identical gratings of 10 % reflectance.

Assuming linearity between change in optical phase and longitudinal strain the deviation away from linearity is  $\pm 1 \mu\epsilon$  per radian.

Using the Butter and Hocker model gives a value of  $0.563 \text{ rad } (\mu\epsilon)^{-1}$ .

Comparing these theoretical results to the experimental results from the two resonators shows good agreement. Experimentally for the single mirror  $R \sim 5\%$  resonator an average constant of proportionality between change in optical phase and longitudinal strain was found to be  $0.566 \pm 0.033 \text{ rad } (\mu\epsilon)^{-1}$ , which is within 0.2% error of the expected theoretical result with a standard deviation of 5%. Figure 79, shows some typical results obtained from the single mirror  $R \sim 5\%$  resonator. The deviation from linearity ( resolution ) was found to be  $\pm 0.426 \mu\epsilon$ .

Experimentally for the single mirror  $R \sim 10\%$  resonator an average constant of proportionality between change in optical phase and longitudinal strain was found to be  $0.587 \pm 0.099 \text{ rad } (\mu\epsilon)^{-1}$  with error percentage of 3.3% to the expected theoretical result with a standard deviation percentage error of 17%. Figure 80 shows some typical results from various runs with the 10% resonator. The deviation from linearity ( resolution ) was found to be  $\pm 2.0 \mu\epsilon$ .

The modified grating resonators (14-3-3 and 14-3-4) go some way to having a finite range for the longitudinal strain but a problem remains with the implementation of the modified gratings and standardisation of fabrication of the gratings. Experimentally for resonator (14-3-3) an average constant of proportionality between change in optical phase and longitudinal strain was found to be  $0.013 \pm 0.0007 \text{ rad } (\mu\epsilon)^{-1}$  with a deviation away from linearity of  $\pm 35 \mu\epsilon$  per radian. The predicted theoretical value for the constant of proportionality between phase and longitudinal strain using the T-matrix formalism with the model of the signal processing is  $0.017 \text{ rad } (\mu\epsilon)^{-1}$  with a deviation away from linearity of  $\pm 16 \mu\epsilon$  per radian. The difference between the experimental and the theoretical value is quite large but this is expected because of the profile distortion.

Experimentally for resonator (14-3-4) an average constant of proportionality between change in optical phase and longitudinal strain was found to be  $0.015 \pm 0.0002 \text{ rad } (\mu\epsilon)^{-1}$  with a deviation away from linearity of  $\pm 12 \mu\epsilon$  per radian.

Again, comparing these experimental values to the theoretically predicted values of  $0.022 \text{ rad } (\mu\epsilon)^{-1}$  and deviation away from linearity of  $\pm 9 \mu\epsilon$  per radian are in better agreement. The differences between the results is probably due the anomalies on the resonators profile response to longitudinal strain and the deviations in the profile's general shape which is due to the fabrication technique. These two characteristics cause " noise " and limits the strain resolution. The resolution of the two modified resonators is relativity poor compared to the other two resonators but changing the period of the reflectivity profile can change the strain resolution. Figure 81 showing some typical runs for the resonator (14-3-3) and Figure 82 showing the response of the system-using resonator (14-3-4).

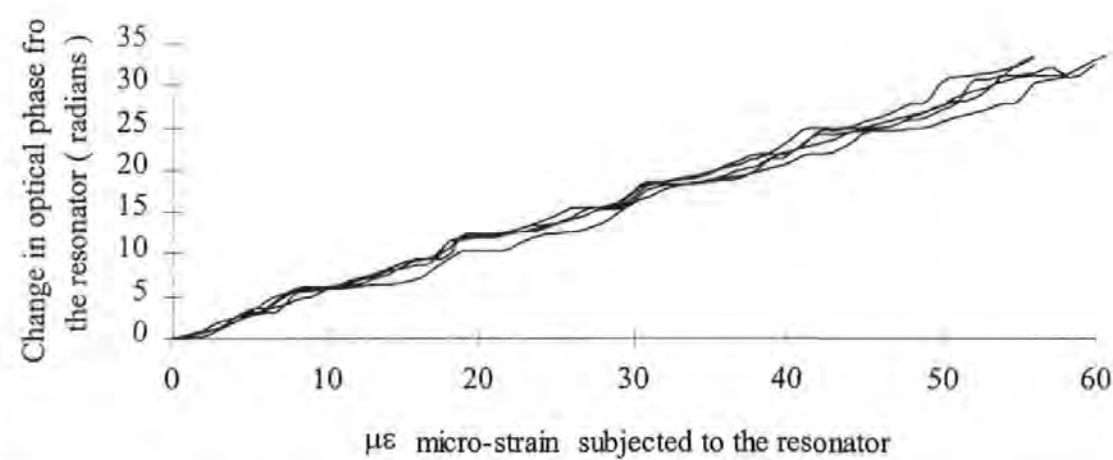


Figure (79). Typical processed experimental data for sensing element F.B.G. resonator 24-4-72

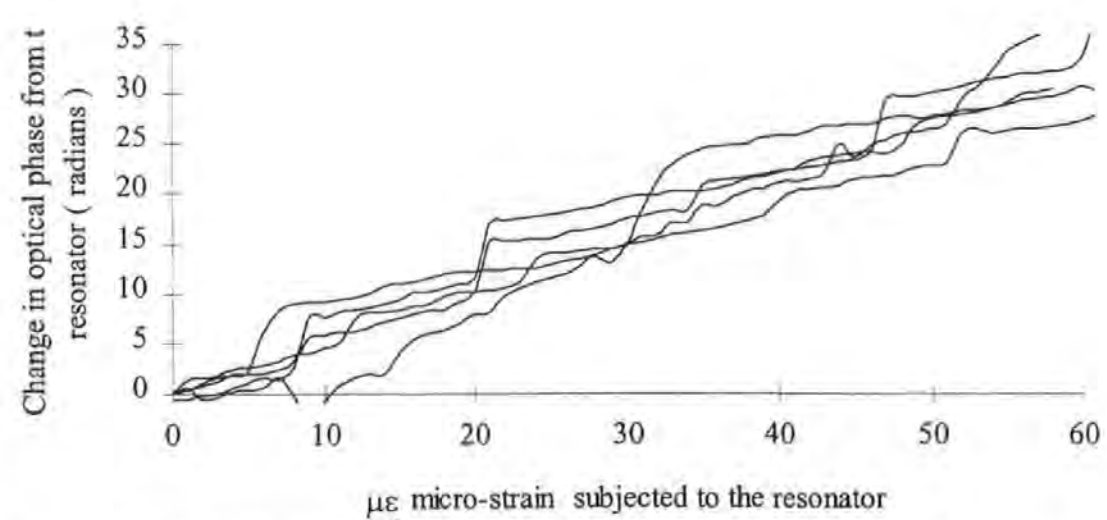


Figure (80). Typical processed experimental data for sensing element F.B.G. resonator 24-4-71

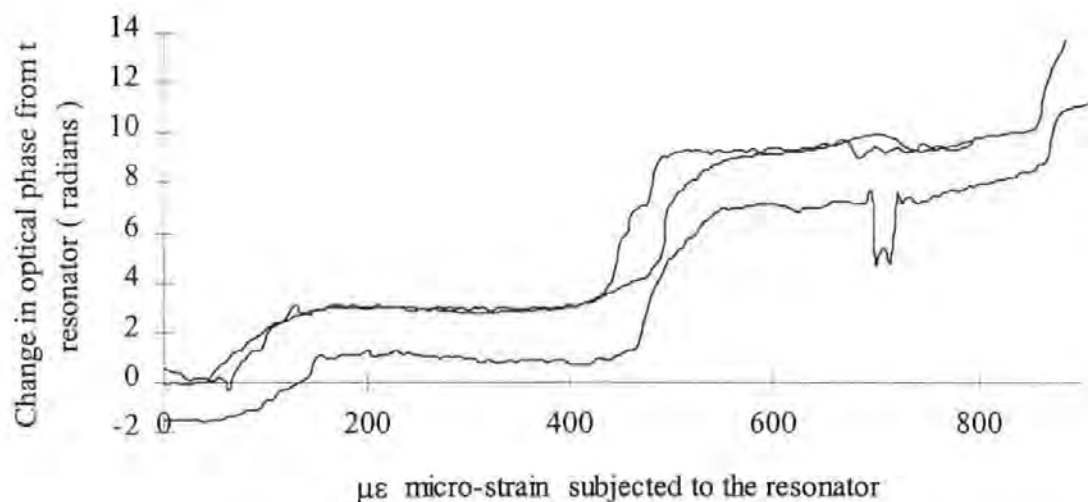


Figure (81) . Typical processed experimental data when using sensing element F.B.G. resonator 14-3-3.

Note the general loss of linearity due to the non-Michelson response of the sensor, thus the approximation assumed in the signal processing to obtain linear relationship no longer applies.

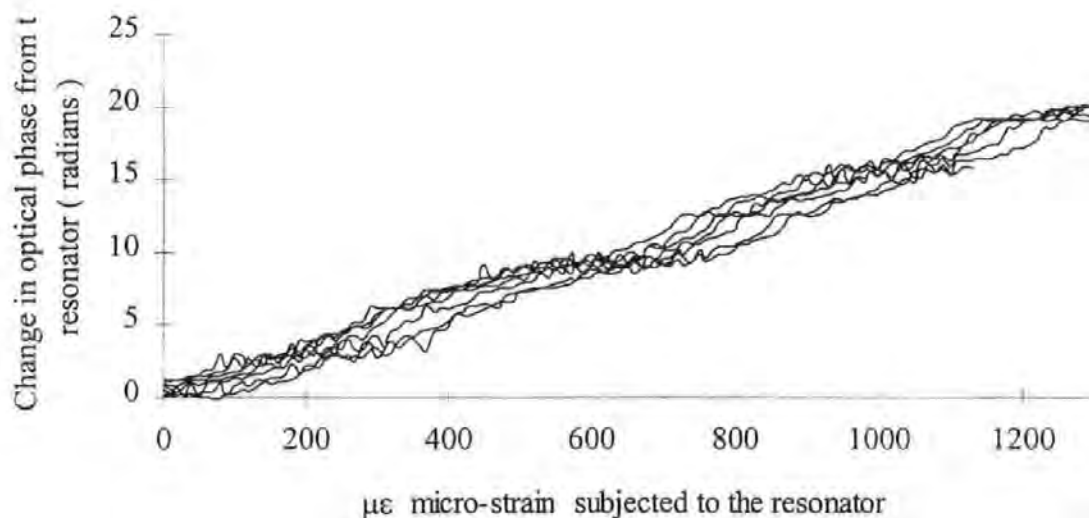


Figure (82) . Typical processed experimental data when using sensing element F.B.G. resonator 14-3-4.

### 5.1 Description of the grating to be investigated and theoretical spectral response.

In the previous chapter the fibre Bragg grating resonator was shown to behave as a fibre Fabry Perot sensor. This also includes some of the F.F.P. sensor's drawbacks: the sensor only measures apparent longitudinal strain and the problems associated with multiplexing such a device. To overcome the aforementioned problems it was decided to try to obtain a fibre Bragg grating structure that would behave like a Michelson interferometric sensor. The sensor would have a finite operational range with unique values over that range. This would give a sensing element that is capable of absolute longitudinal strain measurement, and will use the same signal processing technique.

A detailed study using the T matrix formalism gives rise to two structures that gave promising spectral responses. Figure 83 shows a four peak structural variation in the refractive index modulation and Figure 84 shows a two-peak variation in refractive index modulation of fibre Bragg grating. Each of these structures of gratings also has a linear chirp in the spatial period along the axis of the grating.

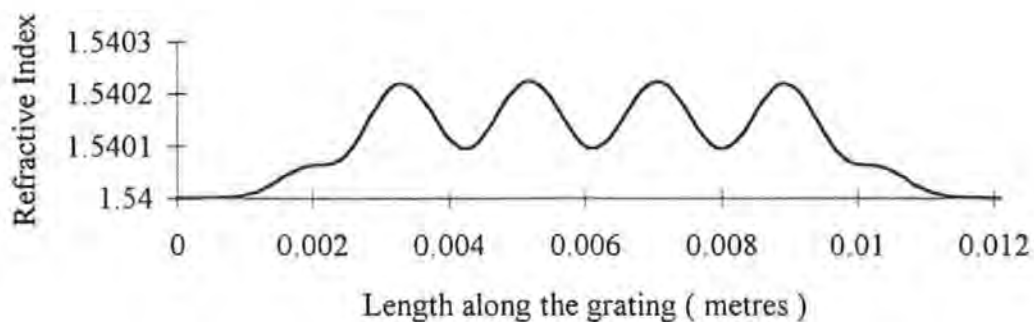


Figure (83) . The refractive index envelope function ( taper function ) variation along the length of this linearly chirped, tophat with a sinusoidal perturbation in the refractive index .

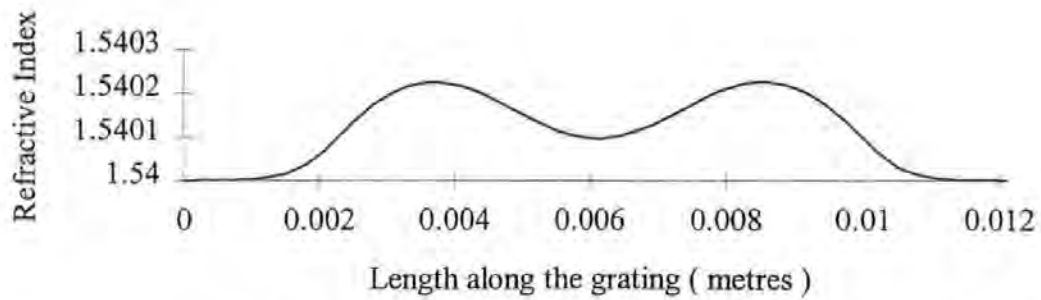


Figure (84) . The variation of the refractive index along the grating's length but the spatial period of the sinusoidal perturbation is longer.

The theoretical spectral responses of the two grating structures are shown in Figures 85, 86. The reason for considering the spectral responses of these proposed structures is that a D.F.B. laser irradiates them, which is single wavelength. As longitudinal strain increases, the spectral response of the grating shifts to longer wavelengths. Assuming that the operational wavelength of the D.F.B. laser is positioned in the spectral domain, at the minima of the spectral profile of the grating then increasing the longitudinal strain will sweep the grating spectral response through the wavelength of the D.F.B. laser. Thus the reflected irradiance from the fibre Bragg grating will have a Michelson interferometric response to longitudinal strain over a finite range.

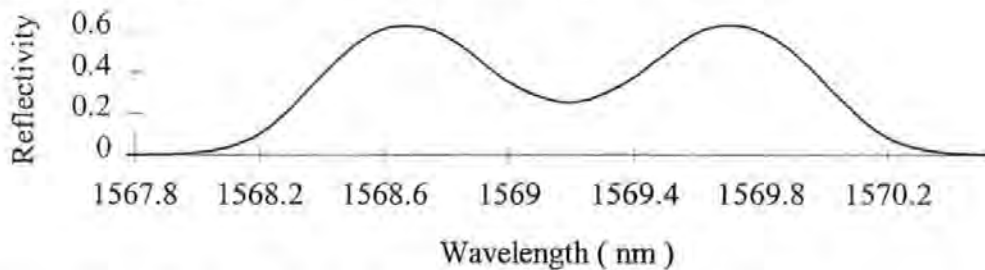


Figure (85). The theoretical reflective spectral response of the structure in figure 84.

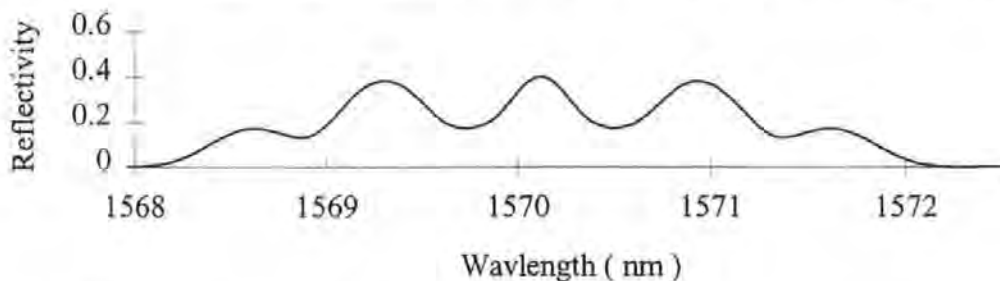


Figure (86) . The theoretical reflective spectral response of the structure in figure 83.

The sensor will produce a sinusoidal response when it experiences a longitudinal strain that can be detected by a photodetector. The sensor's response to longitudinal strain will result in only one and one half complete cardioids generated for longitudinal strain and

one and one half complete cardioids for compression for the spectral response shown in Figure 86. This is due to the effect strain as on the F.B.G., it's spectral response shifts to greater wavelengths and D.F.B. laser's wavelength does not shift, so the spectral profile of the sensor will sweep through the D.F.B. laser's wavelength before coming off the plateau. The plateau being the region of the spectrum where the F.B.G. has high reflectance. Thus the device can measure absolute strain by using a DC cut-off power level of the sensor. The resolution of such a strain sensor is dependent upon the period of the sinusoidal region of the reflectivity profile of the device and the accompanying system. The smaller the bandwidth of this sinusoidal region the greater the sensitivity.

Another possible grating structure is shown in Figure 87. This structure produces very similar results to the design of Figures 83, 84, this is shown in Figure 88. A problem with this design was that continuous phase information across the three sections of the grating is required with no discontinuities between each section. After discussions with researchers at Aston University it was decided that making such a grating would be too difficult, so this design of grating was abandoned in favour of the sinusoidal taper function of the modulation of the refractive index on a linearly chirped Bragg grating.

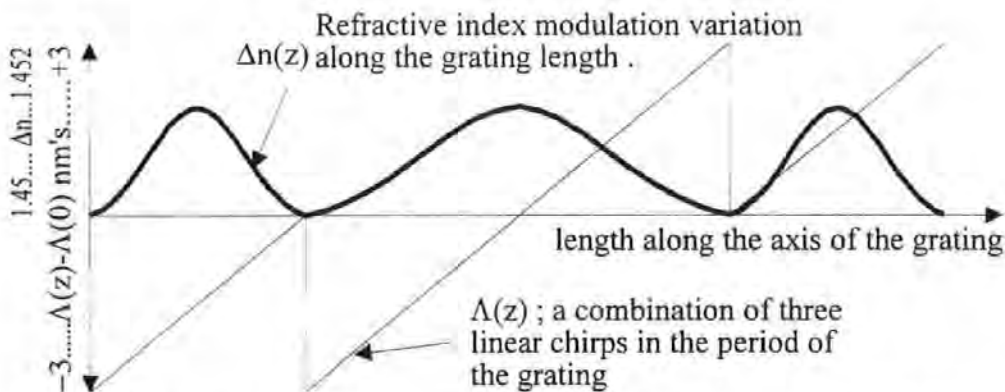


Figure (87) . A theoretical structure consisting of a combination of linear chirps in the spatial period of the refractive index perturbation and a taper function for the modulation of  $\Delta n$  of a fibre Bragg grating.

Figure 87 shows three sections with Gaussian taper function imposed on the depth of modulation of the refractive index. This produces the spectral reflectivity responses given in Figure 88 .Two grating responses were of interest; the parameters of the two gratings are given in Figure 88.

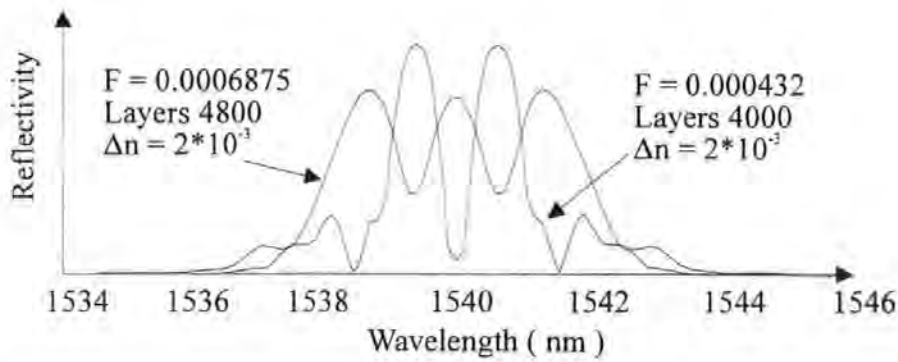


Figure (88) . Spectral responses of the grating structure shown in Figure 87.

## 5.2 The theoretical response of the proposed gratings subjected to a longitudinal strain.

The graphs of Figures 89a and 89b show how the DC reflectivity changes with longitudinal strain at a precise wavelength. The assumption was made that the emission line of the D.F.B. laser diode can be represented by a delta function although in practice a D.F.B. laser has a finite spectral bandwidth of a Lorentzian / Gaussian form. An investigation was performed to see if the approximation of using the delta function for the emission line of the D.F.B. laser diode would be valid. This was achieved by taking the spectral response of the Bragg grating produced by the T-matrix formalism and performing a convolution with a suitable Lorentzian or Gaussian shape that represents the spectral response of the D.F.B. laser. The convolution was performed in a Mathcad +6 program. It was found that using the delta function gave a reasonable approximation to the Lorentzian or Gaussian spectral emission from a D.F.B. laser.

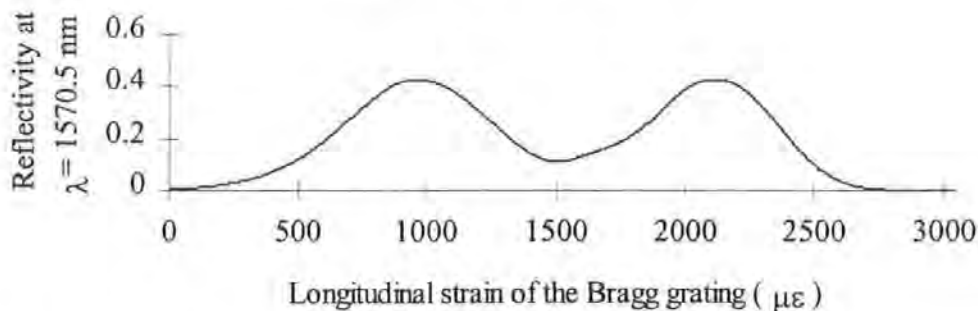


Figure (89a) . The fibre Bragg grating reflectivity response at a single wavelength as a function of longitudinal strain.



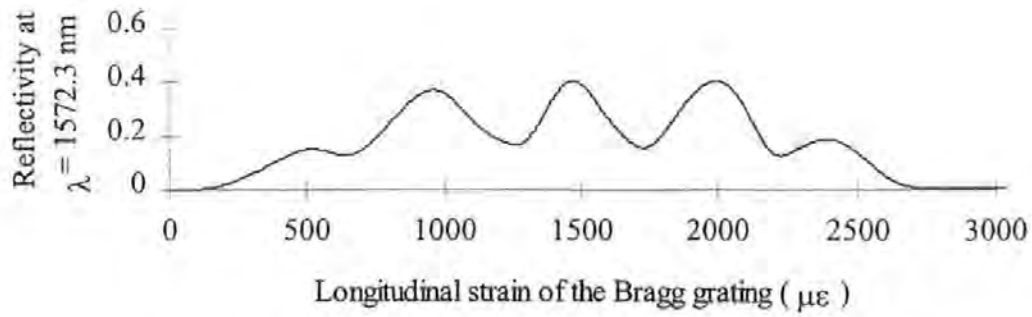


Figure (89b) . The reflectivity at a single wavelength of a fibre Bragg grating as a function of longitudinal strain.

The data shown in Figures 89a and 89b are for a grating specification of which  $\Delta n \sim 2.5 \times 10^{-4}$ , Chirp factor  $\sim 1.729\pi$  with a sinusoidal period in  $\Delta n$  of 4.079 mm for Figure 89a and 1.569 mm for Figure 98b. The total length is  $\sim 10.2$  mm and an initial grating period  $\Lambda(z = 0) = 510$  nm.

Figure 90 shows the combination of linear chirps and a Gaussian taper function for  $\Delta n$ . The following results were found by using the same technique.

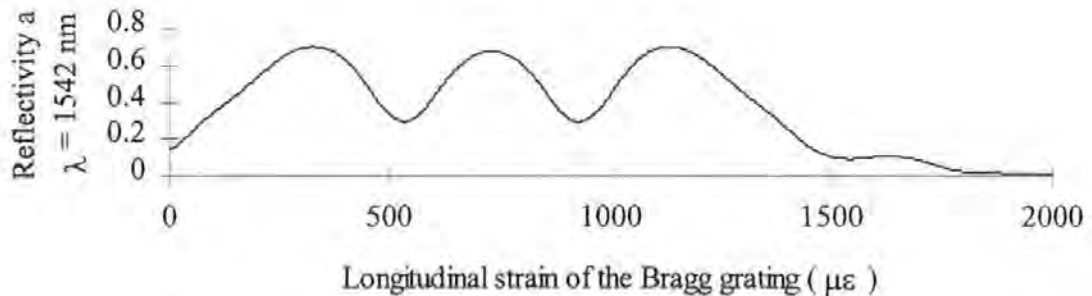


Figure (90) . The fibre Bragg grating combination reflectivity response at a single wavelength as a function of longitudinal strain.

The grating specification is for Figure 90  $\Delta n \sim 2 \times 10^{-3}$ , section one of the grating Chirp factor  $\sim 0.919\pi$  with a total length of 0.6003 mm, section two of the grating Chirp factor  $\sim 0.919\pi$  with a total length of 1.201 mm and section three of the grating Chirp factor  $\sim 0.918\pi$  with a total length is 0.6003 mm with initial grating spatial periods of  $\Lambda_{\text{section1}}(z = 0) = 499\text{nm}$ ,  $\Lambda_{\text{section2}}(z = 0) = 499.175\text{nm}$  and  $\Lambda_{\text{section3}}(z = 0) = 500\text{nm}$ .



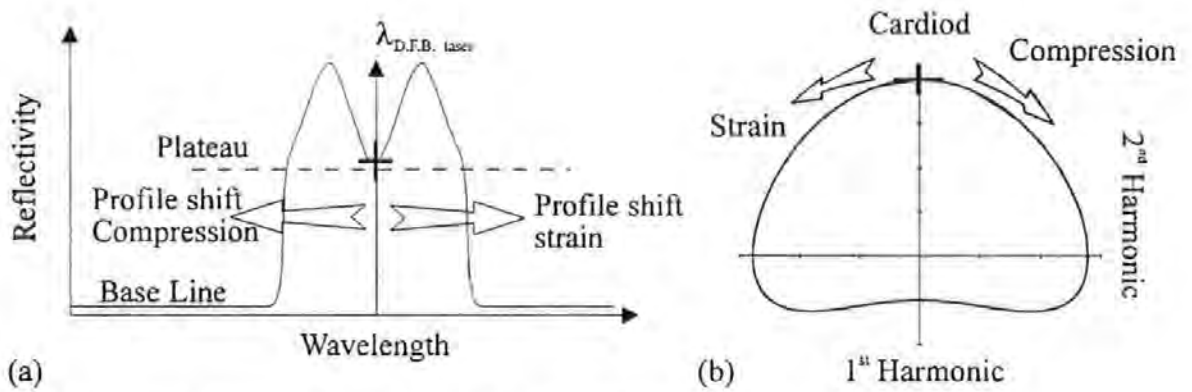


Figure (91) . Response of an idealised Bragg grating sensor and the cardioid generated from the reflected irradiance from the Bragg grating.

One property these two gratings have in common is a sinusoidal response to longitudinal strain, which is similar in behaviour to both the fibre Fabry Perot sensor and Bragg grating resonator, but only over a finite range of strain.

This finite range of operational strain for the sensing element is because the sinusoidal response is raised above the base line see Figure 91a. This behaviour can be used to introduce a reflected irradiance DC cut-off level which would restrict the response of the sensing element providing the D.F.B. laser diode wavelength is situated at the minima (point of symmetry of the reflectivity profile) of the spectral response of the Bragg grating with no strain applied ( see Figure 91a ). As strain is applied to the sensing element then half the sensor's feature will sweep through the D.F.B. laser. The reason being that the Bragg wavelength / condition is given by  $\lambda_B = 2n_{eff} \Lambda$  and  $\Lambda$  is a function of strain. The sensor's reflected irradiance would generate an anti-clockwise cardioids. If the sensor was subjected to a compressional force, and then the sensor's reflected irradiance would generate a clockwise cardioids, see Figure 91b.

### 5.3 Physical interpretation of the fibre Bragg gratings.

Inspection of the mode-coupled equations ( see appendix 1 ) of a Bragg grating with a single linear chirp, a refractive index modulation depth that is a Top-Hat taper function with a sinusoidal variation superimposed on it, shows that the phase term  $\Psi(z)$  of the mode coupled equations includes trigonometric expressions which can be expressed as Bessel functions. In effect one can postulate that if the modulation index of the Bessel function is small only a few harmonics are generated. The fundamental is being the original variation of the modulation depth. The first and second harmonics being side bands to the fundamental harmonic of  $\Delta n(z)$ .

A linearly chirped fibre Bragg grating illuminated by a single wavelength source will have a Bragg condition at one location along the grating's length. The intensity of the reflected light will be dependent upon local properties of the grating at the position where the Bragg condition is satisfied giving rise to local interference. The local optical path differences in that region and the Fresnel reflections at the interfaces will vary according to the refractive index modulation,  $\Delta n(z)$ . The variation of  $\Delta n(z)$  is a tophat with sinusoidal variation superimposed on it, which results in the back-reflected intensity being some kind of sinusoidal variation with wavelength.

This was investigated, using the mode coupled equations, by Fourier analysis of the  $\Psi(z)$  in conjunction with  $\kappa(z)$ ; the coupling coefficient , which varies according to the Taper function for  $\Delta n(z)$  . A reflection-band diagram was constructed to inspect the Bragg condition along the fibre Bragg grating length to obtain more physical understanding as to how the light would interact with the grating, a method used by L. Poladian [88].

A grating with a combination of linear chirps with continuous phase information can be considered as a resonator. If the grating combination is illuminated by a single wavelength there will exist two locations along the grating length where the Bragg condition is satisfied, which are separated by some length of the grating. At some given wavelength there will be effectively two mirrors ( Bragg condition / resonance ) within the grating's length separated by some distance in the grating thus the fibre Fabry - Perot scenario.

This condition will exist for a range of wavelengths because of the linear chirps in the spatial period of the grating, as can be seen on a reflection-band diagram, an example is shown Figure 92. These effects plus the optical path difference between the “ first mirror ” and the “ second mirror ” are what determine the spectral reflectivity profile of that grating.

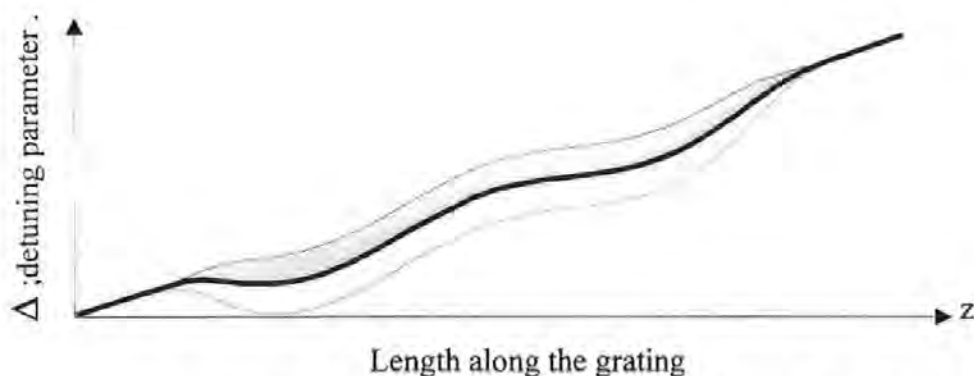


Figure (92) . Reflection-band diagram of the Bragg grating with a single linear chirp, refractive index modulation depth that is a Top-Hat taper function with a sinusoidal variation superimposed on it .

Figure 92 shows the local Bragg condition along the grating length of the Bragg grating sensing element. The symbol  $\Delta$  defines the detuning parameter. For a uniform Bragg grating only one Bragg condition  $\Delta = 0$ . Therefore  $\Delta = 0$  is the solid curve which represents the local Bragg condition and the enclosed shaded / white regions are the extended region of the local photonic band gap at that position along the Bragg grating length. The extent of the region is dependent upon depth of modulation of refractive index in the grating at that position;  $\Delta n(z)$ . So the oscillation on the solid line is due to the changes in the refractive index and the gradient of the line represents the chirp. As the chirp decreases, the slope of solid curve decreases, thus at some value of the chirp factor there will be two or more positions along the grating where the Bragg condition is satisfied, thus a fibre Fabry - Perot scenario will occur.

## 5.4 The fibre Bragg grating strain sensor ( the spectral responses ).

To confirm the spectral behaviour of the grating sensing elements received from our fabricators, a series of measurements were carried out at the Optoelectronics Division of Nortel at Paignton. The test - rig was one normally used for testing Erbium Doped Fibre Amplifiers (EDFA's). A schematic diagram of the system is shown in Figure 93. The EDFA was driven into saturation and therefore operated as a broadband optical source over a range 1540nm to 1560nm. The optical spectrum analyser a Hewlett Packard 70004A O.S.A. had a spectral range of 600nm to 1700nm with a resolution of 0.08nm, the number of sampling points was 800. The gratings were coupled via a 3dB coupler to the system, to obtain the reflective spectral response. Mechanical joints where used to couple the sensing elements to the system, which caused some alignment problems. In this procedure a calibration was performed on the system replacing the coupler and the fibre Bragg grating sensor with an optical short. Figure 94 shows the system response over the spectral bandwidth of interest.

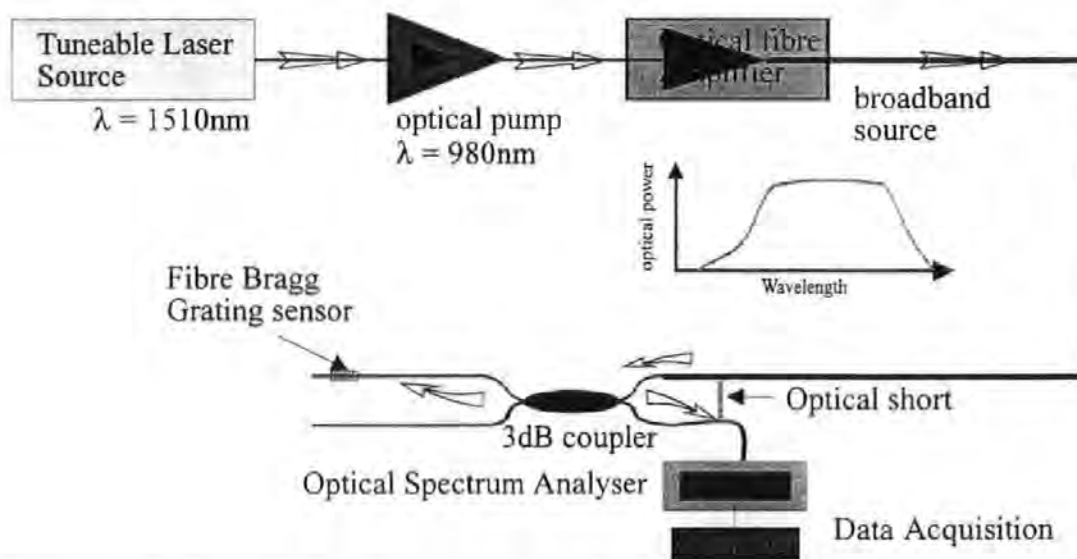


Figure (93) . A schematic of rig used to obtain the spectral response of the gratings.

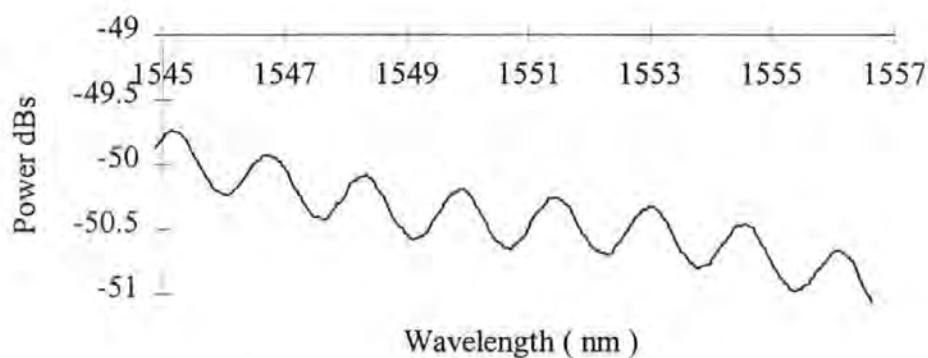


Figure (94) . Spectral response of the rig used to obtain the spectral response of the fibre Bragg gratings to be used on the mechanical test rig.

Some difficulties arose in fabricating the sensors with a raised sinusoid variation on a plateau above the baseline response, Figure 95 shows the ideal spectral response required by the detection scheme.

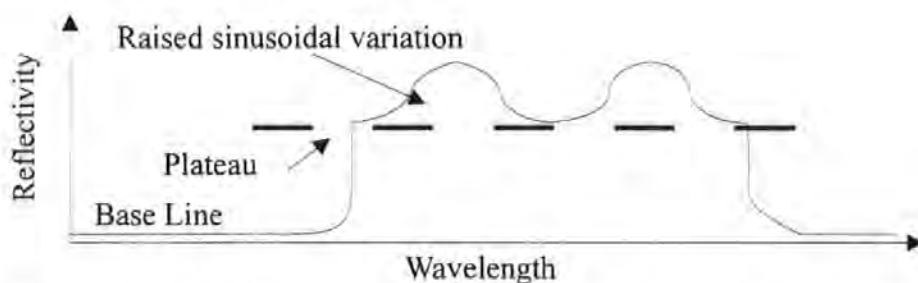


Figure (95) . The ideal spectral response profile of a fibre Bragg grating.

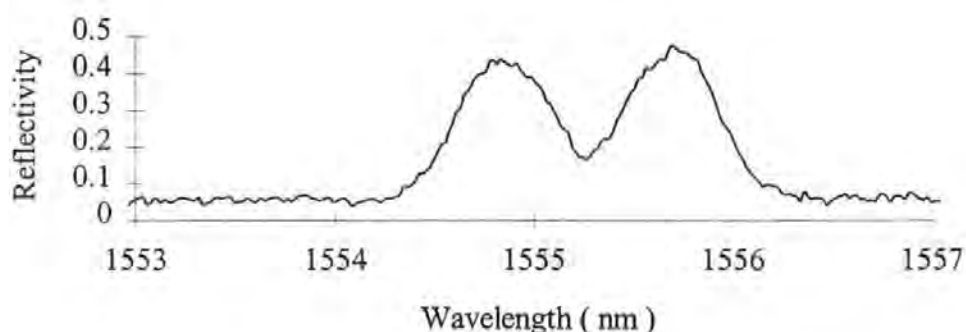


Figure (96) . The spectral response of a linearly chirped and sinusoidal taper function of  $\Delta n$  ( No TOMAR12 ) fibre Bragg grating.

Figure 96 shows the spectral response of a linearly - chirped, sinusoidal - tapered refractive index modulation grating. The spectral characteristic behaviour is in agreement with the theoretical spectral response, section 5.1. The response, although not symmetric or sinusoidal, is quite close to the desired response. It is thought that the deviation from the desired response is due to fabrication effects. The “plateau” at the 20% reflection level allows a D.C. cut-off to be incorporated into the signal processing.

A variation or a deviation in the fabrication technique of the grating gives rise to variation in the spectral profile curves of which Figure 97 is an example. This shows that the base line for the sinusoidal behaviour is raised to around 60% reflectivity. A second difference is that the bandwidth of the raised sinewave in the grating with the response given in Figure 96 is 2.0 nm where has the grating responsible for Figure 97 is 1.5 nm.

Although the general form of the  $\Delta n$  profile is similar for these two gratings, the “stronger grating” of Figure 97 provides higher reflectance and hence narrower bandwidth. It is this feature that controls the strain resolution of the sensor ( see appendix V ).

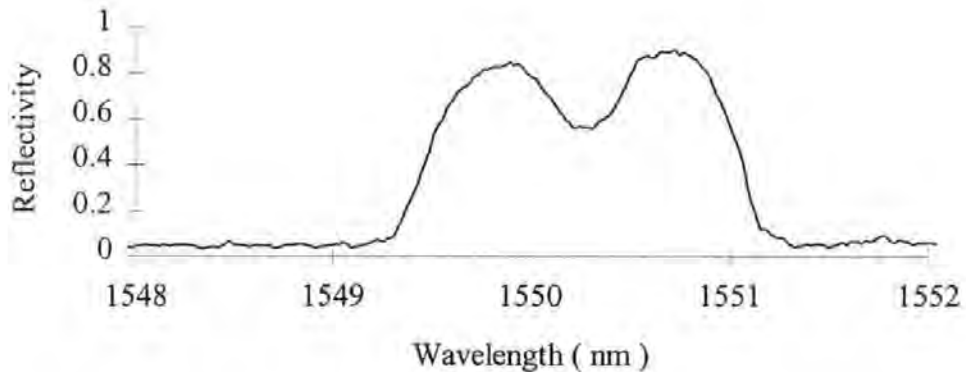


Figure (97). Another spectral response of a linearly chirped and sinusoidal taper function of  $\Delta n$  ( No TOMAR12 ) fibre Bragg grating.

The Figures of 98, 99 and 100 show the spectral characteristics of other gratings produced. The variations in the reflection profiles, centre wavelength and bandwidth plus the anomalies on the profiles themselves is again thought to be due to how the grating is fabrication and procedures adopted in the fabrication process.

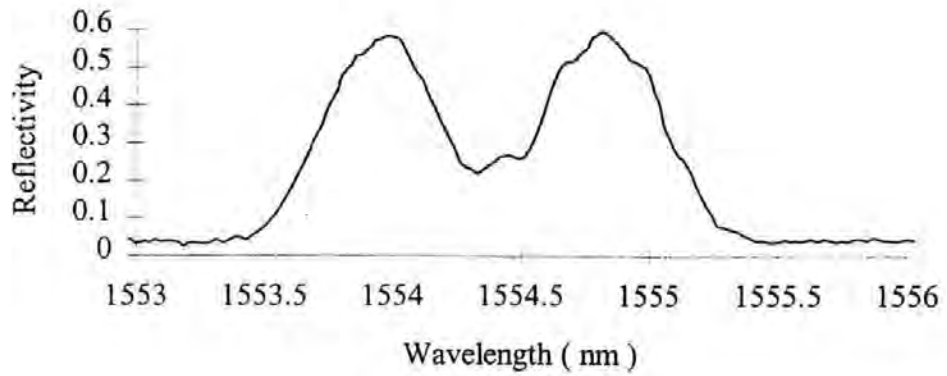


Figure (98) . The spectral response of a linearly chirped and sinusoidal taper function of  $\Delta n$  ( No TOMAR10 ) fibre Bragg grating.

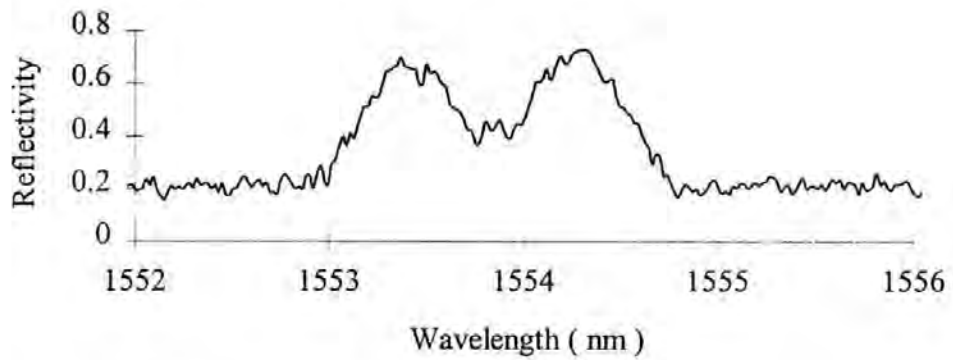


Figure (99) . The spectral response of a linearly chirped and sinusoidal taper function of  $\Delta n$  ( No TOMAR13 ) fibre Bragg grating.

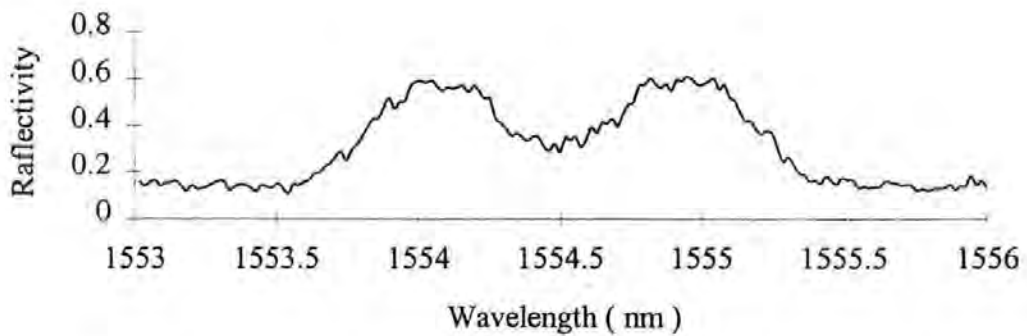


Figure (99) . The spectral response of a linearly chirped and sinusoidal taper function of  $\Delta n$  ( No TOMAR11 ) fibre Bragg grating.



## 5.5 Experimental results from the fibre Bragg grating sensors subjected to longitudinal strain.

The same experimental procedure was used as that for the fibre Bragg grating resonators. Likewise the same strain test rig and the same signal processing technique. Instead of frequency modulation, which has been considered. The interest is in wavelength modulation due to the D.F.B. laser, which can have a wavelength shift. The detection system is the same; detection of the first and second harmonics at the modulation frequency of the wavelength. The operating wavelength of the D.F.B. laser was optimised for each sensing element. This was achieved by changing the temperature control setting of the drive unit of the D.F.B. laser ( LDC100, the temperature servo-control operates to  $\pm 0.1$  °C ). This governs the operating temperature of the D.F.B. laser, and therefore the operational wavelength of the D.F.B. laser. Figure 101 shows the wavelength variation with temperature control voltage. This was done to obtain a wavelength of the D.F.B. laser that could cover the spectral features of the Bragg grating sensing element, so as the grating is subjected to longitudinal strain the complete spectral profile of the grating sweeps through the wavelength of the D.F.B. laser. An additional operation of the sensing system is required, the detection of the DC level of the light reflected back from the sensor ( fibre Bragg grating ) which would give the finite operational range of the sensor.

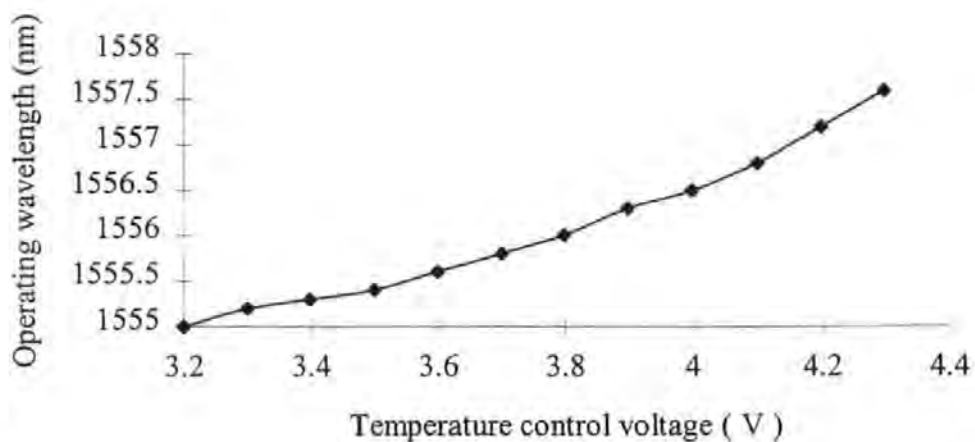


Figure (101) . The variation of the wavelength from the D.F.B. laser using temperature control of the drive unit.



5.5.1 The static reflectivity response of the Bragg grating sensors to longitudinal strain.

Figure 102-106 below shows the output voltage obtained from the photodetector when the grating sensor is subjected to longitudinal strain. The output voltage is proportional to the intensity of reflected irradiance from the sensor and therefore a measurement of the reflectivity-strain profile of the grating.

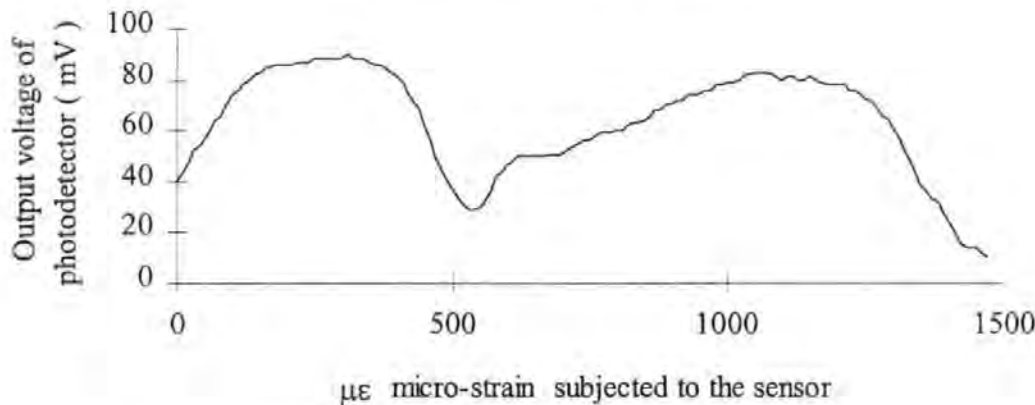


Figure (102) . Static reflectivity-strain profile of sensor TOMAR12.

Comparing Figure 102 to the spectral response shown on Figure 96 shows differences. This may be caused by the strain-optic effect, where strain changes the refractive index of the core and changes the grating's response to strain. This distortion with longitudinal strain has been observed in the theoretical model of this kind of fibre Bragg grating ( see appendix V, section Vh ).

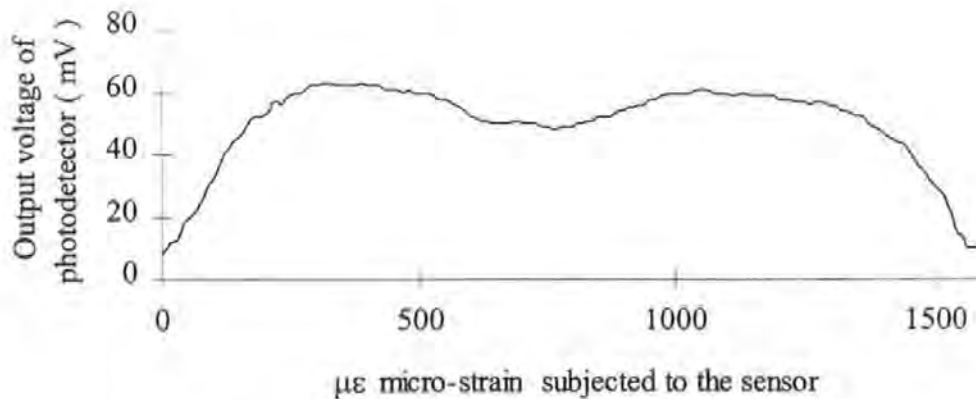


Figure (103) . Static reflectivity-strain profile of sensor TOMAR8.

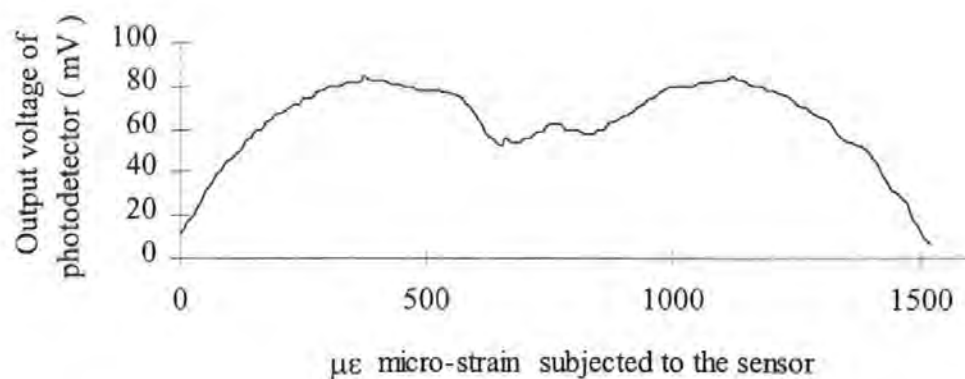


Figure (104) . Static reflectivity-strain profile of sensor TOMAR13.

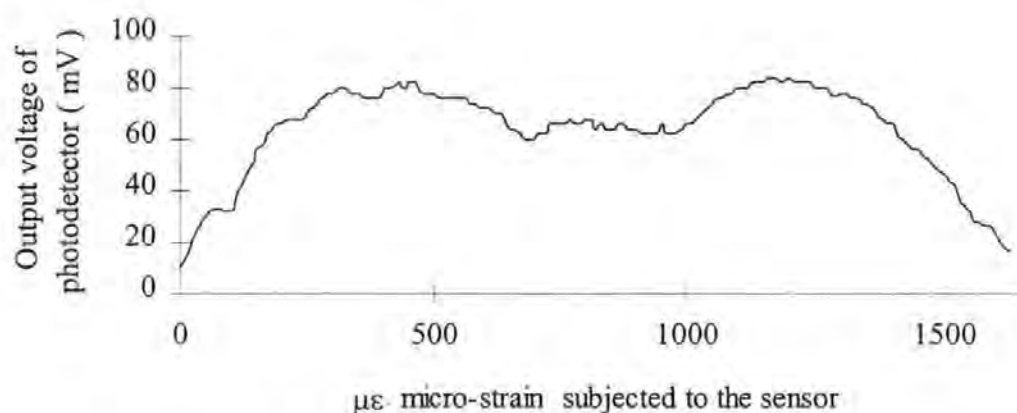


Figure (105) . Static reflectivity-strain profile of sensor TOMAR10.

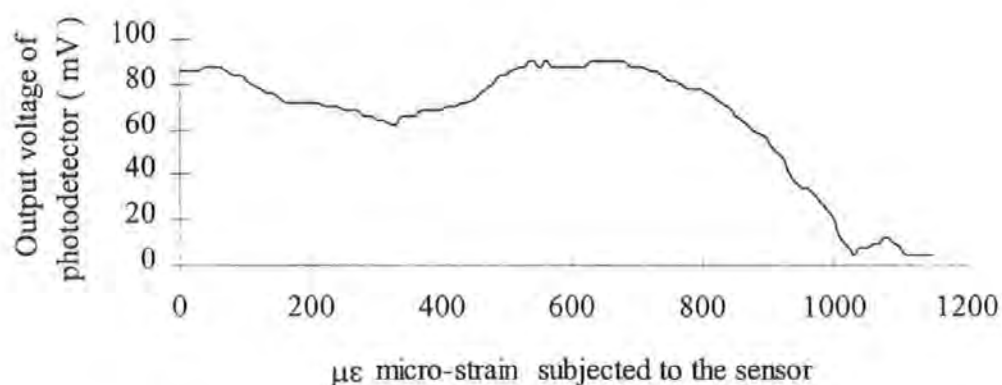


Figure (106) . Static reflectivity-strain profile of sensor TOMAR11.

5.5.2 Experimental results of the sensing system using fibre Bragg grating sensors.

The same test-rig and procedure was used as in section 5.5.1 with the D.F.B. laser being modulated with a 5kHz signal to induce a sinusoidal wavelength modulation. The effective current-to-wavelength conversion factor is dependent upon the current being applied to the D.B.F. laser ( see graph 3 in appendix Vc ). The sensors are mounted on the Aluminium beam and subjected to longitudinal strain. The lock-in-amplifiers measure the first and second harmonics but instead of a change of phase a change in wavelength is used to track the shift of the gratings profile, which is digitised ( AD converter in the electronics of the L.I.A's ) and fed into a computer see Figure 107 below.

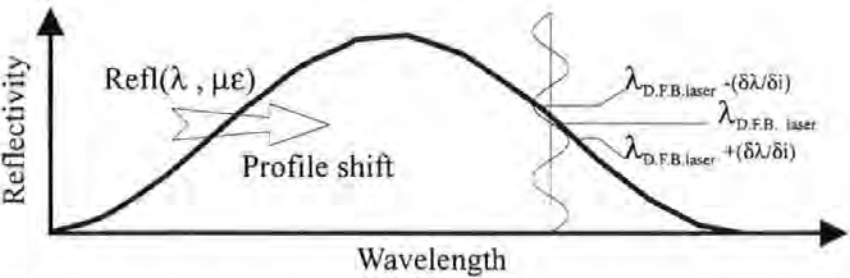


Figure (107) . Generation of the harmonics using wavelength modulation.

The fibre Bragg grating sensors were tested, cardioids were generated in some cases but not in others and diagrams of the first and second harmonics. Most of the sensor gratings generated lissajou figures, which were not useful cardioids for the adopted signal processing technique. The most successful sensor grating was TOMAR12, a profile which was a reasonable approximation to a sinusoidal response to longitudinal strain, see examples of cardioid and lissajou Figures 108, 109, 110.

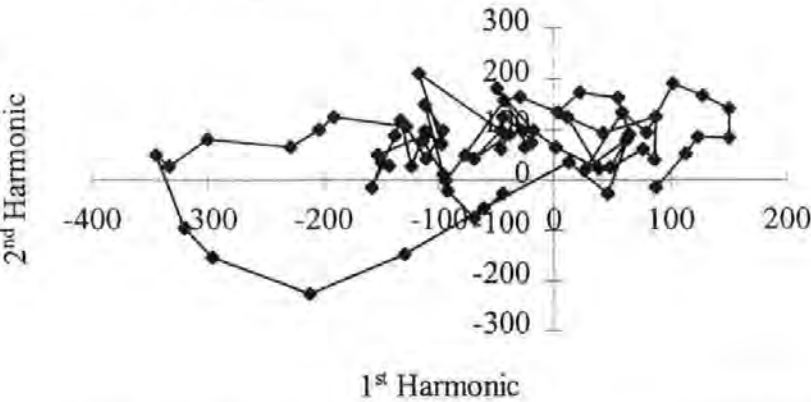


Figure (108) . Cardioid generated using sensing element TOMAR13.

The other grating sensors generated lissajou figures like Figure 108, the signal processing technique adopted worked but resulted in very poor strain resolution. Each mark represents an increase in strain of ten micro-strains. For sensor TOMAR13 only half the range was obtained ( 0 to  $700\mu\epsilon$  ). This was also true for TOMAR10 and no meaningful results were obtained using sensor TOMAR8. Realising that the first and second harmonics can be visualised as the first and second derivatives of the reflectance profile of the grating, any rapid variation of the derivatives would probably give the reason for obtaining bad results. One of the reasons for bad results is the anomalies on the profile ( rapid variation ) and/or the regions of flatness on the profile. To reduce the sensitivity of the signal processing technique to anomalies on the profile an increase in the wavelength modulation amplitude was adopted but this also decreased the response of the sensing system.

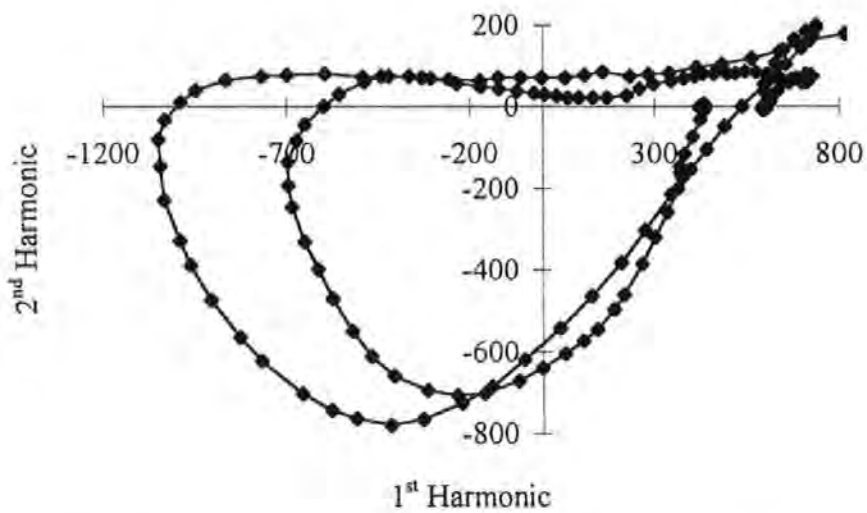


Figure (109) . Cardioid generated using sensing element TOMAR12.

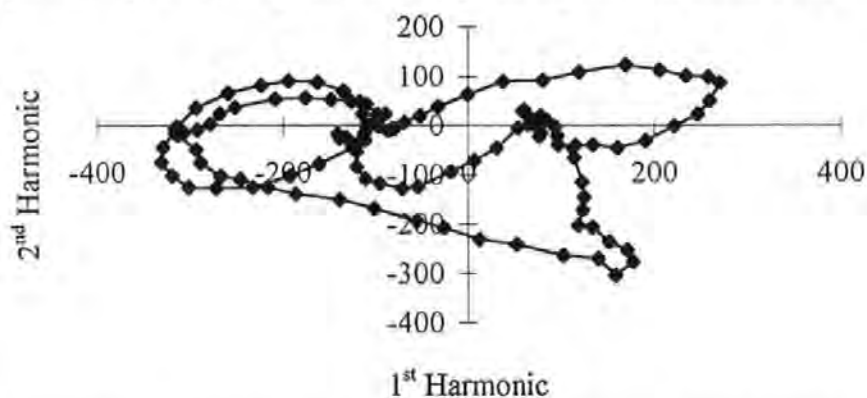


Figure (110) . Cardioid generated using sensing element TOMAR11.

Although the data are processed in the same way as that of the fibre Fabry-Perot sensor, the physical interpretation is different. It is the relative wavelength shift caused by longitudinal strain that is being measured rather than the change in optical phase shift. That is to say an effective wavelength shift takes place across the static reflectivity-strain profile of the sensing element, this being the Bragg grating sensor ( see appendix V, section Vg ). The way in which a change in temperature influences the sensor can be seen in Figure 111 where a hysteresis effect is clearly visible.

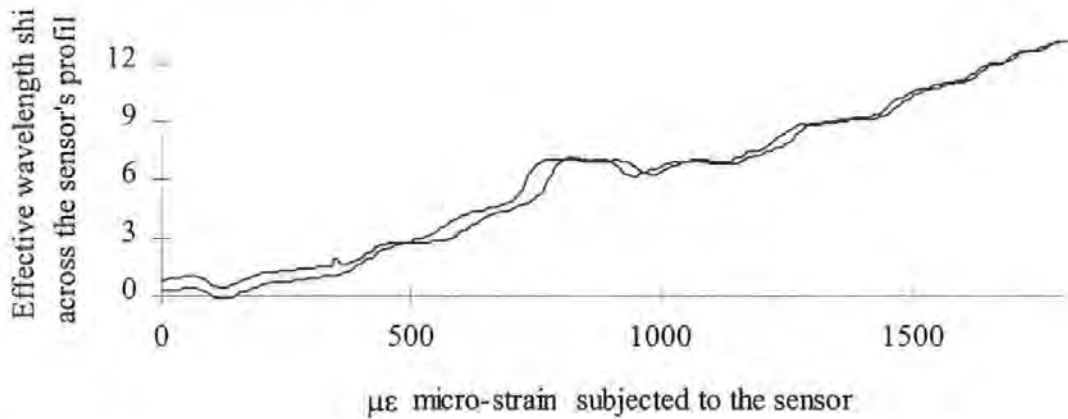


Figure (111) . Experimental processed data from the L.I.A.'s using sensor TOMAR12.

Figure 111 shows the behaviour of sensor TOMAR12 when subjected to an increasing strain up to 1810  $\mu\epsilon$  and then reduced back to 0  $\mu\epsilon$ , which shows the hysteresis.

Figure 112 shows how the measured data compares with theoretical predictions. The graph is composed of three curves **A**, **B** and **C**. A general observation of Figure 112 is that there are two regions of quasi-linearity separated by an inflexion plateau.

**Curve A** is the measured values of the wavelength shift due to strain for a sensor designated TOMAR12, which have been processed, see Figure 112.

**Curve B** is based on using the measured static reflection response of sensing element TOMAR12 when under strain and simulating the signal processing technique ( see appendix V, section Vk ; using a Mathcad program ), see Figure 112.

**Curve C** is a theoretical response, using T-matrix formalism to obtain the grating's response to strain and simulation for the signal processing, see Figure 112.

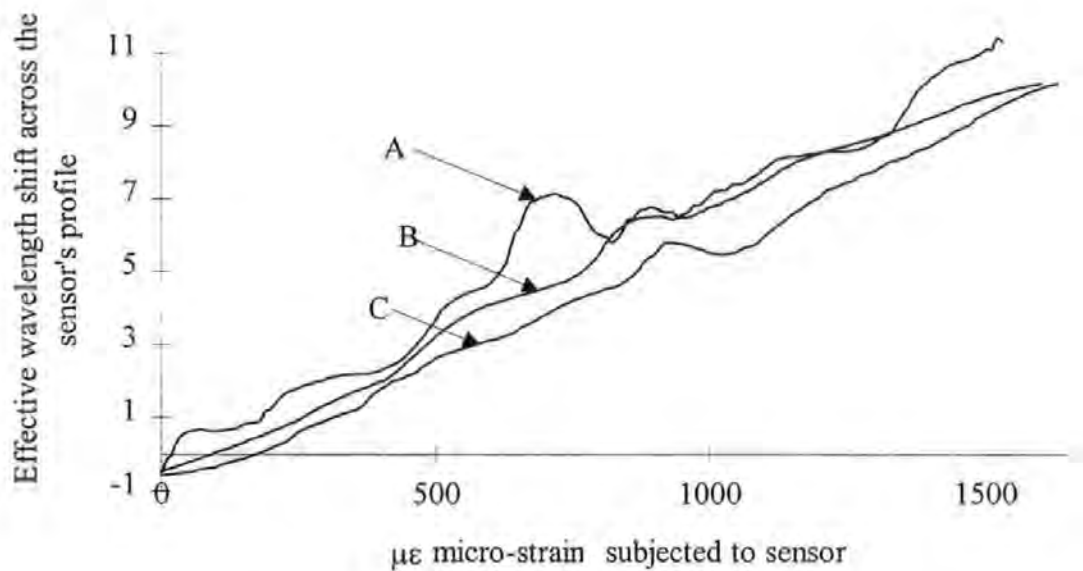


Figure (112) . A comparison between theoretical data from simulations and experimental data from sensor TOMAR12.

The slight differences are probably due to the parameters used in the simulation, which are slightly different to the fabricated fibre Bragg grating structure. This can be seen by comparing the theoretical and actual static reflection responses for longitudinal strain. The reason for the inflexion plateau is unclear but this occurs in both sets of results, theoretical and experimental. This suggests that the strain response is a direct response to the taper function of  $\Delta n$ . Removing the strain-optic effect and Poisson's effect on the material from the refractive index parameters results in this inflexion plateau being less pronounced.

The Experimental data used for Figure 112 was typical processed data from the grating sensing system using TOMAR12, some typical datasets are shown below in Figure 113. The variation of the various lines is probably due to temperature variation and minor adjustments to try and maintain an optimum signal. The sensor TOMAR12 is the only one for which a comparison is made because of the distortion / anomalies present on the other sensors.

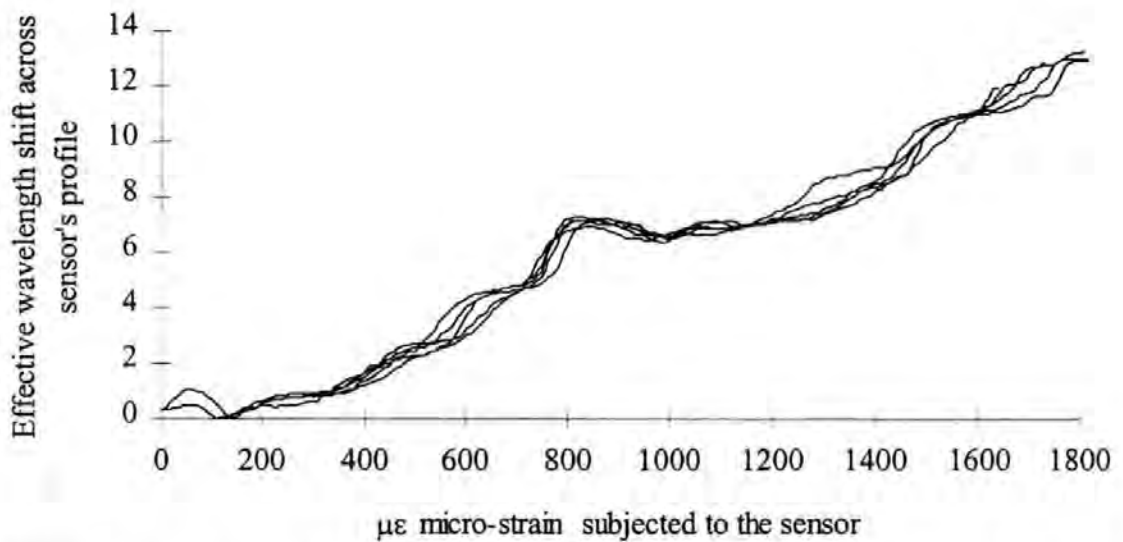


Figure (113) . Processed experimental data from some typical runs on the test -rig using the sensing system with the TOMAR12 fibre Bragg grating sensor.

The following results are taken at two different wavelengths;  $\lambda_1$  and  $\lambda_2$ . The reason behind this is not to over strain the Aluminium beam beyond its elastic limit, to which the sensor is adhered. The wavelengths  $\lambda_1$  and  $\lambda_2$  are chosen so that the complete spectral profile of the sensor can be obtained, when the sensor is strained its spectral profile will shift to longer wavelengths sweeping through the D.F.B. laser wavelength, either  $\lambda_1$  or  $\lambda_2$ . Thereby obtaining the complete response of the sensor to longitudinal strain, see Figure 114 below.

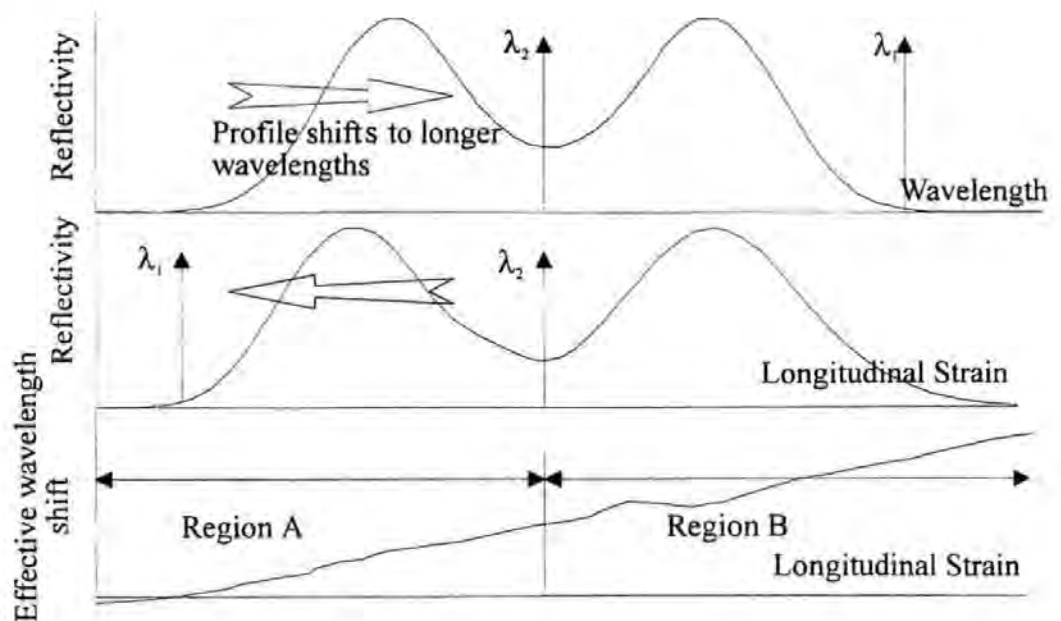


Figure (114) . Indicates where the wavelengths  $\lambda_1$  and  $\lambda_2$  are chosen.



By altering the temperature control facility on the drive circuit, the wavelengths of the D.F.B. laser  $\lambda_1$  and  $\lambda_2$  was adjusted so that  $\lambda_1 = 1557.6\text{nm}$  (temperature control voltage 4.31 V) and  $\lambda_2 = 1557.0\text{nm}$  (temperature control voltage 4.17 V). Measurements of the sensor's response to longitudinal strain were carried out at these two wavelengths.

## **5.6 Observations and results of the sensing system using sensor a Bragg grating that is linearly chirped and has a top-Hat taper function with a sinusoidal variation in the refractive index modulation.**

General inspection of the results obtained in the above section suggests that this type of fibre Bragg grating can be used as a strain sensor with the prescribed signal processing technique. The resolution of this type of sensor is dependent upon the envelope functions, the " period " of the sinusoidal variation of the refractive index modulation. The main problem with this grating sensor is the difficulty of fabrication. The general static reflective-strain response of the gratings gives evidence of this. This is one more step closer to a useful fibre optical strain sensor but for the " inflexion plateau " on the reflectivity - strain profile of the processed data.

The sensitivity was such that the additional pre-amplifier between the photodetector and the L.I.A.'s was not required and the gain of the amplifier was reduced.

The theoretical values for the constants of proportionality between the effective wavelength shift across the sensor's profile and longitudinal strain for regions A and B ( see Figure 114 ) are calculated using the T-matrix formalism to obtain the static reflectivity response to strain and then superimposing a sinusoidal variation on to the response and thus then extracting the first and second harmonics from that information. The parameter variation for the signal processing, such as effective current to wavelength conversion factor, was optimised to produce the most linear response ( see appendix V, section Vh ). The grating specification used in the T-matrix formalism was as follows is the refractive index modulation strength  $\Delta n \sim 1.6 \times 10^{-4}$ , chirp factor of  $1.204\pi$  with a sinusoidal period for the taper envelope function for the refractive index modulation 4.894mm. The total length of the grating is  $\sim 12.24\text{mm}$  and the initial grating period  $\Lambda(z = 0) = 510\text{nm}$ .



Using the above model and parameters and assuming a static sinusoidal reflective response to longitudinal strain a linear relationship can be extracted and hence an inverse tangent function of the ratio of first and second harmonics of the modulated wavelength response from the effective wavelength shift across the sensor's static strain-reflectivity response to applied longitudinal strain. The deviation away from linearity in region **A** is  $\pm 6\mu\epsilon$  with a constant of proportionality  $= 8.060 \times 10^{-3} \mu\epsilon^{-1}$ . In region **B**, a deviation away from linearity is  $\pm 8\mu\epsilon$  with a constant of proportionality  $= 8.131 \times 10^{-3} \mu\epsilon^{-1}$ . The actual static reflection response for longitudinal strain for sensor TOMAR12 ( see appendix V, section Vh ) gives in region **A**, a deviation away from linearity of  $\pm 21\mu\epsilon$  with a constant of proportionality  $= 7.758 \times 10^{-3} \mu\epsilon^{-1}$  and in region **B**, a deviation away from linearity of  $\pm 20\mu\epsilon$  with a constant of proportionality  $= 5.614 \times 10^{-3} \mu\epsilon^{-1}$ .

For region **A** the average constant of proportionality between the effective wavelength shift ( nm per nm ) and the longitudinal strain was found to be  $7.009 \times 10^{-3} \pm 0.315 \times 10^{-3} \mu\epsilon^{-1}$ . This is an error percentage of 11% to the expected theoretical value ( using the actual static reflection response of sensor TOMAR12 ) with a standard deviation percentage error of 11%. The deviation away from linearity was found to be  $\pm 20\mu\epsilon$ . Figure 115 shows some typical processed data from several runs with the D.F.B. laser at  $\lambda_1$  equal to 1557.6nm, region **A**.

For region **B** the average constant of proportionality between the effective wavelength shift ( nm per nm ) and the longitudinal strain was found to be  $6.29 \times 10^{-3} \pm 0.064 \times 10^{-3} \mu\epsilon^{-1}$ . This is an error percentage of 10% to the expected theoretical value ( using the actual static reflection response of sensor TOMAR12 ) with a standard deviation percentage error of 2%. The deviation away from linearity was found to be  $\pm 25\mu\epsilon$ . Figure 116 shows some typical processed data from several runs with the D.F.B. laser at  $\lambda_2$  equal to 1557.0nm, region **B**.

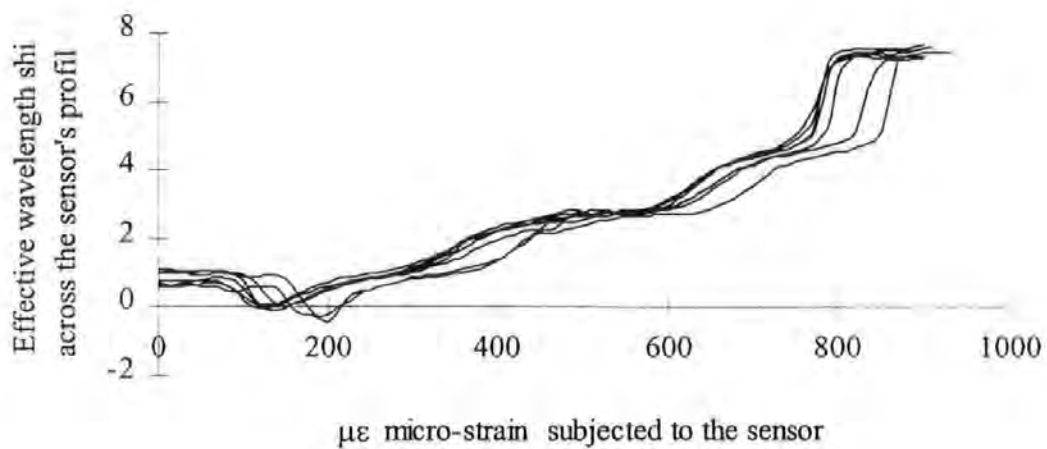


Figure (115) . Typical processed experimental data for region A, using sensor TOMAR12.

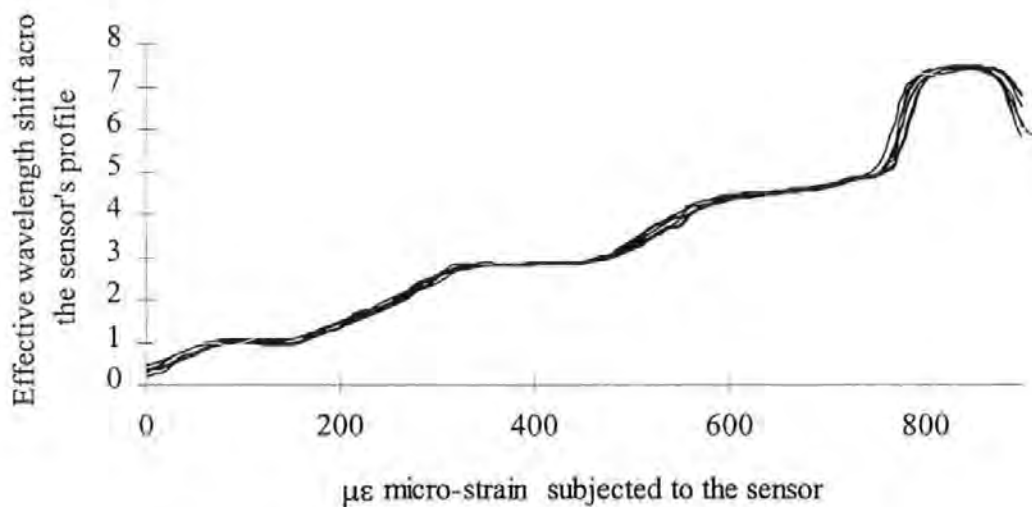


Figure (116) . Typical processed experimental data for region A, using sensor TOMAR12.

A general observation of Figures 115 and 116 is that the runs performed to generate the region **B** at  $\lambda_2$  are less noisy than the runs at  $\lambda_1$  for region A. This may be due to the fact that the D.F.B. laser was run at relatively high temperature to obtain  $\lambda_1$  and was running at the limits of the DF.B. laser, so thermal effects, thus wavelength drift would contribute to the noise.

If the wavelength is set at  $\lambda_2$  then both compression and tensile strain can be measured with this sensor. This sensor would then generate unique values for a given tensile strain or compression ( see section 5.2 ). Also, as the initial value of the wavelength shift for the sensor is known, then over a finite range, the sensing element is capable of measuring absolute strain when using the plateau to give a DC cut-off reflectance level. Strain sensitivity is variable along with the measurable range, which would depend upon application. Temperature effects were less noticeable using this sensor which is to be expected because the rates of the gradient are small compared to the fibre Bragg grating resonators, again this is dependent upon the spectral bandwidth of the grating's profile, that is to say the spectral period of the profile itself.

## **6      Conclusion.**

### **6.1 General discussion.**

The intention, at the start of this study, was to develop a strain gauge based on the principle of operation of a simple Fabry-Perot interferometer. The Fabry-Perot, the strain sensing element, was to be an integral part of a short length of standard, single-mode, and telecommunications optical fibre.

The reasoning behind this decision was two-fold. Firstly, the device would have a good resolution of strain, and secondly, using low values of mirror reflectance, around 5%, a Michelson type sinusoidal variation in irradiance with strain would exist. This sinusoidal response was a crucial fact in the design strategy. This was because the signal processing technique already developed would generate an output electrical signal from an inverse-tangent function of the optical signal which is proportional to the strain ( see section 2.4, 2.5.1 and appendix V ).

A fibre Fabry-Perot device was made using a  $\text{TiO}_2$  layer dielectric as a mirror which demonstrated that the principles of the sensor were sound. It was found however to suffer from a number of drawbacks. These are i) fabrication, ii) problems with multiplexing such a sensor, iii) measuring only apparent strain, iv) the length of sensor to obtain good resolution and associated shear strain.

It was decided that to overcome the major fabrication difficulties associated with the  $\text{TiO}_2$  F.F.P. sensor a move to fibre Bragg grating technology perhaps would provide a solution to this particular problem. Using the reflective properties of a Bragg grating, which has been written into the core of a single-mode optical fibre, could provide a replacement for the  $\text{TiO}_2$  mirror. In order to verify the suitability of this principle, an experiment was conducted to investigate the properties and performance of a Fabry-Perot, fibre Bragg grating resonator using this technology.

The gratings, used to substitute for the mirrors in a Fabry-Perot, were linearly chirped Bragg gratings with a large but finite spectral bandwidth and with a constant reflectance over that spectral range. The results from this study were encouraging and are documented in Chapter 4. Again the other problems associated with the  $\text{TiO}_2$  F.F.P. still

existed using these fibre Bragg grating resonators. Solution to these problems were sought by designing a number of modified Bragg grating resonators which were duly provided by our suppliers. The spectral bandwidth of these gratings was reduced and the separation between the gratings was also reduced. This would give an advantage when addressing the multiplexing problem. The results are reported in section 4.5. The modified grating resonator used did demonstrate that along with the associated theory these sensors could be used with existing signal processing technique.

There were still problems to be overcome with the sensing system operating with a modified resonator and using the existing signal processing technique. Obtaining a finite bandwidth of operation for longitudinal strain and moving away from measuring apparent ( relative ) strain to measuring absolute strain of a given structure.

A solution to the difficulty of measuring absolute longitudinal strain was to generate a single cardioid figure. This would give a unique pair of values for the first and second harmonic at a given value of strain or compression. This could be accomplished by using only a single period of sinusoidal oscillatory response for longitudinal strain or compression. Along with this, a way of detecting a finite range of operation of the sensor must be achieved. It was decided to use the static reflective power from a fibre Bragg grating, this would be used to give an effective cut-off power level for an operational range (see Figure 117 ). To stop shear strain occurring a single fibre Bragg grating would be used, thus reducing the total length of the sensor.

The characteristic behaviour of a single grating under longitudinal strain is to shift the spectral response of that grating to longer wavelengths. In order to make use of this effect the D.F.B. laser's wavelength is modulated ( see appendix V ).

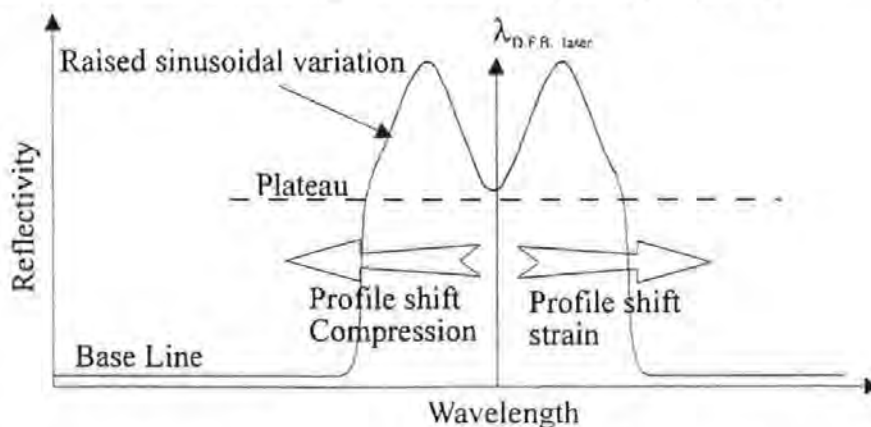


Figure (117) . Ideal spectral response of a fibre Bragg grating sensor required.

After some modelling of various structures of gratings by means of the T-matrix formalism ( see section 3.6, 3.7, 3.8 and appendices IV ) two possibilities emerged which gave the “ sinusoid ” spectral response and the required response to longitudinal strain .

One of the possibilities was discarded, after discussions with the fabricators; owing to the practical difficulties of producing the grating structure. The second grating structure was produced and is documented in chapter 5. The sensing system with this sensing element was demonstrated and the results are documented in sections 5.5 and 5.6. The experimental results were in relatively good agreement with the theoretical predictions, including the “ inflexion plateau ” in both sets of data. The reasoning for this inflexion plateau is not fully understood but using the Butter and Hocker model [50,51] which is a simplified expression for taking into account the strain-optic effect and neglecting the waveguide dispersion effects due to strain, may be the source of the problem. In the experimental data the inflexion plateau is more pronounced than in the theoretical data which suggests that a second order effect may be coming into play. This phenomenon was not present in the theoretical response to strain in the second possible structure. This suggests that the response to strain of the sensor being used is related to the overall effect of the longitudinal strain on the refractive index modulation taper envelope function.

## **6.2 General discussion of the performance of the new sensing element.**

The resolution of this linearly chirped, Top-Hat taper function with a sinusoidal variation in the refractive index modulation fibre Bragg grating sensor is less than the other types of sensing elements but this is dependent upon the period of the refractive index modulation taper envelope function ( see appendix Vg ), which also gives the effective range of operation of the sensor .

One of two problems have to be resolved with this sensor.

1) Fabrication: According to the co-researchers at Aston University this is quite a difficult sensor to produce but probably this problem will be overcome in time as the fabrication technique is refined. Although a  $\sim 1.5$  nm spectral bandwidth sensor has been produced, there would seem to be some additional problems in producing narrower spectral bandwidth sensors at the present time, again due to the adopted fabrication technique. Looking at the reflection band diagram [88] of this type of linearly chirped and tapered

function grating, as the spectral bandwidth decreases the required linear chirp also decreases. So with the required variation in the modulation of the refractive index a “ Fabry-Perot ” effect can occur at a given wavelength ( interaction, Bragg resonance along the grating length at more than one position ). So a reduction in the magnitude of the modulation of the refractive index would be required but also an increase in the quality of spectral profile of the grating is needed. In fact a reduction in the magnitude of the anomalies on the reflective profile of the grating; “ less noise ” would be needed.

2 ) Understanding the origins of the “ inflexion plateau ” and how to counter act it’s effect.

This new sensing element has satisfied the requirements of the project that is to say.

1 ) Fabrication which has difficulties but the sensors can be duplicated.

2 ) Multiplexing can be far easier addressed using the fact that these sensors work only over a small spectral range ( the sensor investigated in chapter 5, bandwidth  $\sim 1.5\text{nm}$  ).

3) This sensor is capable of measuring absolute strain.

4) The sensor’s length of 1cm is less than the  $\text{TiO}_2$  F.F.P. sensor.

### 6.3 General comparison of the three sensing elements.

Table 1 of the results of the project.

Sensor type	Sensitivity	Range of operation	Resolution
F.F.P. sensor (Titanium Oxide)	0.613 rad per $\mu\epsilon$	-	$\pm 1.0\mu\epsilon$
Fibre Bragg grating Resonators			
5% mirrors resonator	0.566 rad per $\mu\epsilon$	-	$\pm 0.5\mu\epsilon$
10% mirrors resonator	0.587 rad per $\mu\epsilon$	-	$\pm 2.0\mu\epsilon$
Modified Fibre Bragg grating Resonators			
No 14-3-3	0.013 rad per $\mu\epsilon$	$\sim 1000\mu\epsilon$	$\pm 35.0\mu\epsilon$
No 14-3-4	0.015 rad per $\mu\epsilon$	$\sim 1500\mu\epsilon$	$\pm 12.0\mu\epsilon$
Fibre Bragg grating sensor			
No TOMAR12			
Region A	0.00701 per $\mu\epsilon$	$\sim 1000\mu\epsilon$	$\pm 20.0\mu\epsilon$
No TOMAR12			
Region B	0.00629 per $\mu\epsilon$	$\sim 1000\mu\epsilon$	$\pm 25.0\mu\epsilon$

The resolution of the modified resonators is poor; this was due to noise on the reflectivity profile and temperature effects. The reason for the poor resolution for the fibre Bragg grating comes from the approximation of a tangent function for the ratio of the first to second harmonic. The modelling of the response of the system to strain needs some more investigating and modifications to the tangent function used. Table 1 also shows that the sensitivity of the  $\text{TiO}_2$  F.F.P. sensor is comparable to the fibre Bragg grating resonator (5% and 10%). This was expected because the gratings were just replacements for the titanium oxide layer and the physical dimensions (approximately the same length between mirrors). The fibre Bragg grating sensor has poor sensitivity compared to the fibre Bragg grating resonator or the  $\text{TiO}_2$  F.F.P. sensor but the sensitivity can be improved (see section 6.1).

Comparing this sensing detection method ( signal processing technique ) with the various sensing elements used in this study, to other systems reported in the literature ( section 1.2.5. and 1.26 ). It seems that the resolution is slightly less for the sensor TOMAR12 but the strain resolution can be improved by reducing the spectral bandwidth of the reflectivity profile of the grating. Some theoretical results are shown in Table 2, three examples and Figure 118, a theoretical prediction of reflectivity as a function of longitudinal strain of the fibre Bragg grating sensor is obtained by using T-matrix formalism ( a C-program ). The modelling of the signal processing technique is done by Mathcad +6 program ( see Figures 118 and 119 for theoretical predictions ); see appendix V and VI. Several theoretical modelling techniques were used to obtain consistent results between the different techniques and to gain confidence in the C-program, which represents the T-matrix formalism.

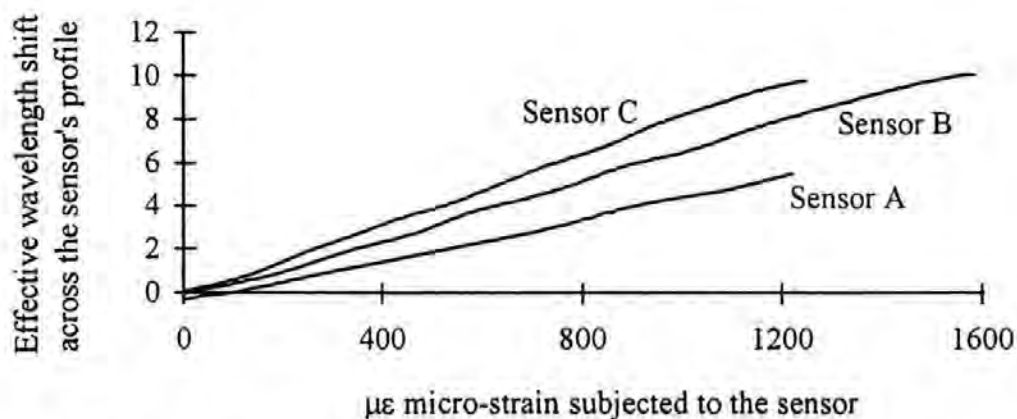


Figure (118) . Theoretical response of three proposed sensors.



Assuming the fabrication difficulties can be overcome. A series of theoretical predictions for proposed sensor gratings using the signal processing technique are shown in Figure 118. General observation of Figure 118 shows improvement in the linearity of the sensors as the spectral bandwidth of the sensors decreases. Note the wavelength modulation in the modelling of the signal processing was the same for all three sensors.

**Table 2 .** Theoretical results from the T-Matrix formalism of fibre Bragg gratings

Fibre Bragg grating sensor	Sensor's physical characteristics				Sensor's response to longitudinal strain		
	Chirp Factor	Depth of index modulation	Spectral Bandwidth	Total Length	Sensitivity	Range of operation	Resolution
Sensor A	3.529 $\pi$	$\Delta n \sim 0.00025$	$\sim 3.75$ nm	7.14 mm	0.00471 per $\mu\epsilon$	$\sim 2300$ $\mu\epsilon$	$\pm 17$ $\mu\epsilon$
Region A					0.00482 per $\mu\epsilon$	$\sim 1250$ $\mu\epsilon$	$\pm 12$ $\mu\epsilon$
Region B					0.00524 per $\mu\epsilon$	$\sim 800$ $\mu\epsilon$	$\pm 12$ $\mu\epsilon$
Sensor B	1.729 $\pi$	$\Delta n \sim 0.00022$	$\sim 2.62$ nm	10.2 mm	0.00679 per $\mu\epsilon$	$\sim 1650$ $\mu\epsilon$	$\pm 11$ $\mu\epsilon$
Region A					0.00664 per $\mu\epsilon$	$\sim 620$ $\mu\epsilon$	$\pm 9$ $\mu\epsilon$
Region B					0.00656 per $\mu\epsilon$	$\sim 800$ $\mu\epsilon$	$\pm 11$ $\mu\epsilon$
Sensor C	1.204 $\pi$	$\Delta n \sim 0.00016$	$\sim 2.16$ nm	12.24 mm	0.00812 per $\mu\epsilon$	$\sim 1340$ $\mu\epsilon$	$\pm 7$ $\mu\epsilon$
Region A					0.00806 per $\mu\epsilon$	$\sim 680$ $\mu\epsilon$	$\pm 6$ $\mu\epsilon$
Region B					0.00813 per $\mu\epsilon$	$\sim 560$ $\mu\epsilon$	$\pm 8$ $\mu\epsilon$

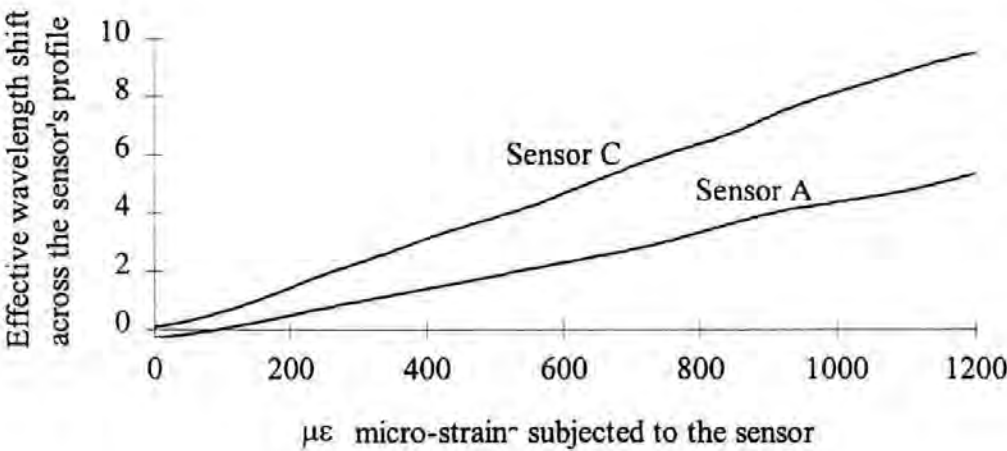


Figure (119) . The optimising of the theoretical response to longitudinal strain by changing the magnitude of the wavelength modulation.

The theoretical results shown in Figure 119 is when the wavelength modulation has been optimised for a given proposed sensor grating. This is achieved by changing the peak-to-peak modulation voltage to the drive unit of the D.F.B. laser and the magnitude of the drive current to the laser.

Temperature effects have not been taken into account with the present sensing system. There is a problem with temperature variation causing a shift in wavelength which is described in the literature and numerical values quoted for the wavelength shift due to temperature are  $\Delta\lambda_T = 1.3 \times 10^{-2} \text{ nm}^\circ\text{C}^{-1}$  and wavelength shift due to strain as  $\Delta\lambda_s = 1.15 \times 10^{-3} \text{ nm}\mu\text{e}^{-1}$  [35]. During the acquisition of data from experimental runs with the sensing system, using the TOMAR12 sensor, variations due to temperature seemed small but this was probably due to the fact that the Aluminium beam acted as a good heat sink, therefore minimising temperature effects. A proposed way of calibrating out temperature effects is to use a control sensor for each sensor used in the array. A simple electronic subtraction after signal processing of the data from both sensors would remove temperature effects.

#### 6.4 Suggestion for multiplexing.

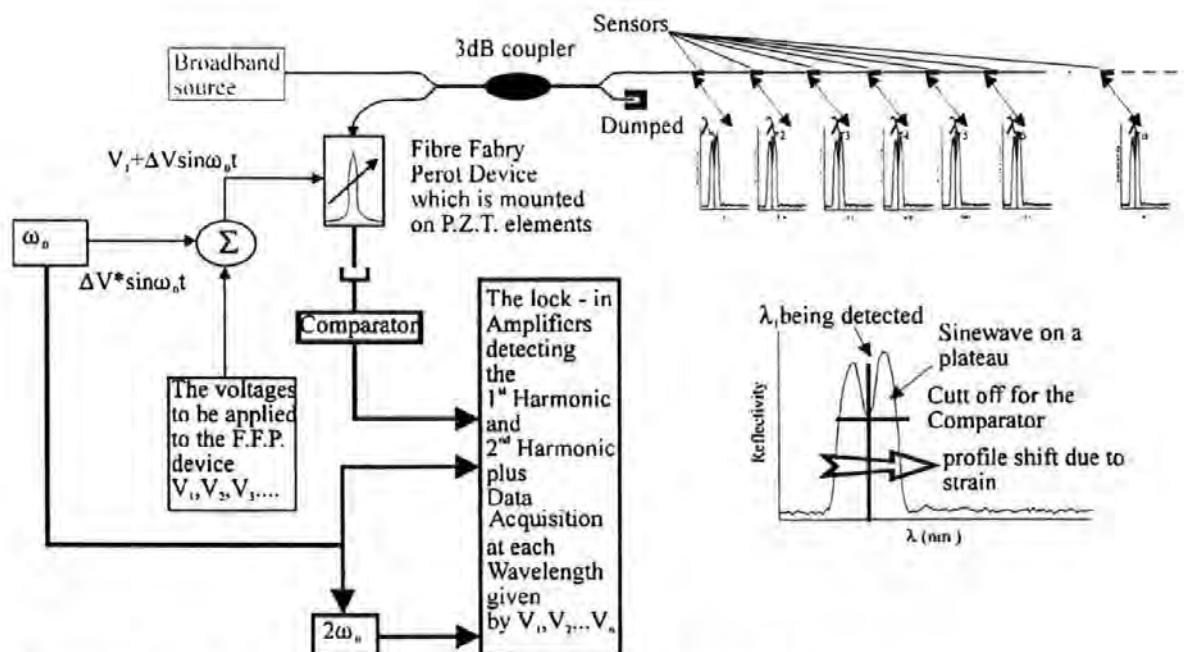


Figure (120) . A proposed scheme using this type of sensing element.

Figure 120 shows a possible scheme of multiplexing that could be used with this sensor. This scheme is dependent upon the fibre Fabry-Perot device; i.e. wavelength resolution. The free spectral range which is dependent on the finesse and thus the mirror reflectivities. An Alternative to the fibre Fabry-Perot device would be an electronically tuneable optical wavelength filter such as the one used in the M.A.S.T. joint project which include British Aerospace Sowerby Research Centre [112]. Another suggestion is to use a similar device such as the one used by T. Coroy et al [113] with an acousto-optic tuneable filter. In this system the wavelengths of the sensors with no longitudinal strain is at the minima of the reflectivity profile. As the sensor is subjected to compression or strain the profile shifts and generates a cardioid. The illuminating light source is broadband; the modulation of the light is achieved at the fibre Fabry-Perot device by a sinusoidal perturbation on the controlling voltage of the P.Z.T. mounts of the F.F.P. device.

Time division multiplexing is possible using an architecture using several D.F.B. lasers matched to each fibre Bragg grating sensors. These are suggestions for the multiplexing problems to illustrate the possibilities that may be used with this type of sensing element.

## **6.5 Robustness of the system.**

It is hard to quantify the robustness of a sensing system but it is easier to compare to another system. In the review of the literature [31- 45, 47-49] the majority of the sensing systems were demonstrated in a laboratory environment, assuming the same laboratory conditions for this project. In general a large percentage of demonstrated schemes using fibre Bragg gratings have used an optical spectrum analyser or some kind of interferometric filtering technique to extract the information meaning to extract the shift in wavelength generally this requires some bulky optical equipment or some additional optics to the fibre optical array. There are alignment problems that have to be considered in a commercial application when additional optics is included in the sensing system. This can also add to the physical size and complexity of the sensing system.

The system demonstrated in this project does not use bulky optical equipment, all optical components are fusion spliced into the fibre optical sensing array, giving an advantage over many of the schemes suggested in the literature. There are no alignment

problems with this scheme, this again is a distinct advantage for this scheme in a commercial application; less sensitive to handling errors and the environmental changes.

Robustness is very much qualitative. The system presented in this report needs to be compared to existing strain-sensing systems that are being used in specific applications such as by D. Roberts and P Foote [112] or P Nellen et al [114]. The D . Roberts and P. Foote sensing scheme uses an acousto-optic tuneable filter which reduces the bulky optical equipment but employs a tree architecture for the sensing array, which increases the possibility of damage due to handling whilst embedding the array.

P Nellen et al [114] uses a 0.5 m grating spectrometer equipped with a 1024 element CCD array for detecting a wavelength shift. Using simple line architecture, which decreases the damage drawing handling and embedding, but the system contains bulky optical equipment and also the increased risk of optical miss-alignment during the process of setting-up the sensing system.

## **6.6 A comparison of specification to existing systems.**

(a) The resolution of P Nellen et al [114] sensing system is  $\pm 1\mu\epsilon$  over a operation strain range of  $\sim 2000 \mu\epsilon$  with an update rate of the sensing system of 10 Hz, due to scanning of the 0.5 m grating spectrometer. The number of sensors in the channel / array is seven.

(b) The scheme adopted by D. Roberts and P Foote [112] is a little bit unclear in the available literature but the specification they are working to has a strain resolution of  $\pm 10\mu\epsilon$ , over an operational range of  $\pm 3500 \mu\epsilon$  with five sensors per channel / total number of sensor in the array is forty, with an update rate per sensor of 500 Hz.

Comparing theoretical predictions using the system investigated, in terms of strain resolution and operational range. The theoretical results seem to give parity with system **b** or better depending on the operational range of the sensor. Comparing experimental strain resolution of the system investigated to system **b**'s resolution, system **b** is better by a factor of two ( this has been discussed in section 6.1 and 6.2 ). Again comparing experimental strain resolution of the system investigated to system **a**'s resolution, system **a** is better by a magnitude but the range of measurement is approximately the same. Theoretical resolution is still less than for system **a** but only by a factor 2.

The update rate for the system under investigation is better by an order of 2 magnitudes than system a and approximately one order of magnitude better than system b.

In general this comparison does not seem favourable for the sensing system which has been investigated but advantages are less bulky optics ( less miss-alignment problems ) and much cheaper ( simple electronics for the signal processing technique ). The main problem is fabrication of the sensors themselves, quality, reducing noise ( increase in resolution ) and the ability to produce other short operational ranges.

## **6.7 Concluding remarks.**

The aim of the project was to produce a sensing element that would yield absolute strain measurement over a useful range of strain values and also have the operational strain resolution of a fibre Fabry-Perot sensor, without the fabrication / characterisation problems of the F.F.P. sensor.

This was achieved in part. A sensor was fabricated that could measure absolute longitudinal strain and overcome the fabrication problems encountered with the F.F.P. sensor but the resolution was not as good as the F.F.P. sensor.

The questions of resolution and operational range of this sensing element are linked and have been discussed in section 6.2 and 6.3 of this report. The longitudinal strain resolution can be improved by using shorter spectral bandwidth sensing elements, which also would decrease the operational range. The sensor design could be tailored to the application for a given resolution or range required.

## **7      References .**

- [1] J.A. Bucaro et al " Fibre optic hydrophones ", Jn. Acoust. Soc. Am. , vol 62 , pp 1302 , 1977 .
- [2] J.H. Cole et al " Fibre optic detection of sound ", Jn. Acoust. Soc. Am. , vol 62 , pp 1136 , 1977 .
- [3] P.A. Tutton et al " Structural health monitoring using embedded fibre optic sensors ", AGARD Conf . Proc. ,Smart struct aircraft and spacecraft, L ndau , Germany , pp 531 , 1993 .
- [4] R. Kist et al " Fibre Fabry Perot Thermometer for medical applications ", Conf. Proc. , 2nd O.F.S. , Stuttgart , Germany , pp165 , 1984 .
- [5] T. Allsop et al " High resolution optical-fibre strain gauge for bio-engineering applications ", Conf. Proc. Bio-Sensors , Vienna , Austria , 1996 .
- [6] R.M. Measures et al " Wavelength demodulation Bragg grating fibre optic sensing systems for addressing smart structure critical issues ", Smart .Mater.Struct. vol 1 , pp36 , 1992 .
- [7] R.M. Measures " Fibre optic sensor - The key to smart structures ", SPIE , vol 1120 , Fibre Optic's 89 , pp161 , 1989 .
- [8] D. Uttamchandani , Jn Elect and Comms Eng , pp237 , 1994 .
- [9] D.A. Jackson " Recent progress in monomode fibre optic sensors ", Meas. Sci. Tech. , vol 5 , pp621 , 1994 .
- [10] T. Berkoff et al " Interferometric fibre displacement / strain sensor based on source coherence synthesis ", Elect. Lett. Vol 26 , no 7 , pp452 , 1990 .
- [11] K.A. Murphy et al " Elliptical core two mode optical fibre sensor implementation methods ", Jn. Lightwave Technol. , vol 8 , no 11 , pp1688 , 1990 .
- [12] P. Neilson et al " Experimental application of phase strain temperature model for polarimetric optical fibre strain sensor ", Conf. Proc. Smart structures and materials Glasgow , pp89 , 1992 .
- [13] H.K. Kim et al " Polarimetric fibre laser sensors " Opt. Lett. , vol 18 , no4 , pp317 , 1993 .
- [14] C.E. Lee et al " Optical fibre Fabry Perot embedded sensor ", Opt. Lett., vol 4, no21 , pp832 , 1989 .

- [15] J.P. Andrews " Hybrid fibre optic sensor resolves directional ambiguity of time multiplexed Fabry Perot ", SPIE Conf. Proc. Active Materials and Adaptive structures , session 34 , Blacksburg ,VA , U.S.A. , 1992 .
- [16] J.S. Sirkis et al " In-line fibre etalon for strain measurement ", Opt. Lett. , vol 18 , no 22 , pp1973 , 1993 .
- [17] K.A. Murphy et al " Quadrature phase-shifted , extrinsic Fabry Perot optical fibre sensors ", Opt Lett , vol 16 , no 4 , pp273 , 1991 .
- [18] C.E. Lee et al " Optical fibre Fabry Perot sensors for smart structures ", SPIE Conf. Proc. Active Materials and Adaptive structures , session 34 , Blacksburg ,VA , U.S.A. , pp657 , 1992 .
- [19] D.Hogg et al " Development of a fibre Fabry Perot strain gauge system ", SPIE Conf. Proc. Active Materials and Adaptive structures , session 34 , Blacksburg ,VA , U.S.A. , pp667 , 1992 .
- [20] J.S. Sirkis et al " In-line fibre etalon fibre optical strain sensor ", Jn. Lightwave Technol. , vol 13 , no 7 , pp1256 , 1995 .
- [21] A Wang et al " Extrinsic Fabry Perot interferometric optical fibre sensor with micro-lens ", SPIE Conf. Proc. Active Materials and Adaptive structures , session 34 , Blacksburg ,VA , U.S.A. , pp19 , 1992 .
- [22] V. Bhatia et al " Application of absolute fibre optic sensors to smart materials and structures ", Conf Proc. 10th Optical Fibre Sensors Conf , Glasgow , vol 1699 , pp17 , 1994 .
- [23] F. Farahi et al " A multiplexed remote fibre optic Fabry Perot sensing system ", Int. Jn. Optoelectronics , vol 3 , no1 , pp79 , 1988 .
- [24] Ph. M. Nellen " Absolute strain measurement with multiplexed low coherence demodulated fibre Fabry Perot ", Conf. Proc. 10th Optical Fibre Sensors , Glasgow , vol 1699 , pp518 , 1994 .
- [25] J.S. Sirkis et al " Complete phase-strain model for structurally embedded interferometric optical fibre sensors ", Jn. Intell. Mater.Syst. and Struct . , vol 2 , pp3 , 1991
- [26] J.S. Sirkis et al " Interferometric strain measurement by arbitrarily configured , surface-mounted , optical fibres " , Jn. Lightwave Technol. , vol 8 , no 10 , pp1497 , 1990 .

- [27] J.S. Sirkis " Unified approach to phase-strain-temperature models for smart structure interferometric optical fibre sensors : part 1 , development ", *Opt. Engineering* , vol 32 , no 4 , pp752 , 1993 .
- [28] K-S. Kim et al " A model of embedded fibre optic Fabry Perot temperature and strain sensors ", *Jn. Composite Mater.* , vol 27 , no 17 , pp1618 , 1993 .
- [29] D.A. Jackson " Monomode optical fibre interferometers for precision measurement ", *Jn. Phys. E. Sci. Instrum.* , vol 18 , pp981 , 1985 .
- [30] A.D. Kersey et al " Overview of multiplexing techniques for interferometric fibre sensors " *Proc. SPIE Fibre Optic and Laser sensors V* , vol 838 , pp184 , 1987 .
- [31] Y-J. Rao " In-fibre Bragg grating sensors ", *Meas. Sci. Tech.* , vol 8 , pp355 , 1997.
- [32] B.Y. Kim et al " Multiplexing of fibre optic sensors ", *Optic News* , pp35 , Nov 1989 .
- [33] S.M. Melle et al " Practical fibre optic Bragg grating strain gauge system ", *Appl. Opt.* , vol 32 , no19 , pp3601 , 1993 .
- [34] T. Coroy et al " Active wavelength demodulation of a Bragg grating fibre optic strain sensor using a quantum well electroabsorption filtering detector ", *Elect. Lett.* Vol 32 , no 19 , pp1811 , 1996 .
- [35] A.D. Kersey et al " Fibre-grating based strain sensor with phase sensitive detection" , *Conf. Proc. Smart Structures and Materials* , Glasgow 1992 , section 2 , pp61 .
- [36] A.D. Kersey et al " Fibre optic Bragg strain sensor with drift-compensated high-resolution interferometric wavelength-shift detection ", *Opt. Lett.* , vol 18 , no 1 , pp72 , 1993 .
- [37] G.P. Bardy " Bragg grating temperature and strain sensor ", *Conf. Proc. 10th Optical Fibre Sensors Conf* , Glasgow , vol 1699 , pp511 , 1994 .
- [38] A. Othonos et al " Fibre Bragg grating laser sensor ", *Opt. Engineering* , vol 32 , no11 , pp2841 1993 .
- [39] Y-J. Rao et al " Combined spatial and time division multiplexing scheme for fibre grating sensors with drift-compensated phase-sensitive detection ", *Opt. Lett.* , vol 20 , no 20 , pp2149 , 1995 .
- [40] A.D. Kersey et al " Multiplexed fibre Bragg grating strain sensor system with a fibre Fabry Perot wavelength filter ", *Opt. Lett.* , vol 18 , no 16 , pp1371 , 1993 .
- [41] D.A. Jackson et al " Simple multiplexing scheme for a fibre optic grating network", *Opt. Lett.* , vol 18 , no 14 , pp1193 , 1993 .



- [42] A.B. Ribeiro et al " Time and spatial multiplexing tree topology for fibre optic Bragg grating sensors with interferometric wavelength-shift detection ", *App. Opt.* , vol 35 , no 13 , pp2267 , 1996 .
- [43] J. Mlodzianowski et al " A simple frequency domain multiplexing system for optical point sensors ", *Jn. Lightwave Technol.* , vol 5 , no 9 , pp1002 , 1987 .
- [44] W.W. Morey et al " Multiplexing fibre Bragg grating sensors ", *Proc. Soc. Photo-opt. Instrum. - Distributed and multiplexed fibre optic sensors* , Boston , U.S.A. , SPIE , vol 1586 , pp216 , 1991 .
- [45] D. Connell et al " Coherence multiplexed fibre optic temperature sensor using a wavelength dithered source ", *Proc. OFC'89* , Houston , U.S.A. , pp145 , 1989 .
- [46] A.D. Kersey et al " Differential polarimetric fibre optic sensor configuration with dual wavelength operation ", *Appl. Opt.* , vol 28 , pp204 , 1989 .
- [47] H. Ishio et al " Review and status of wavelength division mutliplexing technology and its applications ", *Jn. Lightwave Technol.* , vol 2 , pp448 , 1984 .
- [48] Y-J. Rao et al " Extended dynamic range detection system for in fibre Bragg grating strain sensors based on two cascaded interferometric wavelength scanners ", *Meas. Sci. Technol.* , vol 8 , pp1043 , 1997 .
- [49] A.D. Kersey " Interrogation and Multiplexing techniques for fibre Bragg grating strain sensors ", *Conf Proc. 10th Optical Fibre Sensors Conf* , Glasgow , vol 2071 , pp30 , 1994 .
- [50] C.D. Butter and G.B. Hocker " Fibre optics strain gauge ", *Appl. Opt.* , vol 17 , no 18 , pp2867 , 1978 .
- [51] G.B. Hocker " Fibre optic sensing of pressure and temperature ", *Appl. Opt.* , vol 18 , no 9 , pp1445 , 1979 .
- [52] H.W. Haslash et al " Surface mounted optical fibre strain sensor design ", *Appl. Opt.* , vol 30 , no28 , pp4069 , 1991 .
- [53] M. Born , E. Wolf " *Principles of Optics* " , Pergamon , Oxford , 1970 .
- [54] G. Meltz et al " Formation of Bragg gratings in optical fibres by transverse holographic method ", *Opt. Letts* , vol 14 , no 15 , pp823 , 1989 .
- [55] I. Bennion et al " UV written in fibre Bragg gratings ", *Opt. and Quant. Elect.* , vol 28 , pp93 , 1996 .
- [56] P. Yeh " *Optical waves in layered media* " , J. Wiley and Sons .
- [57] A. Yariva " *Optical waves in crystals* " , J. Wiley and Sons , 1983.

- [58] K.O. Hill et al " Photosensitivity in optical fibre waveguides : Application to reflection filter fabrication ", Appl. Phys. Lett. , vol 32 , no 10 , pp647 , 1978 .
- [59] Q. Zhang et al " Linearly and nonlinearly chirped Bragg gratings fabricated on curved fibres ", Opt. Lett. , vol 20 , no 10 , pp1122 , 1995 .
- [60] J.A.R. Williams et al " Fibre Bragg grating fabrication for dispersion slope compensation ", Photon. Technol. Lett. , vol 8 , no9 , pp1187 , 1996 .
- [61] M.C. Farries et al " Very broad reflection bandwidth ( 44nm ) chirped fibre gratings and narrow bandpass filtes produced by the use of an amplitude mask ", Electron. Lett. , vol 30 , no 11 , pp891 , 1994 .
- [62] K.C. Bryon et al " Fabrication of chirped gratings written holographically in optical fibre tapers ", Electronic Lett. , vol 29 , pp1659 , 1993 .
- [63] R. Kashyap et al " Simple technique for apodising chirped and unchirped fibre Bragg gratings ", Electronic Lett. , vol 32 , no 13 , pp1226 , 1996 .
- [64] J. Canning et al " p-phase shifted periodic distributed structures in optical fibres by UV post processing ", Electronic Lett. , vol 30 , no16 , pp1344 , 1994 .
- [65] W.W. Morey et al " Fibre optic Bragg grating sensors ", Proc. SPIE Fibre Optic and Laser sensors VII , vol 1169 , pp98 , 1989 .
- [66] P.J. Lemaire et al " High pressure H<sub>2</sub> loading as a technique for achieving ultrahigh UV photosensitivity and thermal sensitivity in GeO<sub>2</sub> doped optical fibres " ,  
Electronic Lett. , Vol 29 , no13 , pp1191 , 1993 .  
D.L. Williams et al " Enchanced UV photosensitivity in Boron codoped germanosilicate fibres " , Electronic Lett. , Vol 29 , no1 , pp45 , 1993
- [67] B.Malo et al " Single excimer pulse writing fibre gratings by use of a zero order nulled phase mask : grating response and visualisation of index perturbations " ,  
Opt. Lett. , Vol 18 , pp453 , 1993 .
- [68] C.G. Askins et al " Consideration for producing single pulse fibre Bragg gratings " ,  
SPIE Conf. Proc. Distributed and multiplexed Fibre optic sensors 3 , Boston ,  
vol 2071 , paper2 , pp12 , 1993 .
- [69] C.G. Askins et al " Fibre Bragg reflectors prepared by a single excimer pulse " ,  
Opt. Lett. , vol 17 , no 11 , pp833 , 1992 .

- [70] K.O. Hill et al " Bragg gratings fabricated in monomode photosensitive optical fibre by UV exposure through a phase mask ", Appl. Phys. Lett. , vol 62 , no10 , pp1035 , 1993 .
- [71] Q. Zhang et al " Simple prism based scheme for fabricating Bragg gratings in optical fibres ", Opt. Lett. , Vol 19 , no23 , pp2030 , 1994 .
- [72] R.J. Campbell et al " The properties and applications of photosensitive germanosilicate fibre ", Int. Jn. Optoelectron. , vol 9 , no 1 , pp33 , 1994 .
- [73] A. Inoue et al " Fabrication and application of fibre Bragg grating : A review ", Optoelectronics Devices and Technol. , vol 10 , no 1 , pp119 , 1995 .
- [74] V. Mizrahi et al " Physics of photosensitive grating formation in optical fibres ", Physical review A , vol 43 , no1 , pp433 , 1991 .
- [75] D.L. Williams et al " UV spectroscopy of optical fibres and preforms ", SPIE Proc. of the Photo. Opt. Instrumen. Eng. , vol 1516 , pp29 , 1991 .
- [76] L. Dong et al " Photoinduced absorption change in germanosilicate preforms : evidence for the colour centre model of photosensitivity ", Appl. Opt. , vol 34 , no18 , pp3436 , 1995 .
- [77] W. Streifer et al " Analysis of grating coupled radiation in GaAs:GaAlAs lasers and waveguides ", Jn Quant. Electron. , vol QE-12 , no 12 , pp422 , 1976 .
- [78] A. Yariv " Coupled Mode theory for guided wave optics ", Jn Quant. Electron. , vol QE-9 , no 9 , pp919 , 1973 .
- [79] A. Yariv et al " Periodic structures for integrated optics ", Jn Quant. Electron. , vol QE-13 , no 4 , pp233 , 1977 .
- [80] H. Kogelnik " Filter response of nonuniform almost -periodic structures ", The Bell System Technical Journal , vol 55 , no 1 , pp109 , 1976 .
- [81] H. Kogelnik et al " Coupled wave theory of distributed feedback lasers ", Appl. Phys. Lett. , vol 43 , no5 , pp2327 , 1972 .
- [82] J.B. Shellan et al " Theory of chirped gratings in broad band filters ", Opt. Commun., vol 23 , no 3 , pp398 , 1977 .
- [83] C.S. Hong et al " Broad - band grating filters for thin film optical waveguides ", Appl. Phys. Lett. , vol 31 , no7 , pp276 , 1977 .
- [84] M. Matsuhara et al " Optical waveguide band rejection filters : Design " , Appl. Opt., vol 13 , no 12 , pp2886 , 1974 .

- [85] M. Matsuhara et al " Optical waveguide filters : Synthesis ", Jn Opt. Soc. Am. , vo 65 , no 7 , pp804 , 1975 .
- [86] T. Fukuzawa et al " Mode coupling in thin film chirped gratings ", Opt. Lett. , vol 4 , no 11 , pp343 , 1979 .
- [87] B-G. Kim et al " Effect of front -facet reflections on the reffectivity of Bragg reflectors ",Opt. Lett. , vol 16 , no 14 , pp1065 , 1991 .
- [88] L. Poladian " Graphical and WKB analysis of nonuniform Bragg gratings ", Physical Review E , vol 48 , no 6 , pp4759 , 1993 .
- [89] J.E. Sipe et al " Propagation through noniform grating structures ", Jn Opt. Soc. Am. , vol 11 , no 4 , pp1307 , 1994 .
- [90] L.A. Weller-Brophy et al " Analysis of waveguide gratings : application of Rouard's method ", Jn Opt. Soc. Am. , vol 2 , no 6 , pp863 , 1985 .
- [91] L.A. Weller-Brophy et al " Analysis of waveguide gratings : a comparison of the results of Rouard's method and coupled -mode theory ", Jn Opt. Soc. Am. , vol 4 , no 1 , pp60 , 1987 .
- [92] G-H. Song et al " Design of corrugated waveguide filters by the Gel'fand -Levitan-Marchenko inverse scattering method ", Jn Opt. Soc. Am. A. , vol 2 , no 11 , pp1905 , 1985 .
- [93] E. Peral et al " Design of fibre grating dispersion compensators using a novel iterative solution to the Gel'fand -Levitan-Marchenko coupled equations ", Electronic Lett. , vol 32 , no 10 , pp918 , 1996 .
- [94] L. Poladian " Resonance mode expansions and exact solutions for nonuniform gratings ", Physical Review E , vol 54 , no 3 , pp2963 , 1996 .
- [95] D. Kermisch " Nonuniform sinusoidally modulated dielectric gratings ", Jn Opt. Soc.Am. , vol 59 , no 3 , pp1409 , 1969 .
- [97] M. Yamada et al " Analysis of almost periodic distributed feedback slab waveguide via a fundamental matrix approach ", Appl. Opt. , vol 26 , no 16 , pp3474 , 1987 .
- [98] B-G. Kim et al " Comparison between the matrix method and the coupled wave method in the analysis of Bragg reflector structures ", Jn Opt. Soc. Am. A. , vol 9 , no 1 , pp132 , 1992 .
- [99] S. Huang et al " Bragg intragrating structural sensing ", Appl. Opt. , vol 34 , no 22 , pp5003 , 1995 .

- [100] W.W. Morey et al " Fibre Fabry Perot interferometer using side exposed fibre Bragg gratings ", O.F.C. 92 Conf. Proc. Opt. Fibre Communs. , San Jose , WA2 , 1992 .
- [101] G.E. Town et al " Wide band Fabry Perot like Filters in optical fibre ", Photon. Technol. Lett. , vol 7 , no 1 , pp78 , 1995 .
- [102] S. Legoubin et al " Free spectral range variations of grating based Fabry Perot filters photowritten in optical fibre ", Jn Opt. Soc. Am. A. , vol 12 , no 8 , pp1687 , 1995 .
- [103] M. Martinelli " The dynamical behaviour of a single mode optical fibre strain gauge ", Jn Quant. Electron. , vol QE-18 , no 4 , pp666 , 1982 .
- [104] P. Yeh " Optical waves in layered Media " , Wiley , New York , 1988 .
- [105] A. Yariv and P. Yeh " Optical Waves in Crystals " , Wiley , New York , 1984 .
- [106] A. Yariv " Optical Electronics " , Holt-Saunders , New York , 1985 .
- [107] D. Lee " Electromagnetic Principles of Integrated Optics " , Wiley , New York , 1986 .
- [108] T. Tamir " Integrated Optics " , Springer-Verlag , New York , 1975 .
- [109] D. Marcuse " Theory of Dielectric Optical Waveguides , second edition " , Academic Press , Boston , 1991 .
- [110] H. A. Haus " Waves and Fields in Optoelectronics " , Prentice-Hall , New Jersey , 1984 .
- [111] E. Udd " Fiber Optic Sensors , An Introduction for Engineers and Scientists " , Wiley , New York , 1992 .
- [112] D. Roberts and P. Foote " Carbon spars for superyachts and smart technology " , Conf. Proc. The Modern Yacht , Portsmouth , U.K. , paper No 13 , 1998 .
- [113] T. Coroy et al " Applications of Photonic Technonolgy " , pp343 , Plenum Press , New York , 1995 .
- [114] P. Nellen et al " Application of fiber optical and resistance strain gauges for long-term surveillance of civil engineering structures " , Proc. Vol 3043 : Smart Structures and Materials , 3043 , pp77 , 1997 .

## Appendix I. Mode Coupling Theory.

All of the guiding structures that are discussed in the appendix are representatives of a broad class known as cylindrical dielectric waveguides . By definition , a cylindrical dielectric waveguide is a structure whose permittivity is invariant along the propagation direction  $z$  . Assuming a free - space permeability  $\mu_0$  , then the waveguide geometry is completely defined by specifying the variation of the permittivity  $\epsilon$  with  $x$  and  $y$  .

No matter how complicated the function  $\epsilon(x,y)$  is there are several general statements that can be made concerning the nature of the guided modes supported by the structure . These statements / relationships are important for analysis of coupled - mode theory . There are two approaches that are generally used to obtain an exact solution for the mode in the waveguide ( propagation of electromagnetic radiation along the guide ) . One is the Bloch - wave formalism [ 104,105 ] . The other is coupled mode theory [ 106-110 ] due to the variation of the dielectric ( permittivity ) along the axis of the fibre . This is considered as a perturbation that couples the unperturbed normal modes of a structure and the resultant E-field can be expressed as a superposition of unperturbed normal modes .

### Ia ) Coupled Equations of Motion .

Let the unperturbed fields  $\mathbf{E}$  and  $\mathbf{H}$  correspond to the solutions for the  $n$ th mode on the unperturbed waveguide . That is ,

$$\mathbf{E}(x, y, z) = \mathbf{e}_n(x, y)e^{-ik_{zn} z}$$

$$\mathbf{H}(x, y, z) = \mathbf{h}_n(x, y)e^{-ik_{zn} z}$$

where  $\mathbf{e}_n$  and  $\mathbf{h}_n$  are normalised fields .

The perturbed fields  $\mathbf{E}'$  and  $\mathbf{H}'$  can be represented by some superposition of the unperturbed modes . At some fixed arbitrary value of  $z = z_0$  the perturbed fields are only a function of  $x$  and  $y$  . The transverse field components of the unperturbed modes can be shown to be an orthogonal set in any  $xy$  plane , this can shown from the Lorentz reciprocity theorem , assuming that the perturbed permittivity is the same as the unperturbed

permittivity .It is possible to express the transverse components of the perturbed fields in terms of the unperturbed transverse field components , that is

$$\mathbf{E}'_t(x, y, z_0) = \sum_m a_m(z_0) \underline{e}_{mt}(x, y) e^{-ik_m z_0}$$

and

$$\mathbf{H}'_t(x, y, z_0) = \sum_m a_m(z_0) \underline{h}_{mt}(x, y) e^{-ik_m z_0}$$

where the coefficients  $a_m(z_0)$  are constants and the summation is over all guided modes . While the above superposition may be used to represent the perturbed field variation with  $x$  and  $y$  at  $z = z_0$  at some other different but arbitrary point  $z$  along the guide the perturbed field variation with  $x$  and  $y$  might be different . Therefore , the coefficients  $a_m$  must in general vary with  $z$  .Thus , for an arbitrary  $z$  ,  $z$  must be replaced with  $a_m(z)$  . It is possible in some situation to solve for the coefficients  $a_m(z)$  and obtain a complete description of the perturbed fields .

Note that the longitudinal perturbed fields  $\mathbf{E}'_z$  and  $\mathbf{H}'_z$  are obtainable from the transverse component using Maxwell's curl equations . That is ,

$$\underline{z}\mathbf{E}'_z = 1/(i\omega\epsilon') (\nabla_t \times \mathbf{H}'_t)$$

$$\underline{z}\mathbf{H}'_z = 1/(-i\omega\mu_0) (\nabla_t \times \mathbf{E}'_t)$$

Where  $\omega$  is the frequency of the propagating field and  $\mu_0$  has the usual meaning .

Substituting the expansions for  $\mathbf{E}'_t$  and  $\mathbf{H}'_t$  in terms of the unperturbed transverse modes and note that the unperturbed fields satisfy Maxwell's curl equations for the unperturbed geometry defined by  $\epsilon'$  , thus

$$\mathbf{E}'_z = \sum_m a_m(z) \frac{\epsilon}{\epsilon'} \underline{e}_{mz} e^{-ik_m z_0}$$

and

$$\mathbf{H}'_z = \sum_m a_m(z) \underline{h}_{mz} e^{-ik_m z_0}$$

The perturbed dielectric constant  $\epsilon'$  is very close to  $\epsilon$  so that the ratio  $\epsilon / \epsilon'$  can be approximated by unity. Under these conditions, the field expansion simplifies to the following approximate form :

$$\mathbf{E}'(x, y, z) = \sum_m a_m(z) \underline{e_m(x, y)} e^{-ik_z z_0}$$

and

$$\mathbf{H}'(x, y, z) = \sum_m a_m(z) \underline{h_m(x, y)} e^{-ik_z z_0}$$

Using the Lorentz reciprocity theorem for the general class of cylindrical waveguides

$$\iint_S \frac{\partial}{\partial z} (\mathbf{E}_t^* \times \mathbf{H}_t' + \mathbf{E}_t' \times \mathbf{H}_t^*) \cdot \hat{z} dS = -i\omega \iint_S (\epsilon - \epsilon') \mathbf{E}' \cdot \mathbf{E}^* dS$$

where  $\mathbf{E}_t^*$  is the conjugate of the unperturbed transverse field .

$\mathbf{E}_t'$  is the perturbed transverse field .

$\mathbf{E}'$  is the mode for the perturbed waveguide .

$\mathbf{E}^*$  is the mode for the conjugate perturbed waveguide .

This is derived from Maxwell's equations for unperturbed and perturbed permittivity  $\epsilon'(x, y, z)$  :

$$\nabla \times \mathbf{E} = -i\omega\mu\mathbf{H} , \quad \nabla \times \mathbf{E}' = -i\omega\mu\mathbf{H}'$$

and

$$\nabla \times \mathbf{H} = i\omega\epsilon\mathbf{E} , \quad \nabla \times \mathbf{H}' = i\omega\epsilon'\mathbf{E}' .$$

Integrating over the given structure of the dielectric waveguide and making use of the Divergence theorem ; for a closed surface  $S$  enclosing a volume  $\tau$  and vector field  $\mathbf{F}$  ;

$$\int_S \mathbf{F} \cdot d\mathbf{S} = \int_{\tau} \text{div} \mathbf{F} \cdot d\tau .$$

Gauss's theorem : This states that the total electric field in a closed surface  $S$  is the sum of all the localised E-fields within that closing surface ;



$$\int \mathbf{E} \cdot d\mathbf{S} = \sum_{n=1}^N \int \mathbf{E}_n \cdot d\mathbf{S}$$

Using the Lorentz reciprocity theorem on the perturbed fields yields

$$\begin{aligned} \sum_m \left[ i\Delta_{n,m} a_n + \frac{da_m}{dz} \right] e^{i\Delta_{n,m}z} \iint_s \left[ \mathbf{e}_{nt}^* \times \mathbf{h}_{mt} + \mathbf{e}_{mt} \times \mathbf{h}_{nt}^* \right] \cdot \hat{\mathbf{z}} dS \\ = -i\omega \sum_m a_m e^{i\Delta_{n,m}z} \iint_s (\varepsilon - \varepsilon') \mathbf{E}' \cdot \mathbf{E}^* dS \end{aligned}$$

where  $\Delta_{n,m} \equiv k_{zn} - k_{zm}$

and the functional dependence of  $a_m$  on  $z$  has been omitted for convenience . Applying the orthogonality relationship to the integral on the left side of the above equation shows that

$$\iint_s \left[ \mathbf{e}_{nt}^* \times \mathbf{h}_{mt} + \mathbf{e}_{mt} \times \mathbf{h}_{nt}^* \right] \cdot \hat{\mathbf{z}} dS = 2 \operatorname{sgn}(n) \delta_{m,n}$$

The quantity  $\operatorname{sgn}(n)$  is defined to be +1 if  $n$  is positive and -1 if  $n$  is negative .

so the summation over  $m$  on the left side of the above equation selects out only the value of  $m$  equal to  $n$  .Thus obtaining

$$\frac{da_n}{dz} = -i \sum_m a_m e^{i\Delta_{n,m}z} C_{m,n}$$

where

$$C_{m,n} \equiv \frac{\omega}{2} \operatorname{sgn}(n) \iint_s (\varepsilon' - \varepsilon) \underline{\mathbf{e}}_m \cdot \underline{\mathbf{e}}_n^* dS$$

This being the coupling constant between the  $m$  and  $n$  mode .

## Ib . Backward Coupling : The Grating Reflector.

In this section a general method is presented for transferring the power in a forward - travelling mode to that of a backward - travelling mode existing within the same guide. This transfer is accomplished by the introduction of a periodic perturbation in the waveguide dielectric along the propagation direction  $z$  . This waveguide can be consider as perturbation on a simpler uniform slab waveguide Figure (A2) . The perturbation consists of the square wave - shaped region ,  $\Delta\epsilon(x, y)$  Figure (A3) . When either  $h$  or  $\epsilon_2 - \epsilon_1$  or both are small quantities , then the perturbed problem can be described accurately using the coupled - mode formalism . The perturbation can be describe mathematically as

$$\Delta\epsilon(x, y) = u(x)\Delta\epsilon(z)$$

where

$$u(x) = 1 \quad \left| x - d/2 \right| < h/2$$

$$= 0 \quad \text{otherwise}$$

and

$$\Delta\epsilon(z) = \Delta\epsilon_1 \cos \frac{2\pi}{\Lambda} z + \Delta\epsilon_2 \cos \frac{4\pi}{\Lambda} z + \dots + \Delta\epsilon_n \cos \frac{n\pi}{\Lambda} z$$

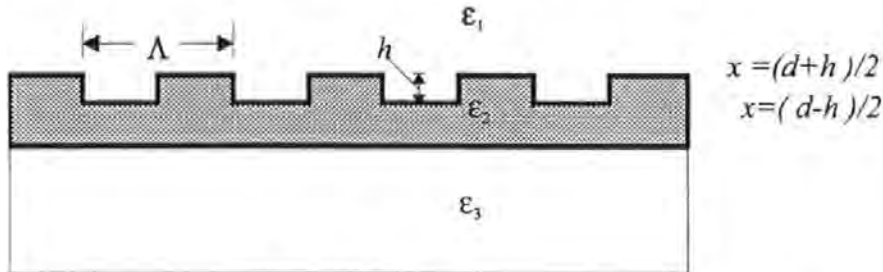


Figure A1

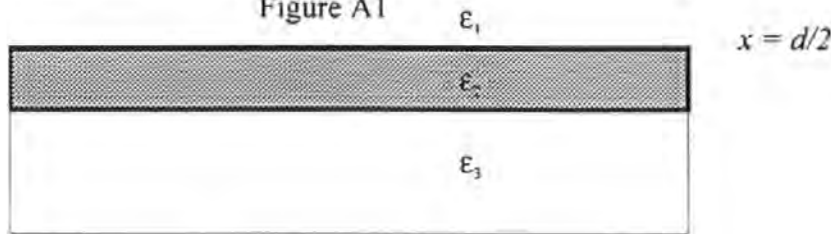


Figure A2

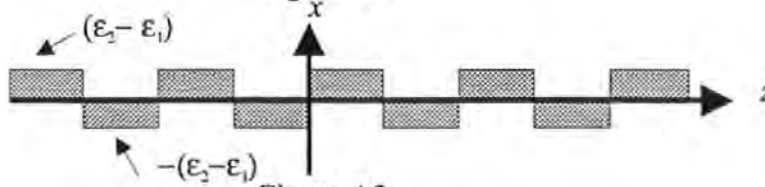


Figure A3

Figures A1 is the grating reflector , A2 ; unperturbed , A3 ; perturbed ..

For a rectangular pulse

$$\Delta \varepsilon_n = \frac{4(\varepsilon_2 - \varepsilon_1)}{\pi n} (-1)^{(n-1)/2} \quad n \text{ odd}$$

$$= 0 \quad n \text{ even}$$

Assuming that unperturbed guide is single mode , capable of supporting one forward mode  $n$  , and one backward mode  $-n$  where  $n$  is a positive integer . The perturbed fields are assumed to be of the form

$$\mathbf{E}'(x, y, z) = a_n(z) \underline{e_n(x, y)} e^{-ik_z n z} + a_{-n}(z) \underline{e_{-n}(x, y)} e^{-ik_z (-n) z}$$

and

$$\mathbf{H}'(x, y, z) = a_n(z) \underline{h_n(x, y)} e^{-ik_z n z} + a_{-n}(z) \underline{h_{-n}(x, y)} e^{-ik_z (-n) z}$$

giving rise to a set of coupled - mode equations which can be reduce by setting the sum to  $m = \pm n$  . Thus obtaining

$$\frac{da_n}{dz} = -i \left( a_n C_{n,n} + a_{-n} e^{i\Delta_{n,-n} z} C_{-n,n} \right)$$

and

$$\frac{da_{-n}}{dz} = -i \left( a_{-n} C_{-n,-n} + a_n e^{i\Delta_{-n,n} z} C_{n,-n} \right)$$

where

$$C_{nn} = \frac{\omega}{2} \Delta \varepsilon_1 \cos(2\pi z / \Lambda) \int_0^w dy \int_{(d-h)/2}^{(d+h)/2} dx |e_n(x, y)|^2$$

with

$$C_{-n,n} = C_{n,n}$$

$$C_{n,-n} = C_{-n,-n} = -C_{n,n}$$

and

$$\Delta_{n,-n} = k_{zn} - k_{z(-n)} = 2k_{zn}$$

$$\Delta_{-n,n} = -2k_{zn}$$

If the grating height  $h$  is small, then the fields  $e_n(x, y)$  and  $e_n^*(x, y)$  may be assumed to be constant over the integration with respect to  $x$  and equal to their value at  $x = d/2$ . Thus,

$$C_{n,n} \cong C_0 \cos\left[\frac{2\pi}{\Lambda} z\right]$$

where

$$C_0 = \frac{\omega}{2} \Delta \epsilon_1 h \int_0^W dy \left| e_n\left(\frac{d}{2}, y\right) \right|^2$$

The pair of coupled equations can be written as ;

$$\frac{da_n}{dz} = -iC_0 (a_n \cos \gamma z + a_{-n} e^{i2k_z n z} \cos \gamma z)$$

$$\frac{da_{-n}}{dz} = +iC_0 (a_{-n} \cos \gamma z + a_n e^{-i2k_z n z} \cos \gamma z)$$

where

$$\gamma \equiv \frac{\pi}{\Lambda}$$

There are several statements that can be made about the behaviour of the two coefficients  $a_n$  and  $a_{-n}$ . As the periodic perturbation approaches zero, then,  $C_0$  approaches zero. In this limit,  $da_n/dz = da_{-n}/dz = 0$ , implying that  $a_n$  and  $a_{-n}$  are constants. For a small but finite perturbation,  $a_n$  and  $a_{-n}$  are no longer constant but are slowly varying functions of  $z$ . Taking one of the above equations and integrating w.r.t.  $z$ , it can be seen from inspection that the first consists of a slowly varying function,  $a_n(z)$ , multiplied by a rapidly oscillating one,  $\cos(\gamma z)$  (Figure (A4)).

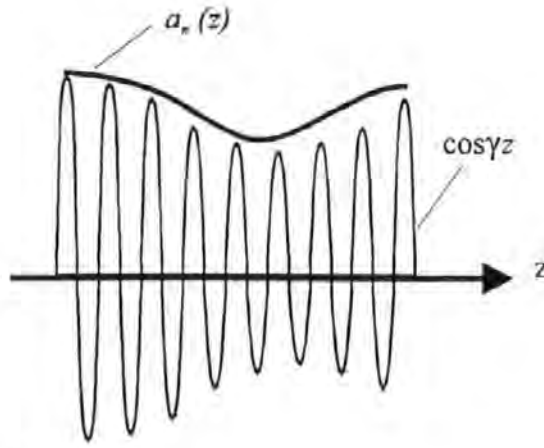


Figure (A4) .

This would mean regardless of the exact functional form of  $a_n(z)$  the oscillating nature of the term  $\cos(\gamma z)$  causes the product of these two terms to average to nearly zero when integrated over  $z$  . The second term can be written has

$$a_{-n}(z)e^{i2k_{zn}z}\cos\gamma z = a_{-n}(z)\left[\frac{e^{i(\gamma+2k_{zn})z} + e^{-i(\gamma-2k_{zn})z}}{2}\right]$$

Both the real and imaginary parts of the first term in square brackets are rapidly oscillating and therefore their product with  $a_n(z)$  also tends to give negligible contribution when integrated over  $z$  . The second term in the square brackets may contribute to the final solution ; if the grating periodicity is chosen such that  $2k_{zn} - \gamma \equiv \delta k$  where  $\delta k$  is small , then this term can also be slowly varying and thus the integral of its product with  $a_n(z)$  will not be negligible. So when the grating periodicity is chosen so that  $\delta k$  is small then the coupled mode equations can be written as

$$\frac{da_n}{dz} = -i\frac{C_0}{2}a_{-n}e^{i\delta kz}$$

And the same arguments for the other equation .

$$\frac{da_{-n}}{dz} = +i\frac{C_0}{2}a_n e^{-i\delta kz}$$

These two expressions are commonly known as the mode coupled equations for a Bragg Grating . They can be written in the more familiar form by recognising that  $2k_{zn} - \gamma \equiv \delta k$  where  $\delta k$  is the differential propagation constant associated with detuning from the Bragg condition , so  $2k_{zn} - \gamma \equiv \delta k$  in terms of  $\Delta\beta$  where  $\Delta\beta = \beta - \beta_0 = 2n\pi/\lambda - \pi/\Lambda$  and that the terms  $+i\frac{C_0}{2} \equiv +i\kappa$  so  $\frac{C_0}{2}$  is the coupling coefficient . The above coupled mode equation can be rewritten has ,

$$\frac{da_n}{dz} = -i\kappa^* a_{-n} e^{i2(\Delta\beta)z}$$

and

$$\frac{da_{-n}}{dz} = +i\kappa a_n e^{-i2(\Delta\beta)z}$$

### Ic . Solution to the Mode Coupled Equations(Uniform Grating ).

Let  $\Delta\beta = \Delta$  ,  $a_n$  is the complex amplitude of the electric field of the forward mode in the grating , so  $a_n = B(z)$  . The function  $a_{-n}$  is the complex amplitude of the electric field of the backward mode in the grating ; so  $a_{-n} = A(z)$  . The coupled mode equations become

$$\frac{dB(z)}{dz} = -i\kappa^* A(z) e^{i2\Delta z}$$

and

$$\frac{dA(z)}{dz} = +i\kappa B(z) e^{-i2\Delta z}$$

$$e^{i\Delta z} \frac{dA(z)}{dz} = +i\kappa B(z)e^{-i\Delta z} \text{ and } e^{-i\Delta z} \frac{dB(z)}{dz} = -i\kappa^* A(z)e^{i\Delta z}$$

which can be written as

$$\frac{d}{dz} \left[ e^{i\Delta z} A(z) \right] = i\Delta A(z)e^{i\Delta z} + i\kappa B(z)e^{-i\Delta z}$$

and

$$\frac{d}{dz} \left[ e^{-i\Delta z} B(z) \right] = -i\Delta B(z)e^{-i\Delta z} - i\kappa^* A(z)e^{i\Delta z}$$

Letting  $p(z) = e^{i\Delta z} A(z)$  and  $q(z) = e^{-i\Delta z} B(z)$

then

$$\frac{dp(z)}{dz} = i\Delta p(z) + i\kappa q(z)$$

and

$$\frac{dq(z)}{dz} = -i\Delta q(z) - i\kappa^* p(z)$$

Which can be written in matrix form ,

$$\frac{d}{dz} \begin{bmatrix} p(z) \\ q(z) \end{bmatrix} = \begin{bmatrix} i\Delta & i\kappa \\ -i\kappa^* & -i\Delta \end{bmatrix} \begin{bmatrix} p(z) \\ q(z) \end{bmatrix}$$

thus

$$\begin{bmatrix} p(z) \\ q(z) \end{bmatrix} = e^{\begin{bmatrix} i\Delta & i\kappa \\ -i\kappa^* & -i\Delta \end{bmatrix} z} \begin{bmatrix} p(0) \\ q(0) \end{bmatrix}$$

The eigenvalues of the matrix are

$$\begin{vmatrix} \lambda - i\Delta & -i\kappa \\ i\kappa^* & \lambda + i\Delta \end{vmatrix} = 0$$

$$\lambda^2 + \Delta^2 - |\kappa|^2 = 0$$

Hence

$$\lambda_1 = +\sqrt{|\kappa|^2 - \Delta^2}$$

and

$$\lambda_2 = -\sqrt{|\kappa|^2 - \Delta^2}$$

Eigenvectors, let  $\lambda = \lambda_1$

so

$$\begin{bmatrix} \lambda_1 - i\Delta & -i\kappa \\ i\kappa^* & \lambda_1 + i\Delta \end{bmatrix} \begin{bmatrix} e_1 \\ f_1 \end{bmatrix} = 0$$

Thus  $e_1 = i\kappa$  and  $f_1 = \lambda_1 - i\Delta$  and by a similar process

for  $\lambda_2$  giving  $e_2 = i\kappa$  and  $f_2 = \lambda_2 - i\Delta$

thus

$$e^{\begin{bmatrix} i\Delta & i\kappa \\ -i\kappa^* & -i\Delta \end{bmatrix} z} = \begin{bmatrix} e_1 & e_2 \\ f_1 & f_2 \end{bmatrix} \begin{bmatrix} e^{\lambda_1 z} & 0 \\ 0 & e^{\lambda_2 z} \end{bmatrix} \begin{bmatrix} e_1 & e_2 \\ f_1 & f_2 \end{bmatrix}^{-1}$$



Thus

$$\begin{bmatrix} p(z) \\ q(z) \end{bmatrix} = \begin{bmatrix} e_1 & e_2 \\ f_1 & f_2 \end{bmatrix} \begin{bmatrix} e^{\lambda_1 z} & 0 \\ 0 & e^{\lambda_2 z} \end{bmatrix} \begin{bmatrix} e_1 & e_2 \\ f_1 & f_2 \end{bmatrix}^{-1} \begin{bmatrix} p(0) \\ q(0) \end{bmatrix}$$

and

$$\begin{bmatrix} e_1 & e_2 \\ f_1 & f_2 \end{bmatrix}^{-1} \begin{bmatrix} p(z) \\ q(z) \end{bmatrix} = \begin{bmatrix} e^{\lambda_1 z} & 0 \\ 0 & e^{\lambda_2 z} \end{bmatrix} \begin{bmatrix} e_1 & e_2 \\ f_1 & f_2 \end{bmatrix}^{-1} \begin{bmatrix} p(0) \\ q(0) \end{bmatrix}$$

which can be rewritten as

$$\begin{bmatrix} e_1 & e_2 \\ f_1 & f_2 \end{bmatrix}^{-1} \begin{bmatrix} \exp(-i\beta_0 l) a(l) \\ \exp(+i\beta_0 l) b(l) \end{bmatrix} = \begin{bmatrix} e^{\lambda_1 l} & 0 \\ 0 & e^{\lambda_2 l} \end{bmatrix} \begin{bmatrix} e_1 & e_2 \\ f_1 & f_2 \end{bmatrix}^{-1} \begin{bmatrix} p(0) \\ q(0) \end{bmatrix}$$

By setting  $z = l$  , the length of the grating , and using the fact that the electric fields of the backward and forward modes in the grating can be expressed as  $a(z) = A(z)\exp(i\beta z)$  and  $b(z) = B(z)\exp(-i\beta z)$  respectively where  $\beta$  is the wave propagation constant . Using these facts and by some matrices manipulation the following is obtained.

$$\begin{bmatrix} f_2 e^{\lambda_1 l} & e_2 e^{i\beta_0 l} \\ f_1 e^{\lambda_2 l} & e_1 e^{i\beta_0 l} \end{bmatrix} \begin{bmatrix} a(0) \\ b(l) \end{bmatrix} = \begin{bmatrix} f_2 e^{-i\beta_0 l} & e_2 e^{\lambda_1 l} \\ f_1 e^{-i\beta_0 l} & e_1 e^{\lambda_2 l} \end{bmatrix} \begin{bmatrix} a(l) \\ b(0) \end{bmatrix}$$

thus

$$\begin{bmatrix} a(0) \\ b(l) \end{bmatrix} = \begin{bmatrix} f_2 e^{\lambda_1 l} & e_2 e^{i\beta_0 l} \\ f_1 e^{\lambda_2 l} & e_1 e^{i\beta_0 l} \end{bmatrix}^{-1} \begin{bmatrix} f_2 e^{-i\beta_0 l} & e_2 e^{\lambda_1 l} \\ f_1 e^{-i\beta_0 l} & e_1 e^{\lambda_2 l} \end{bmatrix} \begin{bmatrix} a(l) \\ b(0) \end{bmatrix}$$

and this gives a scattering matrix for the Bragg grating by substituting  $\lambda_1, \lambda_2, e_1, e_2, f_1$  and  $f_2$  and the identities hyperbolic functions i.e.

Thus the scattering is :

$$\begin{bmatrix} a(0) \\ b(l) \end{bmatrix} = \begin{bmatrix} S_{11} & S_{12} \\ S_{21} & S_{22} \end{bmatrix} \begin{bmatrix} a(l) \\ b(0) \end{bmatrix}$$

$$\begin{bmatrix} S_{11} & S_{12} \\ S_{21} & S_{22} \end{bmatrix} = \begin{bmatrix} \frac{is \exp(-i\beta_0 l)}{-\Delta\beta \sinh(sl) + is \cosh(sl)} & \frac{\kappa \sinh(sl)}{-\Delta\beta \sinh(sl) + is \cosh(sl)} \\ \frac{\kappa \sinh(sl)}{-\Delta\beta \sinh(sl) + is \cosh(sl)} \exp(-2i\beta_0 l) & \frac{is \exp(-i\beta_0 l)}{-\Delta\beta \sinh(sl) + is \cosh(sl)} \end{bmatrix}$$

where  $s = \sqrt{|\kappa|^2 - \Delta\beta^2}$

Using the conditions that  $a(l) = \exp(i\beta l)$  and  $b(0) = B_0$  the transfer matrix expression for the uniform grating is obtained i.e.

$$\begin{bmatrix} a(0) \\ b(0) \end{bmatrix} = \begin{bmatrix} T_{11} & T_{12} \\ T_{21} & T_{22} \end{bmatrix} \begin{bmatrix} a(l) \\ b(l) \end{bmatrix}$$

where

$$T_{11} = T_{22}^* = \frac{\Delta\beta \sinh(sl) + is \cosh(sl)}{is} \exp(-i\beta_0 l) ,$$

and

$$T_{12} = T_{21}^* = \frac{\kappa \sinh(sl)}{is} \exp(i\beta_0 l) .$$

The T - matrix relates the left - side vector  $[a(0) \ b(0)]$  to the right - side vector  $[a(0) \ b(0)]$  and is therefore well suited for analysis of a cascade of gratings . For example , if a uniform grating as a total length of  $L$  , then using this method of analysis the single grating of length  $L$  can be divided into small gratings where the sum of the lengths of the small gratings equals the total length of the single grating .The small gratings lengths are  $l_1, l_2, \dots, l_n$  and  $L = l_1 + l_2 + \dots + l_n$  ,it can be verified analytically that

$$\begin{bmatrix} T_L \end{bmatrix} = \begin{bmatrix} T_{l_1} \end{bmatrix} \cdot \begin{bmatrix} T_{l_2} \end{bmatrix} \cdot \dots \cdot \begin{bmatrix} T_{l_n} \end{bmatrix}$$

where  $\begin{bmatrix} T_L \end{bmatrix}$  denotes the T - matrix for the complete grating of length  $L$  ;  $\begin{bmatrix} T_{l_i} \end{bmatrix}$  denotes the T - matrix for the  $i$ th small grating ( $i = 1, 2, 3, \dots, n$ ) . This method is not limited by the selection length of the grating chosen for this analysis . For example  $N_i$  is an integer number ,so for a sub-grating  $l_i = N_i \Lambda$  ,  $N_i$  is the number of periods per sub-grating . This can be chosen to be as short as only one pitch / period .

The mode coupling between the forward and the backward waves is a continuous process taking place at all  $z$  - positions in the grating , and the coupling efficiency depends on how synchronically the varying of  $\Delta n(z)$  matches the differential phase between the two waves . If  $\Delta n(z)$  is sinusoidal , the coupling becomes efficient because the varying of  $\Delta n(z)$  just synchronically matches the mode phase difference everywhere in the grating . If  $\Delta n(z)$  is not sinusoidal , then finding a corresponding harmonic that would produce a net coupling efficiency . Therefore the local coupling efficiency within one pitch / period is actually determined by the internal  $\Delta n(z)$  function and independent on the condition outside of this period / pitch .

### Id . Nonuniform Gratings .

It was pointed out above that the T- matrix Formalism is valid even if the length of the sub grating is chosen to be one period . Using this approach variations in the period i.e.(a linear, cubic chirp in the period or apodisation / variations in  $\Delta n(z)$ ) can taken into account by choosing a suitable sub - grating length or for accuracy producing a T - matrix for each period in the grating .Then multiplying all the T - matrices together to obtain the response of the complete grating . If there are n periods in the grating then ;

$$\begin{bmatrix} a(0) \\ b(0) \end{bmatrix} = \begin{bmatrix} T_{l_n} \\ T_{l_{n-1}} \end{bmatrix} \dots \begin{bmatrix} T_{l_j} \\ T_{l_1} \end{bmatrix} \begin{bmatrix} a(L) \\ b(L) \end{bmatrix}$$

or

$$\begin{bmatrix} a(0) \\ b(0) \end{bmatrix} = \prod_{j=n}^0 \begin{bmatrix} T_{l_j} \\ T_{l_j} \end{bmatrix} \begin{bmatrix} a(L) \\ b(L) \end{bmatrix}$$

or

$$\begin{bmatrix} a(0) \\ b(0) \end{bmatrix} = \prod_{j=n}^0 \begin{bmatrix} (T_{11})_{l_j} & (T_{12})_{l_j} \\ (T_{21})_{l_j} & (T_{22})_{l_j} \end{bmatrix} \begin{bmatrix} a(L) \\ b(L) \end{bmatrix}$$

## **Appendix II . The Runge-Kutta method for solving the coupled mode equations .**

The generalised coupled mode equations can be written as :

$$\frac{dA(z)}{dz} = -i\kappa B(z)e^{-i\psi(z)} \quad \text{and} \quad \frac{dB(z)}{dz} = +i\kappa A(z)e^{+i\psi(z)}$$

where

$$\psi(z) = \int_z \frac{2\pi}{\Lambda(z)} dz - 2\beta z$$

$\beta$  is the propagation constant of the unperturbed guide . Assuming a linear chirp is defined as :

$$\frac{2\pi}{\Lambda(z)} = \frac{2\pi}{\Lambda(0)} - 2\gamma z$$

where  $\Lambda(0)$  is the period at the beginning of the grating and  $\gamma$  is the chirp factor , then

$$\psi(z) = \int_z \left( \frac{2\pi}{\Lambda(0)} - 2\gamma z \right) dz - 2\beta z = 2 \left( \frac{2\pi}{\Lambda(0)} - \beta \right) z - \gamma z^2 + c$$

### **IIa . Derivation of the equations used in the Runge-Kutta Method .**

Using the above definitions of the various parameters that define a linearly chirped period variation in a Bragg grating the coupled mode equations become

$$\frac{dA(z)}{dz} = -i\kappa B(z)e^{-i \left[ 2(\beta_0 - \beta)z - \gamma z^2 \right]} = -i\kappa B(z)e^{-i2\delta z} \cdot e^{+i\gamma z^2}$$

and

$$\frac{dB(z)}{dz} = +i\kappa A(z)e^{+i\left[2(\beta_0 - \beta)z - \gamma z^2\right]} = +i\kappa A(z)e^{+i2\delta z} \cdot e^{-i\gamma z^2}$$

where  $\delta = \beta_0 - \beta$

The E-field of the backward and forward modes can be expressed in terms of a reference propagation constants  $a(z)$  and  $b(z)$  of the grating :

$$a(z) = A(z)e^{+i\delta z} \text{ and } b(z) = B(z)e^{-i\delta z}$$

Differentiating  $a(z)$  and  $b(z)$  with respect to  $z$  yields :

$$\frac{da(z)}{dz} = \frac{dA(z)}{dz} \cdot e^{+i\delta z} + i\delta e^{+i\delta z} A(z) = \frac{dA(z)}{dz} \cdot e^{+i\delta z} + i\delta \cdot a(z)$$

and

$$\frac{db(z)}{dz} = \frac{dB(z)}{dz} \cdot e^{-i\delta z} - i\delta e^{-i\delta z} B(z) = \frac{dB(z)}{dz} \cdot e^{-i\delta z} - i\delta \cdot b(z)$$

Using the two equations above and the definitions of the modes , the coupled mode equations become :

$$\frac{db(z)}{dz} + i\delta \cdot b(z) = \left[ i\kappa A(z)e^{+i2\delta z} \cdot e^{-i\gamma \cdot z^2} \right] e^{-i\delta \cdot z}$$

$$\text{thus } \frac{db(z)}{dz} + i\delta \cdot b(z) = i\kappa a(z)e^{-i\gamma \cdot z^2} \quad (\text{II})$$

and

$$\frac{da(z)}{dz} - i\delta \cdot a(z) = \left[ -i\kappa B(z)e^{-i2\delta z} \cdot e^{+i\gamma \cdot z^2} \right] e^{+i\delta \cdot z}$$

thus 
$$\frac{da(z)}{dz} - i\delta \cdot a(z) = -i\kappa b(z)e^{+i\gamma \cdot z^2} \quad (II2)$$

### **IIb . The implementation of the Runge-Kutta Method .**

The equations II1 and II2 are translated into FORTRAN90 and are listed as the two complex functions in the program **FNF1** and **FNF2** . The procedure of the 4th order Runge-Kutta technique is to solve for these two equations . Letting  $a = a_{Re} + ia_{Im}$  and  $b = b_{Re} + ib_{Im}$  to separate the real and imagery parts of the solutions . Using the boundary conditions  $a(z=0) = 1$  and  $b(z=l) = 0$  and estimating  $b(z=0) = 0$  as an initial value of  $b(z=0)$ .

The spectral range which is considered is determined by the value of the variable **lamdamin** ; The minimum value for wavelength and **lamdamax** is the variable for the maximum value of the wavelength . The reflectivity is obtained by the variable **BS(3)** ; **B** , the resultant values for reflectivity are outputted to a file ; name **tomdata.csv** and contains also the wavelength for a given reflectivity . The number of iterations for the Runge-Kutta method is divided into 10,000 sections . The variables **K1** , **K2** , **K3** and **L1** , **L2** , **L3** are the intermediate values along the grating length . The initial condition are given in the variable values of **BS(1)** , **BS(2)** for the reflected wave and the incident wave condition given by **A**

## IIC . Listing of the FORTRAN90 program for Runge-Kutta method

```
REAL*8 L,K,GAM,DELTA,H,Z,AA,CAPGAM,BETA,N,lamda,pi
real*8 lamdamin,lamdamax
COMPLEX*16 A,B,BS,BE,K1,L1,K2,L2,K3,L3,K4,L4
COMPLEX f1,f2
INTEGER*4 NPTS,I,J,m,lamj
COMMON K,DELTA,GAM

DIMENSION BS(3),BE(3),AA(20000)
open(unit=24, file='tomdata.csv',status='unknown')
pi=4d0*atan(1d0)
NPTS=10000
L=1.989d-4
N=1.54D0
GAM=60d0
CAPGAM=492D-9

GAM=8d-9*pi/(CAPGAM**2*L)
print*, 'gam=',gam
H=L/NPTS
m=100
print *,delta
lamdamin=1510d-9
lamdamax=1560d-9

do 200 lamj=0,m
  LAMDA=lamdamin+lamj*(lamdamax-lamdamin)/m
  K=pi*1.5d-3/lamda
  BETA=2D0*pi*N/LAMDA
  DELTA=PI/CAPGAM-BETA

  BS(1)=(0D0,0D0)
  BS(2)=(1D0,1D0)

  DO 120 I=1,3

    A=(1D0,0D0)
    B=BS(1)

    DO 110 J=0,NPTS-1

      Z=J*H
      K1=H*f1(A,B,Z)
      L1=H*f2(A,B,Z)

      K2=H*f1(A+K1/2,B+L1/2,Z+H/2)
      L2=H*f2(A+K1/2,B+L1/2,Z+H/2)
```



```

K3=H*Π(A+K2/2,B+L2/2,Z+H/2)
L3=H*Π2(A+K2/2,B+L2/2,Z+H/2)

K4=H*Π(A+K3,B+L3,Z+H)
L4=H*Π2(A+K3,B+L3,Z+H)

A=A+(K1+2D0*K2+2D0*K3+K4)/6D0
B=B+(L1+2D0*L2+2D0*L3+L4)/6D0
AA(J+1)=ABS(A)
c  print *,aa(j+1)
110  CONTINUE

BE(I)=B
IF(I.EQ.2) THEN
  BS(3)=BS(1)-BE(1)*(BS(2)-BS(1))/(BE(2)-BE(1))
END IF
120  CONTINUE
c  PRINT*,BE(3)
c  PRINT*, ""
  PRINT*,lamda," ",ABS(BS(3)**2)
  write(24,500) lamda,abs(bs(3)**2)
200  continue
c  DO 130 J=1,NPTS
c  PRINT*,AA(J)
c 130  CONTINUE

500  format(e14.6,',',e14.6)

END

COMPLEX FUNCTION Π(A,B,Z)
  COMPLEX*16 A,B
  REAL*8 Z,K,DELTA,GAM
  COMMON K,DELTA,GAM
  Π=(0D0,1D0)*DELTA*A-(0D0,1D0)*K*B*(DCOS(GAM*Z**2)
$  +(0D0,1D0)*DSIN(GAM*Z**2))
  RETURN
END

COMPLEX FUNCTION Π2(A,B,Z)
  COMPLEX*16 A,B
  REAL*8 Z,K,DELTA,GAM
  COMMON K,DELTA,GAM
  Π2=-(0D0,1D0)*DELTA*B+(0D0,1D0)*K*A*(DCOS(GAM*Z**2)
$  -(0D0,1D0)*DSIN(GAM*Z**2))
  RETURN
END

```

### **Appendix III . The Analytical solution to a linearly chirped Bragg grating**

Using the two coupled mode equations in appendix II as the starting point .

$$\frac{da(z)}{dz} - i\delta \cdot a(z) = -i\kappa b(z) e^{+i\gamma \cdot z^2}$$

and

$$\frac{db(z)}{dz} + i\delta \cdot b(z) = i\kappa a(z) e^{-i\gamma \cdot z^2}$$

These equations can be presented in a different way , this being :

$$\exp\left(\frac{-i\gamma \cdot z^2}{2}\right) \frac{da}{dz} - i\delta \cdot a \exp\left(\frac{-i\gamma \cdot z^2}{2}\right) = -i\kappa \cdot b \exp\left(\frac{+i\gamma \cdot z^2}{2}\right)$$

and

$$\exp\left(\frac{+i\gamma \cdot z^2}{2}\right) \frac{db}{dz} + i\delta \cdot b \exp\left(\frac{+i\gamma \cdot z^2}{2}\right) = +i\kappa \cdot a \exp\left(\frac{-i\gamma \cdot z^2}{2}\right)$$

#### **IIIa . Derivation of the two independent second order ordinary differential equations .**

Letting

$$U \equiv a \cdot \exp\left(\frac{-i\gamma \cdot z^2}{2}\right) . \text{ This being the incident light .}$$

and

$$V \equiv b \cdot \exp\left(\frac{+i\gamma \cdot z^2}{2}\right) . \text{ This being the reflected light.}$$

The physical interpretation of  $U$  is that it presents how the complex amplitude of the incident light behaves as it goes through the grating with a linear chirp of  $\gamma$ . This is the same for  $V$  which is the complex amplitude reflected light. Also remembering the  $a$  and  $b$  are also functions of  $z$ ;  $a(z)$  and  $b(z)$ , this being :

$$a(z) = A(z)e^{+i\delta z} \text{ and } b(z) = B(z)e^{-i\delta z}$$

where  $\delta = \beta_0 - \beta$ , this being the phase miss-match between the Bragg condition and the wavelength of the incident light upon the grating and it's position within the grating.

Thus the coupled mode equations become :

$$\exp\left(\frac{-i\gamma \cdot z^2}{2}\right) \frac{da}{dz} - i\delta \cdot U = -i\kappa \cdot V$$

and

Result 1

$$\exp\left(\frac{+i\gamma \cdot z^2}{2}\right) \frac{db}{dz} + i\delta \cdot V = +i\kappa \cdot U$$

Now from the definitions of  $U$  and  $V$

$$\frac{dU}{dz} = \exp\left(\frac{-i\gamma \cdot z^2}{2}\right) \frac{da}{dz} - i\gamma \cdot zU$$

and

$$\frac{dV}{dz} = \exp\left(\frac{+i\gamma \cdot z^2}{2}\right) \frac{db}{dz} + i\gamma \cdot zV$$

hence

$$\exp\left(\frac{-i\gamma \cdot z^2}{2}\right) \frac{da}{dz} = \frac{dU}{dz} + i\gamma \cdot zU$$

and

$$\exp\left(\frac{+i\gamma \cdot z^2}{2}\right) \frac{db}{dz} = \frac{dV}{dz} - i\gamma \cdot zV$$

So that Result 1 reduces to

$$\frac{dU}{dz} + i(\gamma \cdot z - \delta)U = -i\kappa \cdot V$$

and

Result 2

$$\frac{dV}{dz} - i(\gamma \cdot z - \delta)V = +i\kappa \cdot U$$

Now

$$\frac{d^2U}{dz^2} + i(\gamma \cdot z - \delta) \frac{dU}{dz} + i\gamma \cdot U = -i\kappa \cdot \frac{dV}{dz} \quad (a)$$

and

$$\frac{d^2V}{dz^2} - i(\gamma \cdot z - \delta) \frac{dV}{dz} - i\gamma \cdot V = +i\kappa \cdot \frac{dU}{dz} \quad (b)$$

and substituting for  $\frac{dV}{dz}$  in R.H.S. of equation (a) and  $\frac{dU}{dz}$  in the R.H.S. of equation (b)

from Result 2 .

$$\frac{d^2U}{dz^2} + i(\gamma \cdot z - \delta) \frac{dU}{dz} + i\gamma \cdot U = -i\kappa (+i\kappa \cdot U + i(\gamma \cdot z - \delta) \cdot V)$$

and

$$\frac{d^2V}{dz^2} - i(\gamma \cdot z - \delta) \frac{dV}{dz} - i\gamma \cdot V = +i\kappa \cdot (-i\kappa \cdot V - i(\gamma \cdot z - \delta) \cdot U)$$

i.e.

$$\frac{d^2U}{dz^2} + i(\gamma \cdot z - \delta) \frac{dU}{dz} - i(\kappa^2 - i\gamma) \cdot U = -i\kappa (+i(\gamma \cdot z - \delta) \cdot V)$$

and

Result 3

$$\frac{d^2V}{dz^2} - i(\gamma \cdot z - \delta) \frac{dV}{dz} - i(\kappa^2 + i\gamma) \cdot V = +i\kappa \cdot (-i(\gamma \cdot z - \delta) \cdot U)$$

Substituting for  $-i\kappa V$  and  $+i\kappa U$  from Result 2 in to Result 3

Hence

$$\frac{d^2U}{dz^2} + \left[ (\gamma \cdot z - \delta)^2 - \kappa^2 + i\gamma \right] U = 0 \quad (\text{B1})$$

and

$$\frac{d^2V}{dz^2} + \left[ (\gamma \cdot z - \delta)^2 - \kappa^2 - i\gamma \right] V = 0 \quad (\text{B2})$$

Considering equation involving  $U$

$$\frac{d^2U}{dz^2} + \gamma^2 \cdot \left[ \left( z - \frac{\delta}{\gamma} \right)^2 - \frac{\kappa^2}{\gamma^2} + \frac{i}{\gamma} \right] U = 0$$

making a substitution  $z - \frac{\delta}{\gamma} = \frac{x}{\sqrt{2\gamma}}$

$$\text{thus } \frac{dU}{dz} = \frac{dU}{dx} \cdot \frac{dx}{dz} = \sqrt{2\gamma} \cdot \frac{dU}{dx}$$

$$\text{and } \frac{d^2U}{dz^2} = \frac{d}{dz} \left( \frac{dU}{dz} \right) = \frac{d}{dx} \left( \frac{dU}{dz} \right) \cdot \frac{dx}{dz} = \frac{d}{dx} \left( \sqrt{2\gamma} \cdot \frac{dU}{dx} \right) \cdot \sqrt{2\gamma}$$

$$\text{so } \frac{d^2U}{dz^2} = 2\gamma \cdot \frac{d^2U}{dx^2}$$

Equation B1 becomes

$$2\gamma \cdot \frac{d^2U}{dx^2} + \gamma^2 \cdot \left[ \left( \frac{x}{\sqrt{2\gamma}} \right)^2 - \frac{\kappa^2}{\gamma^2} + \frac{i}{\gamma} \right] U = 0$$

$$\text{thus } \frac{d^2U}{dx^2} + \left[ \frac{x^2}{4} - \frac{\kappa^2}{\gamma^2} + \frac{i}{\gamma} \right] U = 0 \quad (\text{B3})$$

and similar for the equation involving  $V$

Equation B2 becomes

$$2\gamma \cdot \frac{d^2 V}{dx^2} + \gamma^2 \cdot \left[ \left( \frac{x}{\sqrt{2\gamma}} \right)^2 - \frac{\kappa^2}{\gamma^2} - \frac{i}{\gamma} \right] V = 0$$

thus

$$\frac{d^2 V}{dx^2} + \left[ \frac{x^2}{4} - \frac{\kappa^2}{\gamma^2} - \frac{i}{\gamma} \right] V = 0 \quad (B4)$$

### **IIIb . Parabolic Cylinder Function and it's relationship to Confluent Hypergeometric Functions .**

The ordinary differential equation of the form

$$\frac{d^2 y}{dx^2} + (ax^2 + bx + c)y = 0$$

can be expressed has

$$\frac{d^2 y}{dx^2} - \left( \frac{x^2}{4} + a \right) y = 0 \quad (B5)$$

and

$$\frac{d^2 y}{dx^2} + \left( \frac{x^2}{4} - a \right) y = 0 \quad (B6)$$

Where  $y$  is a Parabolic Cylinder function [111] with real solutions for

$$y(a, x), y(a, -x) \\ y(-a, ix), y(-a, -ix)$$

Equation B5 transforms into equation B6 with  $a$  being replaced by  $-ia$  and  $x$  being replaced by  $x \exp\left(\frac{1}{4}i\pi\right)$ .

Thus the solutions to equation B3 are :

$$y_1 = e^{-\frac{1}{4}x^2} M\left(\frac{1}{2}a + \frac{1}{4}, \frac{1}{2}, \frac{1}{2}x^2\right)$$

and

$$y_2 = x \cdot e^{-\frac{1}{4}x^2} M\left(\frac{1}{2}a + \frac{3}{4}, \frac{3}{2}, \frac{1}{2}x^2\right)$$

Also replacing  $a$  by  $-ia$  and  $x$  by  $x \exp\left(\frac{1}{4}i\pi\right)$

Note that  $x^2 = x^2 \cdot e^{i\frac{\pi}{2}} = ix^2$  the solutions become

$$y_3 = e^{-\frac{i}{4}x^2} M\left(\frac{-i}{2}a + \frac{1}{4}, \frac{1}{2}, \frac{i}{2}x^2\right)$$

and

$$y_4 = x \cdot e^{\frac{i\pi}{4}} \cdot e^{-\frac{1}{4}x^2} M\left(\frac{-i}{2}a + \frac{3}{4}, \frac{3}{2}, \frac{i}{2}x^2\right)$$

From equations B3 and B4 the two values of  $a$  are :

$$a = \frac{+\kappa^2}{2\gamma} \pm \frac{i}{2}$$



$M(a, b, z)$  is a confluent hypergeometric function [111] ; a Kummer's function which can be expressed as :

$$M(a, b, z) = 1 + \frac{az}{b} + \frac{(a)_2 z^2}{(b)_2 2!} + \dots + \frac{(a)_n z^n}{(b)_n n!} + \dots$$

where

$$(a)_n = a(a+1)(a+2)\dots(a+n-1), (a)_0 = 1$$

Also the confluent hypergeometric function has an integral representation :

$$M(a, b, z) = \frac{\Gamma(b)}{\Gamma(b-a)\Gamma(a)} \cdot \int_0^1 e^{zt} \cdot t^{a-1} (1-t)^{b-a-1} dt$$

thus giving  $y_1$  has :

$$e^{\frac{-1}{4}x^2} \cdot M\left(\frac{a}{2} + \frac{1}{4}, \frac{1}{2}, \frac{x^2}{2}\right) = e^{\frac{-1}{4}x^2} \cdot \left[ \frac{\Gamma\left(\frac{1}{2}\right)}{\Gamma\left(\frac{1}{4} - \frac{a}{2}\right) \cdot \Gamma\left(\frac{a}{2} + \frac{1}{4}\right)} \right] \cdot \int_0^1 e^{\frac{-x^2}{4}t} \cdot t^{\left(\frac{a}{2} - \frac{3}{4}\right)} \cdot (1-t)^{-\left(\frac{a}{2} + \frac{1}{4}\right)} \cdot dt$$

and similar expression for  $y_2$ ,  $y_3$  and  $y_4$ .

Using the Kummer's function to solve the equations B3 and B4, the result is two equations of the form :

$$U = a1 \cdot y_1 + b1 \cdot y_2 ; \text{ where } a(z) \cdot e^{-i\frac{\gamma}{2}z^2} = U(z)$$

and

$$V = c1 \cdot y_3 + d1 \cdot y_4 ; \text{ where } b(z) \cdot e^{+i\frac{\gamma}{2}z^2} = V(z)$$

**IIIc . Using the boundary conditions at  $z = 0$  and  $z = L$  , plus the derivatives at those points to obtain the constants of integration .**

$a1, b1, c1$  and  $d1$  are arbitrary constant of integration which can be determined by using the boundary conditions ( note 4 unknowns , 4 boundary conditions ; 4 equations ) .

Remembering that  $a(0) = 1$  and  $b(L) = 0$  :

Therefore  $a(0) = 1 \rightarrow U(0) = 1$  and  $b(L) = 0 \rightarrow V(L) = 0$

So at  $z = 0$

$$U \text{ becomes } 1 = a1 \cdot y_1(0) + b1 \cdot y_2(0) \Rightarrow a1 = \frac{1 - b1 \cdot y_2(0)}{y_1(0)}$$

and

$$V \text{ becomes } 0 = c1 \cdot y_3(L) + d1 y_4(L) \Rightarrow d1 = -c1 \cdot \frac{y_3(L)}{y_4(L)}$$

Using the first order derivatives

$$\frac{dU}{dz} + i(\gamma \cdot z - \delta)U = -i\kappa \cdot V \quad (\text{B7})$$

and

$$\frac{dV}{dz} - i(\gamma \cdot z - \delta)V = +i\kappa \cdot U \quad (\text{B8})$$

Putting  $z = L$  into equation B7

$$a1 \cdot y_1'(L) + b1 \cdot y_2'(L) + i(\gamma \cdot L - \delta)[a1 y_1(L) + b1 y_2(L)] = 0 \quad (\text{B9})$$

Putting  $z = 0$  into equation B8

$$c1 \cdot y_3'(0) + d1 \cdot y_4'(0) + i\delta \cdot [c1 \cdot y_3(0) + d1 \cdot y_4(0)] = i\kappa \quad (\text{B10})$$

Substituting  $a1$  from First boundary condition into equation B9 , so B9 becomes

$$\left[ \frac{1 - b1 \cdot y_2(0)}{y_1(0)} \right] \cdot y_1'(L) + b1 \cdot y_2'(L) + i(\gamma \cdot L - \delta) \left[ \frac{1 - b1 \cdot y_2(0)}{y_1(0)} \right] \cdot y_1(L) + b1 \cdot y_2(L) = 0$$

So therefore

$$b1 = \frac{i(\gamma \cdot L - \delta)y_1(L) + y_1'(L)}{y_2(0) \cdot y_1'(L) + i(\gamma \cdot L - \delta)[y_1(L)y_2(0) - y_1(0)y_2(L)] - y_2'(L) \cdot y_1(0)} \quad (\text{B11})$$

thus  $a1$  is also defined .

$$a1 = \frac{1 - b1 \cdot y_2(0)}{y_1(0)} \quad (\text{B12})$$

Substituting  $d1$  from the first boundary condition into equation B10 .

$$c1 \cdot y_3'(0) + \left[ -c1 \cdot \frac{y_3(L)}{y_4(L)} \right] \cdot y_4'(0) + i\delta \cdot \left[ c1 \cdot y_3(0) + \left[ -c1 \cdot \frac{y_3(L)}{y_4(L)} \right] \cdot y_4(0) \right] = i\kappa$$

Thus

$$c1 = \frac{i\kappa}{\left[ y_3'(0) - \frac{y_3(L)}{y_4(L)} \cdot y_4'(0) \right] + i\delta \cdot \left[ y_3(0) - \frac{y_3(L)}{y_4(L)} \cdot y_4(0) \right]} \quad (\text{B13})$$

and again  $d1$  is defined because

$$d1 = -c1 \cdot \frac{y_3(L)}{y_4(L)} \quad (B14)$$

### III d . The implementation of the Mathematica Program .

The solutions of  $y_1$  ,  $y_2$  ,  $y_3$  and  $y_4$  and equations B11 to B14 give the complete solution to a single linearly chirped grating with a chirp factor of  $\gamma$  and a coupling coefficient of  $\kappa$  .

The various parameters in the equations B11 to B14 are calculated in the program in the notation of :

$$y_1(0) \equiv y10 \text{ , } y'_1(0) \equiv dy10$$

to

$$y_4(0) \equiv y40 \text{ , } y'_4(0) \equiv dy40$$

and

$$y_1(L) \equiv y1L \text{ , } y'_1(L) \equiv dy1L$$

to

$$y_4(L) \equiv y4L \text{ , } y'_4(L) \equiv dy4L$$

Thus the reflectivity of the proposed grating is given by taking the modulus squared of the reflected complex amplitude and evaluating it at the beginning of the grating ;  $z = 0$  .

$$\left| b(0)_{\text{reflection}} \right|^2 = \left| b(z)_{\text{reflec}} \cdot e^{-i\delta \cdot z} \cdot e^{+i\frac{\gamma}{2}z^2} \right|^2 \bigg|_{z=0} = \left| c1 \cdot y_3(0) + d1 \cdot y_4(0) \right|^2$$

### ( IIIe ) Listing of the MATHEMATICA 2.2 program .

```
ClearAll[a,b,c,d,c1,x,lamda,gamma,L,delta,k,z,y1L,y2L,dy1L,dy2L,y10,y20,dy10,dy20,u,v]
```

```
ow=OpenWrite["tommath.csv"];
```

```
st=",";
```

```
npts=100; -This is for the number of points in the spectral Bandwidth . -
```

```
Array[g,npts];
```

```
x=Sqrt[2 gamma]*(z-delta/gamma); - Defined from the above appendix . -
```

```
c1=k^2/(2 gamma)-I/2;
```

```
c2=k^2/(2 gamma)+I/2;
```

-The parameters y1,y2,y3 and y4 are the numerical values of the Kummer's function . -

```
y1=Exp[-x^2 I/4] Hypergeometric1F1[-c1 I/2+1/4,1/2,x^2 I/2];
```

```
y2=x Exp[I Pi/4] Exp[-x^2 I/4] Hypergeometric1F1[-c1 I/2+3/4,3/2,x^2 I/2];
```

```
y3=Exp[-x^2 I/4] Hypergeometric1F1[-c2 I/2+1/4,1/2,x^2 I/2];
```

```
y4=x Exp[I Pi/4] Exp[-x^2 I/4] Hypergeometric1F1[-c2 I/2+3/4,3/2,x^2 I/2];
```

```
dy1=D[y1,{z,1}];
```

```
dy2=D[y2,{z,1}];
```

```
dy3=D[y3,{z,1}];
```

```
dy4=D[y4,{z,1}];
```

```
d2y1=D[y1,{z,2}];
```

```
d2y2=D[y2,{z,2}];
```

```
d2y3=D[y3,{z,2}];
```

```
d2y4=D[y4,{z,2}];
```

```
Do[
```

```
z=0;
```

```
lamda=N[1510*10^-9+50*10^-9 j/npts]; - Defines the spectral bandwidth . -
```

```
k=Pi*1.5*10^-3/lamda; - This is the coupling coefficient . -
```

```
capgamma=492*10^-9; - capgamma is the initial period of the Bragg grating . -
```

```
L=1.989*10^-4; - L ; the total length of the grating . -
```

```
gamma=8*10^-9*Pi/(capgamma^2*L); -gamma ; the linear chirp factor . -
```

```
beta=2.0*Pi*1.5415/lamda; - beta ; the propagation constant of the fibre . -
```

```
delta=Pi/capgamma-beta; - delta ; the differential propagation constant . -
```

```
z=L;
```

```
y1L=N[y1,20];
```

```
y2L=N[y2,20];
```

```
y3L=N[y3,20];
```

```
y4L=N[y4,20];
```

```
dy1L=N[dy1,20];
```

```
dy2L=N[dy2,20];
```

```
dy3L=N[dy3,20];
```

```
dy4L=N[dy4,20];
```

```
z=0;
```

```
y10=N[y1,20];
```

```
y20=N[y2,20];
```

```
y30=N[y3,20];
```

```
y40=N[y4,20];
```

```

dy10=N[dy1,20];
dy20=N[dy2,20];
dy30=N[dy3,20];
dy40=N[dy4,20];

denom=y20 dy1L-y10 dy2L+I(L gamma-delta)(y20 y1L-y10 y2L);
b=(dy1L+I(L gamma-delta)y1L)/denom;
a=(1-b y20)/y10;
c=I k/(dy30-y3L dy40/y4L+delta I(y30-y3L y40/y4L));
d=-c y3L/y4L;
z=0;
u=N[a y1 + b y2,20];
v=N[c y3 + d y4,20];
z=L;
u=N[a y1 + b y2,20];
v=N[c y3 + d y4,20];
N[a,20];
N[b,20];
N[c,20];
N[d,20];
N[c y30+d y40,20];
exactr=N[(Abs[c y30+d y40])^2,10];
N[y10,20];
N[y20,20];
N[b,20];
zb=N[delta/gamma];

alpha=0;
r2=N[1-Exp[-Pi k^2/gamma]];
r3=N[k^2 Pi Exp[-2 alpha zb]/gamma];

N[-c1 L/2+1/4];
N[x^2 L/2];
z=L/2;
N[a dy1 +b dy2+I(gamma z-delta)(a y1+b y2)];
N[-I k (c y3+d y4)];
N[c dy3+d dy4-I(gamma z-delta)(c y3+d y4)];
N[I k (a y1+b y2)];

g[j]=N[(Abs[c y30 +d y40])^2];

WriteString[ow,FortranForm[lamda],st,FortranForm[g[j]]];
Write[ow];
Print[lamda," ",g[j]],{j,0,npts}]
t=Table[g[j],{j,0,npts}];
Close["tommath.csv"];

```

(IVa) Results ( spectral response ) for a uniform Bragg grating using Rouard's Method , T-Matrix formalism and the Derived Analytical expression .

( Note Mathcad +6 program name TECH1.mcd )

### Rouard's Method

The Parameters below are as follows :

I : The of layers in the Bragg grating

I := 40

F: This is the chirp factor , the rate of change of the period per period of the grating :

F :=

- 0.02 10<sup>-9</sup>

n0 : The perturbed index of refraction due to photobleaching :

n0 := 1.54

n1 : The unperturbed index of refraction :

n1 := 1.5

( Note that the values of the refractive index are high but this is only a demonstration of the technique , to obtain theoretical consistence , with increasing n1 , n2 the spectral response shifts up in wavelength )

j and i are two counters for increase of wavelength and number labelling for the periods in the grating :

i := 0..I

j := 0..10

Λ<sub>mode</sub> : The initial period of the grating (nm) :

Λ<sub>mode</sub> := 500 10<sup>-9</sup>

λ<sub>j</sub> : The wavelengths used in this model (nm):

λ<sub>j</sub> := (1510 + 0.5·j) · 10<sup>-9</sup>

d<sub>i</sub> : The period variation along the grating length (nm) :

d<sub>i</sub> := Λ<sub>mode</sub> + F·

d<sub>I+1</sub> :=

Is part of the number count of the periods in the grating

Δβ<sub>i,j</sub> : The phase mismatch between the grating

and the illuminating radiation's wavelength

Per wavelength and period :

$$\Delta\beta_{i,j} := \frac{2 \cdot \pi \cdot \left[ \left( \frac{n1 - n0}{2} \right) + n0 \right]}{\lambda_j} - \frac{\pi}{d_i}$$

κ<sub>j</sub> : Coupling coefficient per wavelength :

$$\kappa_j := \frac{\pi \cdot (n1 - n0)}{\lambda_j}$$

s<sub>i,j</sub> : The s parameter defines the photonic band

gap where wavelength is reflected :

$$s_{i,j} := \sqrt{(\kappa_j)^2 - (\Delta\beta_{i,j})^2}$$

$r_{i+1,j}$  : Represents the reflection coefficient

for each period in the grating :

$$r_{i+1,j} := \frac{-\kappa_j \sinh(s_{i,j} \cdot d_{i+1})}{s_{i,j} \cosh(s_{i,j} \cdot d_{i+1}) - i \cdot \Delta\beta_{i,j} \sinh(s_{i,j} \cdot d_{i+1})}$$

$\epsilon_{i,j}$  : The additional phase information obtained as the light travels through each period per wavelength :

$$\epsilon_{i,j} := \exp\left(\frac{-i \cdot 4 \cdot \pi \cdot n_0 \cdot d_i}{\lambda_j}\right)$$

ii : Is a count from the back end of the grating which used to calculate the net / effective reflection coefficient has it goes through the grating :

$$ii := I, I - 1..$$

$\rho_{I,j}$  : Is the effective interface with a reflection coefficient :

At the I layer of the grating at all wavelengths

$$\rho_{I,j} := \frac{r_{I-1,j} + r_{I,j} \cdot \epsilon_{I,j}}{1 + r_{I-1,j} \cdot r_{I,j} \cdot \epsilon_{I,j}}$$

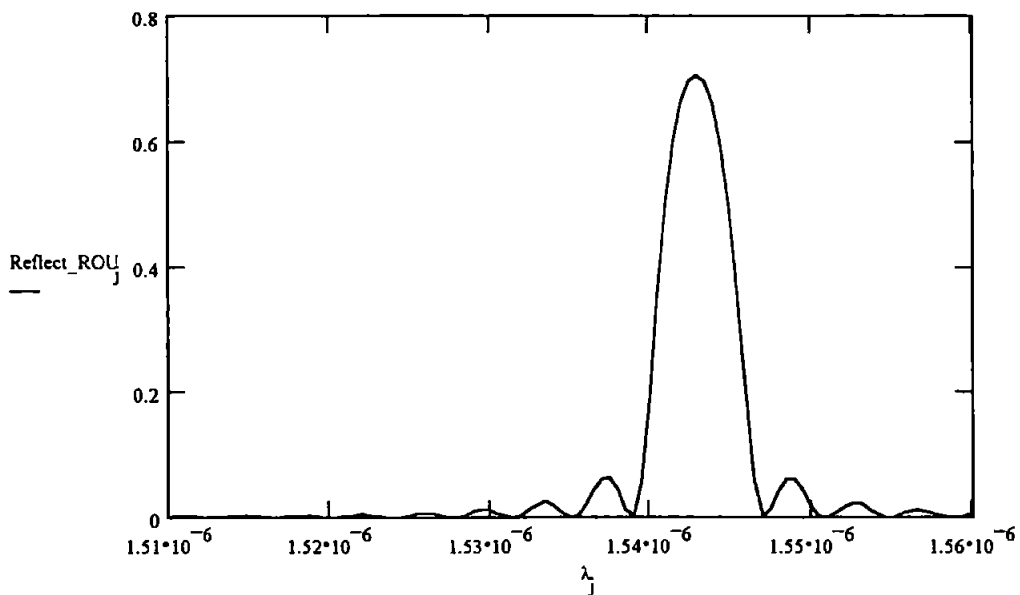
$\rho_{ii-1,j}$  : Calculates the effective reflection coefficient at the beginning of the grating

$$\rho_{ii-1,j} := \frac{r_{ii-1,j} + \rho_{ii,j} \cdot \epsilon_{ii,j}}{1 + r_{ii-1,j} \cdot \rho_{ii,j} \cdot \epsilon_{ii,j}}$$

Reflect\_ROU<sub>j</sub> : The reflectivity of the grating at the wavelengths :

$$\text{Reflect\_ROU}_j := \rho_{0,j} \cdot \rho_{0,j}$$

A Graph of the purposed grating's Reflectivity Vs wavelength using Rouard's method :





## T-Matrix Formalism technique

$z := 0..40$

$\Lambda_{1z} := \Lambda_{\text{mode}} + F \cdot$

These parameters have the same meaning  
has in the Rouard's Method :

$$\Delta\beta_{j,z} := \frac{2 \cdot \pi \cdot (0 + n_0)}{\lambda_j} - \frac{\pi}{\Lambda_{1z}}$$

$$\kappa_{1j} := \frac{\pi \cdot (n_1 - n_0)}{\lambda_j}$$

$$s_{1j,z} := \sqrt{(|\kappa_{1j}|)^2 - (\Delta\beta_{1j,z})^2}$$

$A_{j,z}$  and  $B_{j,z}$  are  
functions derived from  
the T-matrix formalism  
for each layer in the  
grating and at a given  
wavelength.

( see appendix 1 )  
with the variables

C and D are the  
conjugates .

$$A_{j,z} := \frac{\Delta\beta_{1j,z} \cdot \sinh(s_{1j,z} \cdot \Lambda_{1z}) + i \cdot s_{1j,z} \cdot \cosh(s_{1j,z} \cdot \Lambda_{1z})}{i \cdot s_{1j,z}} \cdot \exp\left(-i \cdot \pi \cdot \frac{\Lambda_{1z}}{\Lambda_{\text{mode}}}\right)$$

$$B_{j,z} := \frac{\kappa_{1j} \cdot \sinh(s_{1j,z} \cdot \Lambda_{1z})}{i \cdot s_{1j,z}} \cdot \exp\left(i \cdot \pi \cdot \frac{\Lambda_{1z}}{\Lambda_{\text{mode}}}\right)$$

The generation of the conjugate elements :

$C := \overline{\quad}$

$D := \overline{A}$

The Net effect of the each period in the grating can be represented by a scattering matrix

$\begin{pmatrix} A_{j,z} & B_{j,z} \\ C_{j,z} & D_{j,z} \end{pmatrix}$  and resultant scattering matrix for all the grating is given by Resultant\_Mj , a  
summation .

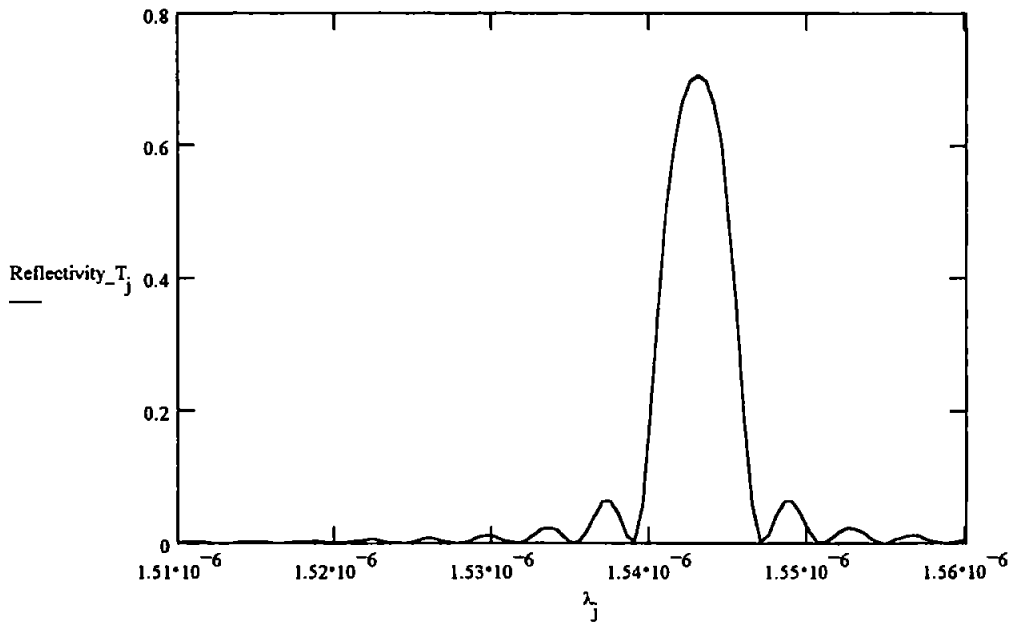
$$\text{Resultant\_M}_j := \left[ \prod_{z=400}^0 \begin{pmatrix} A_{j,z} & B_{j,z} \\ C_{j,z} & D_{j,z} \end{pmatrix} \right]$$

The net reflectivity of the scattering matrix of the  
grating is given by Reflectivity\_Tj

( see appendix 1 )

$$\text{Reflectivity\_T}_j := \left[ \left| \frac{(\text{Resultant\_M}_j)_{0,1}}{(\text{Resultant\_M}_j)_{0,0}} \right| \right]^2$$

A Graph of the purposed grating's Reflectivity Vs wavelength using T-matrix formalism method :



### Derived Analytical Expression

The expression is :

$$R = \frac{\kappa^2 \cdot \sinh(s \cdot L)^2}{s^2 \cdot \cosh(s \cdot L)^2 + \left(\frac{\Delta k}{2}\right)^2 \cdot \sinh(s \cdot L)^2}$$

$k_{0j}$  is coupling coefficient at a given wavelength  $\lambda_j$  :

$$k_{0j} := \frac{2 \cdot \pi \cdot n_0}{\lambda_j}$$

$\delta$  is the resonant frequency of the grating :

$$\delta := \frac{2 \cdot \pi}{\Lambda_{\text{mode}}}$$

$\Delta k_j$  : The phase mismatch between the grating and the illuminating radiation's wavelength

Per wavelength and period :

$$\Delta k_j := 2 \cdot k_{0j} - \delta$$

$s_{2j}$  : The  $s$  parameter defines the photonic band gap where wavelength is reflected :

$$s_{2j} := \sqrt{\left(\left|\kappa_j\right|\right)^2 - \left(\frac{\Delta k_j}{2}\right)^2}$$

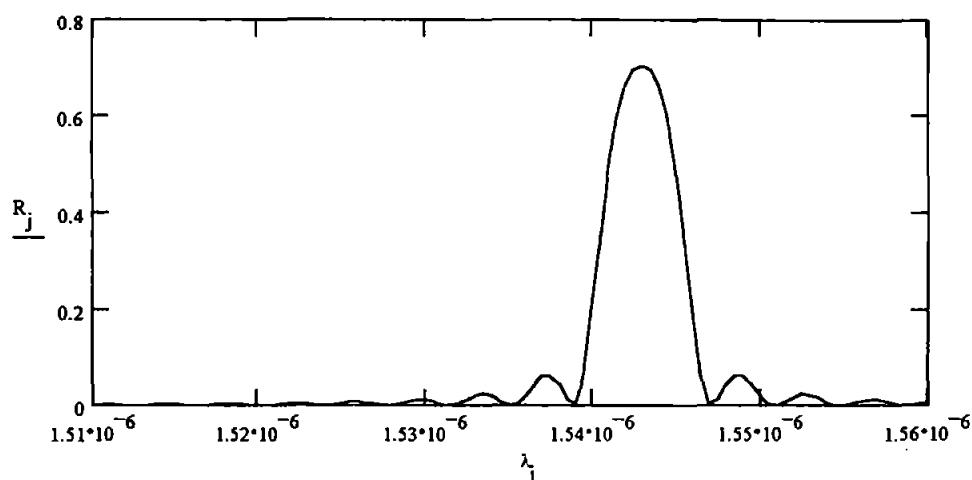
$L$  is the total length of the grating :

$$L := I \cdot \Lambda_{\text{mode}}$$

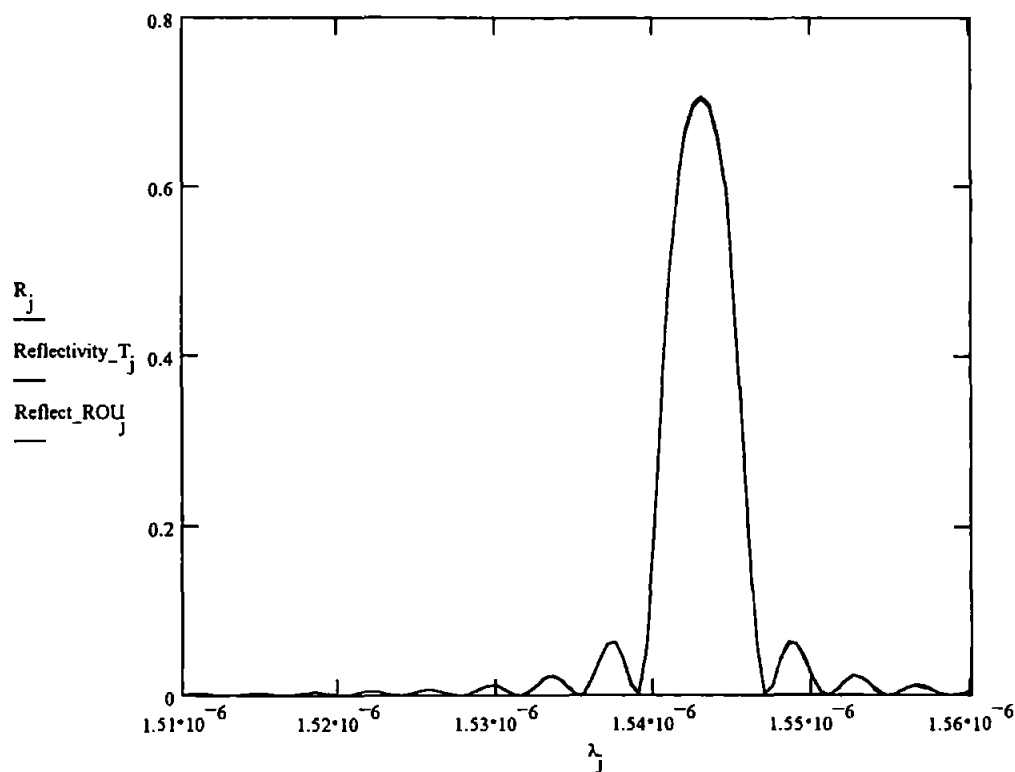
$R_j$  is the analytical expression obtained from the mode-coupled equations ,when solving for a uniform Bragg grating .

$$R_j := \frac{(\kappa_j)^2 \cdot \sinh(s_{2j} \cdot L)^2}{(s_{2j})^2 \cdot \cosh(s_{2j} \cdot L)^2 + \left(\frac{\Delta k_j}{2}\right)^2 \cdot \sinh(s_{2j} \cdot L)^2}$$

A Graph of the purposed grating's Reflectivity Vs wavelength using the analytical expression  
for a uniform grating :



The graph below shows the theoretical results for three techniques for uniform grating , the analytical expression , the T-matrix formalism and Rouard's method , which produce the same spectral response .



**(IVb) Results ( spectral response ) uniform grating and nonuniform grating ( linearly chirped period ) with constant  $\Delta n$  using Rouard's Method .**

( Note Mathcad +6 program name TECH1R.mcd )

**n0 is the peak perturbed refractive index :**

$$n0 := 1.54$$

**n1 is the original core refractive index :**

$$n1 := 1.5$$

**$\Lambda_{\text{mode}}$  is the either the initial half period of the grating  $\Lambda(z=0)$  in the case of a chirped grating or otherwise the uniform half period :**

$$\Lambda_{\text{mode}} := 500 \cdot 10^{-9}$$

**F is the chirp factor which is in nanometers change in period per period of the grating**

$$F := -0.02 \cdot 10^{-9}$$

**I is the number of periods in the grating :**

$$I := 40$$

**i and j are used to increment the periods ; I and j incrementing the wavelength range**

$$i := 0..$$

$$j := 0..10$$

**The wavelength range in nano meters :**

$$\lambda_j := (1510 + 0.5 \cdot j) \cdot 10^{-9}$$

**The variation of the period per period :**

$$d_i := \Lambda_{\text{mode}} + F \cdot$$

$$d_{I+1} :=$$

**The effective refractive index can be considered as the average which is :**

$$n_{\text{eff}} := \left( \frac{n1 - n0}{2} \right) + n$$

**$\Delta\beta$  is the differential propagation constant which is associated with the detuning from the Bragg condition which varies according to the wavelength and the position within the grating :**

$$\Delta\beta_{i,j} := \frac{2 \cdot \pi \cdot n_{\text{eff}}}{\lambda_j} - \frac{\pi}{d_i}$$

**$\kappa$  is the coupling coefficient of the grating :**

$$\kappa_j := \frac{\pi \cdot (n1 - n0)}{\lambda_j}$$

$$s_{i,j} := \sqrt{(\kappa_j)^2 - (\Delta\beta_{i,j})^2}$$

**r reflectivity amplitude which is derived from the coupled mode equations were the the perturbation of the refractive index is described by**

$$n(z) = n + \Delta n \cdot \sin\left(\frac{2 \cdot \pi}{\Lambda} \cdot z\right)$$

$$r_{i+1,j} := \frac{-\kappa_j \cdot \sinh(s_{i,j} \cdot d_{i+1})}{s_{i,j} \cdot \cosh(s_{i,j} \cdot d_{i+1}) - i \cdot \Delta\beta_{i,j} \cdot \sinh(s_{i,j} \cdot d_{i+1})}$$

This section calculates the effective interfaces from layer to layer  
 $\epsilon$  is the phase information for each layer  
 being viewed in reflection :

$$\epsilon_{i,j} := \exp\left(\frac{-i \cdot 4 \cdot \pi \cdot n0 \cdot d_i}{\lambda_j}\right)$$

ii is the effective count from the back end of the grating down to  
 the front face ( perturbation of the refractive index :

$$ii := I, I - 1 ..$$

Calculating the effective interface for the back face  
 perturbation of the grating :

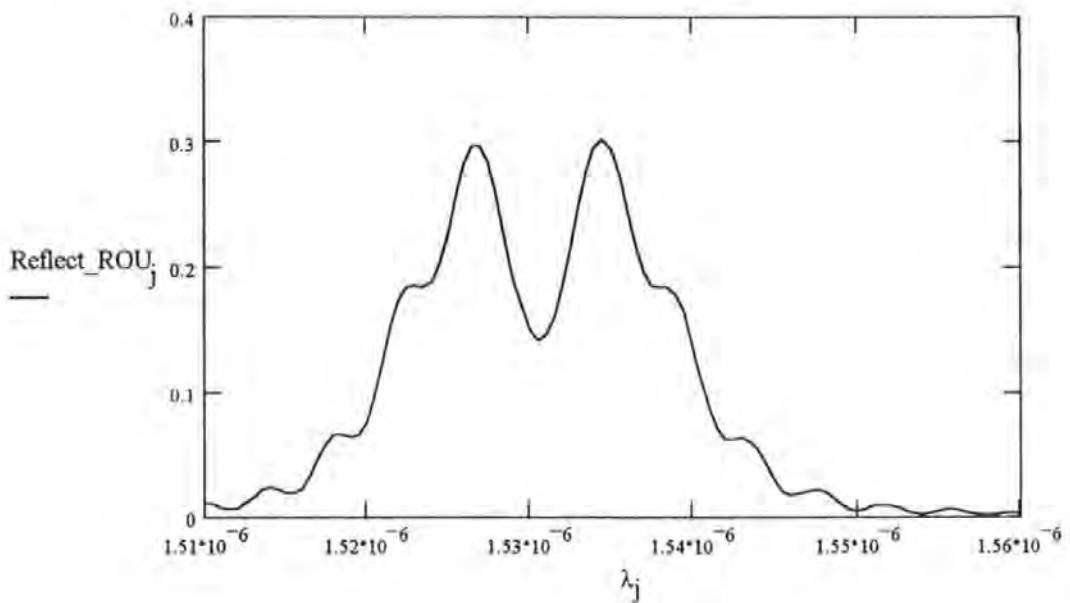
$$\rho_{I,j} := \frac{r_{I-1,j} + r_{I,j} \cdot \epsilon_{I,j}}{1 + r_{I-1,j} \cdot r_{I,j} \cdot \epsilon_{I,j}}$$

The calculations of the effective interfaces from the  
 back face to the front face :

$$\rho_{ii-1,j} := \frac{r_{ii-1,j} + \rho_{ii,j} \cdot \epsilon_{ii,j}}{1 + r_{ii-1,j} \cdot \rho_{ii,j} \cdot \epsilon_{ii,j}}$$

Reflect\_ROU is the total reflection characteristic of the grating :

$$\text{Reflect\_ROU}_j := \rho_{0,j} \cdot \rho_{0,j}$$



# **(IVc) Results ( spectral response ) for a uniform and nonuniform grating ( linearly chirped period ) with constant $\Delta n$ using T-Matrix Formalism .**

( Note Mathcad +6 program name TECH1T.mcd )

**n0 is the peak perturbed refractive index :**

$$n0 := 1.54$$

**n1 is the original core refractive index :**

$$n1 := 1.5$$

**$\Lambda_{\text{mode}}$  is the either the initial half period of the grating  $\Lambda(z=0)$  in the case of a chirped grating or otherwise the uniform half period :**

$$\Lambda_{\text{mode}} := 500 \cdot 10^{-9}$$

**F is the chirp factor which is in nanometers change in period per period of the grating :**

$$F := \frac{-0.02 \cdot 10^{-9}}{2}$$

Note :

$$F_{\text{T\_Matrix}} = \frac{F_{\text{Rouards}}}{2}$$

**I is the number of periods in the grating :**

$$I := 400$$

**i and j are used to increment the periods ; i and j incrementing the wavelength range**

$$z := 0..I$$

$$j := 0..100$$

**The wavelength range in nano meters :**

$$\lambda_j := (1510 + 0.5 \cdot j) \cdot 10^{-9}$$

**The variation of the period per period :**

$$\Lambda l_z := \Lambda_{\text{mode}} + F \cdot z$$

**The effective refractive index can be considered as the average which is :**

$$n_{\text{eff}} = \left( \frac{n1 - n0}{2} \right) + n0$$

**$\Delta\beta$  is the differential propagation constant which is associated with the detuning from the Bragg condition which varies according to the wavelength and the position within the grating :**

$$\Delta\beta l_{j,z} = \frac{2 \cdot \pi \cdot n_{\text{eff}}}{\lambda_j} - \frac{\pi}{\Lambda l_z}$$

**$\kappa$  is the coupling coefficient of the grating :**

$$\kappa l_j = \frac{\pi \cdot (n1 - n0)}{\lambda_j}$$

$$sl_{j,z} = \sqrt{(|\kappa l_j|)^2 - (\Delta\beta l_{j,z})}$$

The Expressions for A , B ,C , D are derived in Appendix I of the thesis .These expression form the elements of the scattering matrix which represents the behaviour of the grating for a given length .In this case the length is one period of the grating .

$$A_{j,z} = \frac{\Delta\beta l_{j,z} \cdot \sinh(sl_{j,z} \cdot \Lambda l_z) + i \cdot sl_{j,z} \cdot \cosh(sl_{j,z} \cdot \Lambda l_z)}{i \cdot sl_{j,z}} \cdot \exp\left(-i \cdot \pi \cdot \frac{\Lambda l_z}{\Lambda_{mode}}\right)$$

$$B_{j,z} = \frac{\kappa l_j \cdot \sinh(sl_{j,z} \cdot \Lambda l_z)}{i \cdot sl_{j,z}} \cdot \exp\left(i \cdot \pi \cdot \frac{\Lambda l_z}{\Lambda_{mode}}\right)$$

The vectors C and D are the conjugates of A and B :

$$C := \overline{A}$$

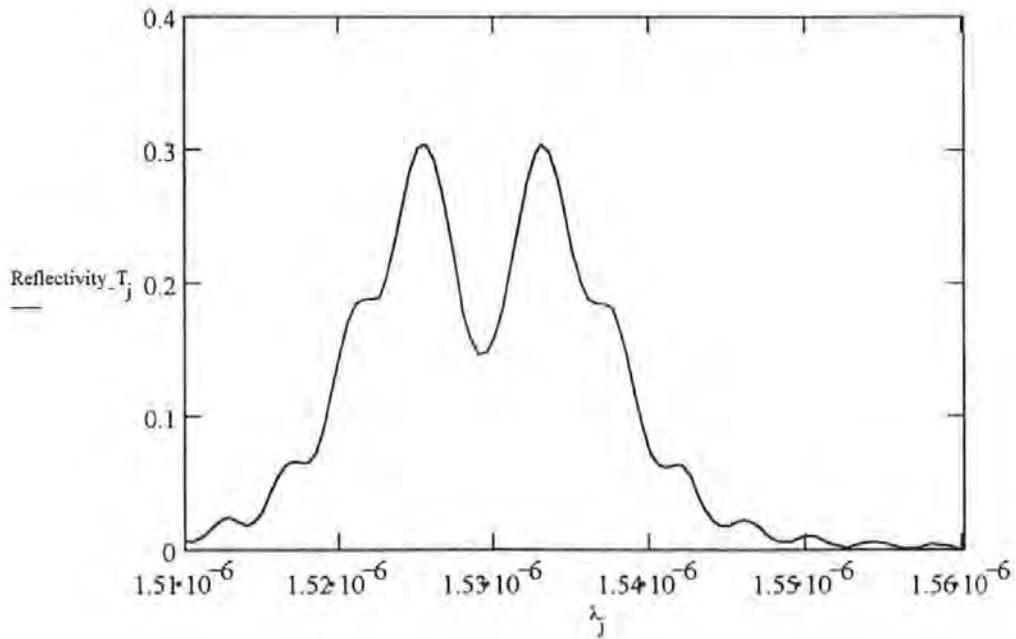
$$D := \overline{B}$$

The variable Resultant\_M<sub>j</sub> is the combined effect of the all the scattering matrix ; of the length of the grating at the front face of the grating ; reflective amplitude response at various wavelengths .

$$Resultant\_M_j = \left[ \prod_{z=400}^0 \begin{pmatrix} A_{j,z} & B_{j,z} \\ C_{j,z} & D_{j,z} \end{pmatrix} \right]$$

Referring to the theory in the chapter 3 of the main body of text of the thesis , the reflectivity of the is calculated below :

$$Reflectivity\_T_j = \left[ \frac{(Resultant\_M_j)_{0,1}}{(Resultant\_M_j)_{0,0}} \right]$$



**(IVd)Results ( spectral response ) for a combination of nonuniform grating ( linearly chirped period three gratings ) constant  $\Delta n$  using Rouard's Method .**

( Note Mathcad +6 program name TECHIRC.mcd )

**n0 is the peak perturbed refractive index :**

$$n0 := 1.54$$

**n1 is the original core refractive index :**

$$n1 := 1.5$$

**$\Lambda_{\text{mode}}$  is the either the initial half period of the grating  $\Lambda(z=0)$  in the case of a chirped grating or otherwise the uniform half period :**

$$\Lambda_{\text{mode}} := 500 \cdot 10^{-9}$$

**F is the chirp factor which is in nanometers change in period per period of the grating :**

$$F := -0.04 \cdot 10^{-9}$$

**I is the number of periods in the grating :**

$$I := 40$$

**i and j are used to increment the periods ; i and j incrementing the wavelength range**

$$i := 0..$$

$$j := 0..10$$

**The wavelength range in nano meters :**

$$\lambda_j := (1510 + 0.5 \cdot j) \cdot 10^{-9}$$

**The variation of the period per period :**

$$d_i = \Lambda_{\text{mode}} + F \cdot$$

$$Z_{\text{max}} :=$$

$$d_{I+1} :=$$

$$z := 0..Z_{\text{ma}}$$

**Section (ii) - obtaining the pattern of the chirps involved in this grating .**

$$\text{centre} := \frac{Z_{\text{ma}}}{2}$$

$$\text{centre} = 200$$

**These variables are used to determine the structure of the grating .**

$$\text{third} := \frac{3 \cdot Z_{\text{ma}}}{4}$$

$$\text{third} = 300$$

$$\text{quarter} := \frac{Z_{\text{ma}}}{4}$$

$$\text{quarter} = 100$$



**Calculating the changes of the period along the grating length .**

$$t = Z_{\max} \cdot \text{thir}$$

$$d_t = \Lambda_{\text{mode}} + F \cdot ((1 + \text{third}) - t)$$

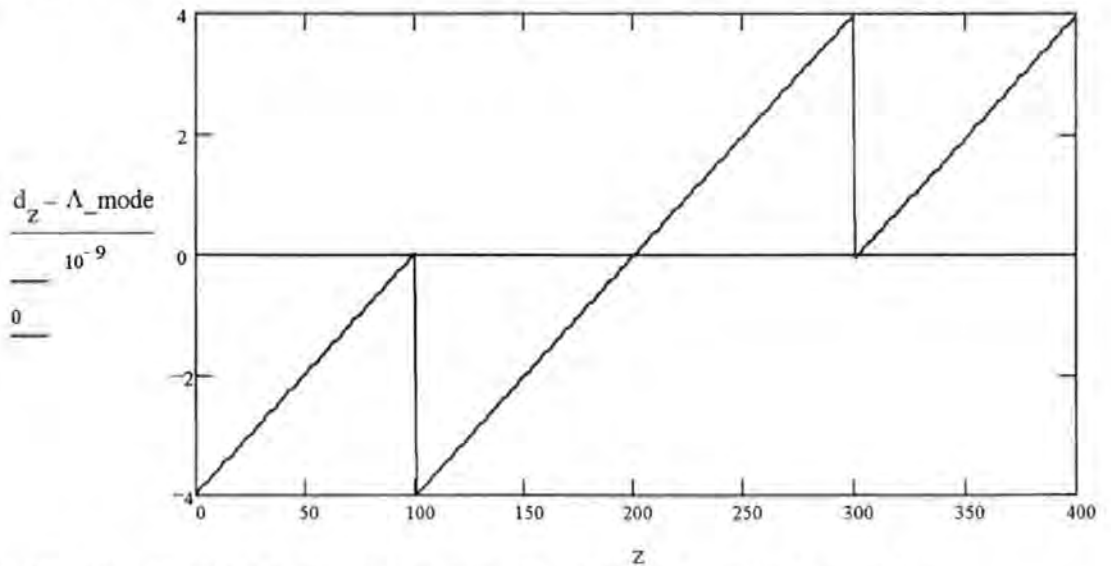
$$t_2 = \text{third} - 1 \cdot \text{quarter} +$$

$$d_{t_2} = \Lambda_{\text{mode}} + F \cdot (\text{centre} - t_2)$$

$$t_3 = \text{quarter} \cdot$$

$$d_{t_3} = \Lambda_{\text{mode}} + F \cdot ((\text{quarter} - t_3) - 1)$$

**The graph below shows the variation of the period along the grating length .**



**The effective refractive index can be considered as the average which is :**

$$n_{\text{eff}} = \left( \frac{n_1 - n_0}{2} \right) + n$$

$\Delta\beta$  is the differential propagation constant which is associated with the detuning from the Bragg condition which varies according to the wavelength and the position within the grating :

$$\Delta\beta_{i,j} = \frac{2 \cdot \pi \cdot n_{\text{eff}}}{\lambda_j} - \frac{\pi}{d_i}$$

$\kappa$  is the coupling coefficient of the grating :

$$\kappa_j = \frac{\pi \cdot (n_1 - n_0)}{\lambda_j}$$

$$s_{i,j} = \sqrt{(|\kappa_j|)^2 - (\Delta\beta_{i,j})^2}$$

**r** reflectivity amplitude which is derived from the coupled mode equations were the the perturbation of the refractive index is described by

$$n(z) = n + \Delta n \cdot \sin\left(\frac{2 \cdot \pi}{\Lambda} \cdot z\right)$$

$$r_{i+1,j} = \frac{-\kappa_j \sinh(s_{i,j} \cdot d_{i+1})}{s_{i,j} \cosh(s_{i,j} \cdot d_{i+1}) - i \cdot \Delta\beta_{i,j} \sinh(s_{i,j} \cdot d_{i+1})}$$

This section calculates the effective interfaces from layer to layer  
 $\varepsilon$  is the phase information for each layer  
 being viewed in reflection :

$$\varepsilon_{i,j} = \exp\left(\frac{-i \cdot 4 \cdot \pi \cdot n_0 \cdot d_i}{\lambda_j}\right)$$

ii is the effective count from the back end of the grating down to  
 the front face ( perturbation of the refractive index :

$$ii = I, I - 1 ..$$

Calculating the effective interface for the back face  
 perturbation of the grating :

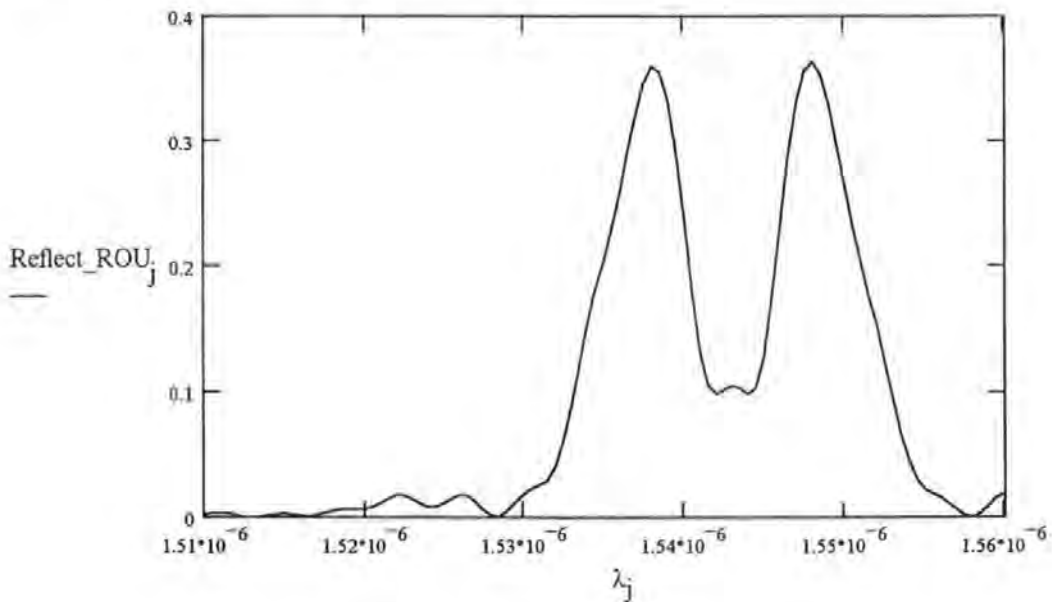
$$\rho_{I,j} = \frac{r_{I-1,j} + r_{I,j} \cdot \varepsilon_{I,j}}{1 + r_{I-1,j} \cdot r_{I,j} \cdot \varepsilon_{I,j}}$$

The calculations of the effective interfaces from the  
 back face to the front face :

$$\rho_{ii-1,j} = \frac{r_{ii-1,j} + \rho_{ii,j} \cdot \varepsilon_{ii,j}}{1 + r_{ii-1,j} \cdot \rho_{ii,j} \cdot \varepsilon_{ii,j}}$$

Reflect\_ROU is the total reflection characteristic of the grating :

$$\text{Reflect\_ROU}_j = \rho_{0,j} \cdot \rho_{0,j}$$



**(IVe) Results ( spectral response ) for a combination of nonuniform grating ( linearly chirped period ) with constant  $\Delta n$  using T-Matrix Formalism .**

( Note Mathcad +6 program name TECHTT.mcd )

**n0 is the peak perturbed refractive index :**

$$n0 := 1.54$$

**n1 is the original core refractive index :**

$$n1 := 1.5$$

**$\Lambda_{\text{mode}}$  is the either the initial half period of the grating  $\Lambda(z=0)$  in the case of a chirped grating or otherwise the uniform half period :**

$$\Lambda_{\text{mode}} := 500 \cdot 10^{-9}$$

**F is the chirp factor which is in nanometers change in period per period of the grating :**

$$F := \frac{-0.04 \cdot 10^{-9}}{2}$$

Note :

$$F_{\text{T\_Matrix}} = \frac{F_{\text{Rouards}}}{2}$$

**I is the number of periods in the grating :**

$$I := 400$$

$$Z_{\text{max}} :=$$

**Section (ii) - obtaining the pattern of the chirps involved in this grating .**

$$\text{centre} := \frac{Z_{\text{ma}}}{2}$$

$$\text{centre} = 200$$

**These variables are used to determine the structure of the grating .**

$$\text{third} := \frac{3 \cdot Z_{\text{ma}}}{4}$$

$$\text{third} = 300$$

$$\text{quarter} := \frac{Z_{\text{ma}}}{4}$$

$$\text{quarter} = 100$$

**Calculating the changes of the period along the grating length .**

$$t := Z_{\text{max}} \cdot \text{third}$$

$$\Lambda_{1_t} = \Lambda_{\text{mode}} + F \cdot [(1 + \text{third}) - t]$$

$$t2 = \text{third} - 1 \cdot \text{quarter} + 1$$

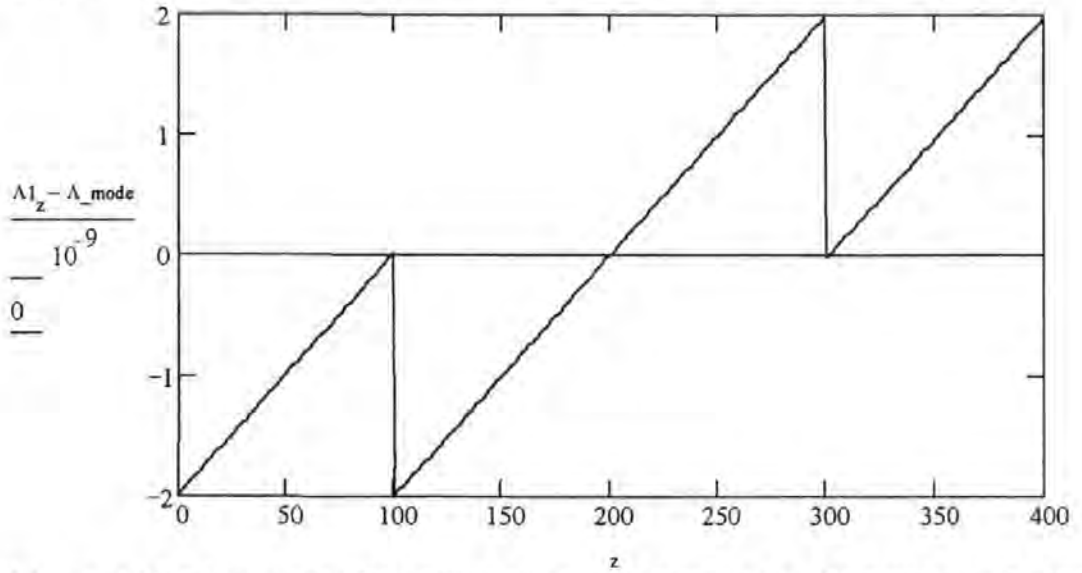
$$\Lambda_{1_{t2}} = \Lambda_{\text{mode}} + F \cdot (\text{centre} - t2)$$

$$t3 = \text{quarter} \cdot 0$$

$$\Lambda_{1_{t3}} = \Lambda_{\text{mode}} + F \cdot [(\text{quarter} - t3) - 1]$$

$$z = 0..Z_{ma}$$

The graph below shows the variation of the period along the grating length .



**i** and **j** are used to increment the periods ; **i** and **j** incrementing the wavelength range

$$z = 0..I$$

$$j = 0..100$$

The wavelength range in nano meters :

$$\lambda_j = (1510 + 0.5 \cdot j) \cdot 10^{-9}$$

The effective refractive index can be considered as the average which is :

$$n_{eff} = \left( \frac{n1 - n0}{2} \right) + n0$$

$\Delta\beta$  is the differential propagation constant which is associated with the detuning from the Bragg condition which varies according to the wavelength and the position within the grating :

$$\Delta\beta_{j,z} = \frac{2 \cdot \pi \cdot n_{eff}}{\lambda_j} - \frac{\pi}{\Lambda l_z}$$

$\kappa$  is the coupling coefficient of the grating :

$$\kappa_{l_j} = \frac{\pi \cdot (n1 - n0)}{\lambda_j}$$

$$sl_{j,z} = \sqrt{(\kappa_{l_j})^2 - (\Delta\beta_{j,z})^2}$$

The Expressions for A , B ,C , D elements for the scattering matrix are derived in appendix I of the thesis .These expression form the elements of the scattering matrix which represents the behaviour of the grating for a given length .In this case the length is one period of the grating .

$$\Lambda_{j,z} = \frac{\Delta\beta_{j,z} \cdot \sinh(sl_{j,z} \cdot \Lambda l_z) + i \cdot sl_{j,z} \cdot \cosh(sl_{j,z} \cdot \Lambda l_z)}{i \cdot sl_{j,z}} \cdot \exp\left(-i \cdot \pi \cdot \frac{\Lambda l_z}{\Lambda_{mode}}\right)$$

$$B_{j,z} = \frac{\kappa l_j \sinh(s l_{j,z} \Lambda l_z)}{j \cdot s l_{j,z}} \exp\left(i \cdot \pi \frac{\Lambda l_z}{\Lambda_{\text{mode}}}\right)$$

C, D are the conjugates of scattering matrix elements A and B .

$$C = \overline{A}$$

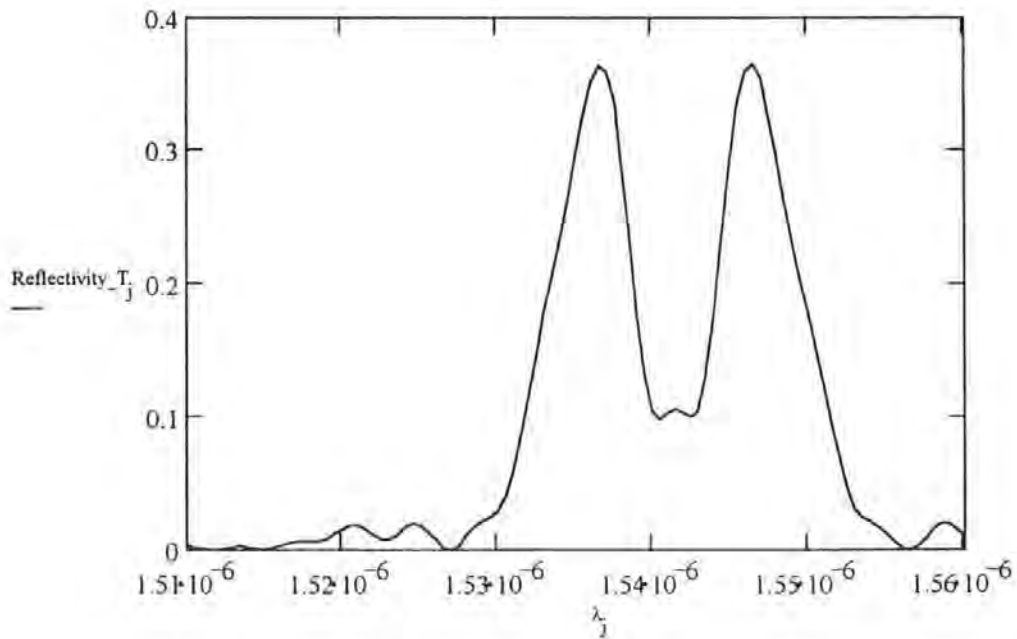
$$D = \overline{B}$$

The variable Resultant\_M<sub>j</sub> is the combined effect of the all the scattering matrix ; of the length of the grating at the front face of the grating ; reflective amplitude response at various wavelengths , assuming there is a no discontinuities between each section of, the grating .

$$\text{Resultant\_M}_j = \left[ \prod_{z=400}^0 \begin{pmatrix} A_{j,z} & B_{j,z} \\ C_{j,z} & D_{j,z} \end{pmatrix} \right]$$

Referring to the theory in the section 3 of the main body of text of the thesis , the reflectivity of the is calculated below :

$$\text{Reflectivity\_T}_j = \left[ \frac{(\text{Resultant\_M}_j)_{0,1}}{(\text{Resultant\_M}_j)_{0,0}} \right]$$



**(IVf) Resultant response ( single wavelength ) for a uniform and nonuniform grating ( linearly chirped period ) constant  $\Delta n$  subjected to a longitudinal strain using Rouard's Method .**

( Note Mathcad +6 program name TECH1RS.mcd )

**n0** is the peak perturbed refractive index :  $n0 := 1.54$

**n1** is the original core refractive index :  $n1 := 1.5$

**$\Lambda\_mode$**  is the either the initial half period of the grating  $\Lambda(z=0)$  in the case of a chirped grating or otherwise the uniform half period :  $\Lambda\_mode := 500 \cdot 10^{-9}$

**F** is the chirp factor which is in nanometers change in period per period of the grating :  
 $F := -0.02 \cdot 10^{-9}$

**I** is the number of periods in the grating :  $I := 40$

**i** and **j** are used to increment the periods ; **i** and **j** incrementing of the longitudinal strain  
 $i := 0..$

$j := 0..10$

The grating is illuminated by a single wavelength :

$\lambda_0 := 1557 \cdot 10^{-9}$

The variation of the period per period :

$d_i := \Lambda\_mode + F \cdot$

Also there is the variation the period by the longitudinal strain which is :

$d1_{i,j} := d_i \cdot (1 + 250 \cdot 10^{-6} \cdot j)$

$d1_{I+1,j} :=$

The effective refractive index can be considered as the average which is :

$n_{eff} := \left( \frac{n1 - n0}{2} \right) + n$

**$\Delta\beta$**  is the differential propagation constant which is associated with the detuning from the Bragg condition which varies according to the period which varies due to the longitudinal strain and the position within the grating :

$\Delta\beta_{i,j} := \frac{2 \cdot \pi \cdot n_{eff}}{\lambda_0} - \frac{\pi}{d1_{i,j}}$

**$\kappa$**  is the coupling coefficient of the grating :  $\kappa := \frac{\pi \cdot (n1 - n0)}{\lambda_0}$

$s_{i,j} := \sqrt{(|\kappa|)^2 - (\Delta\beta_{i,j})^2}$

**r** reflectivity amplitude which is derived from the coupled mode equations were the the perturbation of the refractive index is described by  $n(z) = n + \Delta n \cdot \sin\left(\frac{2 \cdot \pi}{\Lambda} \cdot z\right)$

$$r_{i+1,j} = \frac{-\kappa \sinh(s_{i,j} \cdot dl_{i+1,j})}{s_{i,j} \cosh(s_{i,j} \cdot dl_{i+1,j}) - i \cdot \Delta\beta_{i,j} \sinh(s_{i,j} \cdot dl_{i+1,j})}$$

This section calculates the effective interfaces form layer to layer  
 $\varepsilon$  is the phase information for each layer being viewed in reflection :

$$\varepsilon_{i,j} = \exp\left(\frac{-i \cdot 4 \cdot \pi \cdot n_0 \cdot dl_{i,j}}{\lambda_0}\right)$$

ii is the effective count from the back end of the grating down to the front face ( perturbation of the refractive index :

$$ii = I, I - 1 ..$$

Calculating the effective interface for the back face perturbation of the grating :

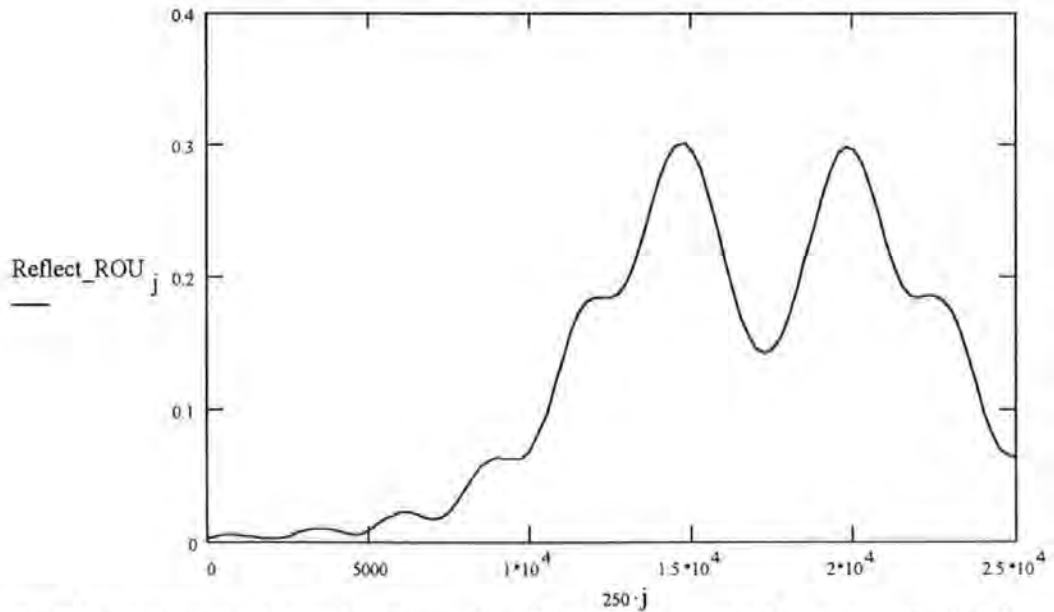
$$\rho_{I,j} = \frac{r_{I-1,j} + r_{I,j} \varepsilon_{I,j}}{1 + r_{I-1,j} \cdot r_{I,j} \varepsilon_{I,j}}$$

The calculations of the effective interfaces from the back face to the front face :

$$\rho_{ii-1,j} = \frac{r_{ii-1,j} + \rho_{ii,j} \varepsilon_{ii,j}}{1 + r_{ii-1,j} \cdot \rho_{ii,j} \varepsilon_{ii,j}}$$

Reflect\_ROU is the total reflection characteristic of the grating due to longitudinal strain

$$\text{Reflect\_ROU}_j = \rho_{0,j} \cdot \rho_{0,j}$$



Note The theoretical results from the Rouard's method for longitudinal strain was compared to the theoretical results from T-matrix formalism technique when longitudinal strain was applied using the same specification for the Bragg grating . Both techniques give the same theoretical response .

**(IVg) spectral response using the T-Matrix Formalism technique a single uniform grating and single nonuniform grating ( linearly chirped ) with envelope function for  $\Delta n$  ( a sinusoidal variation with a Top-Hat function )**

( Note Mathcad +6 program name TECH1T2.mcd )

**n1 is the peak perturbed refractive index :  $n1 := 1.54$**

**n0 is the original core refractive index :  $n0 := 1.5$**

**$\Lambda_{\text{mode}}$  is the either the initial half period of the grating  $\Lambda(z=0)$  in the case of a chirped grating or otherwise the uniform half period :  $\Lambda_{\text{mode}} := 505 \cdot 10^{-9}$**

**F is the chirp factor which is in nanometers change in period per period of the grating :**

$$F = -6.25 \cdot 10^{-1} \quad \text{Note : } F_{\text{T\_Matrix}} = \frac{F_{\text{Rouards}}}{2}$$

$$\left( \frac{600}{1200} \right)^2 \cdot 0.025 \cdot 10^{-9} = -6.25 \cdot 10^{-12}$$

**No\_periods=600**

**condition1 =  $F = -0.025$ , sin\_Mod = 0.2I, No\_pksR=2, period\_sine=2.5**

**condition2 =  $F = -0.025$ , sin\_Mod = 0.2I, No\_pksR=3, period\_sine=3.5**

**condition3 =  $F = -0.025$ , sin\_Mod = 0.3I, No\_pksR=3, period\_sine=4.5**

**I is the number of periods in the grating :**

**I = 1200**

**400**

**i and j are used to increment the periods ; i and j incrementing the wavelength range**

**z := 0..I**

**j := 0..100**

**The wavelength range in nano meters :  $\lambda_j = (1500 + 1 \cdot j) \cdot 10^{-9}$**

**The variation of the period per period :  $\Lambda I_z = \Lambda_{\text{mode}} + F \cdot$**

$$\text{The total length of the grating is : } L = \sum_{z=0}^I \Lambda I_z \quad L = 6.02 \cdot 10^{-4}$$

**The effective refractive index can be considered as an envelope function over the main modulation of  $\Delta n$  :  $\Delta n := \left( \frac{n1 - n0}{2} \right)$**

**Where the parameters a and S define the envelope function of modulation of  $\Delta n$  :**

**a = 1. , S = 13**



$Fn_z$  generates a top hat envelope function  $\Delta n$

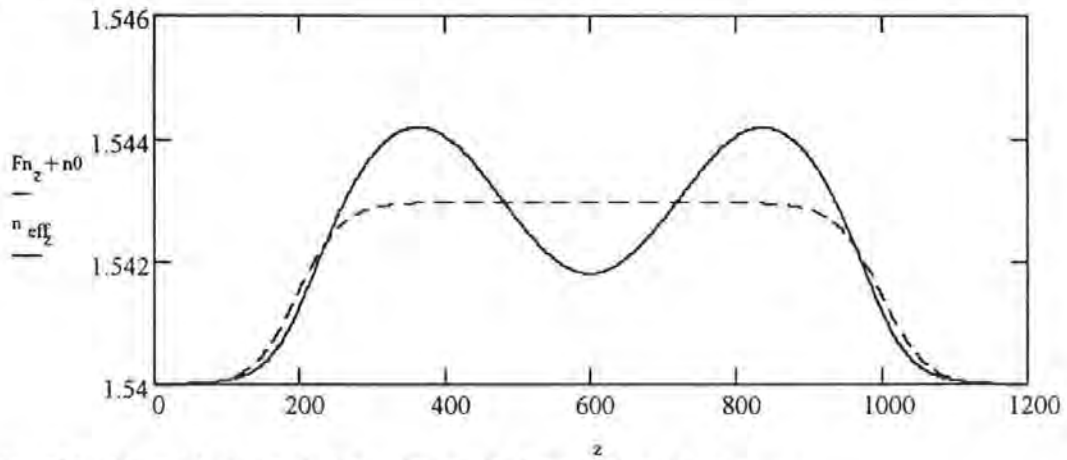
$$Fn_z = \Delta n \cdot \left[ 1 + \tanh \left[ S \cdot \left[ \frac{1}{2} + \frac{\left[ \sum_{z=0}^z \Lambda l_z - \frac{L}{2} \right] \cdot a}{L} \right] \right] \cdot \tanh \left[ S \cdot \left[ \frac{1}{2} - \frac{\left[ \sum_{z=0}^z \Lambda l_z - \frac{L}{2} \right] \cdot a}{L} \right] \right] \right]$$

$Kons = 0$ .

$n_{effz}$  generates a top hat envelope function  $\Delta n$  and superimposing a sine variation on the top of the hat .

$$n_{effz} = Fn_z \cdot \left[ 1 - Kons \cdot \sin \left[ \frac{2 \cdot \pi \cdot (z)}{\left( \frac{I}{2.5} \right)} \right] \right] + n0$$

The graph below the variation of the refractive modulation strength along the Bragg grating length .



The effective refractive index through the grating is :  $n_{core}$

$$\sum_{z=0}^I n_{effz}$$

Which is defined as :  $n_{core} = \frac{\sum_{z=0}^I n_{effz}}{I + 1}$

$\Delta\beta$  is the differential propagation constant which is associated with the detuning from the Bragg condition which varies according to the wavelength and the position within the grating :

$$\Delta\beta_{j,z} = \frac{2 \cdot \pi \cdot n_{core}}{\lambda_j} - \frac{\pi}{\Lambda l_z}$$

$\kappa$  is the coupling coefficient of the grating :  $\kappa_{j,z} = \frac{\pi \cdot (n_{effz} - n0)}{\lambda_j}$

$$sl_{j,z} := \sqrt{(|\kappa l_{j,z}|)^2 - (\Delta\beta l_{j,z})}$$

The Expressions for A , B ,C , D are derived in chapter 3 of the thesis .These expression form the elements of the scattering matrix which represents the behaviour of the grating for a given length . In this case the length is one period of the grating .

$$A_{j,z} := \frac{\Delta\beta l_{j,z} \cdot \sinh(sl_{j,z} \cdot \Lambda l_z) + i \cdot sl_{j,z} \cdot \cosh(sl_{j,z} \cdot \Lambda l_z)}{i \cdot sl_{j,z}} \cdot \exp\left(-i \cdot \pi \cdot \frac{\Lambda l_z}{\Lambda_{mode}}\right)$$

$$B_{j,z} := \frac{\kappa l_{j,z} \cdot \sinh(sl_{j,z} \cdot \Lambda l_z)}{i \cdot sl_{j,z}} \cdot \exp\left(i \cdot \pi \cdot \frac{\Lambda l_z}{\Lambda_{mode}}\right)$$

$$C := -$$

$$D := A$$

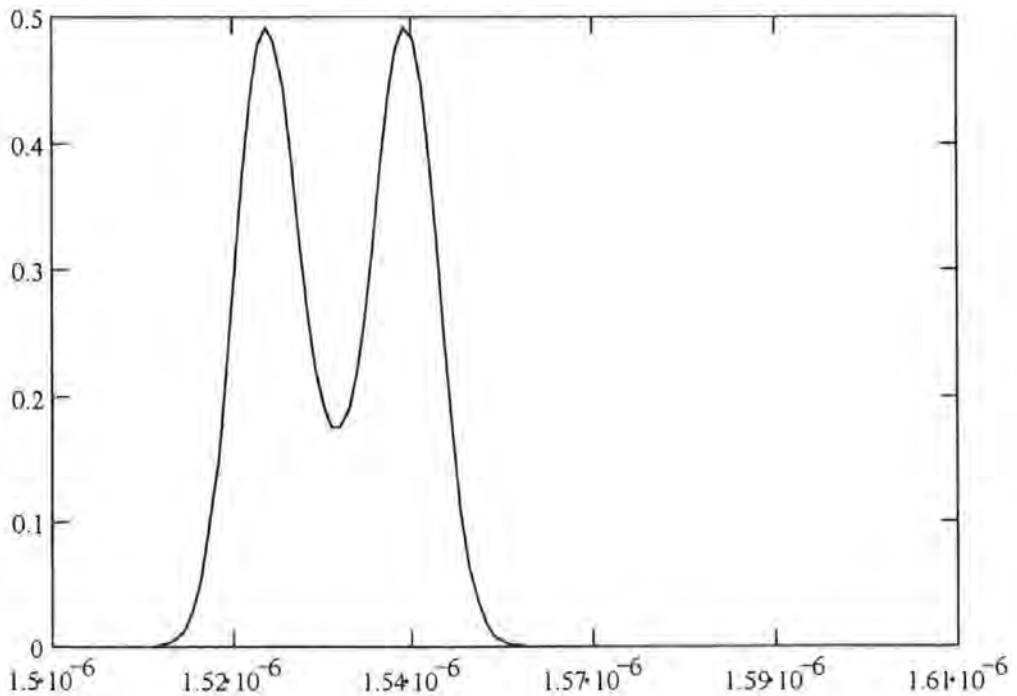
The variable Resultant\_Mj is the combined effect of the all the scattering matrix ; of the length of the grating at the front face of the grating ; reflective amplitude response at various wavelengths .

$$\text{Resultant\_M}_j := \left[ \prod_{z=1200}^0 \begin{pmatrix} A_{j,z} & B_{j,z} \\ C_{j,z} & D_{j,z} \end{pmatrix} \right]$$

Referring to the theory in the chapter 3 of the main body of text of the thesis , the reflectivity of the is calculated below :

$$\text{Reflectivity\_T}_j = \left[ \frac{(\text{Resultant\_M}_j)_{0,1}}{(\text{Resultant\_M}_j)_{0,0}} \right]$$

The graph below shows the spectral response of the proposed Bragg grating



**(IVh) Resultant response ( single wavelength ) for either a single or combination of uniform or nonuniform ( linearly chirped ) with  $\Delta n$  constant or a Taper function for  $\Delta n$  subjected to a longitudinal strain using the T-Matrix Formalism .**

( Note Mathcad +6 program name HOPE2S.mcd )

**Section (i)**

Parameters used for the calculation if of the reflectivity spectrum of the given grating .

The unperturbed refractive index is :  $n_2 = 1.5$

The maximum perturbed refractive index is :  $n_1 = 1.54$

The index modulation depth is :  $n_1 - n_2 = 2 \cdot 10^{-3}$

The original  $\Lambda_0$  is the value used to obtain the grating structure is centred on

$\Lambda_0 = 500 \cdot 10^{-9}$

F is the chirp factor ; this being the linear rate of change in the period per period along the grating length and it is measured in nanometers .  $F = 0.019210^{-9}$

The response of the grating is calculated for a series of increases in micro - strains at a specific wavelength .  $\lambda_0 = 1560 \cdot 10^{-9}$

Zmax represents the number periods in the grating .  $Z_{\max} = 40$

$z = 0 \dots Z_{\max}$

**Section (ii)** - obtaining the pattern of the chirps involved in this grating .

centre =  $\frac{Z_{\max}}{2}$

centre = 200

These variables are used to determine the structure of the grating .

third =  $\frac{3 \cdot Z_{\max}}{4}$

third = 300

quarter =  $\frac{Z_{\max}}{4}$

quarter = 100

Calculating the changes of the period along the grating length ,

$t = Z_{\max} \dots \text{third}$

$\Lambda_1 = \Lambda_0 - F \cdot ((1 + \text{third}) - t)$

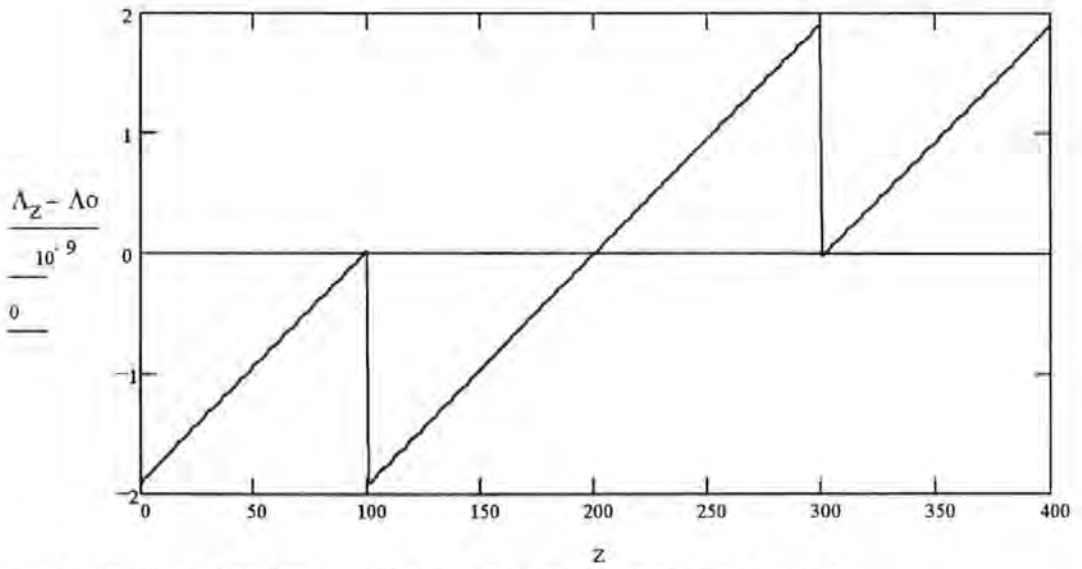
$t_2 = \text{third} - 1 \dots \text{quarter} +$

$\Lambda_{t_2} = \Lambda_0 - F \cdot (\text{centre} - t_2)$

$t_3 = \text{quarter} \dots$

$\Lambda_{t_3} = \Lambda_0 - F \cdot ((\text{quarter} - t_3) - 1)$

The graph below shows the variation of the period along the grating length .



Gaussian - distributed index modulation depth with the chirped period .

L1 represents the total length of the grating :  $L1 = \frac{Z_{ma}}{2}$

ngx gives the variation and the values of the average / effective refractive along the grating length . The reason for introducing this distribution is that currently the gratings that are being fabricated , in general have this kind of Gaussian distribution of the effective refractive index due to laser own Gaussian distribution in irradiance . a1 determines the width of the Gaussian shape :  $a1 := 1$  ,  $a2 := 1$  ,  $S := 1$

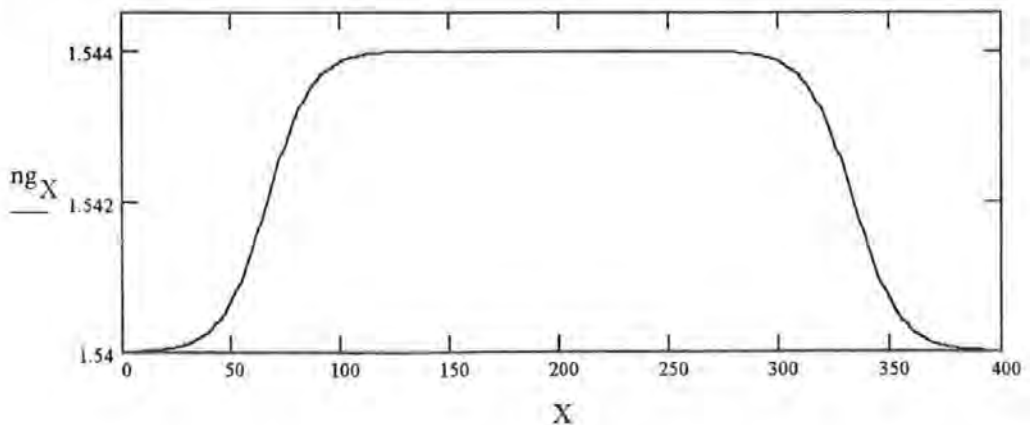
a2 and S determines the shape of the top -hat function  $X := 0..Z_{ma}$

$$(n1 - n2) \cdot \exp \left[ -a1 \cdot \left[ \frac{(X - L1)}{L1} \right]^2 \right] + n$$

$$ng_X = (n1 - n2) \cdot \left[ 1 + \dots \right] + n$$

$$\left[ + 1 \cdot \tanh \left[ S \cdot \left[ \frac{1}{2} + \frac{(X - L1) \cdot a2}{Z_{max}} \right] \right] \cdot \tanh \left[ S \cdot \left[ \frac{1}{2} - \frac{(X - L1) \cdot a2}{Z_{max}} \right] \right] \right]$$

A graph showing the variation of the effective refractive index along the grating length



Remembering that refractive index of the fibre will change due to the optic strain effect.

$$n(z) = n - \frac{1}{2} \cdot n^3 \cdot [P_{12} - \nu(P_{11} + P_{12})] \cdot \varepsilon(z)$$

where

$P_{11}$

and

$P_{12}$

are photoelastic constants and

is the Poisson's ratio for the fibre and  $\varepsilon(z)$  is the strain .

$$P_{11} = 0.11$$

$$P_{12} = 0.25$$

$$\nu = 0.1$$

$a$  is used to increment the strain , the theoretical strain which is subjected on the Bragg grating . The size of the increment is  $200 \mu\epsilon$ 's .

$$a = 0..10$$

The variable  $\Lambda_{1,z,a}$  is the physical variation of the period due to longitudinal strain :

$$\Lambda_{1,z,a} = \Lambda_z \cdot (1 + a \cdot 200 \cdot 10^{-6})$$

The variable  $ng_{1,z,a}$  and  $n_{21,a}$  is the change in the refractive index due to the photoelastic effect

$$ng_{1,z,a} = ng_z - \frac{1}{2} \cdot (ng_z)^3 \cdot [P_{12} - \nu(P_{11} + P_{12})] \cdot a \cdot 200 \cdot 10^{-6}$$

$$n_{21,a} = n_2 - \frac{1}{2} \cdot n_2^3 \cdot [P_{12} - \nu(P_{11} + P_{12})] \cdot a \cdot 200 \cdot 10^{-6}$$

### **Section (iii) - The mode coupled equations**

The electric fields of the backward and forward modes of a grating can be express as :  $a(z) = A(z) \cdot \exp(i \cdot \beta \cdot z)$  and  $b(z) = B(z) \cdot \exp(-i \cdot \beta \cdot z)$  respectively where  $\beta$  is the wave propagation constant . Their complex amplitudes  $A(z)$  and  $B(z)$  obey the coupled mode equations :

$$\frac{d}{dz} A(z) = i \cdot \kappa \cdot B(z) \cdot \exp(-i \cdot 2 \cdot (\Delta\beta) \cdot z)$$

$$\frac{d}{dz} B(z) = -i \cdot \kappa \cdot A(z) \cdot \exp(i \cdot 2 \cdot (\Delta\beta) \cdot z)$$

Where  $\Delta\beta = \beta - \beta_0 = \frac{2\pi \cdot \pi}{\lambda} - \frac{\pi}{\Lambda}$  is the differential propagation constant associated with

detuning from the Bragg condition  $\beta_0$  .

$n$  is the average / effective refractive index .

$\kappa$  is the coupling coefficient .

For a uniform grating i.e. no chirp in the period ,  $\kappa$  is a constant and related to the index modulation depth  $\Delta n$  . For a sinusoidal modulated refractive with the form of

$$n(z) = n + \Delta n(z) = n + \Delta n \cdot \cos\left(\frac{2 \cdot \pi \cdot z}{\Lambda}\right)$$

$\kappa$  is real :

$$\kappa = \frac{\pi \cdot \Delta n}{\lambda}$$

Based on the boundary conditions of  $B(0) = B_0$  and  $A(L) = A_1$ , it is straightforward to obtain the close form solutions for  $A(z)$  and  $B(z)$  from the coupled - mode equations and therefore the closed form solutions for  $a(z)$  and  $b(z)$ . Consequently the backward output ( reflection ),  $a(0)$  and the forward output ( transmission ),  $b(l)$ , from the grating can expressed by means of a scattering matrix .

$$\begin{pmatrix} a(0) \\ b(l) \end{pmatrix} = \begin{pmatrix} S_{11} & S_{12} \\ S_{21} & S_{22} \end{pmatrix} \cdot \begin{pmatrix} a(l) \\ b(0) \end{pmatrix}$$

with  $a(l) = A_1 \exp(i \cdot \beta \cdot l)$  and  $b(0) = B_0$ ; and

$$S_{11} = S_{22} = \frac{i \cdot s \cdot \exp(-i \cdot \beta \cdot l)}{-\Delta\beta \cdot \sinh(s \cdot l) + i \cdot s \cdot \cosh(s \cdot l)}$$

$$S_{12} = S_{21} \cdot \exp(2i \cdot \beta \cdot l) = \frac{\kappa \sinh(s \cdot l)}{-\Delta\beta \cdot \sinh(s \cdot l) + i \cdot s \cdot \cosh(s \cdot l)}$$

where

$$s = \sqrt{(\kappa)^2 - \Delta\beta^2}$$

Based on the scattering - matrix expression one can obtain the transfer - matrix expression

$$\begin{pmatrix} a(0) \\ b(0) \end{pmatrix} = \begin{pmatrix} T_{11} & T_{12} \\ T_{21} & T_{22} \end{pmatrix} \cdot \begin{pmatrix} a(l) \\ b(l) \end{pmatrix}$$

Where ...

$$T_{11} = T_{22} = \frac{\Delta\beta \cdot \sinh(s \cdot l) + i \cdot s \cdot \cosh(s \cdot l)}{i \cdot s} \cdot \exp(-i \cdot \beta \cdot l)$$

$$S_{12} = T_{21} = \frac{\kappa \sinh(s \cdot l)}{i \cdot s} \cdot \exp(i \cdot \beta \cdot l)$$

The T - matrix relates the left - side vector  $(a(0) \ b(0))$  the right - side vector  $(a(l) \ b(l))$  and is well suited to analyse a cascade of gratings . A uniform grating of length of  $L$  can be consider as a cascade of many small uniform gratings with length  $l_1, l_2, l_3, \dots, l_m$ . It can be verified that .

$$(T_L) = (T_{l_1}) \cdot (T_{l_1}) \cdot \dots \cdot (T_{l_m})$$

where  $(T_L)$  denotes the T - matrix for the original grating ; and  $(T_{l_i})$  denotes the T - matrix for the  $i$ th small grating (  $i = 1, 2, \dots, m$  ) .

Note , that  $l_i$  can be as short as one period of the grating ; this is what happens in the calculations below .... Thus nonuniform grating ( a chirp in the period ) and distribution in  $\Delta n(z)$  can be taken into account .

#### Section (iv) Calculations using the T - matrix formalism .

The calculation of the differential propagation constants taking into account the variation of the period along the length of the grating and variations of the effective refractive index in each period due strain.

$$\Delta\beta_{z,a} = \frac{\left(\frac{ngl_{z,a}}{2} + \frac{n2l_a}{2}\right) \cdot \pi \cdot 2}{\lambda_0} - \frac{\pi}{\Lambda l_{z,a}}$$

$\kappa$  is  $KK_{a,z}$  taking variations of refractive index and know the coupling coefficient varies with a longitudinal strain .

$$KK_{z,a} = \frac{(ngl_{z,a} - n2l_a) \cdot \pi}{\lambda_0}$$

$$s = \sqrt{(\kappa)^2 - \Delta\beta^2} \text{ is :}$$

$$s_{z,a} = \sqrt{\left(|KK_{z,a}|\right)^2 - \left(\frac{1}{2} \Delta\beta_{z,a}\right)^2}$$

The below are to calculate the elements of the transfer - matrix ( Appendix I )

$$T_{11_{z,a}} = \left( \frac{\Delta\beta_{z,a} \cdot \sinh(s_{z,a} \cdot \Lambda l_{z,a}) + i \cdot s_{z,a} \cdot \cosh(s_{z,a} \cdot \Lambda l_{z,a})}{i \cdot s_{z,a}} \right) \cdot \exp\left(-i \cdot \Lambda l_{z,a} \cdot \frac{\pi}{\Lambda_0}\right)$$

$$T_{12_{z,a}} = \left( \frac{KK_{z,a} \cdot \sinh(s_{z,a} \cdot \Lambda l_{z,a})}{i \cdot s_{z,a}} \right) \cdot \exp\left(i \cdot \Lambda l_{z,a} \cdot \frac{\pi}{\Lambda_0}\right)$$

$$T_{22} := \overline{T_{11}}$$

Variables  $T_{22}$  and  $T_{21}$  are the conjugates of the elements of the  $T_{11}$  and  $T_{12}$  .

$$T_{21} := \overline{T_{12}}$$

$Ml_a$  is calculation of all the gratings in this case of one period

$(T_L) = (T_{l_1}) \cdot (T_{l_1}) \cdot \dots \cdot (T_{l_m})$  but  $m = Z_{max}$  , the reflection is of interest and this is way the geometrical summation is from  $z = Z_{max}$  to  $z = 0$  . Each  $z$  value represents one period of the grating .

$$Ml_a = \left[ \prod_{z=Z_{max}}^0 \begin{pmatrix} T_{11_{z,a}} & T_{12_{z,a}} \\ T_{21_{z,a}} & T_{22_{z,a}} \end{pmatrix} \right]$$

Let

$$\begin{pmatrix} A & B \\ C & D \end{pmatrix} = \prod_{z=Z_{\max}}^0 \begin{pmatrix} T_{11_{a,z}} & T_{12_{a,z}} \\ T_{21_{a,z}} & T_{22_{a,z}} \end{pmatrix}$$

The coefficient reflection is given by :

$$r_{Z_{\max}} = \left( \frac{b(0)}{a(0)} \right)_{b(Z_{\max})=0}$$

So

$$\begin{pmatrix} a(0) \\ b(0) \end{pmatrix} = \begin{pmatrix} A & B \\ C & D \end{pmatrix} \begin{pmatrix} a(Z_{\max}) \\ b(Z_{\max}) \end{pmatrix}$$

$$\begin{pmatrix} a(0) \\ b(0) \end{pmatrix} = \begin{pmatrix} A & B \\ C & D \end{pmatrix} \begin{pmatrix} a(Z_{\max}) \\ 0 \end{pmatrix}$$

Thus...

$$\begin{pmatrix} a(0) \\ b(0) \end{pmatrix} = \begin{pmatrix} A \cdot a(Z_{\max}) \\ C \cdot a(Z_{\max}) \end{pmatrix}$$

Therefore ...  $a(0) = A \cdot a(Z_{\max})$  and  $b(0) = C \cdot a(Z_{\max})$  so the coefficient of reflection is for a given wavelength ( $\lambda$ ).

$$r_{Z_{\max}}_{\mu\epsilon} = \left[ \left( \frac{b(0)}{a(0)} \right)_{b(Z_{\max})=0} \right]_{\mu\epsilon} = \left( \frac{A}{C} \right)_{\mu\epsilon}$$

In terms of the given variables a Mathcad notation

$$A = (M1_a)_{1,0}$$

and

$$C = (M1_a)_{1,1}$$

So the Reflectivity for a given strain  $\mu\epsilon$  of the grating structure is determined by using the definition that

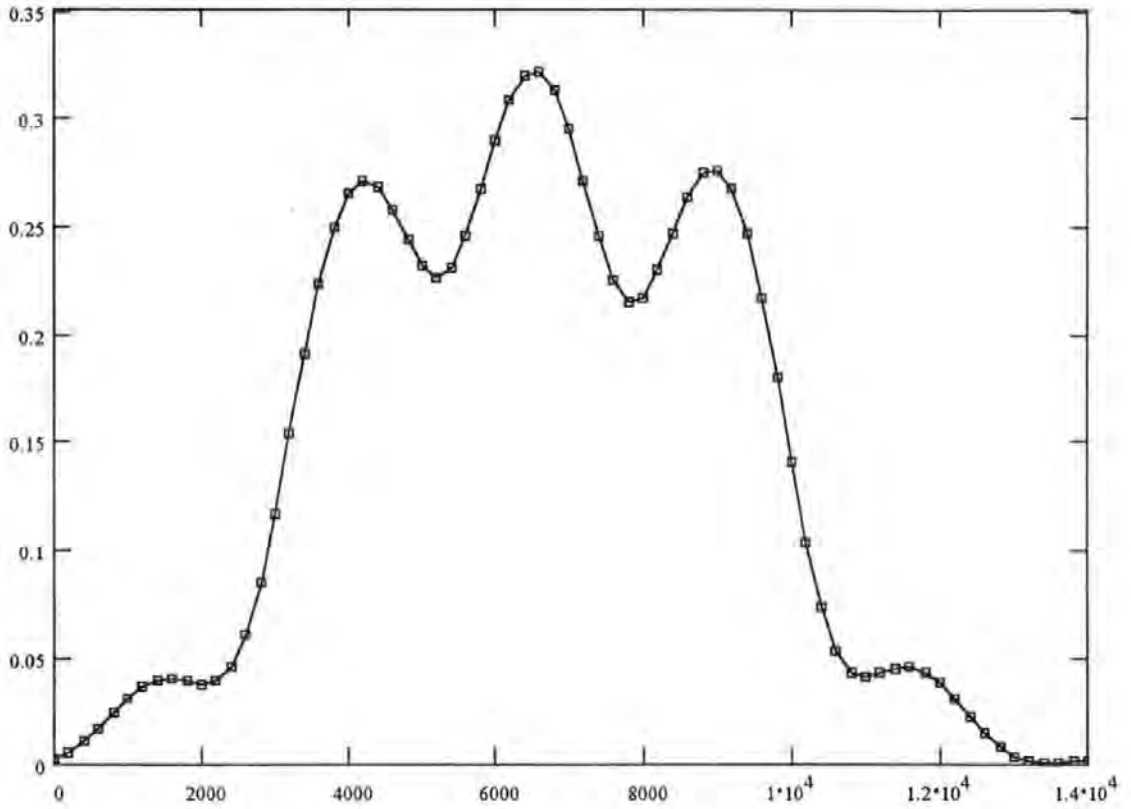
$$\text{Reflectivity}_{\mu\epsilon} = \left[ \left( |r_{Z_{\max}}| \right)_{\mu\epsilon} \right]^2 = Rm_{\mu}$$

$$Rm_a = \left[ \left| \frac{(M1_a)_{1,0}}{(M1_a)_{1,1}} \right| \right]^2$$



$$Rm_a = \left[ \frac{\left( M1_a \right)_{1,0}}{\left( M1_a \right)_{1,1}} \right]^2$$

The graph below shows how the reflectivity changes for a given wavelength at a particular longitudinal strain being subjected to the proposed fibre Bragg grating structure .



The reason for looking at the three linearly chirped Bragg grating and the single linear chirped grating with a Top-Hat taper function of  $\Delta n$  with a sinusoidal perturbation superimposed on it .Is the reflective response to longitudinal strain which would help to overcome some of the drawbacks of a Fibre Fabry-Perot sensor.

Also the reflective response to longitudinal strain of the second grating is investigated more in the main body of text of this report and in the signal processing appendix ( V ) . All the proposed Bragg grating structures have been looked at by T-Matrix formalism and Rouard's method which have gave the approximately the same theoretical predictions .

Also a general note the gratings length are very small this limitation is due to computer resources available to run the Mathcad +6 package . To reduce the computational time and to model more realistic Bragg grating a C program has been developed for spectral response and reflective response to longitudinal strain .

**Appendix V . The modelling of the signal processing technique  
employed by this scheme .**

**Va . The general implementation and modelling of the strain sensing system  
for a Fabry - Perot configured sensor .**

The C program of the T matrix formalism generates an output file of the variations of the reflectivity with respect to longitudinal strain ; *Datafile* . This is then imported into a relevant Mathcad program , this being dependent upon the type of sensor under investigation. A fibre Fabry - Perot sensor ( a  $\text{TiO}_2$  mirror one and endface mirror ) or series of two identical fibre Bragg gratings ( fibre Bragg grating resonator ) the same procedure is used , a variation in optical phase change of the irradiance from the sensor under longitudinal strain ,

The demodulation techniques is known as a phase - generated carrier technique ; a demodulation of the resultant output with respect to the modulation frequency of the laser (  $\omega_0$  ) ; first harmonic and twice the modulation frequency of the laser (  $2\omega_0$  ) ; second harmonic . This is a well established technique for interferometric sensors .

The file *Datafile* holds information how the static reflectivity changes with respect to longitudinal strain of the length of the sensor . Knowing this information , the refractive indices of the fibre core and the wavelength of the irradiance , the optical phase difference can be calculated from this information .

So *Datafile*(  $\mu\epsilon$  )  $\rightarrow$  reflectivity(  $\theta$  ) ; thus also knowing the individual reflectivities of each mirror one is able to model the results in the *Datafile* file . This being :

$$I_{reflec}(\mu\epsilon) = \frac{I_0}{2} \left( \frac{F}{F+1} \right) (1 - \cos(\theta))$$

where  $F = \frac{4R}{(1-R)^2}$  F being the finesse and R being the reflectivity of the mirrors

Thus

$$\theta = \cos^{-1} \left( 1 - 2I_{reflec}(\mu\varepsilon) \left( \frac{1+F}{F} \right) \right)$$

The D.F.B. laser has a sinusoidal modulation on the injection current to the laser ;  $\Delta i \sin(\varpi_0 t)$  in turn this produces a phase shift given by :

$$\Delta\theta = \frac{2\pi\Delta L n}{c} \cdot \Delta i \frac{\delta v}{\delta i} \cdot \sin(\varpi_0 t)$$

The sensor is interferometric in behaviour then the following is true

$$I_{reflec}(\mu\varepsilon) = \frac{I_0}{2} \left( \frac{F}{F+1} \right) \left( 1 - \cos(\theta + \Delta\theta \sin(\varpi_0 t)) \right)$$

Using the Bessel function trigonometric identities for  $\cos(\theta + \Delta\theta \sin(\omega_0 t))$  this leads to at the first harmonic

$$\frac{I_0}{2} \left( \frac{F}{F+1} \right) 2J_1(\Delta\theta) \sin(\theta)$$

and

at the second harmonic

$$\frac{-I_0}{2} \left( \frac{F}{F+1} \right) 2J_2(\Delta\theta) \cos(\theta)$$

or using the general expression for a Fabry -Perot cavity ;  $I_{reflect} = I_0 \left( 1 - \frac{1}{F \sin^2 \left( \frac{\theta}{2} \right)} \right)$

again using the Bessel functions the harmonics become :

First harmonic

$$I_0 \left( \left[ 2F - \frac{3F^2}{2} \right] \cdot \sin(\theta) - F^2 J_2(\Delta\theta) \sin(2\theta) \right) \cdot J_1(\Delta\theta)$$

and

Second harmonic

$$I_0 \left( \frac{3F^2}{2} - 2F \right) \cdot J_2(\Delta\theta) \cos(\theta)$$

Knowing the intensities at the first and second harmonics it is possible to calculate the current generated by the photodetector at  $\omega_0$  and  $2\omega_0$  by using the responsivity of the detector . These currents are inputted in an operation amplifier and the output of the photodetector is converted to a voltage ,the voltage is easily obtainable from the specification of the amplifier ( gain , gain resistance ,etc. ) ; see Mathcad +6 programs in this appendix .

**Vb . The general implementation and modelling for a strain sensing system for a individual fibre Bragg grating sensor .**

There was two methods employed to investigate the system with the individual fibre Bragg grating sensor .

**Method one :** The reflectivity spectral response is obtained by the C program for T matrix formalism by incorporating a small sinusoidal perturbation on the wavelength being subjected to the grating , i.e.

$$\lambda_0 \rightarrow \lambda_0 + \Delta\lambda \sin(\omega_0 t)$$

where  $\Delta\lambda$  is defined by the characteristics of the D.F.B. laser ; the effective current to wavelength coefficient ;  $\frac{\delta\lambda}{\delta i} \Rightarrow \Delta\lambda = \frac{\delta\lambda}{\delta i} \cdot \Delta i$  . With a frequency of oscillation given by  $\omega_0$  which is 5KHz in this case . The generates a output data file ; sampling the reflectivity response at a given time interval . Thus a file is generated as such :

R e f l e c t i v i t y			T i m e			
S t r a i n	t = 0	t = t1	t = t2			t = tn
R ( $\lambda = 0$ )						
R ( $\lambda = 1$ )						
R ( $\lambda = 2$ )						
-						
-						
-						
-						
-						
-						
R ( $\lambda = n$ )						

This datafile is imported to a Mathcad program . This program determines the magnitudes of the 1<sup>st</sup> , 2<sup>nd</sup> harmonics which are found (  $\omega_0$  ,  $2\omega_0$  ) by Fourier analysis . Therefore the induced current generated by the 1<sup>st</sup> harmonic is :

$$[I_0 \varepsilon] \{ Mag_{harmonic} \}$$

and likewise for the second harmonic . This is again followed by the same procedure as above to obtain the input voltages to the lock in amplifiers .

**Method two :** The reflectivity spectral response is obtained by the C program for T matrix formalism for a single wavelength  $\lambda$  for the D.F.B. laser when the proposed grating structure is subject to static increase in longitudinal strain . This generates a output data file (*Datafile ; refl( $\mu\epsilon$ )* ) from the C program containing static reflectivities for a given longitudinal strain .

The sinusoidal perturbation of the D.F.B. laser can be translated to a sinusoidal perturbation of the longitudinal strain , this is achieved by owning the fractional change in the Bragg wavelength with a longitudinal strain  $\epsilon$  is given by :

$$\frac{\Delta\lambda_b}{\lambda_b} = (1 - p_e)\epsilon$$

where  $p_e$  is the effective photoelastic constant which is by strain optic tensor , the refractive index of the core and Poisson's ratio for the optical fibre (see section 1.4.1 ) . This gives strain to wavelength shift responsivity , in this case it is assumed that  $\lambda_b$  is the same wavelength has the D.F.B. laser giving :  $\frac{\delta\lambda}{\delta\epsilon}$

Using  $\frac{\delta\lambda}{\delta\epsilon}$  and from the specification of the D.F.B. laser and it's drive unit for a given voltage modulation to the system a  $\Delta\lambda$  can be found . So an equivalent sinusoidal perturbation in longitudinal strain by using  $\frac{\delta\epsilon}{\delta\lambda} \cdot \Delta\lambda$  has twice the amplitude of a sine wave variation at some given frequency  $\omega_0$  .

Using the above information and the *data file* in a Mathcad program a sinusoidal perturbation is introduced ; has parameter on the data generated by the for T matrix formalism , therefore :

$$refl(\mu\epsilon_{static}) \rightarrow refl\left(\mu\epsilon_{static} + \frac{1}{2}\left(\frac{\delta\mu\epsilon}{\delta\lambda} \cdot \Delta\lambda\right) \sin(\omega_0 t)\right)$$

The modified data is stored and the harmonics are extracted by Fourier analysis.

To ensure that this signal processing technique would produce large enough variation in the output voltage from the lock in amplifiers with the variations of the wavelength a Mathcad program was generated to simulate a sinusoidal Bragg grating

reflectivity response with variation in wavelength using a typical value for the fractional change in the Bragg wavelength with longitudinal strain . It was found that to obtain reasonable resolution a period of 1nm or less in the sinusoidal region of the reflectivity is required ( see Mathcad program in appendix V , Vh ) .

### Vc . Schematic of the strain sensing system .

Schematic of the system being modelled

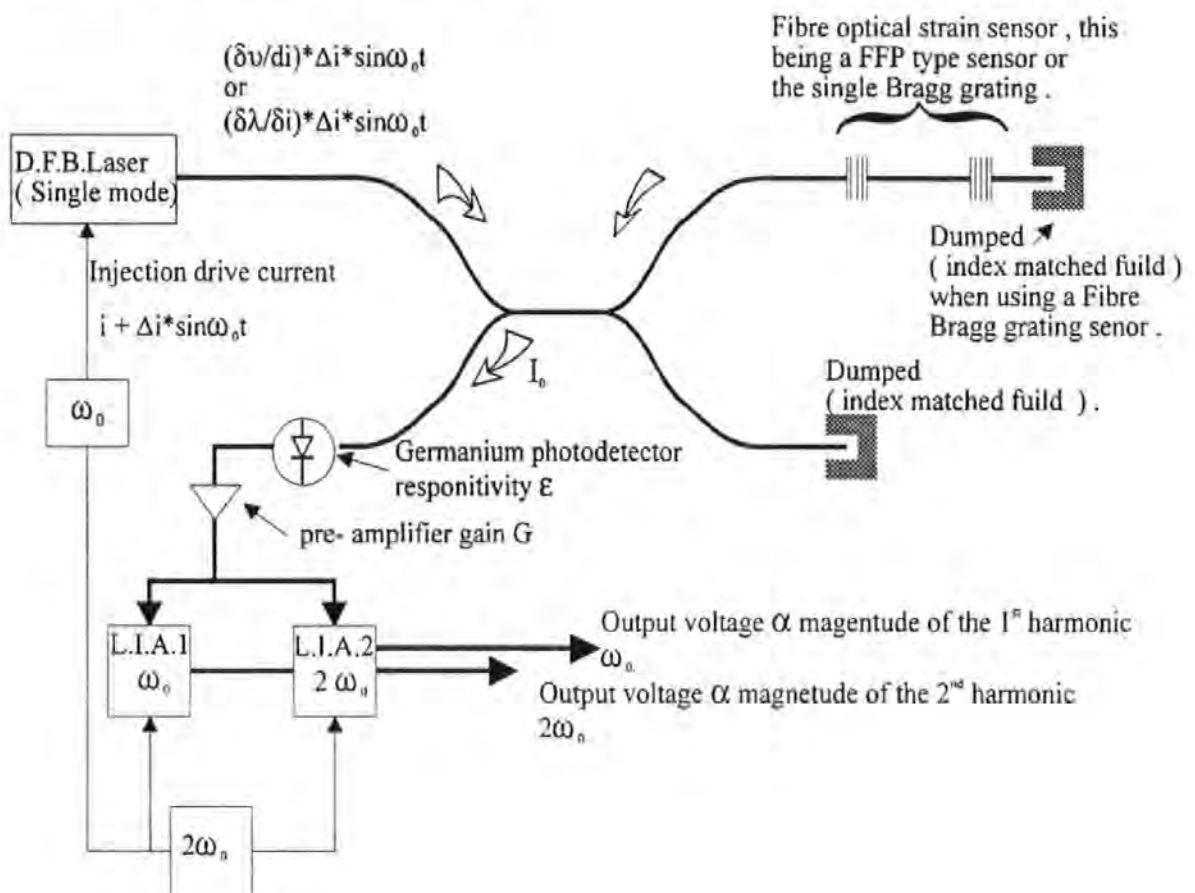


Figure (A5)

For the system :

D.F.B. Laser : A small sinusoidal perturbation of the injection drive current is introduced ;  $i + \Delta i \cdot \sin(\omega_0 t)$  . This in turn produces a sinusoidal variation in

Frequency given by  $\frac{\delta \nu}{\delta i} \cdot \Delta i \cdot \sin(\omega_0 t)$

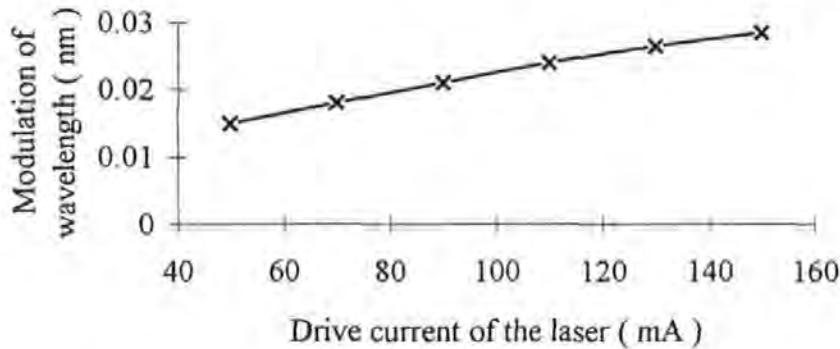
or

Wavelength given by  $\frac{\delta \lambda}{\delta i} \cdot \Delta i \cdot \sin(\omega_0 t)$

There is an effective current to frequency conversion factor  $\left(\frac{\delta \nu}{\delta i}\right)$  which is a constant for a D.F.B. laser :  $\left(\frac{\delta \nu}{\delta i}\right) = 3.5 \times 10^9 \text{ HzmA}^{-1}$ .

Also there is an effective current to wavelength conversion factor  $\left(\frac{\delta \lambda}{\delta i}\right)$  which changes depending on the current being applied to the D.F.B. laser ( see graph 3 below )

The dependence of the modulation of the wavelength upon the drive current of the D.F.B. Laser



Graph (3)

With a sine wave modulation in voltage is used to obtain the modulation of the injection current for the D.F.B. laser , from the specification of the drive unit of the laser ( LDC 100 OEM laser driver unit with a thermoelectric cooler control ) a modulation coefficient of the laser current to peak to peak modulation of  $40 \text{ mA V}^{-1}$

In the modelling it is assumed there is synchronous detection with the Lock - in - Amplifiers , at  $\omega_0$  and  $2\omega_0$  . Also the internal gain of the L.I.A.'s is taken into consideration .



The L.I.A.'s incorporate phase sensitive detectors with a wide dynamic range . The relationship between the D.C. output of the phase sensitive detectors and the input signal is  $V_o = V_s G_s G_e \cos(\phi_r - \phi_s)$  where the frequency of the reference and signal voltage are the same , this is assumed in the modelling .

The signal and reference are also in phase i.e.  $\phi_r = \phi_s$ , thus  $V_o = V_s G_s G_e$  .

$V_o$  is the output of the low-pass filter , the voltage from the L.I.A.'s .

$V_s$  is the root mean squared value of the input signal ; this is generated by the photodetector and the pre-amplifier .

$G_s$  is the signal channel A.C. gain .

$G_e$  is the output stage D.C. gain .

Both the A.C. and the D.C. gains are digitally controlled by the computer with gains available ( 1,10 or 100 ) .

**(Vd) A derivation of the magnitudes of the first and second harmonics from the system using a Fabry-Perot type sensor and the signal processing described .**

( Note Mathcad +6 program name THYSIG2.mcd )

**The Reflectivity of a Fabry - Perot is given by :**

$$R(\mu\varepsilon) = 1 - \frac{1}{1 + F \cdot \sin\left(\frac{\theta(\mu\varepsilon)}{2}\right)^2}$$

**OR**

$$R(\mu\varepsilon) = \frac{\cos(\theta) \cdot F - F}{(\cos(\theta) \cdot F - F - 2)}$$

**because of the trigonometric identity**

$$\sin\left(\frac{\theta(\mu\varepsilon)}{2}\right)^2 = \frac{1}{2} - \frac{1}{2} \cdot \cos(\theta(\mu\varepsilon))$$

**This section is dealing with the response of a photo-detector when the light source is modulated ; in this case there is phase modulation which turn modulates the intensity of the reflected power from the sensor ( grating resonator ) .**

**The photodetector converts the intensity to electrical currents ; the general form of the function that describes the current is :**

$$i = \varepsilon \cdot I_0 \cdot \alpha \cdot \left[ 1 - \frac{1}{1 + F \cdot \sin\left(\frac{\theta + \Delta\theta \cdot \sin(\omega_0 \cdot t)}{2}\right)^2} \right] = \varepsilon \cdot I_0 \cdot \alpha \cdot \left[ \frac{\cos(\theta + \Delta\theta \cdot \sin(\omega_0 \cdot t)) \cdot F - F}{(\cos(\theta + \Delta\theta \cdot \sin(\omega_0 \cdot t)) \cdot F - F - 2)} \right]$$

**With a small perturbation in the injection current for the laser so:**

$$i_{\text{injection}} = i_{\text{const}} + \delta i \cdot \sin(\omega_c \cdot t)$$

**where  $\omega_c$  is the frequency of modulation in this case it is approximately  $\sim 5\text{KHz}$**

**The D.F.B. laser phase modulation is :**

$$v(t, \mu\varepsilon) = \frac{\Delta v(\mu\varepsilon)}{\Delta i} \cdot \delta i \cdot \sin(\omega_c \cdot t)$$

**The reflected Intensity output of the system is dependent upon phase which is dependent upon strain ;  $\mu\varepsilon$**

$$I_{\text{out}} = I_{\text{in}} \cdot R(\phi) = I_{\text{in}} \cdot R(\phi(t, \mu\varepsilon)) = \dots$$

**Remembering the modulation of phase w.r.t. time**

$$R(\phi(t)) = A \cdot \left[ \frac{\cos(\theta + \Delta\theta \cdot \sin(\omega_0 \cdot t)) \cdot F - F}{(\cos(\theta + \Delta\theta \cdot \sin(\omega_0 \cdot t)) \cdot F - F - 2)} \right]$$

**So**

$$R(\phi(t)) = A \cdot \left[ \frac{\cos(\theta(\mu\varepsilon) + \Delta\theta \cdot \sin(\omega_0 \cdot t)) \cdot F - F}{(\cos(\theta(\mu\varepsilon) + \Delta\theta \cdot \sin(\omega_0 \cdot t)) \cdot F - F - 2)} \right]$$

**But Reflection is also dependent upon strain**

$$R(\phi(t, \mu\varepsilon)) = A \cdot \left[ \frac{\cos(\theta(\mu\varepsilon) + \Delta\theta(\mu\varepsilon) \cdot \sin(\omega_0 \cdot t)) \cdot F - F}{(\cos(\theta(\mu\varepsilon) + \Delta\theta(\mu\varepsilon) \cdot \sin(\omega_0 \cdot t)) \cdot F - F - 2)} \right]$$

**But it is know that there is an effective current - to - frequency conversion factor which is  $\delta v \cdot \delta$  , and the magnitude of the modulation current is known  $\Delta$  .**

$$\Delta\theta(\mu\varepsilon) = \frac{\Delta\theta(\mu\varepsilon)}{\Delta i} \cdot \Delta$$

$$R(\phi(t, \mu\varepsilon)) = A \cdot \left[ \frac{\cos\left(\theta(\mu\varepsilon) + \frac{\Delta\theta(\mu\varepsilon)}{\Delta i} \cdot \Delta i \cdot \sin(\omega_0 \cdot t)\right) \cdot F - F}{\left(\cos\left(\theta(\mu\varepsilon) + \frac{\Delta\theta(\mu\varepsilon)}{\Delta i} \cdot \Delta i \cdot \sin(\omega_0 \cdot t)\right) \cdot F - F - 2\right)} \right]$$

**This gives the change in phase . This can be converted to the reflectivity and strain .**

**From the data  $\frac{\Delta R(\mu\varepsilon)}{\Delta \mu\varepsilon}$  and thus  $\frac{\Delta R(\mu\varepsilon)}{\Delta \theta(\mu\varepsilon)}$**

**Thus electrical current is:**

$$R(\lambda(t, \mu\varepsilon)) = A \cdot \left[ \frac{\cos\left(\theta(\mu\varepsilon) + \frac{\Delta\theta(\mu\varepsilon)}{\Delta i} \cdot \Delta i \cdot \sin(\omega_0 \cdot t)\right) \cdot F - F}{\left(\cos\left(\theta(\mu\varepsilon) + \frac{\Delta\theta(\mu\varepsilon)}{\Delta i} \cdot \Delta i \cdot \sin(\omega_0 \cdot t)\right) \cdot F - F - 2\right)} \right]$$

$$i(t, \mu\varepsilon) = \varepsilon \cdot I_{in} \cdot \alpha \cdot R(\phi(t, \mu\varepsilon))$$

$$i(t, \mu\varepsilon) = \varepsilon \cdot I_{in} \cdot \alpha \cdot \left[ \frac{\cos\left(\theta(\mu\varepsilon) + \frac{\Delta\theta(\mu\varepsilon)}{\Delta i} \cdot \Delta i \cdot \sin(\omega_0 \cdot t)\right) \cdot F - F}{\left(\cos\left(\theta(\mu\varepsilon) + \frac{\Delta\theta(\mu\varepsilon)}{\Delta i} \cdot \Delta i \cdot \sin(\omega_0 \cdot t)\right) \cdot F - F - 2\right)} \right]$$

$$i(t, \mu\varepsilon) = \varepsilon \cdot I_{in} \cdot \alpha \cdot \left[ \frac{\cos\left[\theta(\mu\varepsilon) + \frac{\Delta R(\mu\varepsilon)}{\Delta \theta(\mu\varepsilon)} \cdot \frac{\Delta \theta(\mu\varepsilon)}{\Delta v} \cdot \left(\frac{\delta v}{\delta i} \cdot \Delta i\right) \cdot \sin(\omega_0 \cdot t)\right] \cdot F - F}{\left[\cos\left[\theta(\mu\varepsilon) + \frac{\Delta R(\mu\varepsilon)}{\Delta \theta(\mu\varepsilon)} \cdot \frac{\Delta \theta(\mu\varepsilon)}{\Delta v} \cdot \left(\frac{\delta v}{\delta i} \cdot \Delta i\right) \cdot \sin(\omega_0 \cdot t)\right] \cdot F - F - 2\right]} \right]$$

$$i(t, \mu\varepsilon) = \varepsilon \cdot I_{in} \cdot \alpha \cdot \left[ \frac{\cos(\theta(\mu\varepsilon) + \Delta\theta(\mu\varepsilon) \cdot \sin(\omega_0 \cdot t)) \cdot F - F}{(\cos(\theta(\mu\varepsilon) + \Delta\theta(\mu\varepsilon) \cdot \sin(\omega_0 \cdot t)) \cdot F - F - 2)} \right]$$

**This can be expressed and expanded in terms of the harmonics of  $\omega_c$**

$$\cos(z_1 + z_2) = \cos(z_1) \cdot \cos(z_2) - \sin(z_1) \cdot \sin(z_2)$$

**Where**

$$z_1 =$$

**and**

$$z_2 = \Delta\theta \cdot \sin(\omega_c \cdot t)$$

**Thus**

$$\cos(\theta + \Delta\theta \cdot \sin(\omega_c \cdot t)) = \cos(\theta) \cdot \cos(\Delta\theta \cdot \sin(\omega_c \cdot t)) - \sin(\theta) \cdot \sin(\Delta\theta \cdot \sin(\omega_c \cdot t))$$

$$R(\mu\varepsilon) = \frac{(\cos(\theta) \cdot \cos(\Delta\theta \cdot \sin(\omega_c \cdot t)) - \sin(\theta) \cdot \sin(\Delta\theta \cdot \sin(\omega_c \cdot t))) \cdot F - F}{[(\cos(\theta) \cdot \cos(\Delta\theta \cdot \sin(\omega_c \cdot t)) - \sin(\theta) \cdot \sin(\Delta\theta \cdot \sin(\omega_c \cdot t))) \cdot F - F - 2]}$$

**This is achieved by using Bessel identity for trigonometric functions .**

$$\cos(z \cdot \sin(\theta)) = J_0(z) + 2 \cdot \sum_{k=1}^{\infty} J_{2k}(z) \cdot \cos(2 \cdot k \cdot \theta)$$

**and**

$$\sin(z \cdot \sin(\theta)) = 2 \cdot \sum_{k=0}^{\infty} J_{2k+1}(z) \cdot \sin((2 \cdot k + 1) \cdot \theta)$$

**THUS.....**

$$\cos(\theta + \Delta\theta \cdot \sin(\omega_c \cdot t)) = \dots\dots$$

$$\begin{aligned} \cos(\theta) \cdot \cos(\Delta\theta \cdot \sin(\omega_c \cdot t)) &= \cos(\theta) \cdot \left[ J_0(\Delta\theta) + 2 \cdot \sum_{k=1}^{\infty} J_{2k}(\Delta\theta) \cdot \cos[2 \cdot k \cdot (\omega_c \cdot t)] \right] \\ - \sin(\theta) \cdot \sin(\Delta\theta \cdot \sin(\omega_c \cdot t)) &= - \sin(\theta) \cdot \left[ 2 \cdot \sum_{k=0}^{\infty} J_{2k+1}(\Delta\theta) \cdot \sin[(2 \cdot k + 1) \cdot (\omega_c \cdot t)] \right] \end{aligned}$$

**Expanding the Bessel functions**

$$\begin{aligned} \left[ J_0(\Delta\theta) + 2 \cdot \sum_{k=1}^{\infty} J_{2k}(\Delta\theta) \cdot \cos[2 \cdot k \cdot (\omega_c \cdot t)] \right] &= \dots\dots \\ J_0(\Delta\theta) + 2 \cdot [J_2(\Delta\theta) \cdot \cos(2 \cdot \omega_c \cdot t) + J_4(\Delta\theta) \cdot \cos(4 \cdot \omega_c \cdot t)] & \end{aligned}$$

$$\begin{aligned} \left[ 2 \cdot \sum_{k=0}^{\infty} J_{2k+1}(\Delta\theta) \cdot \sin[(2 \cdot k + 1) \cdot (\omega_c \cdot t)] \right] &= \dots\dots\dots \\ J(\Delta\theta)_1 \cdot \sin(\omega_c \cdot t) + J(\Delta\theta)_3 \cdot \sin(3 \cdot \omega_c \cdot t) & \end{aligned}$$

**Therefore :**

$$\cos(\theta) \cdot \cos(\Delta\theta \cdot \sin(\omega_c \cdot t)) = \cos(\theta) \cdot [J_0(\Delta\theta) + 2 \cdot [J_2(\Delta\theta) \cdot \cos(2 \cdot \omega_c \cdot t) + J_4(\Delta\theta) \cdot \cos(4 \cdot \omega_c \cdot t)]]$$

**and**

$$-\sin(\theta) \cdot \sin(\Delta\theta \cdot \sin(\omega_c \cdot t)) = -2\sin(\theta) \cdot (J(\Delta\theta)_1 \cdot \sin(\omega_c \cdot t) + J(\Delta\theta)_3 \cdot \sin(3\omega_c \cdot t))$$

$$R(\mu\epsilon) = \frac{(\cos(\theta) \cdot \cos(\Delta\theta \cdot \sin(\omega_c \cdot t)) - \sin(\theta) \cdot \sin(\Delta\theta \cdot \sin(\omega_c \cdot t))) \cdot F - F}{[(\cos(\theta) \cdot \cos(\Delta\theta \cdot \sin(\omega_c \cdot t)) - \sin(\theta) \cdot \sin(\Delta\theta \cdot \sin(\omega_c \cdot t))) \cdot F - F - 2]}$$

**Substituting in the Bessel identities we obtain**

$$R(\mu\epsilon) = \frac{\left[ \cos(\theta) \cdot [J_0(\Delta\theta) + 2 \cdot [J_2(\Delta\theta) \cdot \cos(2\omega_c \cdot t) + J_4(\Delta\theta) \cdot \cos(4\omega_c \cdot t)]] \dots \right] \cdot F - F}{\left[ \cos(\theta) \cdot [J_0(\Delta\theta) + 2 \cdot [J_2(\Delta\theta) \cdot \cos(2\omega_c \cdot t) + J_4(\Delta\theta) \cdot \cos(4\omega_c \cdot t)]] \dots \right] \cdot F - F - 2 + \left[ 2 \cdot \sin(\theta) \cdot (J(\Delta\theta)_1 \cdot \sin(\omega_c \cdot t) + J(\Delta\theta)_3 \cdot \sin(3\omega_c \cdot t)) \right]}$$

**Only concerned with the first and second harmonics  
thus the above equation becomes**

$$\frac{[\cos(\theta) \cdot (2 \cdot J_2(\Delta\theta) \cdot \cos(2\omega_c \cdot t)) - 2 \cdot \sin(\theta) \cdot J(\Delta\theta)_1 \cdot \sin(\omega_c \cdot t)] \cdot F - F}{[(\cos(\theta) \cdot (2 \cdot J_2(\Delta\theta) \cdot \cos(2\omega_c \cdot t)) - 2 \cdot \sin(\theta) \cdot J(\Delta\theta)_1 \cdot \sin(\omega_c \cdot t)) \cdot F - F - 2]}$$

**Dividing top and bottom by F/2 and multiplying by -1 obtaining from**

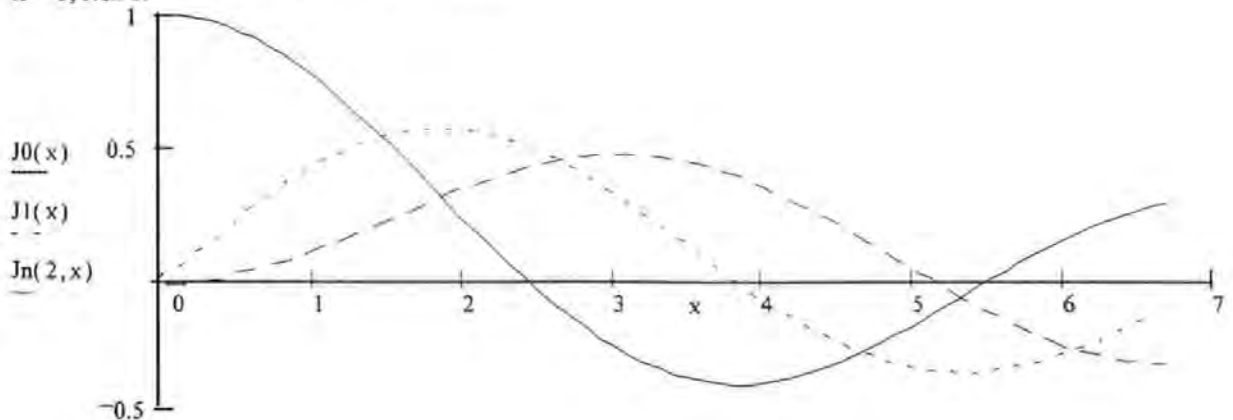
$$\frac{\cos(\theta) \cdot 2 \cdot J_2(\Delta\theta) \cdot \cos(2\omega_c \cdot t) - 2 \cdot \sin(\theta) \cdot J(\Delta\theta)_1 \cdot \sin(\omega_c \cdot t) - 1}{\left[ (\cos(\theta) \cdot 2 \cdot J_2(\Delta\theta) \cdot \cos(2\omega_c \cdot t) - 2 \cdot \sin(\theta) \cdot J(\Delta\theta)_1 \cdot \sin(\omega_c \cdot t)) - 1 - \frac{2}{F} \right]}$$

**To**

$$\frac{\left[ \left( \frac{1}{2} + 2 \cdot \sin(\theta) \cdot J(\Delta\theta)_1 \cdot \sin(\omega_c \cdot t) \right) - \cos(\theta) \cdot 2 \cdot J_2(\Delta\theta) \cdot \cos(2\omega_c \cdot t) \right] \cdot F}{1 - F \cdot \left[ \left( \sin(\theta) \cdot J(\Delta\theta)_1 \cdot \sin(\omega_c \cdot t) + \frac{1}{2} \right) - \cos(\theta) \cdot J_2(\Delta\theta) \cdot \cos(2\omega_c \cdot t) \right]}$$

**The behaviour of the Bessel functions**

$x = 0, 0.1, \dots, 6$



**THUS....**

**We know that  $F$  ,  $J(\Delta\theta)_1$  and  $J(\Delta\theta)_2$  are less than 1**

$$\frac{\left[ \left( \frac{1}{2} + 2 \cdot \sin(\theta) \cdot J(\Delta\theta)_1 \cdot \sin(\omega_c \cdot t) \right) - \cos(\theta) \cdot 2 \cdot J_2(\Delta\theta) \cdot \cos(2 \cdot \omega_c \cdot t) \right] \cdot F}{1 - F \cdot \left[ \left( \sin(\theta) \cdot J(\Delta\theta)_1 \cdot \sin(\omega_c \cdot t) + \frac{1}{2} \right) - \cos(\theta) \cdot J_2(\Delta\theta) \cdot \cos(2 \cdot \omega_c \cdot t) \right]} = f_1(\omega_c \cdot t) \cdot \left( \frac{1}{1 - f_2(\omega_c \cdot t)} \right)$$

**and  $f_2(\omega_c \cdot t) > 1$  , thus using the approximation of  $\frac{1}{1+x} = 1 - x + x^2 - \dots + (-1)^n \cdot x^n$**

**Therefore**

$$\frac{\left[ \left( \frac{1}{2} + 2 \cdot \sin(\theta) \cdot J(\Delta\theta)_1 \cdot \sin(\omega_c \cdot t) \right) - \cos(\theta) \cdot 2 \cdot J_2(\Delta\theta) \cdot \cos(2 \cdot \omega_c \cdot t) \right] \cdot F}{1 - F \cdot \left[ \left( \sin(\theta) \cdot J(\Delta\theta)_1 \cdot \sin(\omega_c \cdot t) + \frac{1}{2} \right) - \cos(\theta) \cdot J_2(\Delta\theta) \cdot \cos(2 \cdot \omega_c \cdot t) \right]}$$

**Becomes .....**

$$1 - F \cdot \left[ \left( \sin(\theta) \cdot J(\Delta\theta)_1 \cdot \sin(\omega_c \cdot t) + \frac{1}{2} \right) - \cos(\theta) \cdot J_2(\Delta\theta) \cdot \cos(2 \cdot \omega_c \cdot t) \right] \dots$$

$$+ F^2 \cdot \left[ \left( \sin(\theta) \cdot J(\Delta\theta)_1 \cdot \sin(\omega_c \cdot t) + \frac{1}{2} \right) - \cos(\theta) \cdot J_2(\Delta\theta) \cdot \cos(2 \cdot \omega_c \cdot t) \right]^2$$

$$F \cdot \left[ \left( \sin(\theta) \cdot J(\Delta\theta)_1 \cdot \sin(\omega_c \cdot t) + \frac{1}{2} \right) - \cos(\theta) \cdot J_2(\Delta\theta) \cdot \cos(2 \cdot \omega_c \cdot t) \right] > \dots$$

$$F^2 \cdot \left[ \left( \sin(\theta) \cdot J(\Delta\theta)_1 \cdot \sin(\omega_c \cdot t) + \frac{1}{2} \right) - \cos(\theta) \cdot J_2(\Delta\theta) \cdot \cos(2 \cdot \omega_c \cdot t) \right]^2$$

**D.C. component :**

$$\frac{1}{2} \cdot F + 2 \cdot (J(\Delta\theta)_1)^2 \cdot F^2 \cdot \cos(\theta)^2 - \frac{1}{4} \cdot F^2 - 2 \cdot (J(\Delta\theta)_1)^2 \cdot F^2$$

$$\text{1st harmonic : } \left[ \left( 2 \cdot F - \frac{3}{2} \cdot F^2 \right) \cdot \sin(\theta) - F^2 \cdot J_2(\Delta\theta) \cdot \sin(2 \cdot \theta) \right] \cdot J(\Delta\theta)_1 \cdot \sin(\omega_c \cdot t)$$

$$\text{2nd harmonic : } \left( \frac{3}{2} \cdot F^2 - 2 \cdot F \right) \cdot J_2(\Delta\theta) \cdot \cos(\theta) \cdot \cos(2 \cdot \omega_c \cdot t)$$

**below is the rest with no 1st or 2nd harmonics components .**

$$2 \cdot (J(\Delta\theta)_1)^2 \cdot F^2 \cdot \cos(\omega_c \cdot t)^2 - 2 \cdot (J(\Delta\theta)_1)^2 \cdot F^2 \cdot \cos(\theta)^2 \cdot \cos(\omega_c \cdot t)^2 - 2 \cdot \cos(\theta)^2 \cdot J_2(\Delta\theta)^2 \cdot \cos(2 \cdot \omega_c \cdot t)^2 \cdot F^2$$

(Ve) Theoretical predictions of response of the system using a Grating Resonator consisting of two approximately 27nm bandwidth and approximately five percent ( sensor 24-7-1 ) reflectivity .

( Note Mathcad +6 program name SIGNAL13.mcd )

$i = 0..300$

Each prediction is taken at increase of point two of a micro - strain .  $\mu\epsilon_i = i \cdot 0.2 \cdot 10^{-6}$

Read data ; the theoretical results from the program based on the T - Matrix formalism of gratings .

$\text{Respon} = \text{READPRN}(\text{dat})$

Maxrange is the max values of strain at / above cut off value of reflectivity ; thus power

$\text{Maxrange} = 100$

start is the min values of strain at / above cut off value of reflectivity ; thus power

start =

Respon is the response from the system with the grating and with the detector having a cut off power level .

$z1 = 0.. \text{Maxrange}$

Changing of the range to accommodate for the cut off of the detector .

$\text{Strain}_{z1} = \left( \text{Respon}^{<1>} \right)_{z1 + \text{start}}$

$\mu\epsilon_{z1} = z1 \cdot 0.$

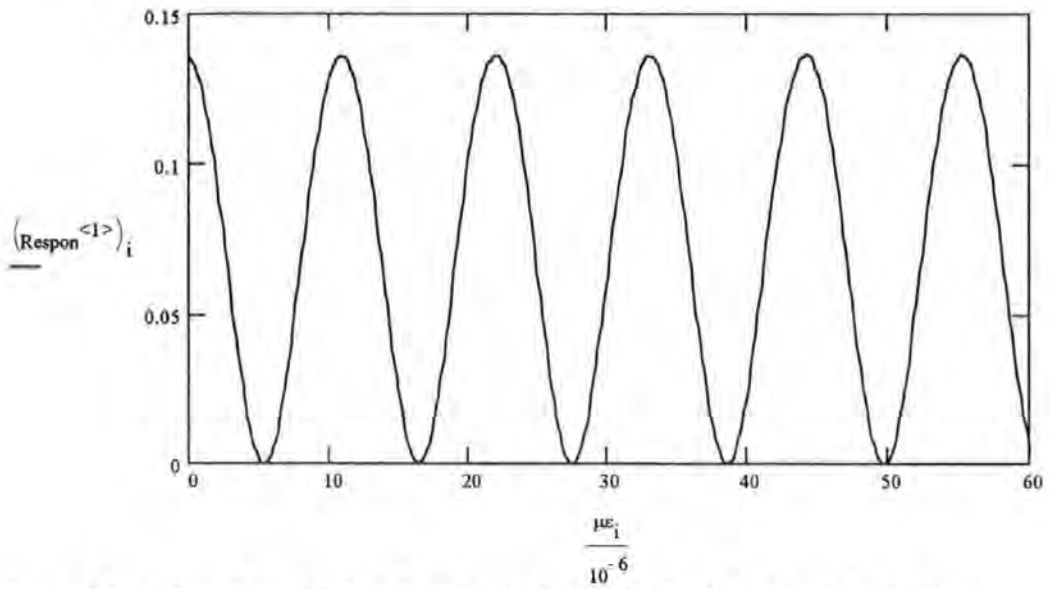
Dstrain is the rate change of reflectivity w.r.t. shift in Phase due to the affect of strain ;

$\frac{d}{d\phi(\mu\epsilon)} R(\mu\epsilon) = \text{Dstrain}$

$$\text{Dstrain}(z1) := \begin{cases} \frac{\text{Strain}_1 - \text{Strain}_0}{\phi\mu\epsilon_1 - \phi\mu\epsilon_0} & \text{if } z1=0 \\ \frac{\text{Strain}_1 - \text{Strain}_0}{\phi\mu\epsilon_1 - \phi\mu\epsilon_0} \\ \frac{\text{Strain}_{z1+1} - \text{Strain}_{z1}}{\phi\mu\epsilon_{z1+1} - \phi\mu\epsilon_{z1}} & \text{if } \text{Maxrange} - 2 \geq z1 \geq 1 \\ \frac{\text{Strain}_{z1+1} - \text{Strain}_{z1}}{\phi\mu\epsilon_{z1+1} - \phi\mu\epsilon_{z1}} \\ \frac{\text{Strain}_{\text{Maxrange}} - \text{Strain}_{\text{Maxrange}-1}}{\phi\mu\epsilon_{\text{Maxrange}} - \phi\mu\epsilon_{\text{Maxrange}-1}} & \text{if } z1=\text{Maxrange} - 1 \\ \frac{\text{Strain}_{\text{Maxrange}} - \text{Strain}_{\text{Maxrange}-1}}{\phi\mu\epsilon_{\text{Maxrange}} - \phi\mu\epsilon_{\text{Maxrange}-1}} \end{cases}$$

$i = 0..99$

The graph below is Reflectivity of the grating at specific wavelength Vs longitudinal strain subjected to the grating .



A single fibre Bragg grating as a reflectivity given by  $R_m$  ,which is 3.7% ;

$$R_m := 0.03$$

This reflectivity defines the coefficient of finesse as :

$$Fin := \frac{4R_m}{(1 - R_m)^2} \quad Fin = 0.159591273807945$$

Assuming the response of the resonator as :  $R(\mu\epsilon) = 1 - \frac{1}{1 + F \cdot \sin^2\left(\frac{\theta(\mu\epsilon)}{2}\right)^2}$

$$\cos(\theta(\mu\epsilon)) = \frac{1 - \left(1 + \frac{2}{Fin}\right) \cdot R(\mu\epsilon)}{1 - R(\mu\epsilon)}$$

Thus the phase can be defined as :  $\theta = \pi - \arccos\left[\frac{1 - \left(1 + \frac{2}{Fin}\right) \cdot R(\mu\epsilon)}{(R(\mu\epsilon) - 1)}\right]$

The problem with this is that inverse cosine function ranges from 0 to  $\pi$  . So to track which quadrant the phase we use the gradient of the original cosine function and monitor the sign of the gradient , using Dstrain(i)

The sine wave generated by the original data file :

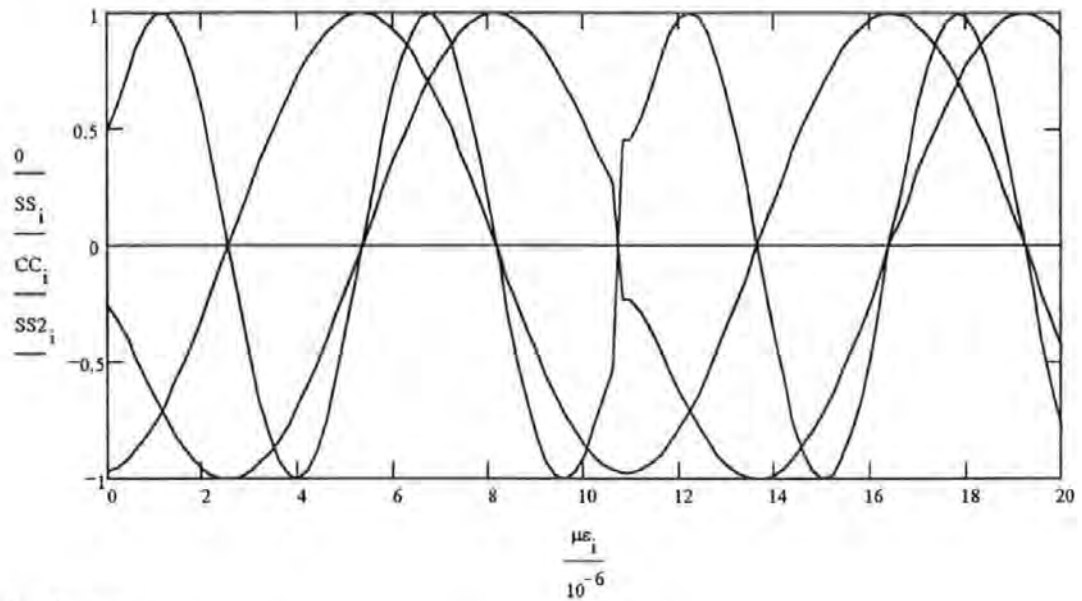
$$SS_1 := \sin\left[\left[\pi - \arccos\left[\frac{1 - \left(1 + \frac{2}{Fin}\right) \cdot (Respon<1>)_i}{(Respon<1>)_i - 1}\right]\right] \cdot Dstrain(i)\right]$$

$$SS_2 := \sin\left[2 \cdot \left[\pi - \arccos\left[\frac{1 - \left(1 + \frac{2}{Fin}\right) \cdot (Respon<1>)_i}{(Respon<1>)_i - 1}\right]\right] \cdot Dstrain(i)\right]$$

The cosine wave generated by the original data file :



$$CC_i = \cos \left[ \pi - \arccos \left[ \frac{\left[ 1 - \left( 1 + \frac{2}{Fin} \right) \cdot (Respon^{<1>})_i \right]}{\left[ (Respon^{<1>})_i - 1 \right]} \right] \right]$$



$z=0$ ..Maxrange -

Data used to calculate the change in wavelength due to strain

The effective refractive index :  $n_{eff} \approx 1.4$

Number\_of\_Periods  $\approx 100$

The chirp factor change period along the grating :  $F \approx 0.013 \cdot 10^{-9}$

The basic half period of the grating :  $\Lambda_0 \approx 510 \cdot 10^{-9}$

The spacing between the gratings :  $L_{spe} \approx 0.0$

$$\text{Total length of the grating : } L_{grt} \approx \left[ \sum_{z=0}^{\text{Number\_of\_Periods}} \Lambda_0 + F \cdot z \right]$$

$$L_{spe} + L_{grt} = 0.0605170165$$

The change in length of the resonator due to strain :

$$\Delta L_{total_{z1}} \approx 2 \cdot \left[ \left( \mu \varepsilon_{z1} \cdot 10^{-6} + 0 \right) \cdot (L_{spe} + 2 \cdot L_{grt}) \right]$$

The change in phase of the resonator due to strain :

Where  $c$  is the velocity of light

$$c \approx 3 \cdot 10^8$$

$$\lambda_{laser} \approx 1535 \cdot 10^{-9}$$

$$\phi \mu \varepsilon$$

Where  $\Delta \nu$  is the modulation of the laser frequency :  $\Delta \nu \approx 5 \cdot 10^3$

$$\phi_{\mu\epsilon_{z1}} = \frac{2 \cdot \pi \cdot \left[ \left( \mu\epsilon_{z1} \cdot 10^{-6} \right) \cdot (L_{spe} + 2 \cdot L_{grt}) \right] \cdot n_{eff}}{\lambda_{laser}}$$

But we also  $\frac{\Delta\phi(\mu\epsilon)}{\Delta\nu}$  which is ;

$$\frac{\Delta\phi(\mu\epsilon)}{\Delta\nu} = \frac{2 \cdot \pi \cdot \left[ \left( \mu\epsilon_{z1} \cdot 10^{-6} + 0 \right) \cdot (L_{spe} + 2 \cdot L_{grt}) \right] \cdot n_{eff}}{c}$$

**The Section below is giving the specification of the D.F.B. laser and the associated drive system .**

sine wave modulation is 1Volt .

Modulation coeff of the laser current 40 mA / V .

Oscillator pk to pk Voltage is 30 mV's which can be varied

$$\Delta i = 4090 \cdot 10^{-3} \Delta i = 3.6 \text{ mA}$$

D.F.B. Laser + Drive Unit

The effective current - to - frequency conversion factor for the D.F.B. laser

$$\delta\nu_{\delta i} = 3.5 \cdot 10^9 \text{ Hz / mA}$$

The effective current - to - wavelength conversion factor

for the D.F.B. laser depending on the drive current

which is  $0.0001865 \times (\text{drivecurrent})$

Drive = 6

$$1.3 \cdot 10^{-4} \cdot \text{Drive} + 0.01 = 0.01884$$

$$\delta\lambda_{\delta i} = 0.019 \cdot 10^{-9} \text{ m / mA}$$

$$0.015 \cdot 10^{-9}$$

$$\delta\lambda_{\delta i} \Delta i = 6.84 \cdot 10^{-11}$$

**Defining Variables used to calculate the resultant current from the photo - detector .**

$\epsilon$  is the responsivity of the photodetector

$\alpha$  is system optical losses

Photodetector  $I_0$  is optical intensity

$$\epsilon = 700 \cdot 10^{-3} \text{ mA / Watt}$$

This section is dealing with the response of a photo-detector when the light source is modulated ; in this case there is phase modulation which in turn modulates the intensity of the reflected power from the sensor ( grating resonator ) .

Data of system with typical values for a given system .

$$c = 3 \cdot 10^8, n_{eff} = 1.5, \Lambda_0 = 500 \cdot 10^{-9}$$

Laser power :

$$I_o = 400 \cdot 10^{-6} \text{ watts}$$

Output amperage of a photo - detector  $I_o \cdot \epsilon = 2.8 \cdot 10^{-4}$

The average power reflected from the device :

$$\beta T_z = \delta v_{\Delta i} \frac{4 \pi \cdot \left[ \left( \mu \epsilon_2 \cdot 10^{-6} + 1 \right) \cdot (L_{spe} + 2 \cdot L_{grt}) \right] \cdot n_{eff}}{c}$$

These expression are derived later

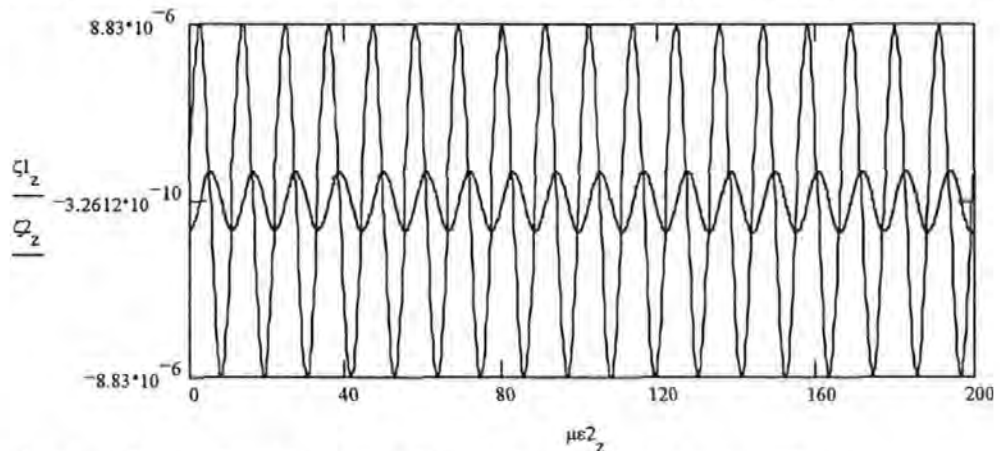
### Harmonics 1st :

$$\zeta 1_z = I_o \cdot \left[ \left[ \left( 2 \cdot Fin - \frac{3}{2} \cdot Fin^2 \right) \cdot SS_z - Fin^2 \cdot Jn(2, \beta T_z) \cdot SS2_z \right] \cdot Jn(1, \beta T_z) \right. \\ \left. \left[ \left( 2 \cdot Fin - \frac{3}{2} \cdot Fin^2 \right) \cdot SS_z - Fin^2 \cdot Jn(2, \beta T_z) \cdot SS2_z \right] \cdot Jn(1, \beta T_z) \right] \cdot \epsilon.$$

### Harmonics 2nd :

$$\zeta 2_z = I_o \cdot \left[ \left( \frac{3}{2} \cdot Fin^2 - 2 \cdot Fin \right) \cdot Jn(2, \beta T_z) \cdot CC \right. \\ \left. \left( \frac{3}{2} \cdot Fin^2 - 2 \cdot Fin \right) \cdot Jn(2, \beta T_z) \cdot CC_z \right] \cdot \epsilon.$$

The current produced at the Detectors when the grating is subjected to longitudinal strain .



There is also an AC coupled Operational Amplifier with a gain of  $\sim 200$  .

Input resistance 1000 ohms .

feedback resistance 200K +10K.

$G := 20$

Operational Amplifier

$R_I = 100$

$R_g = 900 \cdot 10^3$

Arrangement ( photodetector current ) X ( input resistance ) is the input Voltage to the amplifier .

1st Harmonic Voltage input to Amp

$$V1_z = \zeta 1_z \cdot R_I$$

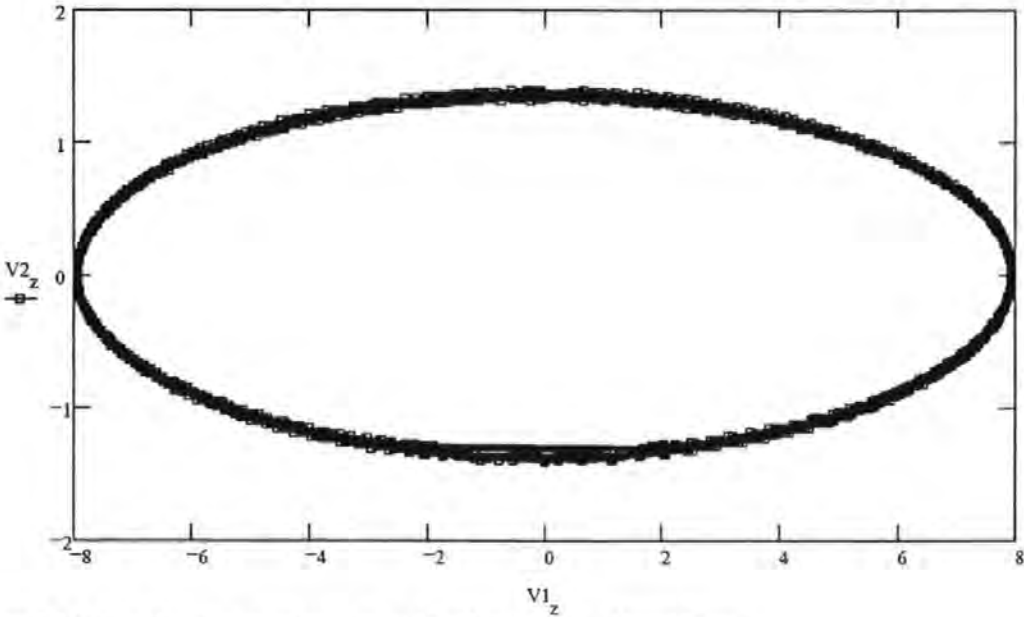
$$V1_z = \zeta 1_z \cdot R_g$$

## 2nd Harmonic Voltage input to Amp

$$V_{2_z} = \zeta_{2_z} \cdot R_I \quad V_{2_z} = \zeta_{2_z} \cdot R_g$$

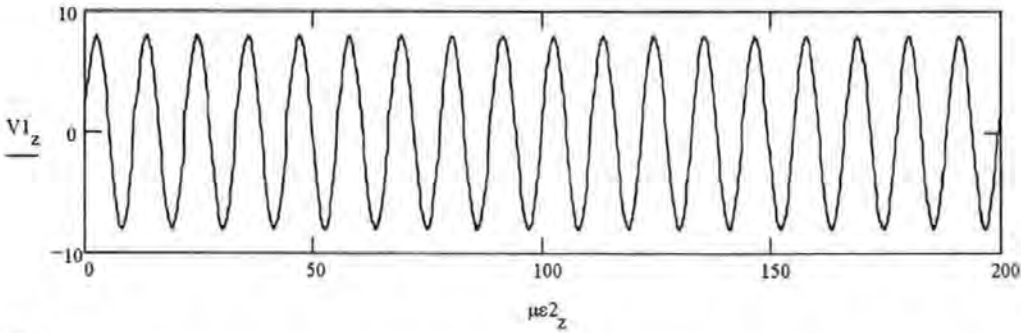
This graph is quadrature diagram of the output voltages generated by the Grating subjected to longitudinal strain, the photodetector and the operational amplifier :

$$\varepsilon \cdot I_{in} \cdot \alpha \cdot R(\lambda(t, \mu\varepsilon)) \rightarrow \frac{7}{10} \cdot I_{in} \cdot \alpha \cdot R(\lambda(t, \mu\varepsilon)) \text{ and thus } i_{out}(\mu\varepsilon) \rightarrow i_{out}(\mu\varepsilon) \text{ .}$$

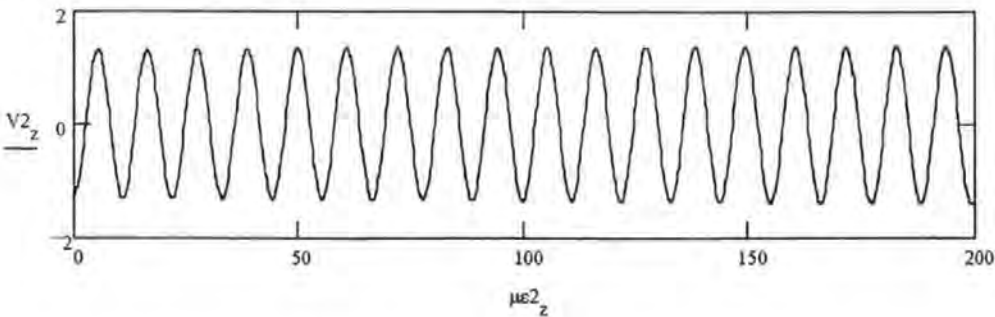


So V2 and V1 are the input voltages to the Lock - In - Amplifiers

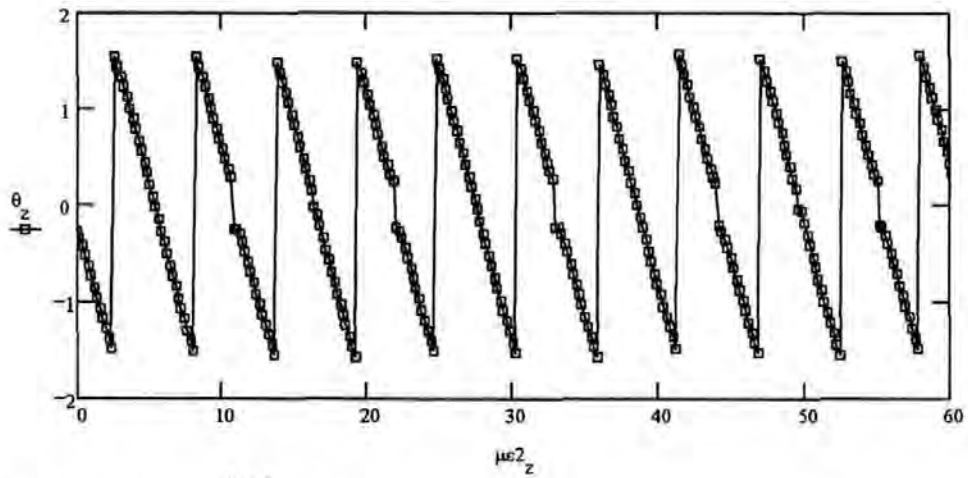
L.I.A (1)



L.I.A. (2)



$$\theta_z = \text{atan} \left( \frac{V1_z}{V2_z \frac{\max(V1)}{\max(V2)}} \right)$$



$$V_o = G_1 \cdot G_2 \cdot V_s \cdot \cos(\phi) = V_f \left( \frac{V_s}{S} \right) \cdot \cos(\phi)$$

But this is synchronous detection .Thus

$$V_o = 5 \cdot G_1 \cdot G_2 \cdot V$$

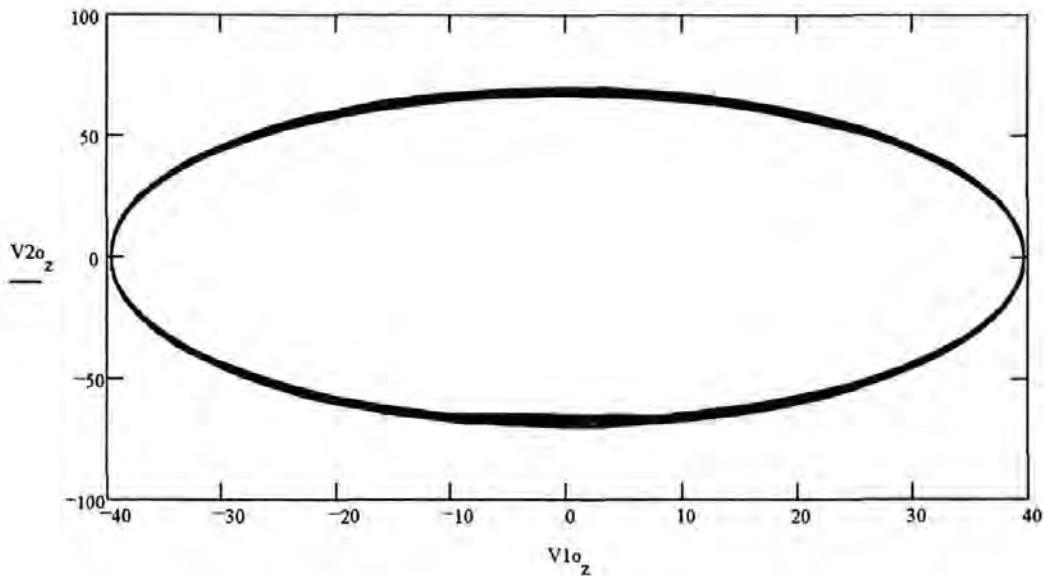
L . I . A.

$V_s$  ; the rms value of the input synchronous

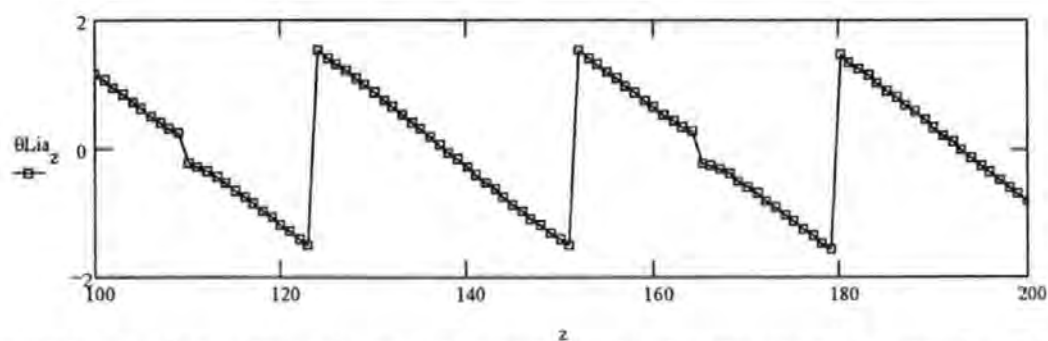
$S$  ; sensitivity selected by the DIP switches

$V_f$  ; full scale output voltage which is 5 Volts

$$S1 := , S2 := 10^{-1}, V_f := , V1_{o_z} = V_f \frac{V1_z}{S1}, V2_{o_z} = V_f \frac{V2_z}{S2}$$



$$\theta Lia_z = \text{atan} \left( \frac{V1o_z}{V2o_z \cdot \frac{\max(V1o)}{\max(V2o)}} \right)$$



Thus using a small program acts on the in coming data to produce a " linear line " by either adding  $\pi$  or subtracting  $\pi$  according the phase being either in retardation or progression .

$z = 0..1 \quad \theta Lia\_Process_z := \theta Lia$

$z = 13..4 \quad \theta Lia\_Process_z := \theta Lia_z - \pi$

$z = 41..6 \quad \theta Lia\_Process_z := \theta Lia_z - 2 \cdot \pi$

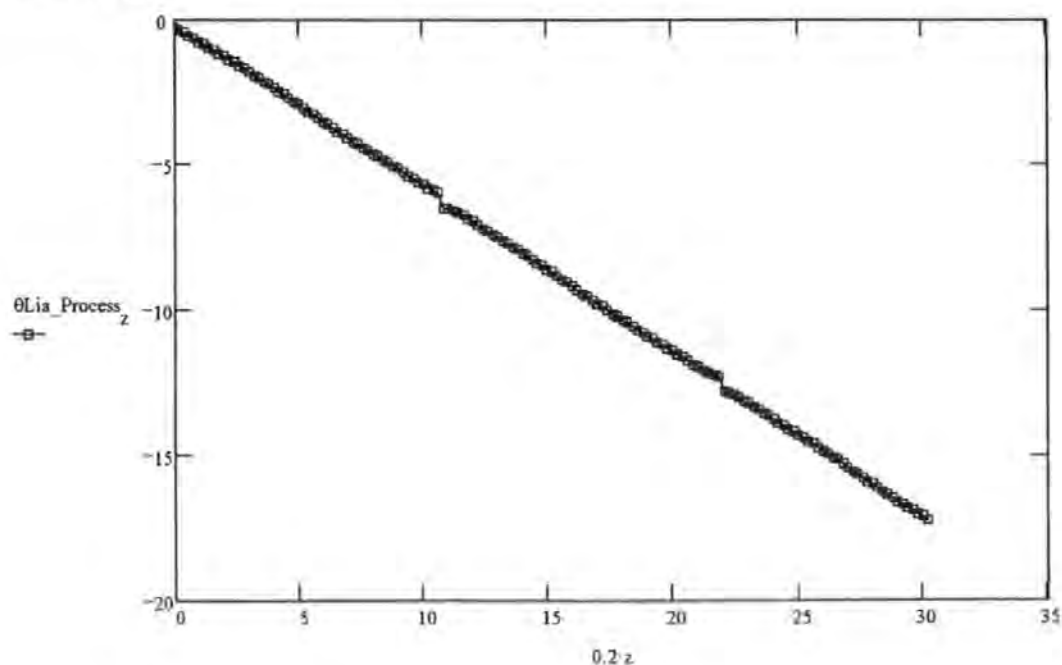
$z = 69..9 \quad \theta Lia\_Process_z := \theta Lia_z - 3 \cdot \pi$

$z = 97..12 \quad \theta Lia\_Process_z := \theta Lia_z - 4 \cdot \pi$

$z = 124..15 \quad \theta Lia\_Process_z := \theta Lia_z - 5 \cdot \pi$

$z = 0..15$

The graph below shows the quasi - linear relationship which can be obtained by the system under investigation .



(Vf) Theoretical predictions of response of the system using a Grating Resonator consisting of two approximately 27nm bandwidth and approximately ten percent ( sensor 24-7-2 ) reflectivity .

( Note Mathcad +6 program name SIGNAL12.mcd )

$i := 0..300$

Each prediction is taken at increase of point two of a micro - strain .  $\mu\epsilon_i := i \cdot 0.2 \cdot 10^{-6}$

Read data ; the theoretical results from the program based on the T - Matrix formalism of gratings .

Respon = READPRN(dat)

**Maxrange** is the max values of strain at / above cut off value of reflectivity ; thus power

Maxrange = 100

**start** is the min values of strain at / above cut off value of reflectivity ; thus power

start =

**Respon** is the response from the system with the grating and with the detector having a cut off power level .

$z1 := 0..Maxrange$

Changing of the range to accommodate for the cut off of the detector .

$Strain_{z1} := (Respon^{<1>})_{z1+start}$

$\mu\epsilon_{z1} := z1 \cdot 0.$

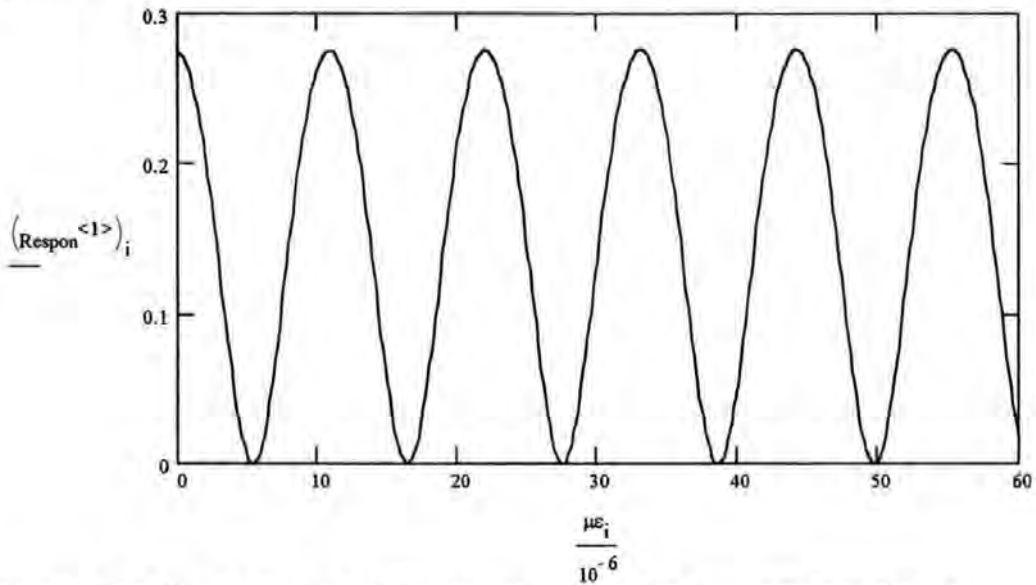
**Dstrain** is the rate change of reflectivity w.r.t. shift in Phase due to the affect of strain ;

$\frac{d}{d\phi(\mu\epsilon)} R(\mu\epsilon) = Dstrain$

$$Dstrain(z1) = \begin{cases} \frac{\frac{Strain_1 - Strain_0}{\phi\mu\epsilon_1 - \phi\mu\epsilon_0}}{\frac{Strain_1 - Strain_0}{\phi\mu\epsilon_1 - \phi\mu\epsilon_0}} & \text{if } z1=0 \\ \frac{\frac{Strain_{z1+1} - Strain_{z1}}{\phi\mu\epsilon_{z1+1} - \phi\mu\epsilon_{z1}}}{\frac{Strain_{z1+1} - Strain_{z1}}{\phi\mu\epsilon_{z1+1} - \phi\mu\epsilon_{z1}}} & \text{if } Maxrange - 2 \geq z1 \geq 1 \\ \frac{\frac{Strain_{Maxrange} - Strain_{Maxrange-1}}{\phi\mu\epsilon_{Maxrange} - \phi\mu\epsilon_{Maxrange-1}}}{\frac{Strain_{Maxrange} - Strain_{Maxrange-1}}{\phi\mu\epsilon_{Maxrange} - \phi\mu\epsilon_{Maxrange-1}}} & \text{if } z1=Maxrange - 1 \end{cases}$$

$i = 0..99$

The graph below is Reflectivity of the grating at specific wavelength Vs longitudinal strain subjected to the grating .



A single fibre Bragg grating as a reflectivity given by  $R_m$  ,which is 10% ;

$$R_m = 0.$$

This reflectivity defines the coefficient of finesse as :

$$Fin := \frac{4 \cdot R_m}{(1 - R_m)^2} \quad Fin = 0.493827160493827$$

Assuming the response of the resonator as :  $R(\mu\epsilon) = 1 - \frac{1}{1 + F \cdot \sin^2\left(\frac{\theta(\mu\epsilon)}{2}\right)^2}$

$$\cos(\theta(\mu\epsilon)) = \frac{1 - \left(1 + \frac{2}{Fin}\right) \cdot R(\mu\epsilon)}{1 - R(\mu\epsilon)}$$

Thus the phase can be defined as :  $\theta = \pi - \arccos\left[\frac{1 - \left(1 + \frac{2}{Fin}\right) \cdot R(\mu\epsilon)}{(R(\mu\epsilon) - 1)}\right]$

The problem with this is that inverse cosine function ranges from 0 to  $\pi$  . So to track which quadrant the phase we use the gradient of the original cosine function and monitor the sign of the gradient , using Dstrain(i)

The sine wave generated by the original data file :

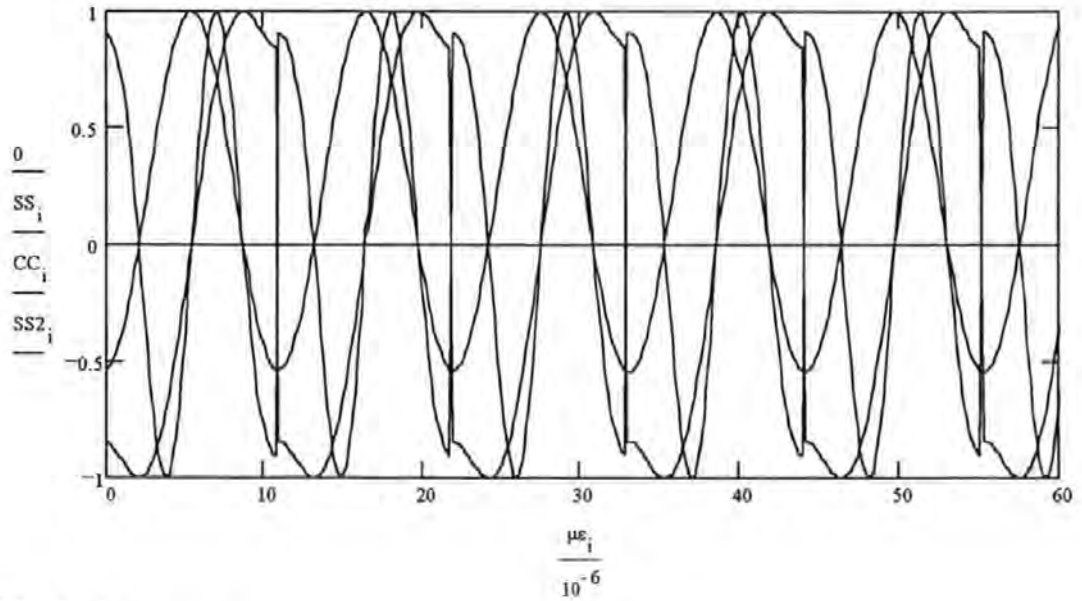
$$SS_i := \sin\left[\left[\pi - \arccos\left[\frac{1 - \left(1 + \frac{2}{Fin}\right) \cdot (Respon^{<1>})_i}{[(Respon^{<1>})_i - 1]}\right]\right] \cdot Dstrain(i)\right]$$



$$SS2_i = \sin \left[ 2 \cdot \left[ \pi - \arccos \left[ \frac{1 - \left( 1 + \frac{2}{Fin} \right) \cdot \langle Respon^{<1>}_i}{\langle Respon^{<1>}_i - 1} \right] \right] \right] \cdot Dstrain(i)$$

**The cosine wave generated by the original data file :**

$$CC_i = \cos \left[ \pi - \arccos \left[ \frac{1 - \left( 1 + \frac{2}{Fin} \right) \cdot \langle Respon^{<1>}_i}{\langle Respon^{<1>}_i - 1} \right] \right]$$



$z \equiv 0.. \text{Maxrange} -$

Data used to calculate the change in wavelength due to strain

The effective refractive index :  $n_{eff} \equiv 1.4$

Number\_of\_Periods  $\equiv 100$

The chirp factor change period along the grating .  $F \equiv 0.013 \cdot 10^{-9}$

The basic half period of the grating :  $\Lambda_0 \equiv 510 \cdot 10^{-9}$

The spacing between the gratings :  $L_{spe} \equiv 0.0$

Total length of the grating :  $L_{grt} \equiv \left[ \sum_{z=0}^{\text{Number\_of\_Periods}} \Lambda_0 + F \cdot z \right]$

$$L_{spe} + L_{grt} = 0.0605170165$$

The change in length of the resonator due to strain :

$$\Delta L_{total_{z1}} \equiv 2 \cdot \left[ (\mu \epsilon_{z1} \cdot 10^{-6} + 0) \cdot (L_{spe} + 2 \cdot L_{grt}) \right]$$

The change in phase of the resonator due to strain : Where  $c$  is the velocity of light

$$c \equiv 3 \cdot 10^8$$

$$\lambda_{laser} \equiv 1535 \cdot 10^{-9}$$

$$\phi \mu \epsilon$$

Where  $\Delta\nu$  is the modulation of the laser frequency :

$$\Delta\nu \approx 5 \cdot 10^3$$

$$\phi_{\mu\epsilon_{z1}} = \frac{2 \cdot \pi \cdot \left[ \left( \mu\epsilon_{z1} \cdot 10^{-6} \right) \cdot (L_{spe} + 2 \cdot L_{grt}) \right] \cdot n_{eff}}{\lambda_{laser}}$$

$$\text{But we also } \frac{\Delta\phi(\mu\epsilon)}{\Delta\nu} \text{ which is : } \frac{\Delta\phi(\mu\epsilon)}{\Delta\nu} = \frac{2 \cdot \pi \cdot \left[ \left( \mu\epsilon_{z1} \cdot 10^{-6} + 0 \right) \cdot (L_{spe} + 2 \cdot L_{grt}) \right] \cdot n_{eff}}{c}$$

**The Section below is giving the specification of the D.F.B. laser and the associated drive system .**

sine wave modulation is 1 Volt ,

Modulation coeff of the laser current 40 mA / V .

Oscillator pk to pk Voltage is 30 mV's which can be varied

$$\Delta i \approx 4090 \cdot 10^{-3}$$

$$\Delta i = 3.6 \text{ mA}$$

D.F.B. Laser + Drive Unit

The effective current - to - frequency conversion factor  
for the D.F.B. laser

$$\delta\nu_{\delta i} \approx 3.5 \cdot 10^9 \text{ Hz / mA}$$

The effective current - to - wavelength conversion factor  
for the D.F.B. laser depending on the drive current  
which is  $0.0001865 \times (\text{drive current})$

$$\text{Drive} = 6$$

$$1.3 \cdot 10^{-4} \cdot \text{Drive} + 0.01 = 0.01884$$

$$\delta\lambda_{\delta i} \approx 0.019 \cdot 10^{-9} \text{ m / mA}$$

$$0.015 \cdot 10^{-9}$$

$$\delta\lambda_{\delta i} \cdot \Delta i = 6.84 \cdot 10^{-11}$$

**Defining Variables used to calculate the resultant current from the photo - detector .**

$\epsilon$  is the responsivity of the photodetector

$\alpha$  is system optical losses

Photodetector  $I_0$  is optical intensity

$$\epsilon = 700 \cdot 10^{-3} \text{ mA / Watt}$$

This section is dealing with the response of a photo-detector when the light source is modulated ; in this case there is phase modulation which in turn modulates the intensity of the reflected power from the sensor ( grating resonator ) .

Data of system with typical values for a given system .

$$c = 3 \cdot 10^8$$

$$n_{eff} = 1.4$$

$$\Lambda_0 = 500 \cdot 10^{-9}$$

$$\text{Laser power : } I_o = 400 \cdot 10^{-6} \text{ watts}$$

Output amperage of a photo - detector  $I_o \cdot \varepsilon = 2.8 \cdot 10^{-4}$

The average power reflected from the device :

$$\beta T_z := \delta v_{\Delta i} \cdot \frac{4 \cdot \pi \cdot \left[ \left( \mu \varepsilon 2_z \cdot 10^{-6} + 1 \right) \cdot \left( L_{spe} + 2 L_{grt} \right) \right] \cdot n_{eff}}{c}$$

These expression are derived later

**Harmonics 1st :**

$$\left[ \left( 2 \cdot Fin - \frac{3}{2} \cdot Fin^2 \right) \cdot SS_z - Fin^2 \cdot J_n(2, \beta T_z) \cdot SS_z^2 \right] \cdot J_n(1, \beta T_z)$$

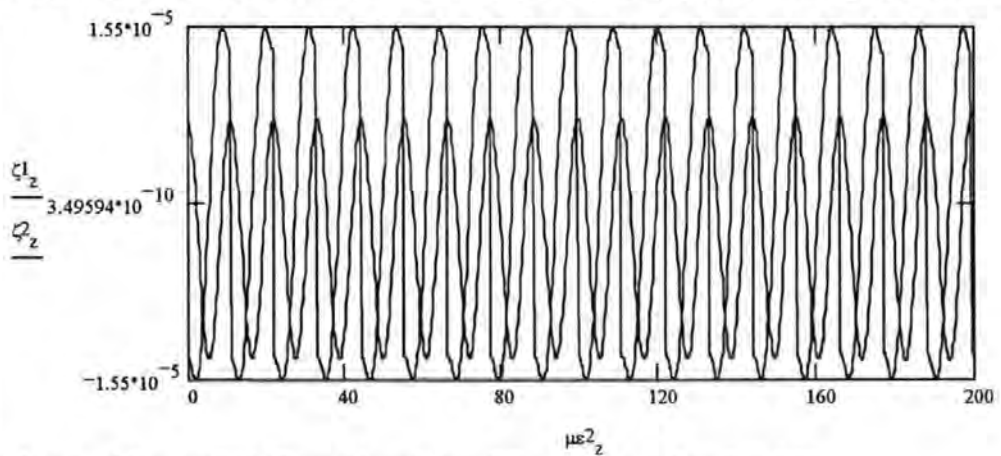
$$\zeta 1_z := I_o \cdot \left[ \left[ \left( 2 \cdot Fin - \frac{3}{2} \cdot Fin^2 \right) \cdot SS_z - Fin^2 \cdot J_n(2, \beta T_z) \cdot SS_z^2 \right] \cdot J_n(1, \beta T_z) \right] \cdot \varepsilon$$

**Harmonics 2nd :**

$$\left( \frac{3}{2} \cdot Fin^2 - 2 \cdot Fin \right) \cdot J_n(2, \beta T_z) \cdot CC$$

$$\zeta 2_z := I_o \cdot \left[ \left( \frac{3}{2} \cdot Fin^2 - 2 \cdot Fin \right) \cdot J_n(2, \beta T_z) \cdot CC_z \right] \cdot \varepsilon$$

The current produced at the Detectors when the grating is subjected to longitudinal strain .



There is also an AC coupled Operational Amplifier with a gain of  $\sim 200$  ,

input resistance 1000 ohms .

feedback resistance 200K +10K.

$G = 20$

Operational Amplifier

$$R_I := 100$$

$$R_g := 900 \cdot 10^3$$

Arrangement ( photodetector current ) X ( input resistance ) is the input Voltage to the amplifier .

**1st Harmonic Voltage input to Amp**

$$V1_z = \zeta 1_z \cdot R_I$$

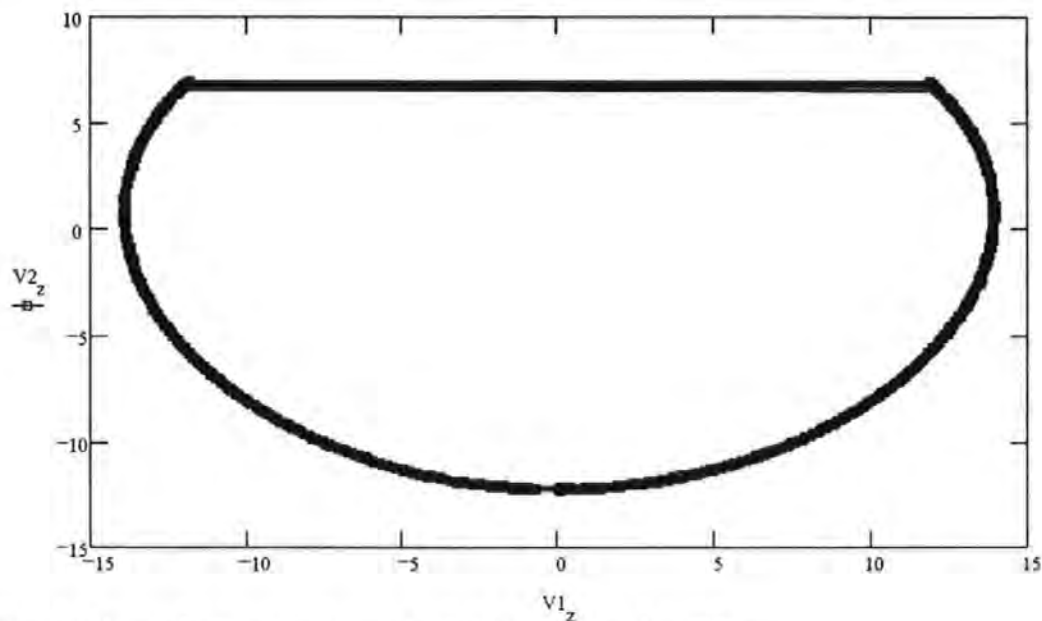
$$V1_z = \zeta 1_z \cdot R_g$$

## 2nd Harmonic Voltage input to Amp

$$V_2 = \zeta_2 \cdot R_I \quad V_2 = \zeta_2 \cdot R_g$$

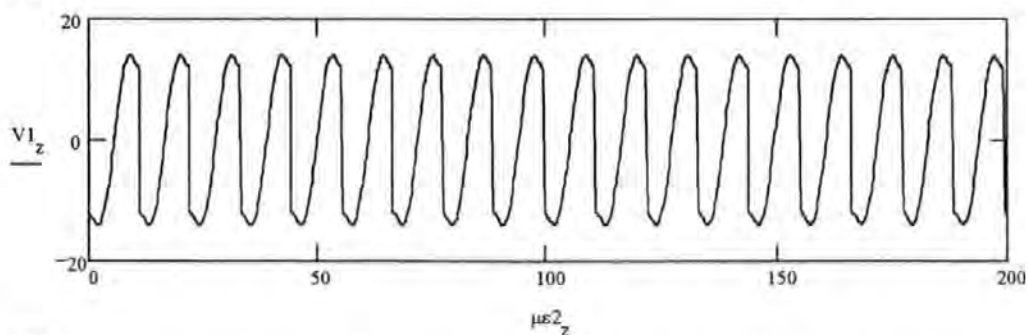
This graph is quadrature diagram of the output voltages generated by the Grating subjected to longitudinal strain, the photodetector and the operational amplifier :

$$\varepsilon \cdot I_{in} \cdot \alpha \cdot R(\lambda(t, \mu\varepsilon)) \rightarrow \frac{7}{10} \cdot I_{in} \cdot \alpha \cdot R(\lambda(t, \mu\varepsilon))_0 \text{ and thus } i_{out}(\mu\varepsilon) \rightarrow i_{out}(\mu\varepsilon)_0$$

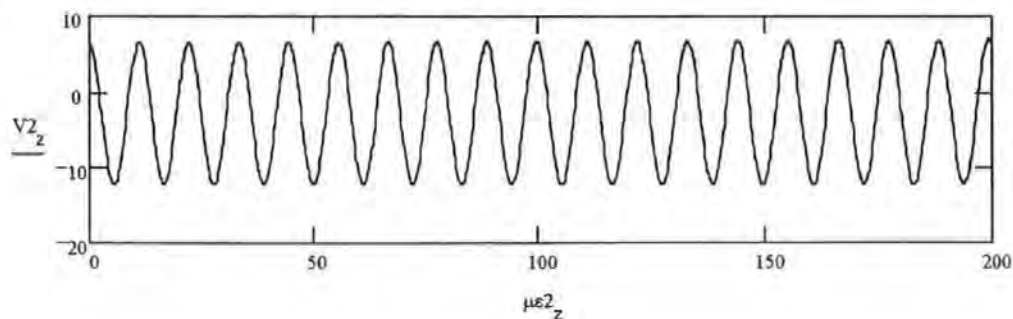


So V2 and V1 are the input voltages to the Lock - In - Amplifiers

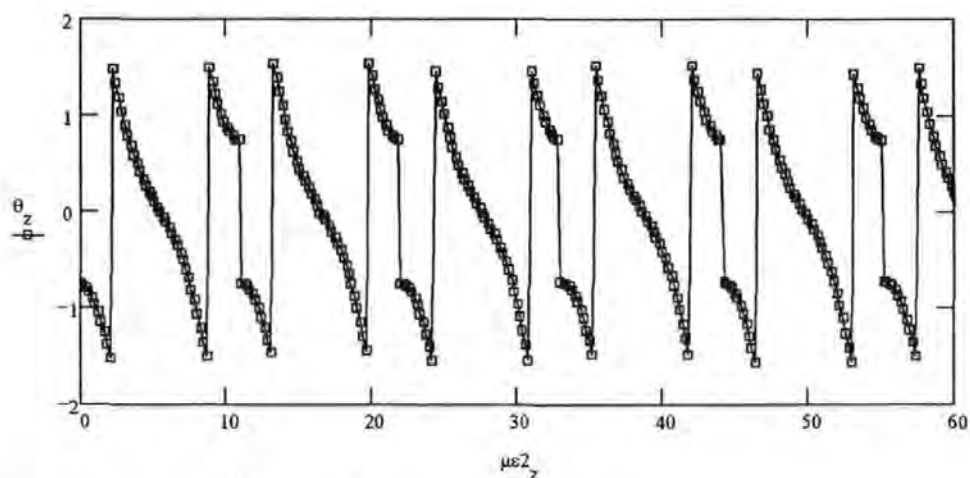
L.I.A. (1)



L.I.A. (2)



$$\theta_z := \text{atan} \left( \frac{V1_z}{V2_z \cdot \frac{\max(V1)}{\max(V2)}} \right)$$



$$V_o = G_1 \cdot G_2 \cdot V_s \cos(\phi) = V_f \left( \frac{V_s}{S} \right) \cdot \cos(\phi)$$

But this is synchronous detection .Thus

$$V_o = 5 \cdot G_1 \cdot G_2 \cdot V$$

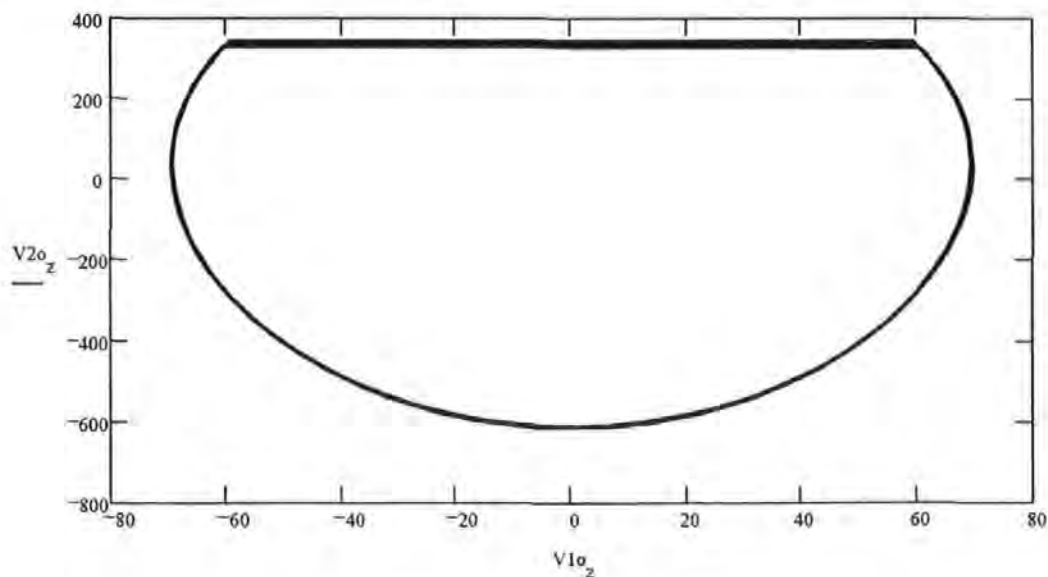
L . I . A.

$V_s$  ; the rms value of the input synchronous

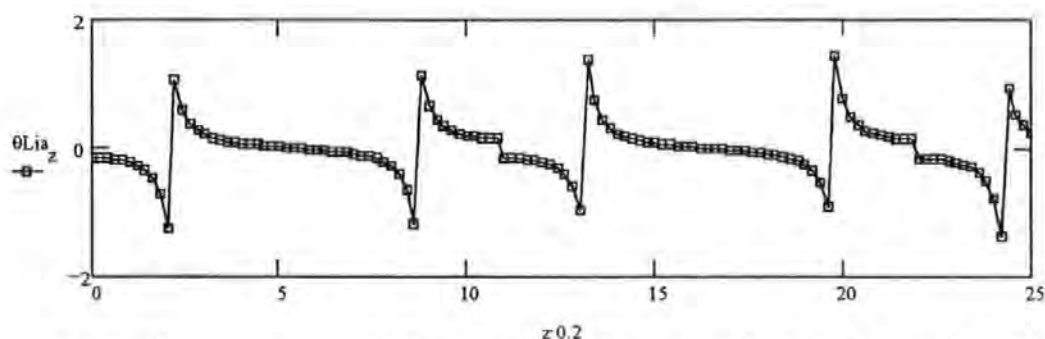
$S$  : sensitivity selected by the DIP switches

$V_f$  ; full scale output voltage which is 5 Volts

$$S1 := , S2 := 10^{-1} , V_f := , V1o_z := V_f \frac{V1_z}{S1} , V2o_z := V_f \frac{V2_z}{S2}$$



$$\theta_{Lia_z} = \text{atan} \left( \frac{V1_{o_z}}{V2_{o_z} \cdot \frac{\max(V1_o)}{\max(V2_o)} \cdot 6} \right)$$



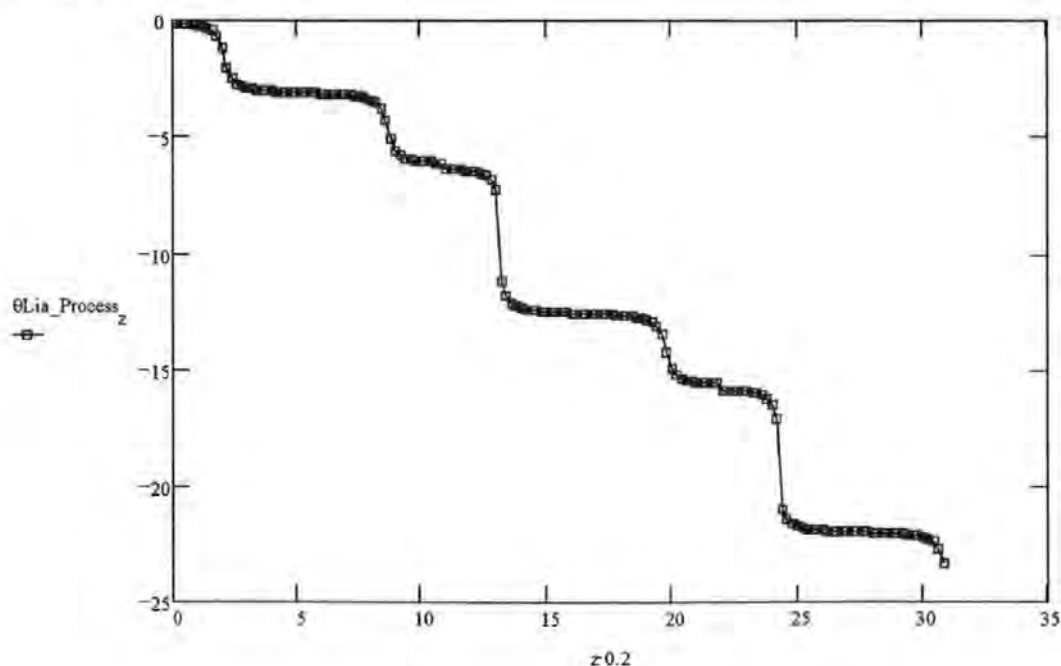
Thus using a small program acts on the in coming data to produce a "linear line" by either adding  $\pi$  or subtracting  $\pi$  according the phase being either in retardation or progression.

```

z = 0..1  theta_Lia_Process_z = theta_Lia
z = 11..4  theta_Lia_Process_z = theta_Lia - pi
z = 44..5  theta_Lia_Process_z = theta_Lia - 2*pi
z = 55..6  theta_Lia_Process_z = theta_Lia - 2*pi
z = 66..9  theta_Lia_Process_z = theta_Lia - 4*pi
z = 99..10  theta_Lia_Process_z = theta_Lia - 5*pi
z = 110..12  theta_Lia_Process_z = theta_Lia - 5*pi
z = 122..15  theta_Lia_Process_z = theta_Lia - 7*pi
z = 0..15

```

The graph below shows the quasi-linear relationship which can be obtained by the system under investigation.



**(Vg) A theoretical prediction of the system using wavelength modulation in conjunction with a fibre Bragg grating which as a sinusoidal behaviour in it's spectral response and is subjected to longitudinal strain .**

( Note Mathcad +6 program name TESTSG.mcd )

Assuming that the D.F.B. laser power illuminating the grating is :

$$I_0 = 400 \cdot 10^{-7} \text{ watts}$$

$$\text{Wavelength of D.F.B. Laser } \lambda_{\text{laser}} := 1555.5 \cdot 10^{-9}$$

$$\text{We know that for a grating under longitudinal strain : } \frac{\delta \lambda}{\lambda} = (1 - p_e) \cdot \frac{\delta l}{l}$$

$$\text{Where } p_e \text{ is given by } \frac{n^2}{2 \cdot [p_{12} - \nu \cdot (p_{11} + p_{12})]}$$

$n$  is the index of refraction of the core

$p_{11}$  and  $p_{12}$  strain - optic coefficients

$\nu$  is Poisson's ratio

$$n = 1.46, p_{11} = 0.11, p_{12} = 0.25, \nu = 0.1$$

$$p_e = \frac{n^2}{2} \cdot [p_{12} - \nu \cdot (p_{11} + p_{12})] \quad p_e = 0.203$$

$$\text{At } 1555.5 \text{ nm the expected sensitivity is : } \delta \lambda_{\delta \varepsilon} = (1 - p_e) \cdot \frac{1555.5 \cdot 10^{-9}}{10^6}$$

$$\delta \lambda_{\delta \varepsilon} = 1.2403092 \cdot 10^{-12} \text{ m} \cdot \mu \varepsilon^{-1}$$

If only consider the region sinusoidal behave , thus :  $\varepsilon = 0..2489$

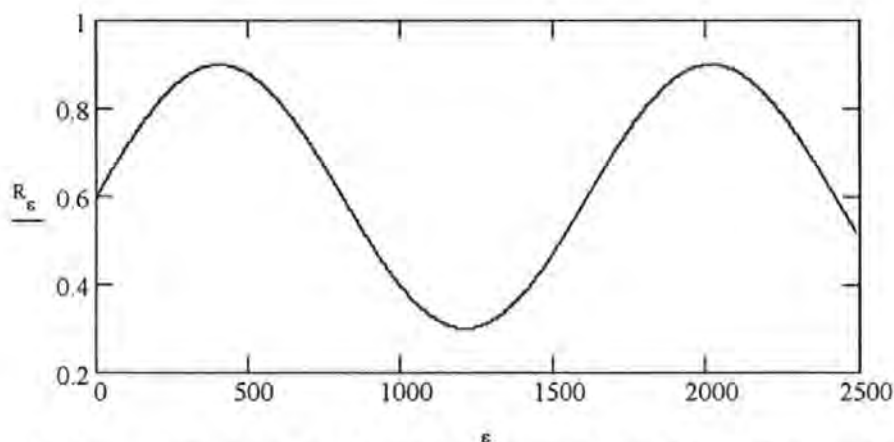
$$\text{The period in the sinusoidal region : } T_\lambda = 2 \cdot 10^{-7} \text{ m}$$

Assuming this Bragg grating has a response of a raised cosine function , being sinusoidal around the 60% reflection

$$K = 0.6$$

$$\text{The Reflectivity to longitudinal strain can be : } R_\varepsilon = \frac{K}{2} \cdot \left( 1 + \cos \left( 2 \cdot \pi \cdot \frac{\lambda_{\text{laser}} + \delta \lambda_{\delta \varepsilon} \cdot \varepsilon}{T_\lambda} \right) \right) + 0.3$$

The graph below shows the behaviour of such a cosine function with longitudinal strain having a dependence upon  $\delta \lambda_{\delta \varepsilon}$



**The Section below is giving the specification of the D.F.B. laser and the associated drive system .**

sine wave modulation is Volt .

Modulation coeff of the laser current 40 mA / V .

Oscillator pk to pk Voltage is 30 mV's which can be varied

$$\Delta i = 40 \cdot 100 \cdot 10^{-6}$$

$$\Delta i = 4 \text{ mA}$$

D.F.B. Laser + Drive Unit

The effective current - to - frequency conversion factor for the D.F.B. laser

$$\delta \nu_{\delta i} = 3.5 \cdot 10^5 \text{ Hz / mA}$$

The effective current - to - wavelength conversion factor for the D.F.B. laser depending on the drive current which is  $0.0001865 \times (\text{drive current})$

$$\text{Drive} = 100$$

$$1.3 \cdot 10^{-4} \cdot \text{Drive} + 0.01 = 0.023$$

$$\delta \lambda_{\delta i} = 0.023 \cdot 10^{-3} \text{ m / mA}$$

$$0.015 \cdot 10^{-3}$$

$$\delta \lambda_{\delta i} \cdot \Delta i = 9.2 \cdot 10^{-11}$$

**Note** that is conversion factor is not constant

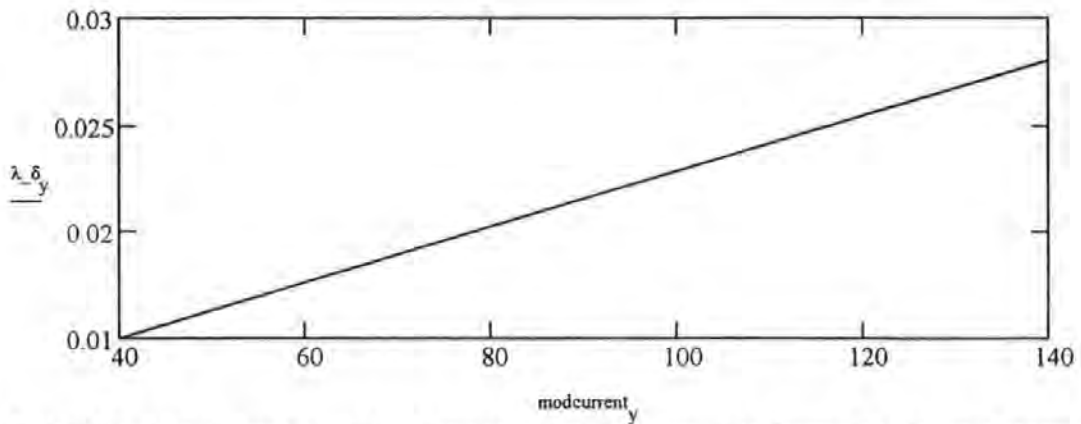
$$y = 0..1$$

$$\text{modcurrent}_y = 40 + 100 \cdot y$$

$$\lambda_{\delta 0} = 0.015, \lambda_{\delta 1} = 0.028$$

$$\text{slope}(\text{modcurrent}, \lambda_{\delta}) = 1.3 \cdot 10^{-4} \quad \text{intercept}(\text{modcurrent}, \lambda_{\delta}) = 9.8 \cdot 10^{-3} \quad y = 0..1$$





**Defining Variables used to calculate the resultant current from the photo-detector .**

$\epsilon$  is the responsivity of the photodetector

$\alpha$  is system optical losses

Photodetector  $I_0$  is optical intensity

$$\epsilon_1 = 700 \cdot 10^{-4} \text{ mA / Watt}$$

Output amperage of a photo - detector

$$I_0 \cdot \epsilon_1 = 2.8 \cdot 10^{-4}$$

Re is now how the reflectivity varies with the sinusoidal variation of the wavelength due to the modulation of the drive current .

$$R_{\epsilon} = \frac{K}{2} \left[ 1 + \cos \left[ 2 \cdot \pi \cdot \left( \frac{\lambda_{\text{laser}} + \delta \lambda_{\epsilon} \cdot \epsilon}{T_{\lambda}} \right) + 2 \cdot \pi \cdot \left( \frac{\delta \lambda_{\epsilon} \cdot \delta i \cdot \Delta i}{T_{\lambda}} \right) \cdot \sin(\omega_0 \cdot t) \right] \right] + 0.3$$

$$\beta T = 2 \cdot \pi \cdot \left( \frac{\delta \lambda_{\epsilon} \cdot \delta i \cdot \Delta i}{T_{\lambda}} \right)$$

The output current of the photo-detector at the fundamental frequency  $\omega_0$

$$\zeta 1_{\epsilon} = I_0 \cdot \epsilon_1 \cdot \frac{K}{2} \cdot J_n(1, \beta T) \cdot \sin \left[ 2 \cdot \pi \cdot \left( \frac{\lambda_{\text{laser}} + \delta \lambda_{\epsilon} \cdot \epsilon}{T_{\lambda}} \right) \right]$$

The output current of the photo-detector at the fundamental frequency  $2 \cdot \omega_0$

$$\zeta 2_{\epsilon} = I_0 \cdot \epsilon_1 \cdot \frac{K}{2} \cdot J_n(2, \beta T) \cdot \cos \left[ 2 \cdot \pi \cdot \left( \frac{\lambda_{\text{laser}} + \delta \lambda_{\epsilon} \cdot \epsilon}{T_{\lambda}} \right) \right]$$

From the Operational Amplifier , the resistance is 200K ohms thus the output voltage to the lock-in-Amplifiers are :

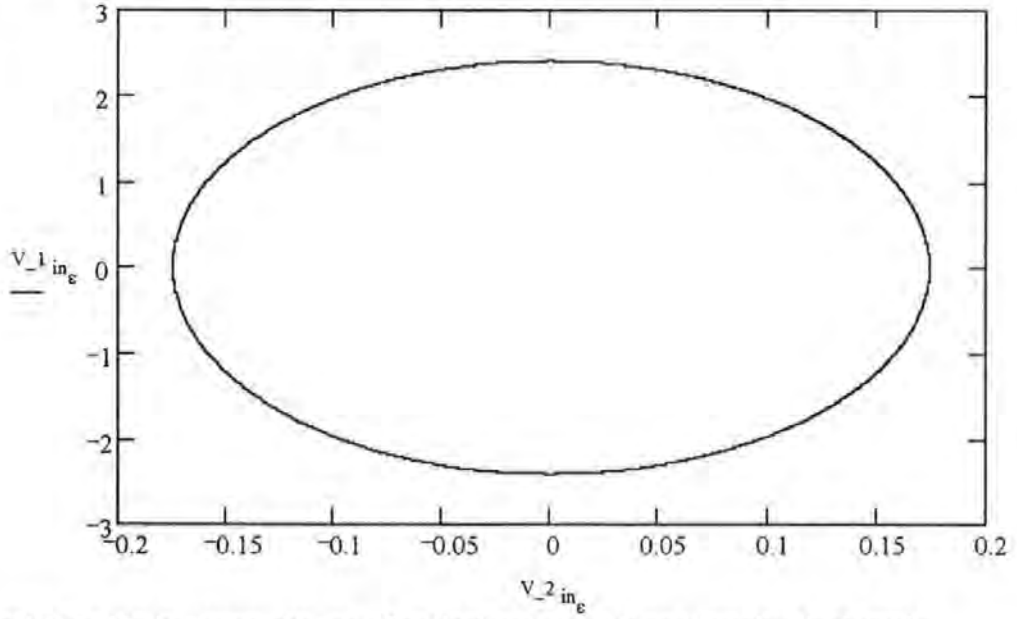
The input voltage to the Lock-In-Amplifiers at the fundamental frequency  $\omega_0$

$$V_{1\text{in}_{\epsilon}} = (200 \cdot 10^3) \cdot \zeta 1$$

The input voltage to the Lock-In-Amplifiers at the fundamental frequency  $2\omega_0$

$$V_{2\text{in}_{\epsilon}} = (200 \cdot 10^3) \cdot \zeta 2$$

The figure below shows the expected cardioid which would be generated from the voltages , from the Lock-In-Amplifiers



The relationship between change of optical wavelength and longitudinal strain using this signal processing technique.

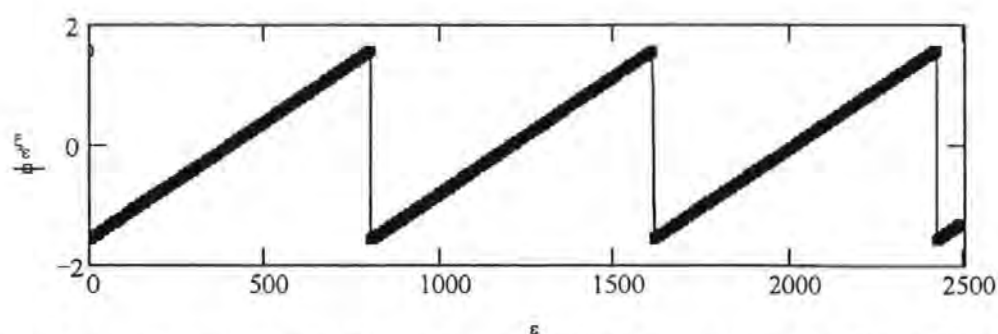
$$\frac{-I_0 \cdot \epsilon l \cdot \frac{K}{2} \cdot J_n(1, \beta T) \cdot \sin \left[ 2 \cdot \pi \cdot \left( \frac{\lambda_{laser} + \delta \lambda_{-} \delta \epsilon \cdot \epsilon}{T_{\lambda}} \right) \right]}{I_0 \cdot \epsilon l \cdot \frac{K}{2} \cdot J_n(2, \beta T) \cdot \cos \left[ 2 \cdot \pi \cdot \left( \frac{\lambda_{laser} + \delta \lambda_{-} \delta \epsilon \cdot \epsilon}{T_{\lambda}} \right) \right]}$$

$$\frac{-J_n(1, \beta T)}{J_n(2, \beta T)} \cdot \frac{\sin \left[ 2 \cdot \pi \cdot \left( \frac{\lambda_{laser} + \delta \lambda_{-} \delta \epsilon \cdot \epsilon}{T_{\lambda}} \right) \right]}{\cos \left[ 2 \cdot \pi \cdot \left( \frac{\lambda_{laser} + \delta \lambda_{-} \delta \epsilon \cdot \epsilon}{T_{\lambda}} \right) \right]} = \frac{-J_n(1, \beta T)}{J_n(2, \beta T)} \cdot \tan \left[ 2 \cdot \pi \cdot \left( \frac{\lambda_{laser} + \delta \lambda_{-} \delta \epsilon \cdot \epsilon}{T_{\lambda}} \right) \right] = \frac{V_{-1} in_{\epsilon}}{V_{-2} in_{\epsilon}}$$

$$\frac{-J_n(1, \beta T)}{J_n(2, \beta T)} = -13.791$$

Using the inverse tangent relationship and multiplicative factor given by  $\frac{-J_n(1, \beta T)}{J_n(2, \beta T)}$  a linear relationship can be extracted between the longitudinal strain subjected to the fibre Bragg grating and the magnitudes of the first and second harmonics generated by this signal processing technique .

$$\xi_{\epsilon} = \text{atan} \left[ \frac{V_{-1} in_{\epsilon}}{V_{-2} in_{\epsilon} \cdot \left( \frac{-J_n(1, \beta T)}{J_n(2, \beta T)} \right)} \right]$$



Thus using a small program acts on the in coming data to produce a " linear line " by either adding  $\pi$  or subtracting  $\pi$  according the phase being either in retardation or progression .

$\varepsilon := 0 \quad \xi_e := \xi_e - \pi$

$\varepsilon := 1..806 \quad \xi_e := \xi$

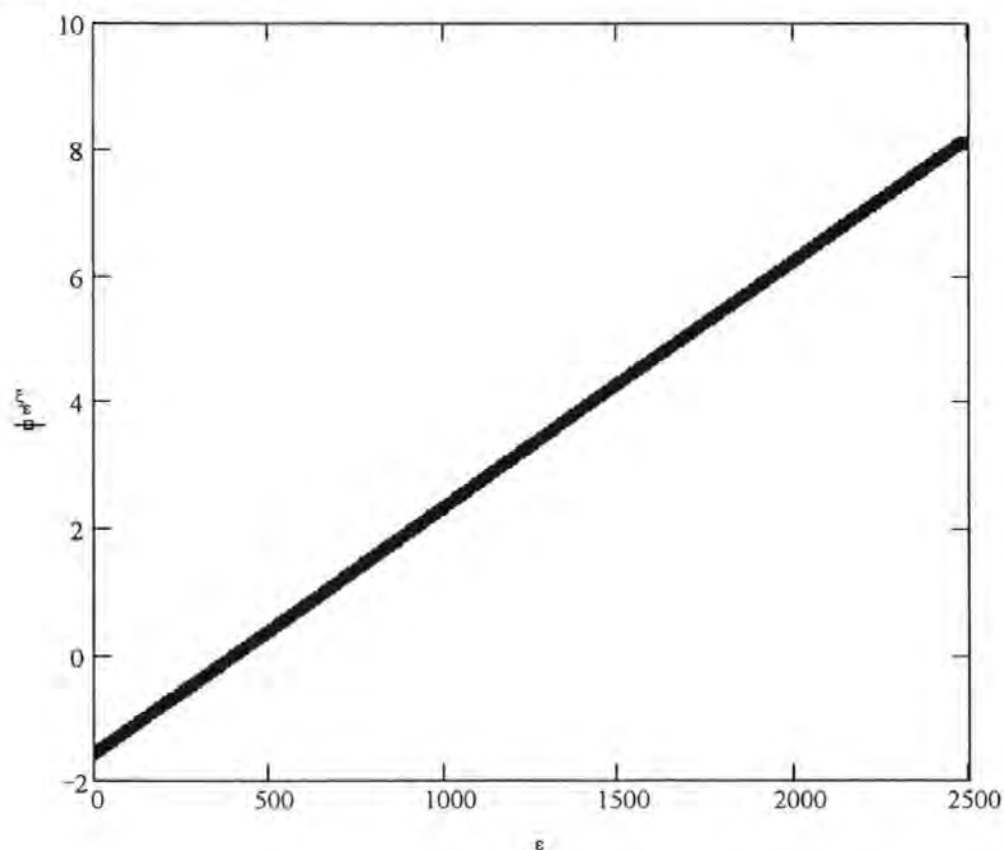
$\varepsilon := 807..1612 \quad \xi_e := \xi_e + \pi$

$\varepsilon := 1613..2418 \quad \xi_e := \xi_e + 2 \cdot \pi$

$\varepsilon := 2419..2489 \quad \xi_e := \xi_e + 3 \cdot \pi$

$\varepsilon := 0..2489$

The graph below shows the quasi - linear relationship which can be obtained by the system under investigation .



THUS

$$\xi = M \cdot \varepsilon + c$$

$$st_{\varepsilon} = \varepsilon$$

A gradient of

$$Theory = slope(st, \xi)$$

$$Theory = 3.897 \cdot 10^{-3} \quad m \cdot \mu\varepsilon^{-1}$$

$$\left( \frac{2 \cdot \pi \cdot \delta \lambda_{-} \delta \varepsilon}{T_{\lambda}} \right) \cdot \varepsilon + \frac{2 \cdot \pi \cdot \lambda_{laser}}{T_{\lambda}} = \operatorname{atan} \left[ \frac{V_{-1} \operatorname{in}_{\varepsilon}}{V_{-2} \operatorname{in}_{\varepsilon} \left( \frac{-J_n(1, \beta T)}{J_n(2, \beta T)} \right)} \right]$$

$$\left( \frac{2 \cdot \pi \cdot \delta \lambda_{-} \delta \varepsilon}{T_{\lambda}} \right) = 3.897 \cdot 10^{-3} \quad \mu\varepsilon^{-1}$$

Therefore a change of one micro-strain causes a change of  $2 \cdot \pi \cdot 6.203 \cdot 10^{-4}$  in the effective change in the " frequency " needing 1612  $\mu\varepsilon$  for one complete cardioid .

$$2 \cdot \pi \cdot 6.203 \cdot 10^{-4} = 3.897 \cdot 10^{-3}$$

**(Vh) A theoretical prediction of the response of the system using a single nonuniform Bragg grating ( linearly chirped with a Taper function ; envelope function for  $\Delta n$  ; a sinusoidal variation with a Top-Hat function .**

$c := 0..200$

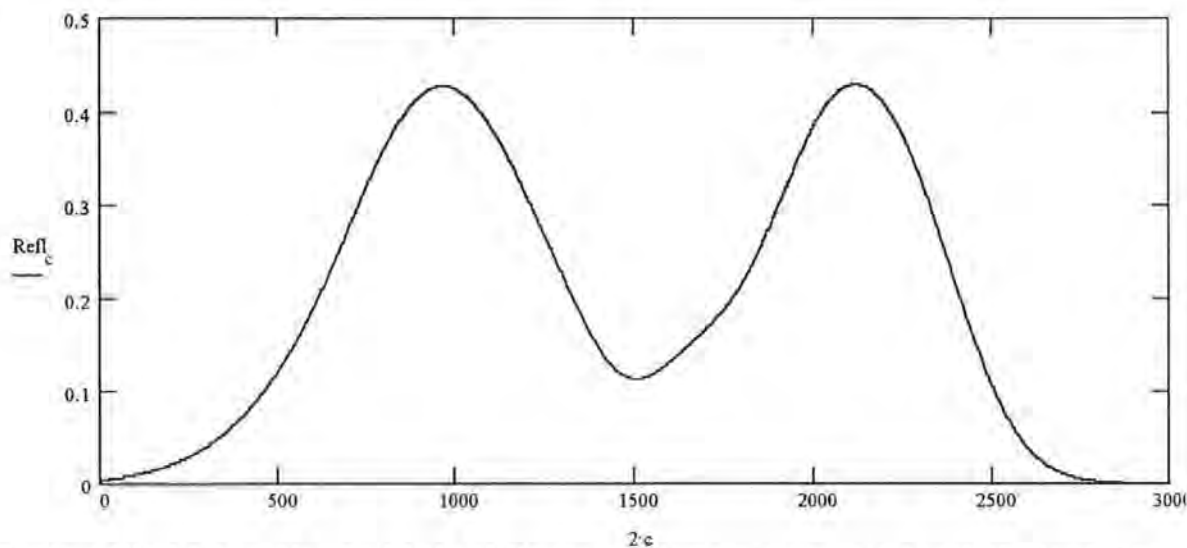
( Note Mathcad +6 program name Finns2.mcd )

Read data : The theoretical results form the C- program which included longitudinal strain , increments readings of reflectivity every two micro-strains .

$\text{Refl} := \text{READPRN}(\text{TOM})$

$\mu\epsilon_c = 2 \cdot c$

The graph below shows the behaviour of the grating at a single wavelength being subjected to strain



This function REFL(x) enables the Mathcad file to superimpose a sinusoidal perturbation to in the strain to take into account the sinusoidal variation the variation of the wavelength eliminating the grating .  $\text{REFL}(x) := \text{Refl}_{\text{floor}(500000 \cdot x + 0.5)}$

Assuming that the D.F.B. laser power illuminating the grating is :  $I_0 = 400 \cdot 10^{-6}$

Wavelength of D.F.B. Laser  $\lambda_{\text{laser}} = 1555.5 \cdot 10^{-9}$

We know that for a grating under longitudinal strain :  $\frac{\delta\lambda}{\lambda} = (1 - p_e) \cdot \frac{\delta l}{l}$

Where  $p_e$  is given by

$$\frac{n^2}{2 \cdot [p_{12} - \nu \cdot (p_{11} + p_{12})]}$$

$n$  is the index of refraction of the core ,  $p_{11}$  and  $p_{12}$  strain - optic coefficients ,  $\nu$  is Poisson's ratio :

$n = 1.5$  ,  $p_{11} = 0.11$  ,  $p_{12} = 0.25$  ,  $\nu = 0.1$

$$p_e = \frac{n^2}{2} \cdot [p_{12} - v(p_{11} + p_{12})] \quad p_e = 0.225$$

At 1555.5nm the expected sensitivity is :

$$\delta\lambda_{\delta\epsilon} = (1 - p_e) \cdot \frac{\lambda_{\text{laser}}}{10^6} \quad \delta\lambda_{\delta\epsilon} = 1.204821410^{-12} \text{ m } \mu\epsilon^{-1}$$

The variation of the wavelength comes from the specification of the system :

**The Section below is giving the specification of the D.F.B. laser and the associated drive system .**

sine wave modulation is Volt .

Modulation coeff of the laser current 40 mA / V .

Oscillator pk to pk Voltage is 30 mV's which can be varied

$$\Delta i = 40 \cdot 100 \cdot 10^{-3}$$

$$\Delta i = 4 \text{ mA}$$

D.F.B. Laser + Drive Unit

The effective current - to - frequency conversion factor for the D.F.B. laser

$$\delta\nu_{\delta i} = 3.5 \cdot 10^9 \text{ Hz / mA}$$

The effective current - to - wavelength conversion factor for the D.F.B. laser depending on the drive current which is  $0.0001865 \times (\text{drivecurrent})$

$$\text{Drive} = 10$$

$$1.3 \cdot 10^{-4} \cdot \text{Drive} + 0.01 = 0.023$$

$$\delta\lambda_{\delta i} = 0.023 \cdot 10^{-9} \text{ m / mA}$$

$$0.015 \cdot 10^{-9}$$

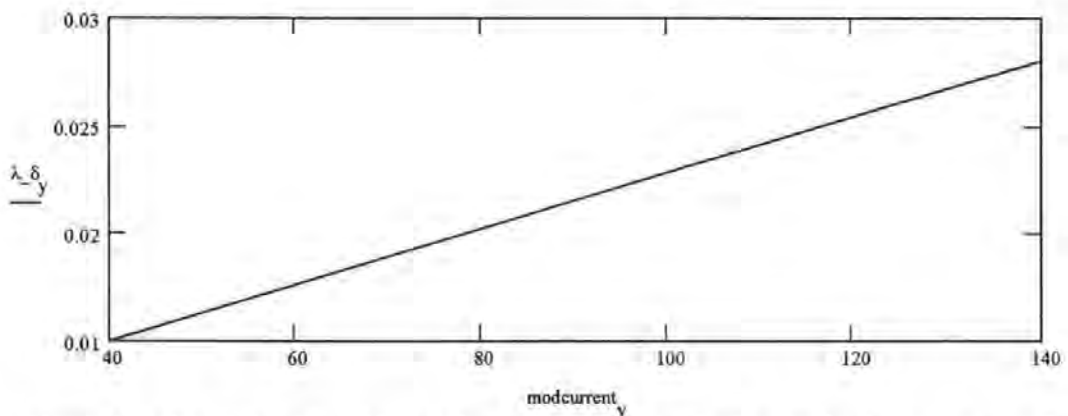
$$\delta\lambda_{\delta i} \cdot \Delta i = 9.2 \cdot 10^{-11}$$

**Note** that is conversion factor is not constant

$$y = 0.. \quad \text{modcurrent}_y = 40 + 100y$$

$$\lambda_{\delta 0} = 0.01, \quad \lambda_{\delta 1} = 0.02, \quad \text{slope}(\text{modcurrent}, \lambda_{\delta}) = 1.3 \cdot 10^{-4}, \quad \text{intercept}(\text{modcurrent}, \lambda_{\delta}) = 9.8 \cdot 10^{-3}$$

$$y = 0..$$



Thus knowing the  $\delta\lambda / \delta\epsilon$  and  $\Delta\lambda$  for the system a equivalent perturbation a longitudinal strain

$$(\delta\lambda_{\delta i} \Delta i) \cdot \left( \frac{1}{\delta\lambda_{\delta\epsilon}} \right) = 76.36$$

**Defining Variables used to calculate the resultant current from the photo-detector .**

$\epsilon$  is the responsivity of the photodetector

$\alpha$  is system optical losses

Photodetector

$I_0$  is optical intensity

$\epsilon l = 700 \cdot 10^{-3} \text{ mA / Watt}$

Output amperage of a photo - detector  $I_0 \cdot \epsilon l = 2.8 \cdot 10^{-4}$

The  $p$  variable is the peak variation of the wavelength which is given by :  $\frac{(\delta\lambda_{\text{ref}} \cdot \delta i \cdot \Delta i)}{2} \left( \frac{1}{\delta\lambda_{\text{ref}} \cdot \delta\epsilon} \right)$

which approximately :  $p = \frac{(\delta\lambda_{\text{ref}} \cdot \delta i \cdot \Delta i)}{2} \left( \frac{1}{\delta\lambda_{\text{ref}} \cdot \delta\epsilon} \right) \cdot 10^{-6} \quad \frac{p}{10^{-6}} = 38.18$

The frequency of the perturbation is  $\nu = 2$

$a$  is just a value of the strain  $a = 1000 \cdot 10^{-6}$

$f(t, a, p)$  generates the the sinusoidal variation about the strain variable  $a$  with a frequency modulation of  $\nu$  :

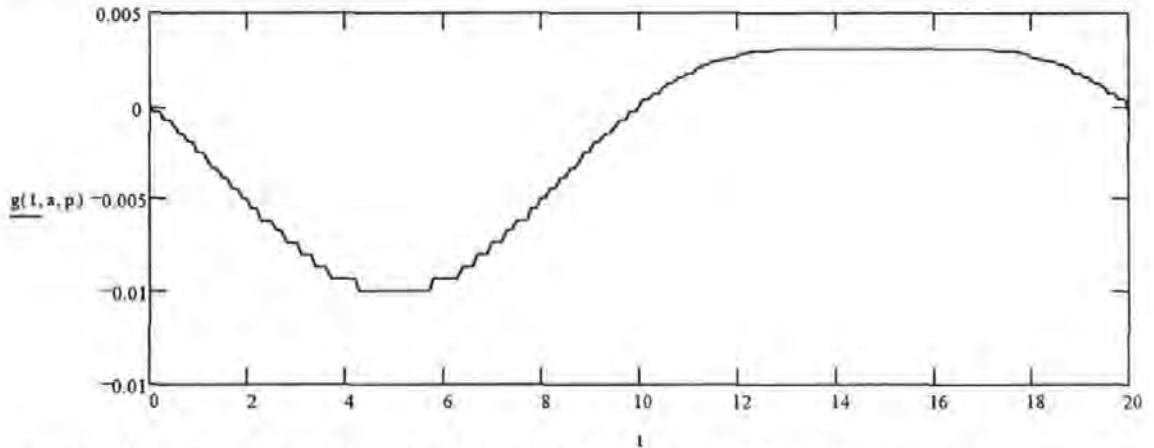
$$f(t, a, p) = a + p \cdot \sin\left(\frac{2 \cdot \pi \cdot t}{\nu}\right)$$

$g(t, a, p)$  removes the DC component of the generated signal a sinusoidal variation about the reflectivity given at strain value of  $a$  with a bandwidth of variation is dependent upon  $p$

$$g(t, a, p) = \text{REFL}(f(t, a, p)) - \text{REFL}(f(0, a, p))$$

The graph below shows the variation of reflectivity over one period of the sine variation

$t = 0, 0.1 \dots 2$



The generation of the harmonics using a Fourier transform D.C. component  $c_0$  :

at  $a$

$$c_0 = \frac{1}{\nu} \int_0^{\nu} g(t, a, p) dt$$

$h = 1 \dots 5$  giving the first 5 harmonics  $c_h$  :

at  $a = h = 1..$

$$c_h = \frac{2}{v} \int_0^v g(t, a, p) \cdot e^{\frac{-i \cdot 2 \cdot \pi \cdot h \cdot t}{v}} dt$$

$\gamma$  gives the range of micro-strains of interest according to min and max :

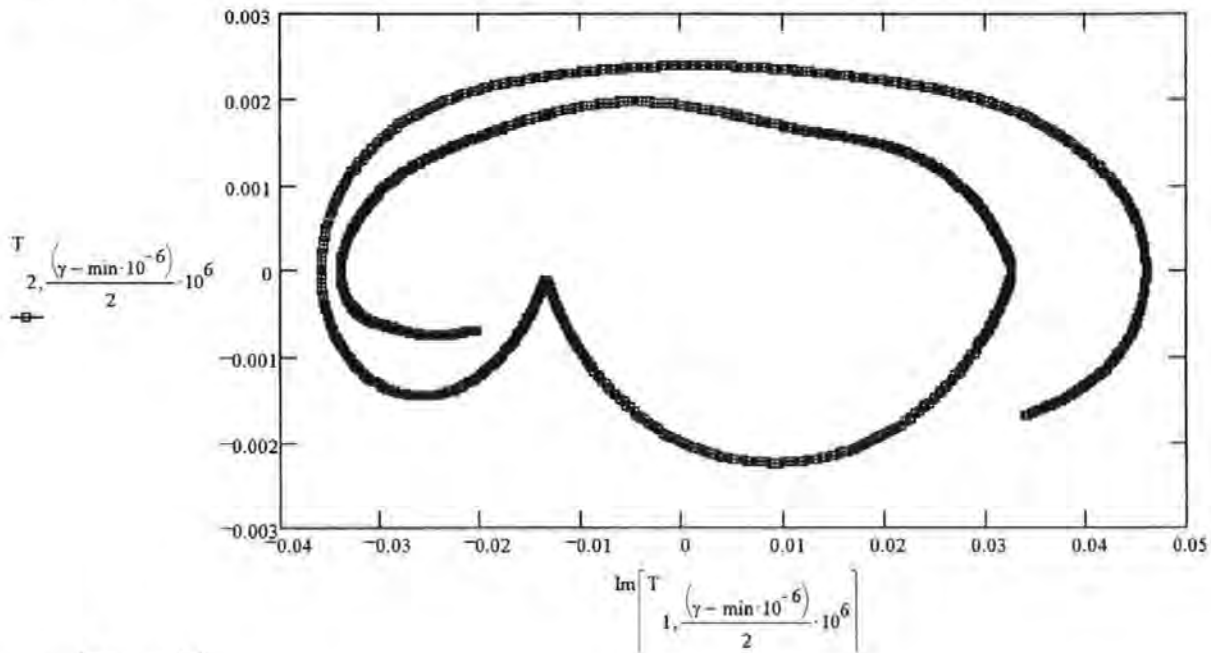
$$\min := 47 \quad , \quad \max := 2.5 \cdot 10^3$$

$$\gamma := \min \cdot 10^{-6}, (\min + 2) \cdot 10^{-6} .. \max \cdot 10^{-6}$$

$$T_{h, \frac{(\gamma - \min \cdot 10^{-6})}{2} \cdot 10^6} = \frac{2}{v} \int_0^v g(t, \gamma, p) \cdot e^{\frac{-i \cdot 2 \cdot \pi \cdot h \cdot t}{v}} dt$$

T calculates all the harmonics over the range of interest :

NOTE : The generation of the cardioid uses the Im for the first harmonic , this is just the way the harmonics have been generated to save time .



$$co = 0., \left( \frac{\max}{2} - \frac{\min}{2} \right)$$

The output current of the photodetector at the fundamental frequency  $v$

$$F1_{co} = I_0 \cdot \varepsilon l \cdot \text{Im}(T_{1,co})$$

The output current of the photodetector at the fundamental frequency  $2v$

$$F2_{co} = I_0 \cdot \varepsilon l \cdot T_{2,c}$$

From the Operational Amplifier , the resistance is 200K ohms thus the output voltage to the lock-in-Amplifiers are :



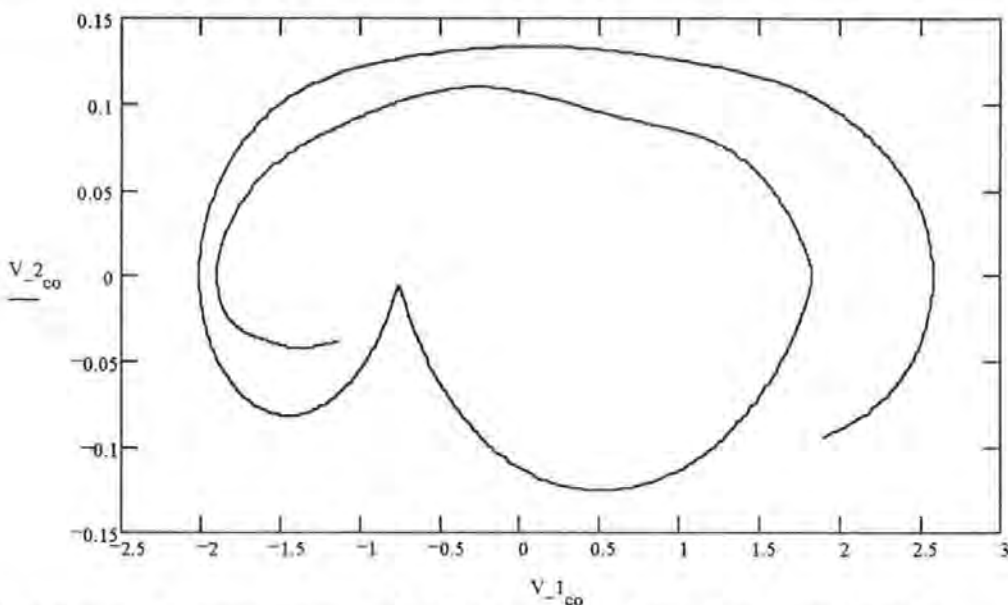
The input voltage to the Lock-In-Amplifiers at the fundamental frequency  $\nu$

$$V_{1_{co}} := (200 \cdot 10^3) \cdot F1_c$$

The input voltage to the Lock-In-Amplifiers at the fundamental frequency  $2\nu$

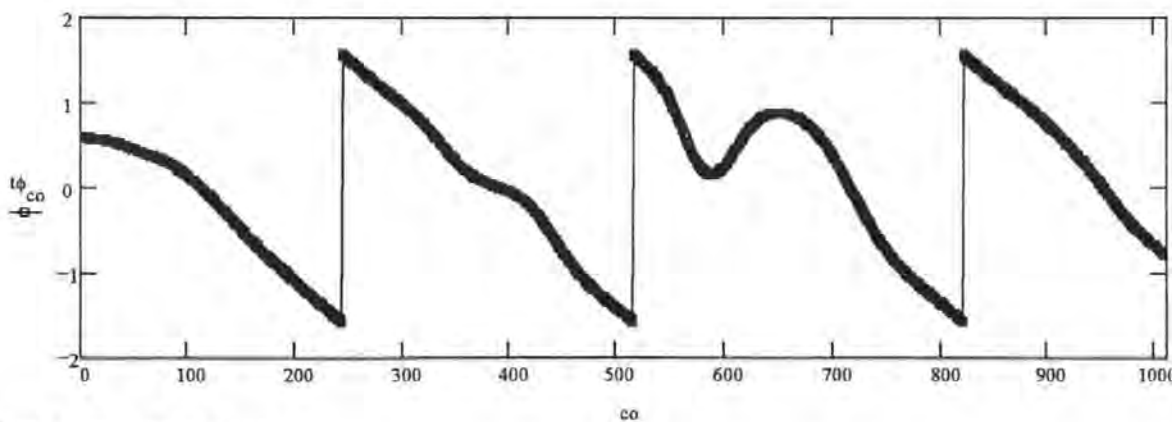
$$V_{2_{co}} := (200 \cdot 10^3) \cdot F2_c$$

The figure below shows the expected cardioid which would be generated from the voltages , from the Lock-In-Amplifiers



The relationship between change of optical wavelength and longitudinal strain using this signal processing technique.

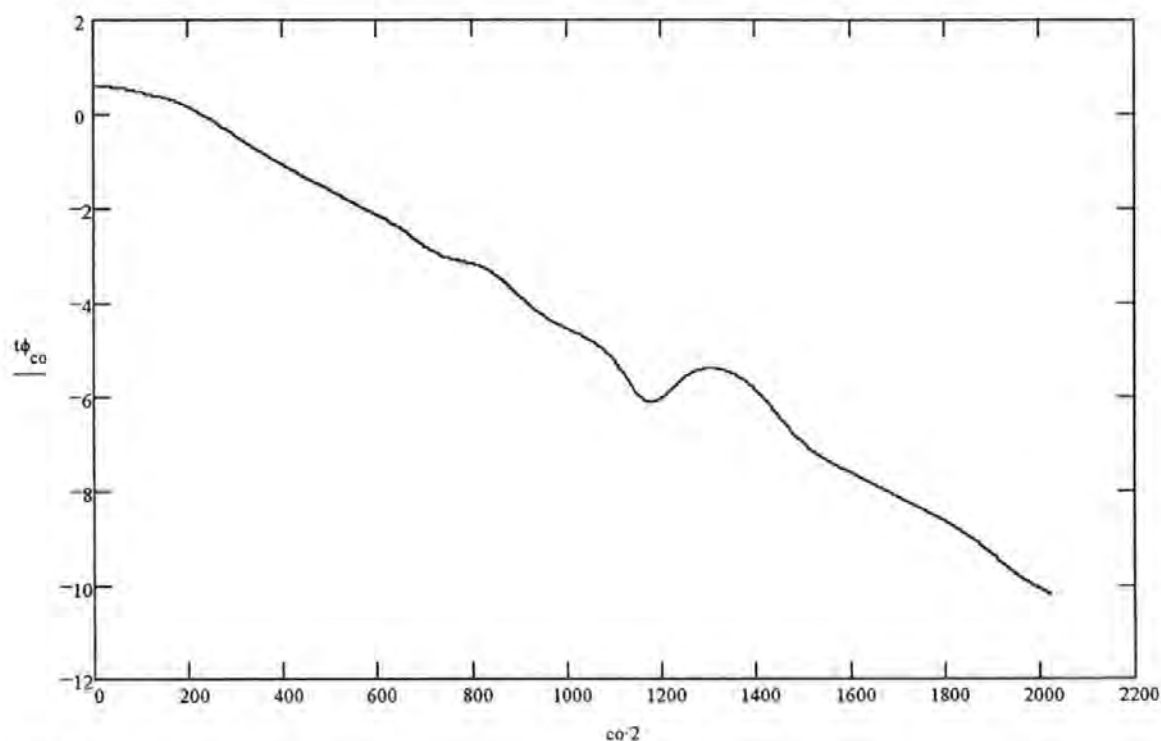
$$t\phi_{co} := \text{atan} \left( \frac{V_{2_{co}}}{V_{1_{co}} \cdot 0.05} \right)$$



Therefore a processed signal :

$$co = 0..24 \quad t\phi_{co} = t\phi_{co} - t\phi_0$$

$$\begin{aligned}co &:= 245.51 & t\phi_{co} &:= t\phi_{co} - \pi - t\phi_0 \\co &:= 517.82 & t\phi_{co} &:= t\phi_{co} - 2 \cdot \pi - t\phi_0 \\co &:= 822.101 & t\phi_{co} &:= t\phi_{co} - 3 \cdot \pi - t\phi_0 \\co &:= 0.. \left( \frac{\max}{2} - \frac{\min}{2} \right)\end{aligned}$$



$$\text{strain}_{co} = co \cdot$$

A gradient of

$$\text{Lin} = \text{slope}(t\phi, \text{strain})$$

$$\text{slope}(t\phi, \text{strain}) = -183.035$$

$$\text{star} = \text{intercept}(t\phi, \text{strain})$$

$$\text{intercept}(t\phi, \text{strain}) = 200.645$$

ERROR.

$$\text{ERROR} = \frac{\left( \frac{\max}{2} - \frac{\min}{2} \right) \sum_{k=0} \sqrt{[\text{strain}_k - (\text{Lin} \cdot t\phi_k + \text{star})]^2}}{\left( \frac{\max}{2} - \frac{\min}{2} \right)}$$

$$\text{ERROR} = 32.219$$

**(Vj) A theoretical prediction of the response of the system using a single nonuniform Bragg grating ( linearly chirped with a Taper function ; envelope function for  $\Delta n$  ; a sinusoidal variation with a Top-Hat function .**

(Note Mathcad +6 program name FINNS3.mcd )

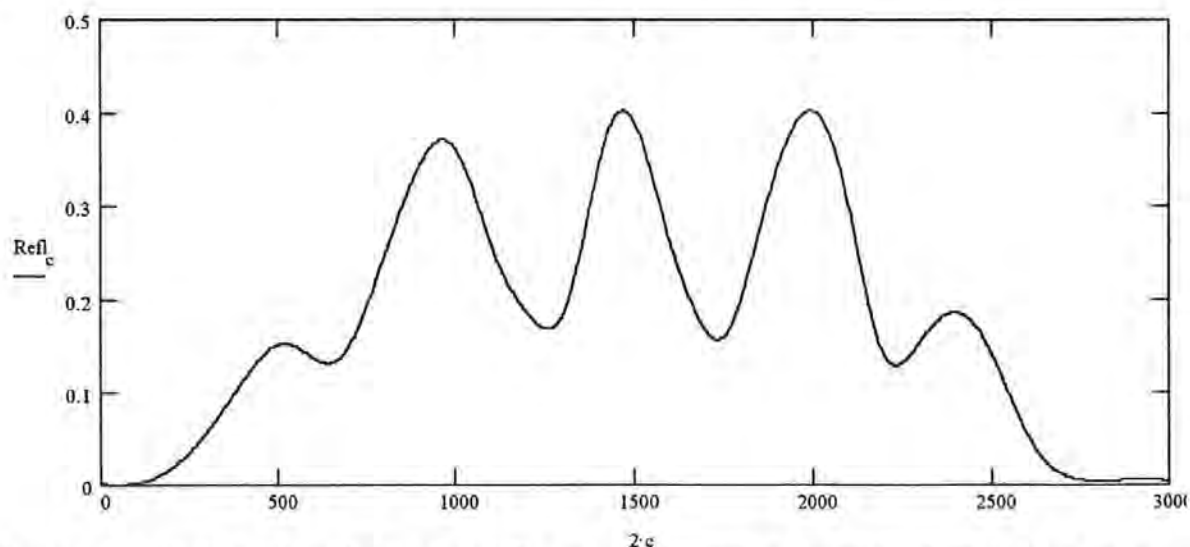
$c := 0..200$

Read data : The theoretical results form the C- program which included longitudinal strain , increments readings of reflectivity every two micro-strains .

$Refl := READPRN(TOM)$

$\mu\epsilon_c := 2 \cdot c$

The graph below shows the behaviour of the grating at a single wavelength being subjected to strain



This function REFL(x) enables the Mathcad file to superimpose a sinusoidal perturbation to in the strain to take into account the sinusoidal variation the variation of the wavelength eliminating the grating .  $REFL(x) := Refl_{floor(500000 \cdot x + 0.5)}$

Assuming that the D.F.B. laser power illuminating the grating is :  $I_0 := 400 \cdot 10^{-6}$

Wavelength of D.F.B. Laser  $\lambda_{laser} = 1555.5 \cdot 10^{-9}$

We know that for a grating under longitudinal strain :  $\frac{\delta \lambda}{\lambda} = (1 - p_e) \cdot \frac{\delta l}{l}$

Where  $p_e$  is given by

$$\frac{n^2}{2 \left[ p_{12} - \nu \cdot (p_{11} + p_{12}) \right]}$$

$n$  is the index of refraction of the core

$p_{11}$  and  $p_{12}$  strain - optic coefficients

$\nu$  is Poisson's ratio

$n = 1.5$  ,  $p_{11} = 0.11$

$$p_{12} = 0.25 , \nu = 0.1 , p_e = \frac{n^2}{2} [p_{12} - \nu(p_{11} + p_{12})]$$

$$p_e = 0.225444$$

At 1555.5nm the expected sensitivity is :

$$\delta\lambda_{\delta\epsilon} = (1 - p_e) \cdot \frac{\lambda_{\text{laser}}}{10^6} \quad \delta\lambda_{\delta\epsilon} = 1.204821410^{-12} \text{ m} \cdot \mu\epsilon^{-1}$$

The variation of the wavelength comes from the specification of the system :

**The Section below is giving the specification of the D.F.B. laser and the associated drive system .**

sine wave modulation is Volt .

Modulation coeff of the laser current 40 mA / V .

Oscillator pk to pk Voltage is 30 mV's which can be varied

$$\Delta i = 40 \cdot 100 \cdot 10^{-3}$$

$$\Delta i = 4 \text{ mA}$$

D.F.B. Laser + Drive Unit

The effective current - to - frequency conversion factor for the D.F.B. laser

$$\delta\nu_{\delta i} = 3.5 \cdot 10^9 \text{ Hz / mA}$$

The effective current - to - wavelength conversion factor for the D.F.B. laser depending on the drive current which is  $0.0001865 \times (\text{drive current})$

$$\text{Drive} = 10$$

$$1.3 \cdot 10^{-4} \cdot \text{Drive} + 0.01 = 0.023$$

$$\delta\lambda_{\delta i} = 0.023 \cdot 10^{-9} \text{ m / mA}$$

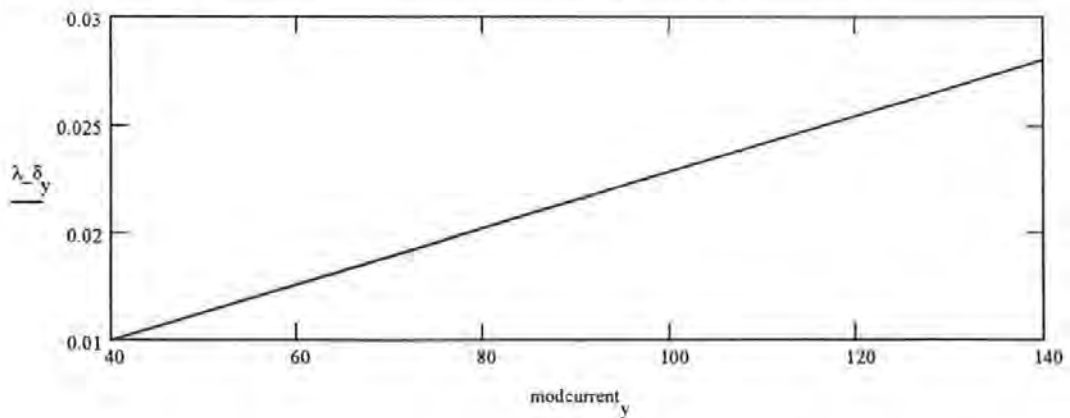
$$0.015 \cdot 10^{-9}$$

$$\delta\lambda_{\delta i} \cdot \Delta i = 9.2 \cdot 10^{-11}$$

**Note** that is conversion factor is not constant

$$y = 0.. , \text{modcurrent}_y = 40 + 100y , \lambda_{\delta 0} = 0.01 , \lambda_{\delta 1} = 0.02$$

$$\text{slope}(\text{modcurrent}, \lambda_{\delta}) = 1.3 \cdot 10^{-4} \quad \text{intercept}(\text{modcurrent}, \lambda_{\delta}) = 9.8 \cdot 10^{-3} \quad y = 0..$$



Thus knowing the  $\delta\lambda / \delta\epsilon$  and  $\Delta\lambda$  for the system a equivalent perturbation a longitudinal strain

$$(\delta\lambda_{-}\delta i \Delta i) \cdot \left( \frac{1}{\delta\lambda_{-}\delta\epsilon} \right) = 76.359866$$

**Defining Variables used to calculate the resultant current from the photo-detector .**

$\epsilon$  is the responsivity of the photodetector

$\alpha$  is system optical losses

Photodetector

$I_0$  is optical intensity

$$\epsilon l = 700 \cdot 10^{-3} \text{mA} / \text{Watt}$$

Output amperage of a photo - detector  $I_0 \cdot \epsilon l = 2.8 \cdot 10^{-4}$

The p variable is the peak variation of the wavelength which is given by :  $\frac{(\delta\lambda_{-}\delta i \Delta i) \cdot \left( \frac{1}{\delta\lambda_{-}\delta\epsilon} \right)}{2}$

$$\text{which approximately : } p = \frac{(\delta\lambda_{-}\delta i \Delta i) \cdot \left( \frac{1}{\delta\lambda_{-}\delta\epsilon} \right)}{2} \cdot 10^{-6} \quad \frac{P}{10^{-6}} = 38.179933$$

The frequency of the perturbation is  $\nu = 2$

a is just a value of the strain  $a = 1000 \cdot 10^{-6}$

$f(t, a, p)$  generates the the sinusoidal variation about the strain variable **a** with a frequency modulation of  $\nu$  :

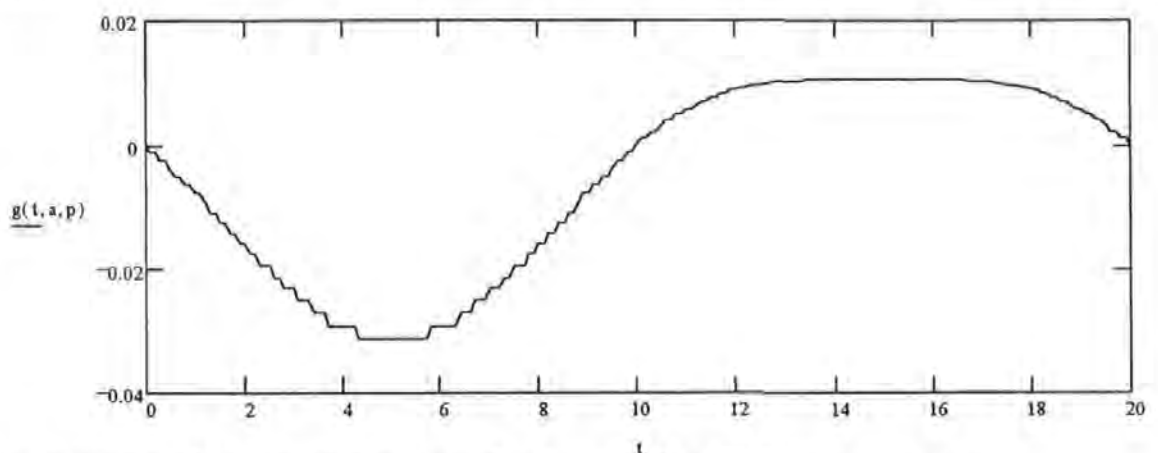
$$f(t, a, p) = a + p \cdot \sin\left(\frac{2 \cdot \pi}{\nu} \cdot t\right)$$

$g(t, a, p)$  removes the DC component of the generated signal a sinusoidal variation about the reflectivity given at strain value of **a** with a bandwidth of variation is dependent upon **p**

$$g(t, a, p) = \text{REFL}(f(t, a, p)) - \text{REFL}(f(0, a, p))$$

The graph below shows the variation of reflectivity over one period of the sine variation

$t = 0, 0.1.. 2$



The generation of the harmonics using a Fourier transform D.C. component  $c_0$  :

at **a**

$$c_0 := \frac{1}{v} \int_0^v g(t, a, p) dt$$

$h = 1 \dots 5$  giving the first 5 harmonics  $c_h$  :

at **a**

$h := 1..$

$$c_h = \frac{2}{v} \int_0^v g(t, a, p) \cdot e^{\frac{-i \cdot 2 \cdot \pi \cdot h \cdot t}{v}} dt$$

$\gamma$  gives the range of micro-strains of interest according to min and max :

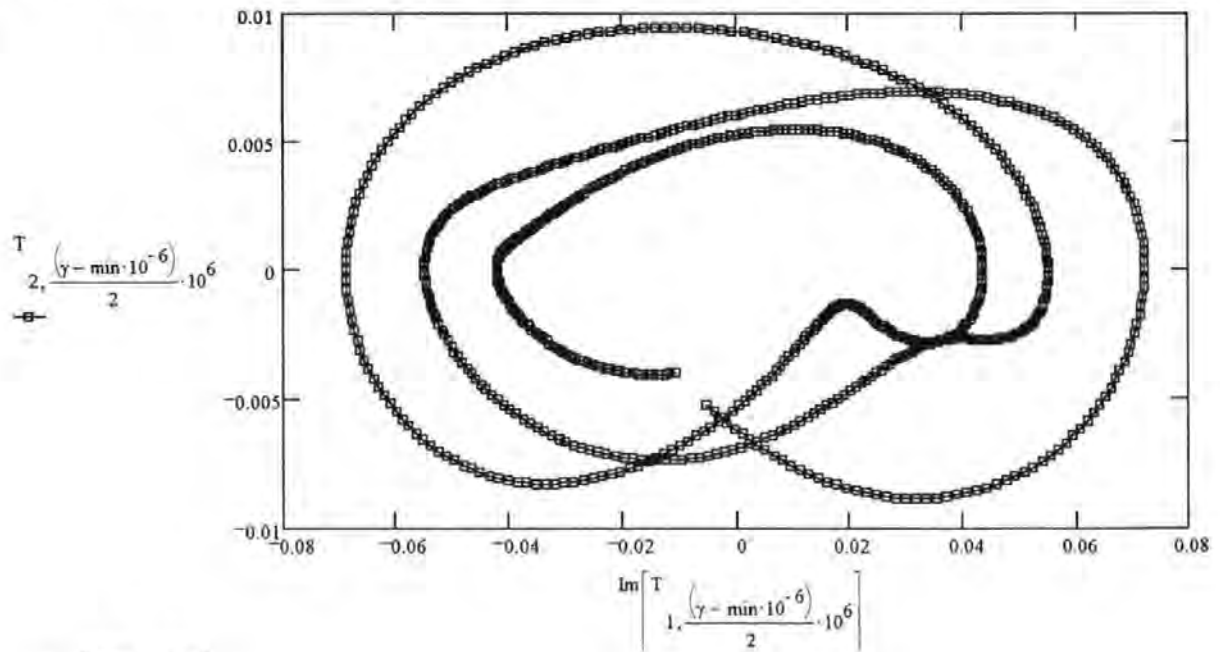
$$\min := 66, \max := 2.24 \cdot 10^3$$

$$\gamma := \min \cdot 10^{-6}, (\min + 2) \cdot 10^{-6} \dots \max \cdot 10^{-6}$$

$$T_{h, \frac{(\gamma - \min \cdot 10^{-6})}{2} \cdot 10^6} = \frac{2}{v} \int_0^v g(t, \gamma, p) \cdot e^{\frac{-i \cdot 2 \cdot \pi \cdot h \cdot t}{v}} dt$$

T calculates all the harmonics over the range of interest :

NOTE : The generation of the cardioid uses the Im for the first harmonic , this is just the way the harmonics have been generated to save time ,



$$co := 0.. \left( \frac{\max}{2} - \frac{\min}{2} \right)$$

The output current of the photodetector at the fundamental frequency  $v$

$$F1_{co} = I_0 \cdot \varepsilon_1 \cdot \text{Im}(T_{1,co})$$

The output current of the photodetector at the fundamental frequency  $2v$

$$F2_{co} = I_0 \cdot \varepsilon_1 \cdot T_{2,e}$$

From the Operational Amplifier , the resistance is 200K ohms thus the output voltage to the

lock-in-Amplifiers are :

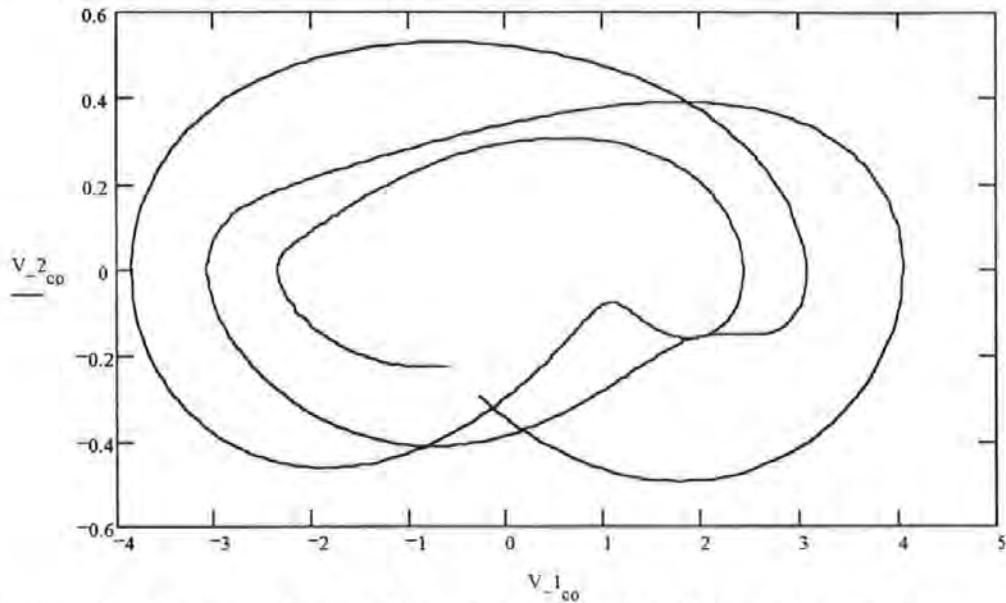
The input voltage to the Lock-In-Amplifiers at the fundamental frequency  $v$

$$V_{1_{co}} := (200 \cdot 10^3) \cdot F1_c$$

The input voltage to the Lock-In-Amplifiers at the fundamental frequency  $2v$

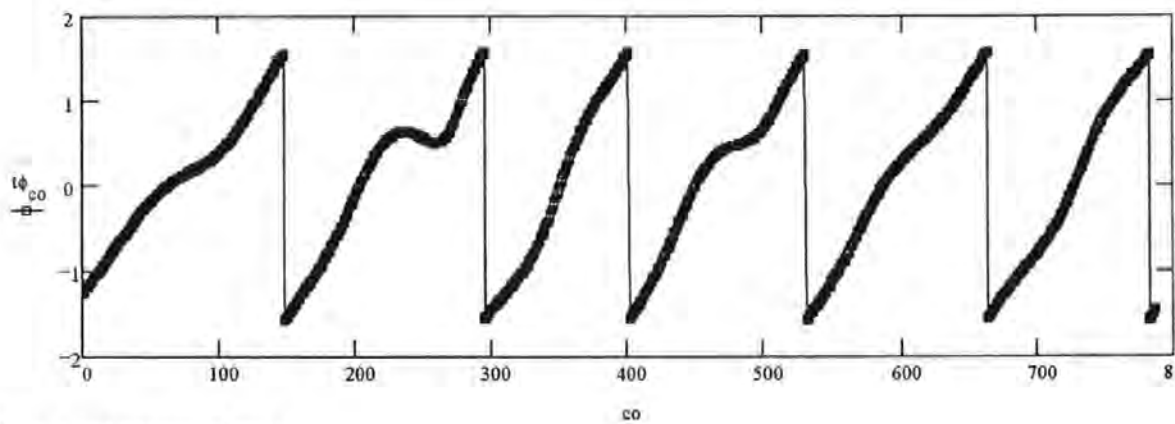
$$V_{2_{co}} := (200 \cdot 10^3) \cdot F2_c$$

The figure below shows the expected cardioid which would be generated from the voltages , from the Lock-In-Amplifiers



The relationship between change of optical wavelength and longitudinal strain using this signal processing technique.

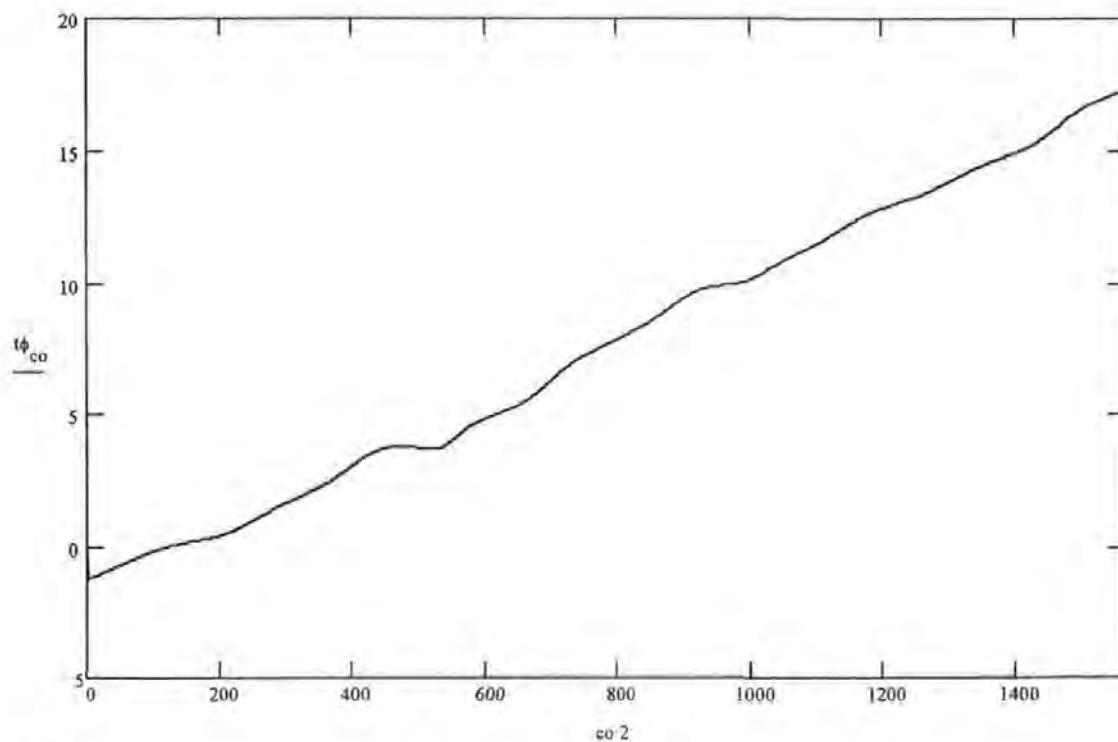
$$t\phi_{co} := \text{atan} \left[ \frac{(V_{2_{co}} - 1)}{V_{1_{co}} \cdot 0.12} \right]$$



Therefore a processed signal :

$$\begin{aligned} co &:= 0..14 & t\phi_{co} &= t\phi_{co} - t\phi_0 \\ co &:= 148..29 & t\phi_{co} &= (t\phi_{co} + \pi) - t\phi_0 \\ co &:= 296..40 & t\phi_{co} &= (t\phi_{co} + 2\pi) - t\phi_0 \end{aligned}$$

$$\begin{aligned}
 co &:= 402.53 & t\phi_{co} &:= (t\phi_{co} + 3 \cdot \pi) - t\phi_0 \\
 co &:= 531.66 & t\phi_{co} &:= (t\phi_{co} + 4 \cdot \pi) - t\phi_0 \\
 co &:= 663.78 & t\phi_{co} &:= (t\phi_{co} + 5 \cdot \pi) - t\phi_0 \\
 co &:= 783.78 & t\phi_{co} &:= (t\phi_{co} + 5 \cdot \pi) - t\phi_0 \\
 co &= 0. \cdot \left( \frac{\max}{2} - \frac{\min}{2} \right)
 \end{aligned}$$



$$\text{strain}_{co} = co \cdot$$

A gradient of

$$\text{Lin} := \text{slope}(t\phi, \text{strain})$$

$$\text{slope}(t\phi, \text{strain}) = 82.56658$$

$$\text{star} := \text{intercept}(t\phi, \text{strain})$$

$$\text{intercept}(t\phi, \text{strain}) = 157.984793$$

ERROR.

$$\text{ERROR} = \frac{\sum_{k=0}^{\left(\frac{\max}{2} - \frac{\min}{2}\right)} \sqrt{\left[\text{strain}_k - (\text{Lin} \cdot t\phi_k + \text{star})\right]^2}}{\left(\frac{\max}{2} - \frac{\min}{2}\right)}$$

$$\text{ERROR} = 20.850805$$



**(Vk) A theoretical prediction of the response of the system using the experimental static reflection response data of the fabricated single nonuniform Bragg grating ( linearly chirped with a Taper function ; envelope function for  $\Delta n$  ; a sinusoidal variation with a Top-Hat function .**

( Note Mathcad +6 program name FINNS5.mcd )

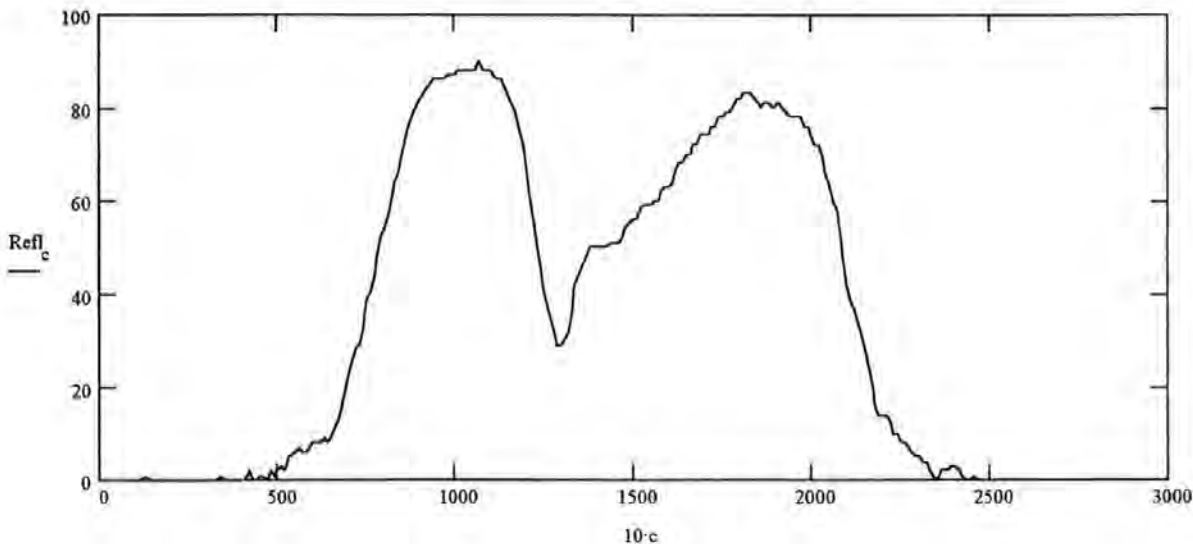
$c := 0..27$

Read data : The theoretical results form the C- program which included longitudinal strain , increments readings of reflectivity every two micro-strains ..

$Refl := READPRN(TOM)$

$\mu\epsilon_c := 10 \cdot c$

The graph below shows the behaviour of the grating at a single wavelength being subjected to strain



This function REFL(x) enables the Mathcad file to superimpose a sinusoidal perturbation to in the strain to take into account the sinusoidal variation the variation of the wavelength illuminating the grating .  $REFL(x) := Refl_{\text{floor}(100000 \cdot x + 0.5)}$

Wavelength of D.F.B. Laser  $\lambda_{\text{laser}} := 1570.5 \cdot 10^{-9}$

We know that for a grating under longitudinal strain :  $\frac{\delta\lambda}{\lambda} = (1 - p_e) \cdot \frac{\delta l}{l}$

Where  $p_e$  is given by 
$$\frac{n^2}{2 \cdot [p_{12} - v \cdot (p_{11} + p_{12})]}$$

$n$  is the index of refraction of the core ,  $p_{11}$  and  $p_{12}$  strain - optic coefficients

$v$  is Poisson's ratio

$n = 1.5$  ,  $p_{11} = 0.11$  ,  $p_{12} = 0.25$  ,  $v = 0.1$   $p_e = \frac{n^2}{2} \cdot [p_{12} - v \cdot (p_{11} + p_{12})]$   $p_e = 0.22544$

At 1555.5nm the expected sensitivity is :  $\delta\lambda_{\delta\epsilon} = (1 - p_e) \frac{\lambda_{\text{laser}}}{10^6} \delta\lambda_{\delta\epsilon} = 1.216439710^{-12} \text{ m} \cdot \mu\epsilon^{-1}$

The variation of the wavelength comes from the specification of the system :

**The Section below is giving the specification of the D.F.B. laser and the associated drive system .**

sine wave modulation is Volt .

Modulation coeff of the laser current 40 mA / V .

Oscillator pk to pk Voltage is 30 mV's which can be varied

$$\Delta i = 40 \cdot 1000 \cdot 10^{-3}$$

$$\Delta i = 40 \text{ mA}$$

D.F.B. Laser + Drive Unit

The effective current - to - frequency conversion factor for the D.F.B. laser

$$\delta\nu_{\delta i} = 3.5 \cdot 10^9 \text{ Hz / mA}$$

The effective current - to - wavelength conversion factor for the D.F.B. laser depending on the drive current which is  $0.0001865 \times (\text{drive current})$

Drive := 5

$$1.3714310^{-4} \cdot \text{Drive} + 0.01 = 0.01686$$

$$\delta\lambda_{\delta i} = 0.016510^{-9} \text{ m / mA}$$

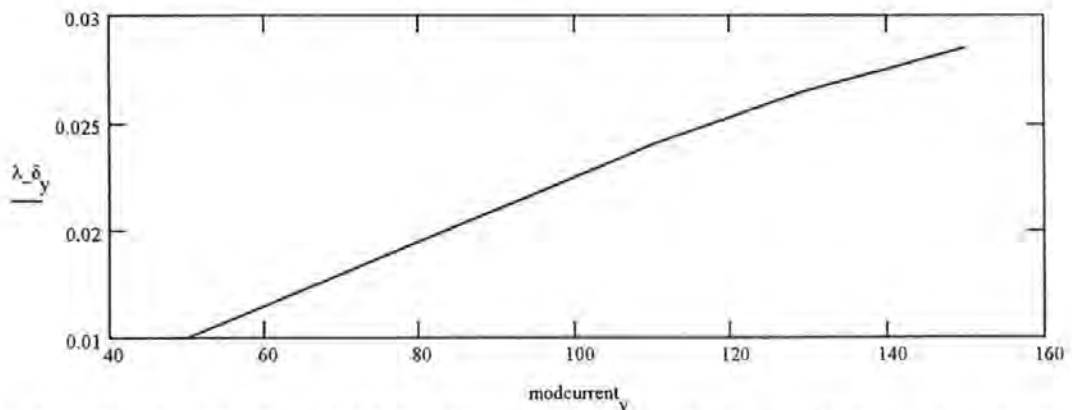
$$0.01510^{-9}$$

$$\delta\lambda_{\delta i} \cdot \Delta i = 6.6 \cdot 10^{-10}$$

**Note** that is conversion factor is not constant

$$y = 0.. \quad \text{modcurrent} = \begin{bmatrix} 50 \\ 70 \\ 90 \\ 110 \\ 130 \\ 150 \end{bmatrix} \quad \lambda_{\delta} = \begin{bmatrix} 0.015 \\ 0.018 \\ 0.021 \\ 0.024 \\ 0.0265 \\ 0.0285 \end{bmatrix}$$

$$\text{slope}(\text{modcurrent}, \lambda_{\delta}) = 1.3714310^{-4} \quad \text{intercept}(\text{modcurrent}, \lambda_{\delta}) = 8.4523810^{-3} \quad y = 0..$$



Thus knowing the  $\delta\lambda / \delta\epsilon$  and  $\Delta\lambda$  for the system a equivalent perturbation a longitudinal strain

$$(\delta\lambda_{\delta i} \cdot \Delta i) \cdot \left( \frac{1}{\delta\lambda_{\delta \epsilon}} \right) = 542.56695$$

**Defining Variables used to calculate the resultant current from the photo-detector .**

$\epsilon$  is the responsivity of the photodetector

$\alpha$  is system optical losses

Photodetector

$I_0$  is optical intensity

$$\epsilon_1 = 700 \cdot 10^{-3} \text{mA / Watt}$$

The  $p$  variable is the peak variation of the wavelength which is given by : 
$$\frac{(\delta\lambda_{\delta i} \cdot \Delta i) \cdot \left( \frac{1}{\delta\lambda_{\delta \epsilon}} \right)}{2}$$

$$\text{which approximately : } p = \frac{(\delta\lambda_{\delta i} \cdot \Delta i) \cdot \left( \frac{1}{\delta\lambda_{\delta \epsilon}} \right)}{2} \cdot 10^{-6} \quad \frac{p}{10^{-6}} = 271.28348$$

The frequency of the perturbation is  $v = 2$

$a$  is just a value of the strain  $a = 700 \cdot 10^{-6}$

$f(t, a, p)$  generates the sinusoidal variation about the strain variable  $a$  with a frequency modulation of  $v$  :

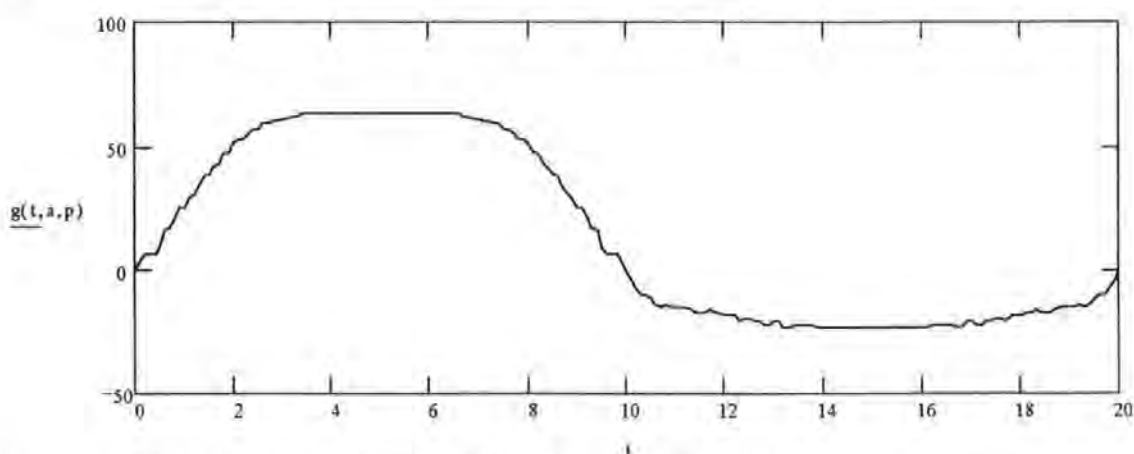
$$f(t, a, p) = a + p \cdot \sin\left(\frac{2\pi}{v} \cdot t\right)$$

$g(t, a, p)$  removes the DC component of the generated signal a sinusoidal variation about the reflectivity given at strain value of  $a$  with a bandwidth of variation is dependent upon  $p$

$$g(t, a, p) = \text{REFL}(f(t, a, p)) - \text{REFL}(f(0, a, p))$$

The graph below shows the variation of reflectivity over one period of the sine variation

$t = 0, 0.1 \dots 2$



The generation of the harmonics using a Fourier transform D.C. component  $c_0$  :

at  $a$

$$c_0 = \frac{1}{v} \int_0^v g(t, a, p) dt$$

$h = 1 \dots 5$  giving the first 5 harmonics  $c_h$  :

at **a**

$h = 1..$

$$c_h = \frac{2}{v} \int_0^v g(t, a, p) \cdot e^{\frac{-i \cdot 2 \cdot \pi \cdot h \cdot t}{v}} dt$$

$\gamma$  gives the range of micro-strains of interest according to min and max :

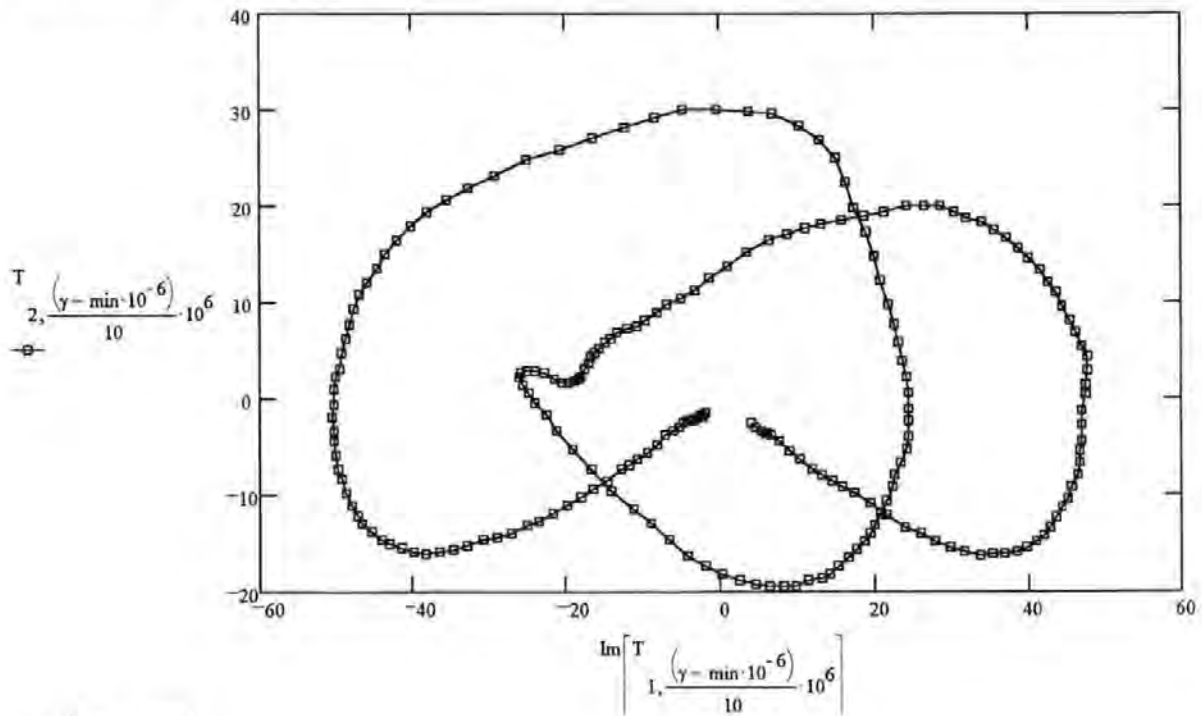
$\min := 28$        $\max := 250$

$\gamma := \min \cdot 10^{-6}, (\min + 10) \cdot 10^{-6}, \max \cdot 10^{-6}$

T calculates all the harmonics over the range of interest :

$$T_{h, \frac{(\gamma - \min \cdot 10^{-6})}{10} \cdot 10^6} = \frac{2}{v} \sum_{k=0}^{99} g\left[\frac{\left(k + \frac{1}{2}\right) \cdot v}{100}, \gamma, p\right] \cdot \left[ \frac{-\exp\left[\frac{-1}{50} \cdot i \cdot \pi \cdot h \cdot (k+1)\right] \cdot v + \exp\left[\frac{-1}{50} \cdot i \cdot \pi \cdot h \cdot k\right] \cdot v}{2 \cdot \pi \cdot i \cdot h} \right]$$

NOTE : The generation of the cardioid uses the Im for the first harmonic , this is just the way the harmonics have been generated to save time .



$$co := 0.. \left( \frac{\max}{10} - \frac{\min}{10} \right)$$

The output Voltage of the photodetector at the fundamental frequency  $v$

$$F1_{co} := \text{Im}(T_{1,co})$$

The output voltage of the photodetector at the fundamental frequency  $2v$

$$F2_{co} := T_{2,c}$$

From the Operational Amplifier , the resistance is 200K ohms thus the output voltage to the lock-in-Amplifiers are :

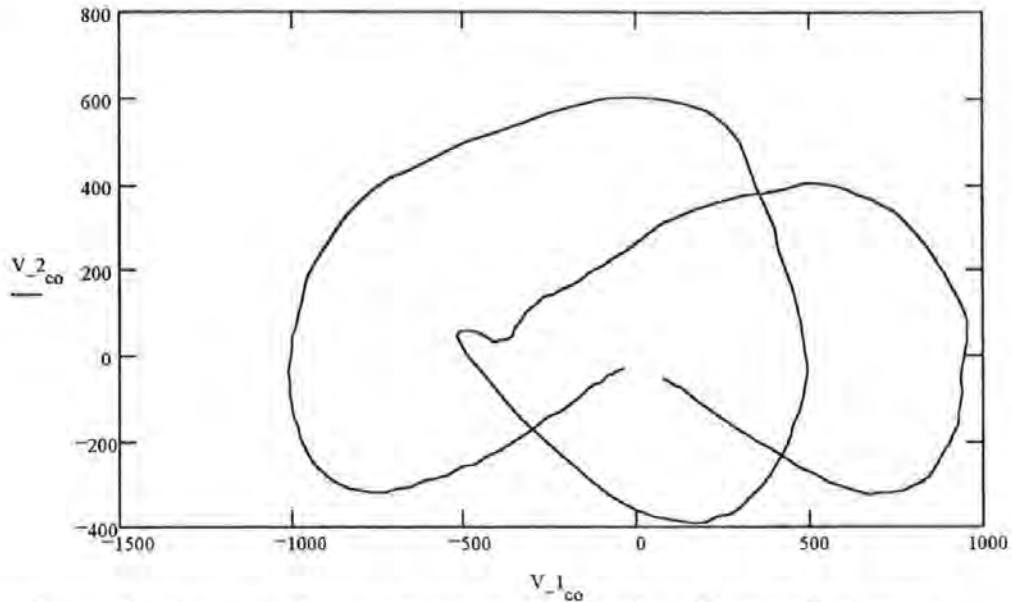
The input voltage to the Lock-In-Amplifiers at the fundamental frequency  $\nu$

$$V_{1_{co}} = 20F1_c$$

The input voltage to the Lock-In-Amplifiers at the fundamental frequency  $2\nu$

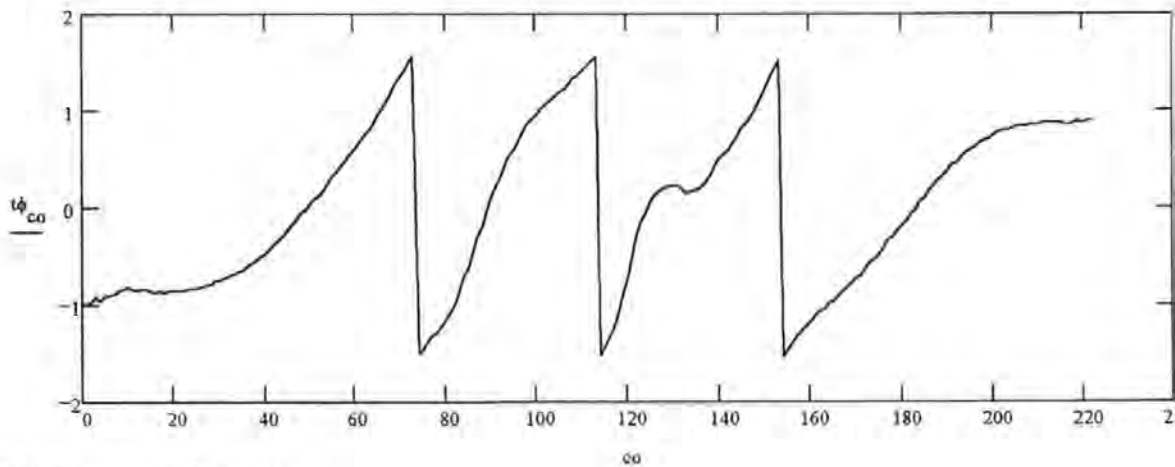
$$V_{2_{co}} = 20F2_c$$

The figure below shows the expected cardioid which would be generated from the voltages , from the Lock-In-Amplifiers



The relationship between change of optical wavelength and longitudinal strain using this signal processing technique.

$$t\phi_{co} = \text{atan} \left( \frac{V_{2_{co}} - 1}{V_{1_{co}} - 0.5} \right)$$



Therefore a processed signal :

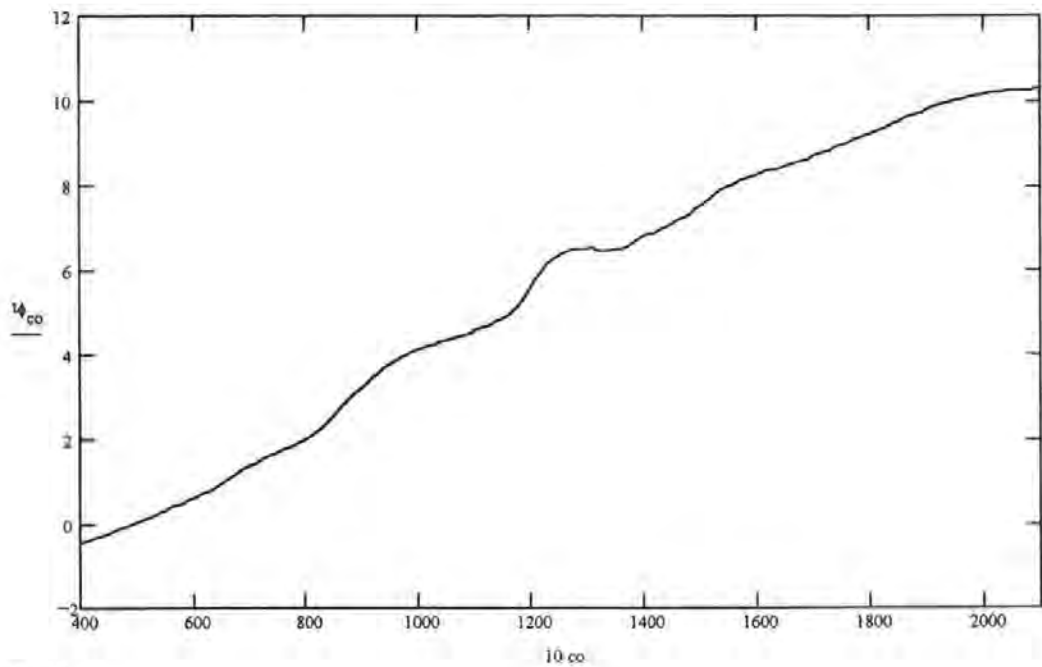
$$co = 0..7$$

$$t\phi_{co} = t\phi_{co} - t\phi_0 \quad co = 74..11$$

$$t\phi_{co} = (t\phi_{co} + \pi) - t\phi_0 \quad co = 114..15$$

$$t\phi_{co} = (t\phi_{co} + 2 \cdot \pi) - t\phi_0 \quad co := 154.22$$

$$t\phi_{co} = (t\phi_{co} + 3 \cdot \pi) - t\phi_0$$



$$co := 40..20$$

$$MAX := 200 - 4$$

$$strain_{co-40} := 10 \cdot (co - 40)$$

$$tt\phi_{co-40} := t\phi_c$$

A gradient of

$$Lin := slope(tt\phi, strain)$$

$$slope(tt\phi, strain) = 139.122598$$

$$star := intercept(tt\phi, strain)$$

$$intercept(tt\phi, strain) = 78.2415$$

$$slope(strain, tt\phi) = 7.1237110^{-3}$$

ERROR.

$$MAX \cdot 10 = 1.6 \cdot 10^3$$

$$MAX \sum_{k=0}^{\quad} \sqrt{[strain_k - (Lin \cdot tt\phi_k + star)]^2}$$

$$ERROR = \frac{\quad}{MAX + 1} \qquad ERROR = 35.75009$$

## VI) The C program that linearises that the optical phase change .

This is achieved by looking for the of  $\pm\pi/2$  from the inverse tangent of the ratio of 2nd harmonic to the 1st harmonic ( first dervative to second dervative ) .

At this point an additional  $\pi$  is added or sudtracted to maintian continuity . This is acheived by obtaining the sign of the gradient of the points ( data of the inverse ratio) this is obtianed from the values of the harmonics .

```
#include <stdio.h>
#include <stdlib.h>
#include <conio.h>
#include <math.h>
#include <dos.h>
#define pi 3.1415927

float *Data;
float *teta;
int n = 0; //Stores number of data points
float factor; // represents the value by which y is divided
float factor1;
float x;
int add = 0;
int i;
char filename2[14], filename[14];
//filename for values file
//filename2 for mathcad uses

FILE *data_ofp, *data_ifp;
/*.....*/
/*.....*/
/*      The setting up of the user interface , V.D.U. screen */
void border(int startx, int starty, int endx, int endy)
{
    register int i;
        gotoxy(1,1);
        for(i=0 ; i<= endx-startx ; i++)  putchar('+');
        gotoxy(1,endy-starty);
        for(i=1 ; i<=endx-startx ; i++)  putchar('+');
        for(i=2 ; i<=endy-starty ; i++) {
```

```

        gotoxy(1,i);
        putchar('+');
        gotoxy(endx-startx+1,i);
        putchar('+');
    } //end for
}

/*****
/*      Asking for the input data file to be used , which contains the values */
/*      of the harmonics .                                     */
void initialization()
{
int i; //For loop counts
int c;

    clrscr();
    window(1,1,80,25);
    border(1,1,80,25);
//Enter filename - open and exit on fail
    gotoxy(10,5);
    printf("Please, enter the name of the data file: ");
    scanf("%s",filename);
    if( ( data_ifp = fopen(filename,"r")) == NULL ){
        fprintf(stderr,"\\n\\n\\t\\tFile open failure - BYE !!!\\n");
        sleep(2);
        exit(0);
    } //end if
//Count number of data points in file - store in n
    while(!feof(data_ifp)){
        fscanf(data_ifp,"%*s");
        n++;
    } //end while
    n--;
//Allocate enough memory for the number of points - exit on failure
    if( (Data = (float*)malloc(n*sizeof(float))) == NULL){
        fprintf(stderr,"Memory allocation failure - Bye !!!");
        exit(0);
    }
}

```



```

//Allocate enough memory for the number of points - exit on failure
    if( (teta = (float*)malloc((n/2)*sizeof(float))) == NULL){
        fprintf(stderr,"Memory allocation failure - Bye !!!!");
        exit(0);
    }

//Go to start of file and read in all the floats to Data array
    rewind(data_ifp);
    for( i = 0; i < n; i++)
        fscanf(data_ifp,"%f",&Data[i]);
    fclose(data_ifp);
    gotoxy(10,6);
    printf("Enter the value of the y division factor : ");
    scanf("%f",&factor);
    gotoxy(10,7);
    printf("Enter the value you want to compare: ");
    scanf("%f",&factor1);
    window(1,10,38,16);
    border(1,10,38,16);
    gotoxy(4,2);
    printf("Enter the name of the file\n");
    gotoxy(4,3);
    printf("where you want to put the results");
    gotoxy(4,4);
    printf("(to use with Mathcad): " );
    scanf("%s",filename2);
    if( ( data_ofp = fopen(filename2,"w")) == NULL ){
        fprintf(stderr,"\n\n\t\tFile open failure - BYE !!!\n");
        sleep(2);
        exit(0);
    } //end if
}

/*****/

void create_teta()
{
    int j;

    for( j = 0 ; j < n/2 ; j++)

```

```

    {
        if(Data[2*j+1]==0 && Data[2*j] < 0) x=-99999;

        if(Data[2*j+1] == 0 && Data[2*j] > 0) x=99999;

        if(Data[2*j+1] != 0) x=factor*Data[2*j]/(7*Data[2*j+1]);

        if(Data[2*j+1] == 0 && Data[2*j] ==0) x=1;

        teta[j] = atan(x);
    }
}

/*****/
void write_to_file( int add , int i )
{
    fprintf(data_ofp, "%4.2f %4.2f %4.4f %4.4f\n",
            Data[2*i],Data[2*i+1],teta[i],teta[i]+add*pi);
}

/*****/

void check_gradient(int j)
{
    int gradient ;
    float delta ;

    if ( teta[j] < teta[j-1] ) gradient = 0 ;
    else gradient = 1 ;
    delta = (teta[j]-teta[j-1]) ;
    if (fabs(delta)>pi*factor1 && gradient==1) add--;
    if (fabs(delta)>pi*factor1 && gradient==0) add++;
    write_to_file(add,j);
}

```

```

/*****
***** Main Procedure *****
*****/

main()
{
    initialization();
    create_teta();
    for(i = 0; i < n/2 ; i++){
        check_gradient(i);
    }
    window(1,18,80,25);
    border(1,18,80,25);
    gotoxy(20,2);
    printf(" You can check the results in files");
    gotoxy(20,3);
    printf(" %s ",filename2);
    gotoxy(30,6);
    printf("BYE-BYE ...!!!");
    sleep(2);
}

```

## VI) A code listing of the C program for the T-Matrix formalism .

```
/* This program performs the T-matrix Formalism which presents */
/* a Bragg grating in an optical fibre . The results from this */
/* program are stored in output files . There is two distinct */
/* sets of results ; these are Reflectivity of the overall */
/* Bragg Gratings Vs Wavelength , the second Reflectivity of */
/* the overall Bragg Gratings at a given wavelenght Vs longitudinal */
/* strain. This is for nonuniform distribution of a grting period */
/* length and refractive index modulation depth . */

/* T.D.P. Allsop 16/6/97 */

/* Include ANSI C standard libraries */

#include <stdio.h>
#include <string.h>
#include <stdlib.h>
#include <math.h>

/* Include local header info */

struct pair
{
    double real, imag ;
} ;

typedef struct pair Complex ;

struct twobytwo
{
    Complex oneone, onetwo, twoone, twotwo ;
} ;

typedef struct twobytwo CMat ;

void InputGlobals(void) ;
Complex Conj(Complex) ;
Complex CAdd(Complex, Complex) ;
Complex CMul(Complex, Complex) ;
CMat CMatAdd(CMat, CMat) ;
CMat CMatMul(CMat, CMat) ;
double Flec(CMat) ;
double Mou(long int) ;

/* Global defines */

#define PI 3.14159

/* Global variables */
```

```

FILE *ofp1 ;          /* file pointer    to single grating save file      */
FILE *ofp2 ;          /* file pointer to ffp configuration save file      */
FILE *ofp3 ;          /* File pointer to result save file                */
FILE *ofp4 ;          /* Flie pointer to sist18 save file                 */
FILE *ofp5 ;          /* Flie pointer to fpstb18 save file               */

int Wave_str ;        /* The choice of code for Wavelength or strain response */
double n0 ;           /* original refractive index                        */
double n11 ;          /* perturbed refractive index                      */
double F ;            /* chirp factor (nano-units)                      */
double lam0 ;         /* initial lambda value (nano-units)              */
double laminc ;       /* lambda increment step                          */
long int j ;          /* number of lambda iterations                   */
double Lambda ;       /* grating period                                 */
double D ;            /* grating separation                             */
long int z ;          /* number of teeth in grating                    */
double epsinc ;       /* strain increment                               */
long int epsmax ;     /* number of strain iterations                   */
int choice ;          /* type of grating wanted ( Gaussian or Uniform ) */
double Para ;         /* For gassian spread                            */
int subM ;            /* SubM is the sub - division of a single period */

```

```

long int      eps ;
long int      y, x1 ;
long int      centre, i ;
int           k ;

double        Tom1, totalL1, n1, total_1, Tom2, totalL2, total_2 ;
double        lamj, Lamlam, G1flec, FFPflec ;
double        t1, t2, t3, t4, t7, t8, temp1, temp2 ;
double        indx, vals, zala ;
double        deltn, deltn1, t88, t89, temp3, temp4 ;

double        Kappa, Beta, S1_2, S1_1, effect ;
double        stra_org, stra_pert ;
double        v, p_12, p_11 ;

Complex A, B, dis ;
Complex      T5, T6 ;
Complex c1, c0 ;
CMat        M, newM, Sep ;

```

```

/* Main program starts here */

```

```

void main1();          /* main1 produces the results of a given */
                      /* structure of a Bragg grating which is */
                      /* subjected to longitudinal strain .    */

```

```

void main2();          /* main2 produces the results for */
                      /* variation of wavelength.         */

```

```

void main()

```

```

{

    InputGlobals();
    c1.real = 1.0 ; c1.imag = c0.real = c0.imag = 0.0 ;

    deltn =(n11-n0);

    if(choice == 1 )
    {
        totalL1 = 0.0 ;
        for(x1 =0 ; x1 <= z ; ++x1)
        {
            Tom1 = Mou(x1) ;
            totalL1 = totalL1 + Tom1 ;
        }
    }
    if ( Wave_str == 1)
    {
        main1() ; /*      For Wavelength */
    }
    else
    {
        main2() ; /*      For Strain */
    }
}

void main2(void)

/*          Both the pitch length change and the average          */
/*          refractive index change caused by strain is taken      */
/*          into account.                                          */
/*          main2() generates output file of a theoretical        */
/*          curve of Reflectivity Vs micro-strains subjected to   */
/*          grating.                                              */

{

    double n00 ;
    long int centre, third, quarter ;

    centre = (z-1L)/2L ; /* These three values help to define */
    third = ((3L*z)-3L)/4L ; /* the structure of the chirps in the */
    quarter = (z-5L)/4L ; /* the Bragg grating. */

    /*          This outer loop is the strain iterations .The variable */
    /*          t1 is for the elongation of a single pitch/period of the */
    /*          grating , each increment is specified in micro - strains. */

    for (eps=0 ; eps<=epsmax ; ++eps)
    {
        t1 = 1.0 + epsinc * ((double)eps) ;
        M.oneone = M.twotwo = c1 ; /* Starting values for */
        M.onetwo = M.twoone = c0 ; /* 2by2 matrices used to */
        total_1 = totalL1 ; /* calculate reflectivity */
        total_2 = totalL2 ;

        /*          This loop represents a single period in the grating the */

```

```

/*      parameter used for the single period is y. This is used */
/*      to calculate the true value of the period by Mou(). */
/*      Input parameter z is the total number of periods in */
/*      the grating , in affect the length y is incremented */
/*      downwards because the interest is in the characteristics */
/*      of the reflection spectrum of the grating i.e. what light */
/*      is reflected at z = 0 ; the front face of the grating . */

    for (y=z ; y>=1 ; --y)
    {
        t2 = Mou(y) ; /*      Brings back the value of */
                    /*      period at that position in */
                    /*      grating in nanometers . */

        printf("\n%ld\t%ld\t%ld",i,eps,y) ;

    }

    /*****/

    v = 0.17 ; /* Poisson's ratio for a germainsilicate fibre... */
    p_12 = 0.252 ; /* Photoelastic constants */
    p_11 = 0.112 ;

    /*****/

    /*      The inner loop is sub - one - period ; this is to */
    /*      accomodate the sinusoidal variation of the modulation */
    /*      of the refractive index over a single period of the */
    /*      grating.Each period sub divided into subM segments. */

    for(k = subM ; k>= 1 ; --k )
    {

    /*****/
    /*      Current Bragg gratings in general have a Gaussian */
    /*      distribution in the modulation depth of the pertubated */
    /*      refractive index . This is due to the methods used to */
    /*      fabricate the gratings , principlably due to the Gaussian */
    /*      profile of the laser's Irradaince used to generate the */
    /*      gratings. */
    /*      This section gives the option of having a single */
    /*      Gaussian distribution in the effective or "average" */
    /*      refractive index over all the grating ,this is achieved */
    /*      by giving the variable " choice " the value 3 .The second */
    /*      option is Gaussian distributions for each section of the */
    /*      grating choice = 1 . The other option is a uniform value */
    /*      the of choice = 2. */
    /*      The variable "Para" determines the width of the */
    /*      Gaussian shape .

    if( choice == 1 )
    {
        if ((y <= z) && (y >= (third+1L)))
        {
            t89 = ((double)y) - 1.0 + (2.0*((double)k)-1.0)/(2.0*((double)subM)-1.0) ;
            t88 = ((double)third)+ ((double) z) / 8.0 ;
            zala = ( ((double) z)/8.0 ) * 2.0 ;
            t8 = (t89 - t88)/ zala ;
            n1 = (n11-n0)*exp(-1.0*Para*t8*t8) + n0 ;
            /*      n00 = (n0)*exp(-1.0*Para*t8*t8) ; */

```

```

n00 = n0 ;

/*      Gaussian distribution 1 for grating 1      */
/*      minimum at z and (third+1) , peaking at   */
/*      third+(z/8) .                               */

}
else if((y <= third) && (y >= (quarter+1L)))
{
t89 = ((double)y) - 1.0 + (2.0*((double)k)-1.0)/(2.0*((double)subM)-1.0) ;
t88 = ((double)centre) ;
zala = ((double)centre) ;
t8 = (t89 - t88)/ zala ;
n1 = (n11-n0)*exp(-1.0*Para*t8*t8) + n0 ;
/*      n00 = (n0)*exp(-1.0*Para*t8*t8) ; */
n00 = n0 ;

/*      Gaussian distribution 2 for grating 2      */
/*      minimum at third and (quarter+1) ,         */
/*      peaking at centre .                       */

}
else if ((y <= quarter) && (y >= 0L))
{
t89 = ((double)y) - 1.0 + (2.0*((double)k)-1.0)/(2.0*((double)subM)-1.0) ;
t88 = ((double) z)/8.0 ;
zala = ((double) z)*2.0/8.0 ;
t8 = (t89 - t88)/ zala ;
n1 = (n11-n0)*exp(-1.0*Para*t8*t8) + n0 ;
/*      n00 = (n0)*exp(-1.0*Para*t8*t8) ; */
n00 = n0 ;
}

/*      Gaussian distribution 3 for grating 3 */
/*      minimum at (quarter) and ( 0 ) ,      */
/*      peaking at (z/8) .                    */

}
else if( choice == 3 )
{
t89 = ((double)y) - 1.0 + (2.0*((double)k)-1.0)/(2.0*((double)subM)-1.0) ;
t88 = ((double)z)/2.0 ;
zala = ((double)z) ;
t8 = (t89 - t88)/ zala ;
n1 = (n11-n0)*exp(-1.0*Para*t8*t8) + n0 ;
/*      n00 = (n0)*exp(-1.0*Para*t8*t8) ; */
n00 = n0 ;
}

/*      This is for a single Gaussian distribution */
/*      that is centred , peaking at y = centre.   */

else
{
n1 = n11 ;
n00 = n0 ;

/*      Uniform value for the refractive index.   */

}

```



```

/*****
/* This section takes into account of the sinusoidal */
/* variation of the modulation of each period and the */
/* effect of longitudinal strain on the refractive index */
/* optic strain effect ( Hocker and Butter model of a */
/* optical fibre under strain ) . */
/* In this program it is assumed that distribution of */
/* longitudinal strain along the fibre is uniform or */
/* constant . */
/* vals is the average value between the (n) and (n-1) */
/* sub sections of a single period. */

stra_org = n00 - 0.5*n00*n00*n00*(p_12 -v*(p_11+p_12)) * epsinc * ((double)eps) ;
stra_pert = n1 - 0.5*n1*n1*n1*(p_12 -v*(p_11+p_12)) * epsinc * ((double)eps) ;
vals = (2.0*((double)k)-1.0) * PI ;
indx = cos( vals / ((double)subM) ) ;
effect = ( stra_pert - stra_org )*indx + stra_org ;

/*****
/* Kappa is the coupling constant between the forward and */
/* backward travelling modes which exist in the grating. */
/* Beta is the differential propagation constant associated */
/* with detuning from the Bragg condition for a given */
/* single period of the grating . Also the strain has to be */
/* taken into account because of the elongation of the period */
/* itself ; which affects the Bragg condition in that period */
/* where original length of the period is given by Mou(). */

Kappa = ( PI * ( stra_pert - stra_org ) * indx) / lam0 ;
Beta = ( effect*PI*2.0 / lam0 ) - ( PI / (t2 * t1) ) ;

/*****
/* The coupled - mode equations for a uniform grating */
/* can yield a closed analytical function solution for */
/* the backward and forward modes in the grating. Consequently */
/* the close form solutions for the grating can be expressed */
/* by means of the scattering matrix and from this a one can */
/* obtain a transfer - matrix expression for the grating ;the */
/* T- matrix .This method can be used for a single period of */
/* grating or a sub - section of one period in the grating */
/* by using this method one can vary the period along the fibre */
/* length and produce a T - matrix for each section. Thus the */
/* total spectral reflectivity of the complete grating is */
/* calculated by multiplying all the 2by2 matrices together */
/* where each matrix represents sub - section , then a period */
/* and thus the grating .

/*****
/* This series of if/else statments represent the three condition */
/* that each section/ sub-section of a period can experience. */
/* These conditions relate to the phase - matching ; Bragg wavelength */
/* and the strength of the coupling constant. Outside of the phase - */
/* matched range there is a sinusoidal response in spectral reflectivity */
/* . Under the condition of being phase matched there is a cosh/sinh */
/* variation which leads to the main features of the spectral reflectivity */
/* grating and the third condition is for continuity . Produces the */
/* elements for the the T - matrices .

if (( Kappa*Kappa ) < (Beta)*(Beta) )

```

```

{
    S1_2 = sqrt( (Beta)*(Beta) - ( Kappa*Kappa ) );
    t3 =( PI * t1 )/((double)subM) ;
    t4 =( S1_2 * t2 * t1 )/ ((double)subM) ;
    T5.real = cos(t3) ; T5.imag = -1.0*sin(t3) ;
    T6.real = cos(t4) ;
    T6.imag = (-1.0 * Beta*sin(t4) )/S1_2 ;
    A = CMul(T5, T6) ;
    T5.imag = 1.0*sin(t3) ;    /* No Matching Condition*/
    T6.real = 0.0 ;
    T6.imag = ( -1.0*Kappa*sin(t4) )/ S1_2 ;
}
else if (( Kappa*Kappa ) > (Beta)*(Beta) )
{
    S1_1 = sqrt( ( Kappa*Kappa ) - (Beta)*(Beta)) ;
    t3 =( PI * t1 )/ ((double)subM) ;
    t4 = ( S1_1 * t2 * t1 )/ ((double)subM) ;
    T5.real = cos(t3) ; T5.imag = -1.0*sin(t3) ;
    T6.real = cosh(t4) ;
    T6.imag = (-1.0*Beta*sinh(t4) )/S1_1 ;
    A = CMul(T5, T6) ;
    T5.imag = 1.0*sin(t3) ;    /* Matching Condition */
    T6.real = 0.0 ;
    T6.imag = ( -1.0*Kappa*sinh(t4) )/S1_1 ;
}
else
{
    S1_1 = sqrt( ( Kappa*Kappa ) - (Beta)*(Beta)) ;
    t3 = ( PI * t1 )/ ((double)subM) ;
    t4 = ( S1_1 * t2 * t1 )/ ((double)subM) ;
    T5.real = cos(t3) ; T5.imag = -1.0*sin(t3) ;
    T6.real = 1.0 ;
    T6.imag = ( -1.0*Beta*t2*t1)/ ((double)subM) ;
    A = CMul(T5, T6) ;
    T5.imag = 1.0*sin(t3) ;    /* Continuity Condition */
    T6.real = 0.0 ;
    T6.imag = (-1.0*Kappa*t2*t1 )/ ((double)subM) ;
}

/*****
/*          This is the multiplication of the 2by2 matrices taking */
/*          n matrix elements and multiplying this by the (n-1) */
/*          matrix . This continues though all of the grating */
/*          taking all variations of period length (chirp) and the */
/*          frensel reflections and also the change in the effective */
/*          refractive index. */

    B = CMul(T5, T6) ;
    newM.oneone = A ;
    newM.onetwo = B ;
    newM.twoone = Conj(B) ;
    newM.twotwo = Conj(A) ;
    M = CMatMul(M, newM) ;
/*    fprintf(ofp3, "%15.12lf ", t2) ; */

}
}

/*****/

```

```

/*          This section is looking at the spectral reflectivity of a          */
/*          Bragg Grating resonator i.e. two identical gratings              */
/*          seperated by some physical distance in the fibre . The main      */
/*          calculation is that of the change of phase over the distance      */
/*          this being the parameter t7 .The result is then stored to file.  */

        G1flec = Flec(M) ;
        fprintf(ofp4, "%lf ", G1flec) ;
        t7 = ((2 * PI * stra_org * D) * t1) / lam0 ;
        dis.real = cos(t7) ; dis.imag = sin(t7) ;
        Sep.oneone = dis ;
        Sep.twotwo = Conj(dis) ;
        Sep.onetwo = Sep.twoone = c0 ;
        newM = CMatMul(CMatMul(M,Sep), M) ;
        FFPflec = Flec(newM) ;
        fprintf(ofp5, "%lf ", FFPflec) ;

        fprintf(ofp4, "\n") ;
        fprintf(ofp5, "\n") ;
    }
    fclose(ofp4) ;
    fclose(ofp5) ;
}

void main1(void)

/*          main2 produces the results for          */
/*          variation of wavelenght ; the total    */
/*          spectral reflectivity of a given grating */
/*          structure ( chirped )/ variation of     */
/*          refractive index .                      */

{

    long int centre, third, quarter ;

    centre = (z-1L)/2L ;
    third = ((3L*z)-3L)/4L ;
    quarter = (z-5L)/4L ;

/*          Main1() and main2() the nearly the same, the structure          */
/*          is different this dealing with the response the grating          */
/*          when irradiated by light with various wavelenghts.              */

/*          *****/
/*          The outer loop is dealing variations in wavelength . This      */
/*          incremented by the parameter i with intial value of lam0        */
/*          in nanometers and increment size is given by laminc . The      */
/*          spectral reflectivity response of the total Bragg grating        */
/*          is stored to file .                                              */

/*          *****/
/*          *****/

    for(i=0 ; i<=j ; ++i)

```

```

{
    /*          printf("\r%d",i);  */
    lamj = lam0 + laminc * ((double)i) ;
    for (eps=0 ; eps<=epsmax ; ++eps)
    {
        t1 = 1.0 + epsinc * ((double)eps) ;
        M.oneone = M.twotwo = c1 ;
        M.onetwo = M.twoone = c0 ;
        total_1 = totalL1 ;

        for( y=z ; y>= 1 ; --y )
        {
            t2 = Mou(y) ;

            printf("\r%d\t%d\t%d",i,eps,y) ;

            for(k = subM ; k>= 1 ; -k )
            {

                if( choice == 1 )
                {
                    if ((y <= z) && (y >= (third+1L)))
                    {
                        t89 = ((double)y) - 1.0 + (2.0*((double)k)-1.0)/(2.0*((double)subM)-1.0) ;
                        t88 = (((double)third) + ((double) z/8L)) ;
                        zala = ((double) z/8L)*2.0 ;
                        t8 = (t89 - t88)/ zala ;
                        deltn1 = (n11-n0)*exp(-1.0*Para*t8*t8) ;
                    }
                    else if((y <= third) && (y >= (quarter+1L)))
                    {
                        t89 = ((double)y) - 1.0 + (2.0*((double)k)-1.0)/(2.0*((double)subM)-1.0) ;
                        t88 = ((double)centre) ;
                        zala = ((double)centre) ;
                        t8 = (t89 - t88)/ zala ;
                        deltn1 = (n11-n0)*exp(-1.0*Para*t8*t8) ;
                    }
                    else if((y <= quarter) && (y >= 0L))
                    {
                        t89 = ((double)y) - 1.0 + (2.0*((double)k)-1.0)/(2.0*((double)subM)-1.0) ;
                        t88 = ((double)z)/2.0 ;
                        zala = ((double)z) ;
                        t8 = (t89 - t88)/ zala ;
                        deltn1 = (n11-n0)*exp(-1.0*Para*t8*t8) ;
                    }
                }
                else if( choice == 3 )
                {
                    t89 = ((double)y) - 1.0 + (2.0*((double)k)-1.0)/(2.0*((double)subM)-1.0) ;
                    t88 = ((double)z)/2.0 ;
                    zala = ((double)z) ;
                    t8 = (t89 - t88)/ zala ;
                    deltn1 = (n11-n0)*exp(-1.0*Para*t8*t8) ;
                }
            }
            else    deltn1 = deltn ;
        }
    }
}

```

/\*\*\*\*\*\*

```

/* In this case main1() has no strain variation */
/* so the parameters " effect ", " Kappa " as no */
/* dependancy on " t1 " and " eps " variables. */

```

```

vals = (2.0*((double)k)-1.0) * PI ;
indx = cos( vals / ((double)subM) ) ;
effect = deltn * indx + n0 ;
Kappa = ( PI * ( deltn1 ) * indx ) / lamj ;

```

```

/*****

```

```

Beta = ( effect*PI*2.0 / lamj ) - ( PI / (t2 * t1) ) ;
if (( Kappa*Kappa ) < (Beta)*(Beta) )
{
S1_2 = sqrt( (Beta)*(Beta) - ( Kappa*Kappa ) ) ;
t3 = ( PI * t1 ) / ((double)subM) ;
t4 = ( S1_2 * t2 * t1 ) / ((double)subM) ;
T5.real = cos(t3) ;          T5.imag = -1.0*sin(t3) ;
T6.real = cos(t4) ;
T6.imag = (-1.0 * Beta*sin(t4) ) / S1_2 ;
A = CMul(T5, T6) ;
T5.imag = 1.0*sin(t3) ;
T6.real = 0.0 ;
T6.imag = (-1.0*Kappa*sin(t4) ) / S1_2 ;
}
else if (( Kappa*Kappa ) > (Beta)*(Beta) )
{
S1_1 = sqrt( ( Kappa*Kappa ) - (Beta)*(Beta) ) ;
t3 = ( PI * t1 ) / ((double)subM) ;
t4 = ( S1_1 * t2 * t1 ) / ((double)subM) ;
T5.real = cos(t3) ;          T5.imag = -1.0*sin(t3) ;
T6.real = cosh(t4) ;
T6.imag = (-1.0*Beta*sinh(t4) ) / S1_1 ;
A = CMul(T5, T6) ;
T5.imag = 1.0*sin(t3) ;
T6.real = 0.0 ;
T6.imag = (-1.0*Kappa*sinh(t4) ) / S1_1 ;
}
else
{
S1_1 = sqrt( ( Kappa*Kappa ) - (Beta)*(Beta) ) ;
t3 = ( PI * t1 ) / ((double)subM) ;
t4 = ( S1_1 * t2 * t1 ) / ((double)subM) ;
T5.real = cos(t3) ;          T5.imag = -1.0*sin(t3) ;
T6.real = 1.0 ;
T6.imag = (-1.0*Beta*t2*t1) / ((double)subM) ;
A = CMul(T5, T6) ;
T5.imag = 1.0*sin(t3) ;
T6.real = 0.0 ;
T6.imag = (-1.0*Kappa*t2*t1) / ((double)subM) ;
}

```

```

B = CMul(T5, T6) ;
newM.oneone = A ;
newM.onetwo = B ;
newM.twoone = Conj(B) ;
newM.twotwo = Conj(A) ;
M = CMatMul(M, newM) ;
/* fprintf(ofp3, "%15.12lf ", t2) ; */

```

```

    }
    }

    fprintf(ofp3, "\n");
    G1flec = Flec(M);
    fprintf(ofp1, "%lf ", G1flec);
    t7 = ((2.0 * PI * n0 * D) * t1) / lamj;
    dis.real = cos(t7); dis.imag = sin(t7);
    Sep.oneone = dis;
    Sep.twotwo = Conj(dis);
    Sep.onetwo = Sep.twoone = c0;
    newM = CMatMul(CMatMul(M, Sep), M);
    FFPflec = Flec(newM);
    fprintf(ofp2, "%lf ", FFPflec);

    }

    fprintf(ofp1, "\n");
    fprintf(ofp2, "\n");

    }
    fclose(ofp1);
    fclose(ofp2);
/*    fclose(ofp3); */

}

/*****
/*****

/* Input global parameters from the keyboard */

void    InputGlobals(void)
{

    printf("Enter (1) for wavelenght or (2) for strain response : ");
    scanf("%d", &Wave_str);

    printf("\n\nEnter original refractive index : ");
    scanf("%lf", &n0);

    printf("Enter perturbed refractive index : ");
    scanf("%lf", &n1);

    printf("Enter (1) for Gaussian , (2) for uniform perturbation : ");
    printf("or (3) Gaussians perturbations for each gratings : ");
    scanf("%d", &choice);

    if(choice == 1){
        printf("Enter parameter for divergance of Gaussian beam : ");
        scanf("%lf", &Para);
    }

    printf("Enter chirp factor (nano-units) : ");
    scanf("%lf", &F);
    F = F * 1.0e-9;
    if(Wave_str == 1 )

```

```

{
printf("Enter initial lambda value (nano-units) : ");
scanf("%lf", &lam0);
lam0 = lam0 * 1.0e-9;

printf("Enter lambda step increment (nano-units) : ");
scanf("%lf", &laminc);
laminc = laminc * 1.0e-9;

printf("Enter number of lambda iterations : ");
scanf("%ld", &j);
}
else
{
printf("Enter lambda value (nano-units) : ");
scanf("%lf", &lam0);
lam0 = lam0 * 1.0e-9;
}
printf("Enter grating Period (nano-units) : ");
scanf("%lf", &Lambda);
Lambda = Lambda * 1.0e-9;

printf("Enter grating separation : ");
scanf("%lf", &D);

printf("Enter number of teeth in grating : ");
scanf("%ld", &z);

printf("Enter the number of sub-division per Period : ");
scanf("%d", &subM);

printf("Enter strain increment (micros) : ");
scanf("%lf", &epsinc);
epsinc = epsinc * 1.0e-6;

printf("Enter number of strain iterations : ");
scanf("%ld", &epsmax);

if(Wave_str == 1)
{
if ((ofp1 = fopen("single.c", "w")) == NULL)
{
printf("\nCan't open file single\n");
exit(1);
}

if ((ofp2 = fopen("ffpcon.c", "w")) == NULL)
{
printf("\nCan't open file ffpcon\n");
exit(1);
}

if ((ofp3 = fopen("result.c", "w")) == NULL)
{
printf("\nCan't open file ffpcon\n");
exit(1);
}
}
else

```

```

        {
            if ((ofp4 = fopen("sistb18.c", "w")) == NULL)
            {
                printf("\nCan't open file single\n");
                exit(1);
            }

            if ((ofp5 = fopen("fpstb18.c", "w")) == NULL)
            {
                printf("\nCan't open file ffpcon\n");
                exit(1);
            }
        }
    }
}

```

/\* Find the complex conjugate \*/

```

Complex Conj(Complex A)
{
    Complex    C;

    C.real = A.real;
    C.imag = -1.0 * A.imag;
    return(C);
}

```

/\* Add two complex variables \*/

```

Complex CAdd(Complex A, Complex B)
{
    Complex    C;

    C.real = A.real + B.real;
    C.imag = A.imag + B.imag;
    return(C);
}

```

/\* Multiply two complex variables \*/

```

Complex CMul(Complex A, Complex B)
{
    Complex    C;

    C.real = A.real * B.real - A.imag * B.imag;
    C.imag = A.real * B.imag + A.imag * B.real;
    return(C);
}

```

/\* Add two complex matrices of size 2x2 \*/

```

CMat    CMatAdd(CMat A, CMat B)
{
    CMat    C;

```



```

        C.oneone = CAdd(A.oneone, B.oneone) ;
        C.onetwo = CAdd(A.onetwo, B.onetwo) ;
        C.twoone = CAdd(A.twoone, B.twoone) ;
        C.twotwo = CAdd(A.twotwo, B.twotwo) ;
        return(C) ;
    }

/* Multiply two complex matrices of size 2x2 */

CMat  CMatMul(CMat A, CMat B)
{
    CMat      C ;

    C.oneone = CAdd(CMul(A.oneone, B.oneone), CMul(A.onetwo, B.twoone)) ;
    C.onetwo = CAdd(CMul(A.oneone, B.onetwo), CMul(A.onetwo, B.twotwo)) ;
    C.twoone = CAdd(CMul(A.twoone, B.oneone), CMul(A.twotwo, B.twoone)) ;
    C.twotwo = CAdd(CMul(A.twoone, B.onetwo), CMul(A.twotwo, B.twotwo)) ;
    return(C) ;
}

/* Calculate flec function of a complex matrix */

double  Flec(CMat M)
{
    Complex      T1, T2, T3 ;
    double      x ;

    T1 = CMul(M.twoone, Conj(M.oneone)) ;
    T2 = CMul(M.oneone, Conj(M.oneone)) ;
    T3 = CMul(T1, Conj(T1)) ;
    x = T3.real / (T2.real * T2.real) ;
    return(x) ;
}

/*****
/*          Centre , third , quarter are parameters that define the      */
/*          structure of the gratings, that is to say the pattren of      */
/*          chirps for the periods of the perturbed indices .The          */
/*          magnitude of the chirp is governed by the input variable */
/*          " F ", in this case it is a combination of three linear      */
/*          chirps , but can be quadratic or cubic . The reason is that */
/*          hese types of chirps can be fabricated .                      */
*****/

/* Calculate grating size */

double  Mou(long int y)
{
    long int  centre ,third , quarter ;
    double  result ;
    result = 0.0 ;
    centre = (z-1L)/2L ;
    third = ((3L*z)-3L)/4L ;
    quarter = (z-5L)/4L ;
/*****
    if ((y <= z) && (y >= (third+1L)))
        result = Lambda + F * ((double) (y-third-1L)) ;

    /*          Chirp One          */
*****/

```

```

/*****/

else if ((y <= third) && (y >= (centre)))
    result = Lambda + F * ((double) (y-centre)) ;
else if ((y <= centre-1L) && (y >= (quarter+1L)))
    result = Lambda + -1.0*F * ((double) (centre-y)) ;

/*          Chirp Two          */

/*****/

else if ((y <= quarter) && (y >= 0L))
    result = Lambda + -1.0*F * ((double) (quarter-y)) ;

/*          Chirp Three          */

/*****/

return (result) ;

}

```